Brigham Young University
BYU ScholarsArchive

All Theses and Dissertations

2012-08-08

Understanding Noble Metal Addition in Cobalt Fischer Tropsch Catalysts

Kari Marie Cook
Brigham Young University - Provo

Follow this and additional works at: https://scholarsarchive.byu.edu/etd

 Part of the Chemical Engineering Commons

BYU ScholarsArchive Citation

Cook, Kari Marie, "Understanding Noble Metal Addition in Cobalt Fischer Tropsch Catalysts" (2012). *All Theses and Dissertations.* 3293.
https://scholarsarchive.byu.edu/etd/3293

This Dissertation is brought to you for free and open access by BYU ScholarsArchive. It has been accepted for inclusion in All Theses and Dissertations by an authorized administrator of BYU ScholarsArchive. For more information, please contact scholarsarchive@byu.edu, ellen_amatangelo@byu.edu.

Understanding Noble Metal Addition in Cobalt Fischer Tropsch Catalysts

Kari Marie Cook

A dissertation submitted to the faculty of
Brigham Young University
in partial fulfillment of the requirements for the degree of

Doctor of Philosophy

William C. Hecker, Chair
Calvin H. Bartholomew
Byron G. Johnson
Larry L. Baxter
David O. Lignell

Department of Chemical Engineering

Brigham Young University

December 2012

Copyright © 2012 Kari Cook

All Rights Reserved

ABSTRACT

Understanding Noble Metal Addition in Cobalt Fischer Tropsch Catalysts

Kari M. Cook
Department of Chemical Engineering
Doctorate of Philosophy

The effects of noble metal (NM) promotion and deposition order (co-deposition of NM with the final Co deposition [co-dep] or sequential deposition of NM after Co deposition [seq-dep]) on surface area, pore size, metal retention, crystallite size, noble metal distribution and bonding in Co Fischer Tropsch (FT) catalysts were studied as were the resulting Co reducibility and Fischer Tropsch activity/selectivity properties. Catalysts containing nominally 25wt% Co with either 0.3 wt% Ru, 0.58 wt% Pt, 0.55wt% Re, or no NM on a La-stabilized-Al_2O_3 support were prepared by wet deposition. The Co, Pt, and Re were uniformly dispersed, but Ru distribution and retention were problematic and deposition-order dependent—85% was lost with co-dep, but it was uniformly distributed while 54% was lost with seq-dep and it was concentrated at the pellet edge. The co-dep catalysts all have smaller reduced Co crystallite size than their corresponding seq-dep catalysts. The average crystallite diameters for all 3 co-dep catalysts are between 4.1 and 4.3nm and ~90% of the crystallites are < 6nm. XAFS measurements showed that after reduction at 360^{o}C, Pt is bonded with Co even with mild calcination between the final Co and the Pt deposition. On the other hand, neither Ru nor Re formed direct bonds with Co. Ru remained in a separate metal phase after reduction even at low loadings. Re remained as Re_2O_7 and still promoted Co reduction well (e.g. 42% reduced to Co metal compared to *none* for the unpromoted catalyst). By all measures of reducibility (TPR, EOR, H_2 uptake), all NM promoted catalysts were more reducible than the unpromoted catalyst. The co-dep catalysts have lower TPR peak temperatures, but lower extents of reduction than their corresponding seq-dep catalysts. The NM type effect on overall extent of reduction trend was Co/Pt-seq>Co/Re-seq>Co/Ru-seq=Co/Pt-co>Co/Re-co>Co/Ru-co>Co. The Co/Pt-co catalyst was the most active of all the catalysts both on rate per mass and per site basis. The co-dep catalysts were all more active than the corresponding sequentially deposited catalysts. The co-dep Pt and Re catalyst activity is greater due to higher activity per site, while co-dep Ru activity is greater due to a higher abundance of active sites.

Keywords: Cobalt, Fischer-Tropsch, noble metal, reducibility, deposition order

.

ACKNOWLEDGMENTS

I wish to thank Dr. William Hecker, my advisor, for his mentoring and guidance through research and writing. Dr. Calvin Bartholomew's mentoring and guidance is also appreciated. I would like to thank Dr. Byron Johnson for mentoring and his industrial perspective. ConocoPhillips is thanked for their financial support through a fellowship. Dr. Jeffrey Miller's mentoring especially in relation to the included XAFS is appreciated. Committee members, Dr. Baxter and Dr. Lignell are also thanked for their support.

Most importantly, I wish to thank my family. I thank my husband, Trevor Cook, for being the best 1 am lab partner anyone could ask for. Kira Cook, I thank for her patience through countless hours of analysis and writing that filled her first year of life. I am grateful also to the examples of my parents, Ed and Regina Guyer, for instilling confidence and a value of education within me.

TABLE OF CONTENTS

LIST OF TABLES

LIST OF FIGURES

1 Introduction

1.1 The Need for Alternative Sources of Petroleum

For several decades, the United States has used petroleum to meet at least 40% of its energy and chemical needs, consuming, for example, 18.8 million barrels per day in 2011 of which more than 50% was imported. While the United States is the largest petroleum consumer in the world, the demand is rising for several other countries including China, who is presently the second largest petroleum consumer and Canada, from whom the United States imports two times more petroleum than any other country (Administration 2012). Evidence of high and increasing demand is demonstrated by (1) rapid growth (especially of motorcycle and automobile transportation) in developing countries and (2) the rising price of crude oil which increased from less than $50/bbl reached as high as $150/bbl and has since stabilized around $80-100/bbl. Environmental concerns surrounding oil production such as impacts of drilling, oil spills, and flaring of coproduced natural gas are causing ever tightening regulations, which in combination with the increase of demand may leave conventional petroleum resources inadequate to meet projected demand.

Thus, there is a clear need for long-term, technically feasible, and economically-favorable alternatives to conventional petroleum resources to supply liquid fuels worldwide. One of the most promising options is the carbon-to-liquids industry in which synthesis gas (carbon

monoxide and hydrogen) produced from stranded, abundant, or otherwise flared natural gas, coal, and renewable, non-food biowaste is converted into high quality synthetic liquid fuels and chemicals via Fischer Tropsch Synthesis (FTS) with little environmental impact. Nearly 500,000 bbl/d of premium fuels (gasoline, diesel, and aviation) and chemical feedstock are presently produced from coal and cheap natural gas by this route.

1.2 Overview of Fischer Tropsch Synthesis Development

The Fischer Tropsch (FT) reaction was discovered by Franz Fischer and Hans Tropsch in 1925. Using a cobalt (Co) catalyst, they produced gaseous and liquid hydrocarbons from coal syngas at 1 bar and 220-250^{o}C (Bartholomew 2003; Bartholomew and Farrauto 2006). The first prominent use of this FT process was production of fuels and wax by Germany during WWII motivated by a lack of access to petroleum but plentiful coal resources. During the decade following the war FT synthesis (FTS) research and development (R&D) surged in the United States until the mid 1950s when it ceased abruptly with the discovery of cheap oil in the Middle East. With work initiated in 1955 by South African Synthetic Oil Limited (SASOL), South Africa was the only place commercial practice of FTS continued as access to petroleum imports was blocked by other nations and coal was plentiful. SASOL's coal-to-liquids (CTL) plants have since expanded and continue to operate.

Following the 1973 oil embargo, most large oil companies including Gulf Oil, Chevron, Shell, Sasol, and Exxon, and universities supported by the United States Department of Energy greatly expanded R&D of FTS (Bartholomew 2003; Bartholomew and Farrauto 2006). In the 1990s, FTS R&D of natural gas to liquids (GTL) by companies including SASOL, Chevron, Conoco-Philips, ExxonMobil, IFP/ENI/Agip, Syntroleum, Marathon, Bechtel, and Amoco

culminated in construction of five GTL plants in Malaysia, Qatar, and Nigeria producing a total of about 250,000 bbl/d (see Table 1-1). This, added to SASOL's expanded CTL production of nearly 200,000 bbl/d, pushed the total world production from FTS to nearly a half-million bbl/d (Bartholomew and Farrauto 2006). Production from FTS is projected to rise significantly due to near record low $2.30 per million BTU natural gas price resulting from shale gas production. This in combination with the high petroleum prices has GTL in the spot light. Shell and Sasol have announced proposals for GTL plants in the United States Gulf Coast (Tullo 2011; Hargreaves 2012; Shell 2012). In fact, the present considerable R&D activities focused on FT catalyst, reactor, and process technologies are likely to provide further improvements to the efficiencies and economics of CTL and GTL processes and in the coming decades make possible the application of FTS to conversion of renewable biowastes in every city and local region of the world. These advancements are demonstrated by at least these six FTS plants currently operating at >10000 barrels/day each and two additional in the planning stage (Table 1-1). Thus, FTS is not only a promising idea, but a proven answer to worldwide liquid fuel needs (Morales and Weckhuysen 2006).

1.3 Statement of Problem/Objectives

While less expensive Fe FT catalysts have been and continue to be used successfully for CTL in South Africa, Co containing catalysts are the most active, selective, and stable catalysts for FTS and are the catalysts of choice for GTL. Previous studies have shown that catalyst support, Co precursor, Co loading, deposition method/solvent, and promoter metal along with drying, calcination, and reduction conditions influence dispersion, particle size, and reducibility of Co, and thus the activity and selectivity of supported Co FT catalysts and that Co FTS

catalysts typically require NMs to achieve optimal reducibility while maintaining Co dispersion (Borg, Froseth et al. 2007; Khodakov, Chu et al. 2007). Even with substantial data from previous literature and the proven commercial viability of noble metal (NM) promoters in numerous patents e.g. (Iglesia, Soled et al. 1988; Eri, Goodwin et al. 1989; Van Berge, Van De Loosdrecht et al. 2008), there is, nevertheless, insufficient information specifying the best type of NM and order of addition. The enormous cost and scarcity of NMs make maximizing their effectiveness and minimizing the amount added to the catalysts critical to acceptable catalyst and possibly overall FT process economics.

Table 1-1. Currently Operating FTS Plants

Location	Company	Production Level (bbl/day)	Start-up Year
South Africa	SASOL	200,000	
South Africa	PetroSA/ SASOL	20,000	1992
Malaysia	Shell	15,000	1993
Qatar	Sasol and Qatar Petroleum (alliance with Chevron)	34000	2005
Nigeria	Chevron Nigeria, a Sasol-Chevron alliance, and Nigerian National Petroleum Company	34,000	2007
Qatar	Shell and Qatar Petroleum	140,000	2011
United States (Louisiana)	Sasol	2-4 million metric tons/yr	2013[a]
United States (Gulf Coast)	Shell	TBA	TBA

[a] Construction starts

The objective of this research was to determine how NM (1) type and (2) deposition order affect the catalysts' physical, chemical, reducibility, and FT activity/selectivity properties for Co/Al_2O_3 catalysts. NMs chosen for this study were Ruthenium (Ru), Platinum (Pt) and Rhenium

(Re) (Objective 1) because they are most commonly claimed in patents and used in commercial practice (Bartholomew and Farrauto 2006). Catalysts incorporating these NMs were prepared by a multi-step bench scale impregnation and the NM was either co-deposited (co-dep) with the final Co deposition step or sequentially deposited (seq-dep) after the final Co deposition step (Objective 2). These planned comparisons are shown by objective in Table 1-2. Note that the wt% for each NM is different in order to maintain the same molar NM:Co ratio a of 0.007.

Table 1-2. Variables to be compared in objectives of this study

Objective	Planned Variations
1. NM Type	0.30 wt% Ru vs. 0.58 wt% Pt vs. 0.55 wt% Re
2. Deposition Order	co-dep vs seq-dep

.

2 Review of Literature

2.1 Representative Co FT Catalyst

Given that the purpose of this study is to determine how NM type and deposition order affect physical, chemical, and reducibility properties and performance of commercially-representative Co FT catalysts, it is important to define nominally desirable properties and performance of commercial Co FT catalysts. Table 2-1 lists several key properties and values that are representative of commercial Co FT catalysts based on a survey of relevant scientific literature and patents.

Cobalt catalysts are almost always supported on a moderately high surface area material in order to obtain and maintain dispersed Co active sites. Heat-treated γ-Al_2O_3 containing textual promoters to improve stabilities is the most commonly used support, due to its higher inherent chemical, thermal, hydrothermal, and mechanical stabilities (Beuther, Kobylinski et al. 1986). Similarly promoted SiO_2 and TiO_2 are also used. Of these three untreated and unstablized supports, γ-Al_2O_3 interacts most strongly with Co and sometimes permits aluminate formation at tetrahedral and octahedral sites thereby decreasing Co reducibility (Culross and Mauldin 1998). Co metal crystallites constitute the active phase and reduction promoters (of which NM are the most effective) are typically added to achieve the most active and selective Co FT catalysts (60-90% reduction to Co metal at low reduction temperatures (i.e. 340-400^{o}C) sufficient to maintain

8-12% dispersion). Thus, γ-Al_2O_3's need for reduction promotion makes it the best choice for this study of NM addition.

Table 2-1. Representative Commercial Co FT catalyst properties (Bartholomew and Farrauto 2006)

Property	Value
Co Weight Loading	20-30 wt%
Noble Weight Loading	0-1[b] wt%
Total Surface Area	100-150 m^2/g
Co Distribution	Uniform at nanoscale
H_2 Uptake	100[c]-300 μmol/g
Reduction Temperature	350-400^oC
Co Dispersion	8-12%
Extent of Reduction	75-95%
Specific Activity (TOF)[a]	20-30 $*10^{-3}$ s^{-1}
C_{5+} Selectivity	85-88%
CH_4 Selectivity	5%

[a] 200^oC, 50% conversion, 20 bar, H_2:CO =2
[b] optimally 0-0.3wt%
[c] optimally 200-300 μmols/g

2.2 NM Effects on Cobalt Reduction

The most prominent effect of NM addition discussed in literature is facilitation of reduction of Co oxides to Co metal at a temperature below 400^oC. Reduction of Co has been shown to occur via two steps i.e., reduction of Co_3O_4 to CoO and CoO to Co^o metal (Brown, Cooper et al. 1982; Sexton, Hughes et al. 1986; Viswanathan and Gopalakrishnan 1986). These earlier findings have been confirmed using temperature programmed reduction (TPR) and most recently using X-ray Adsorption Fine Structure (XAFS) and X-ray Adsorption Near Edge Structure (XANES) analysis (Jacobs, Chaney et al. 2004; Jacobs, Ji et al. 2007).

The generally accepted explanation for Co reduction promotion with NMs is the reduction of NM oxides to metal at a lower temperature than Co oxides reduce to metal. The reduced NM clusters provide centers for H_2 dissociation from which H-atoms spill-over to the Co oxide facilitating its reduction (Kogelbauer, Goodwin et al. 1996; Guczi 2002; Jacobs 2004; Girardon, Constant-Griboval et al. 2005). This effect is depicted in Figure 2-1. Thereafter, Co metal sites formed early in the reduction of the Co oxide phase can also activate H_2 to H-atoms which then accelerate the reduction of nearby Co oxides. This theory fits well with findings that (1) Ru or Re need intimate (though not necessarily direct contact with Co) (Iglesia, 1988; Hilmen, 1996) and (2) NMs with high reduction temperatures do not shift the lower temperature step of Co reduction to a lower temperature (i.e., Re only facilitates the second reduction step CoO to Co metal).

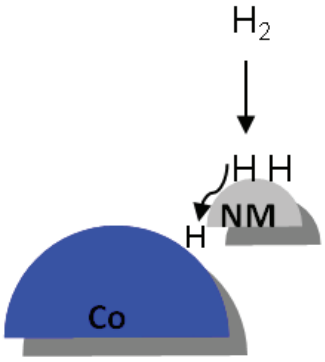

Figure 2-1. Hydrogen spill-over

Temperature programmed reduction (TPR) is one of the most common methods used to measure reducibility in the form of reduction rate as a function of temperature and is done by measuring hydrogen consumption using (a) a thermal conductivity detector or (b) a mass

spectrometer or by (c) a gravimetric measure of oxygen loss (typically using a TGA). These detection methods produce a TPR profile which is the signal from hydrogen consumption or the derivative of the weight change as a function of temperature, and for Co catalysts typically consists of two peaks for the two main steps of the reduction process. Figure 2-2 is a representative TPR profile for an alumina supported Co FT catalysts showing two main peaks corresponding to the two main reduction steps, Co_3O_4 to CoO and CoO to Co^0.

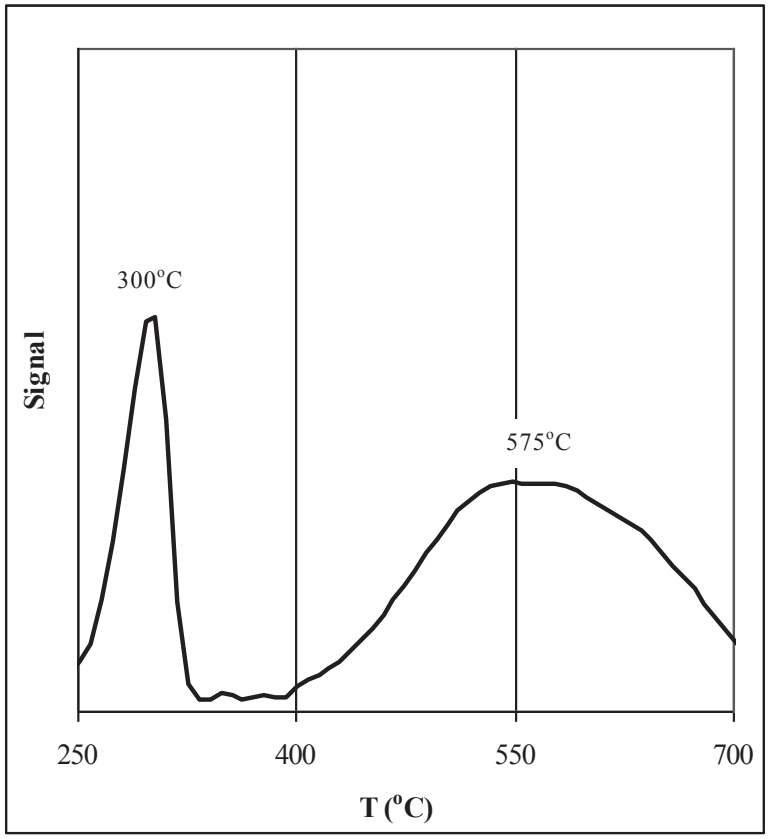

Figure 2-2. Representative TPR showing reduction of calcined Co catalyst

NM promotion effects on reduction temperatures and rates are observed as shifts in one or both of the reduction peaks to lower temperature and changes in peak shape (usually narrowing). The extent of the temperature shift is highly dependent on metal loading, deposition

method, and thermal treatments. A study by Jacobs et al. provides a representative example of shifting reduction peaks to lower temperatures, see Figure 2-3; by adding 0.5 wt% Pt to 25% Co/Al_2O_3 the temperatures of the two main reduction peaks shifted from approximately 325°C and 575°C (bottom bold curve) to 175°C and 425°C (top bold curve), respectively (Jacobs, Das et al. 2002).

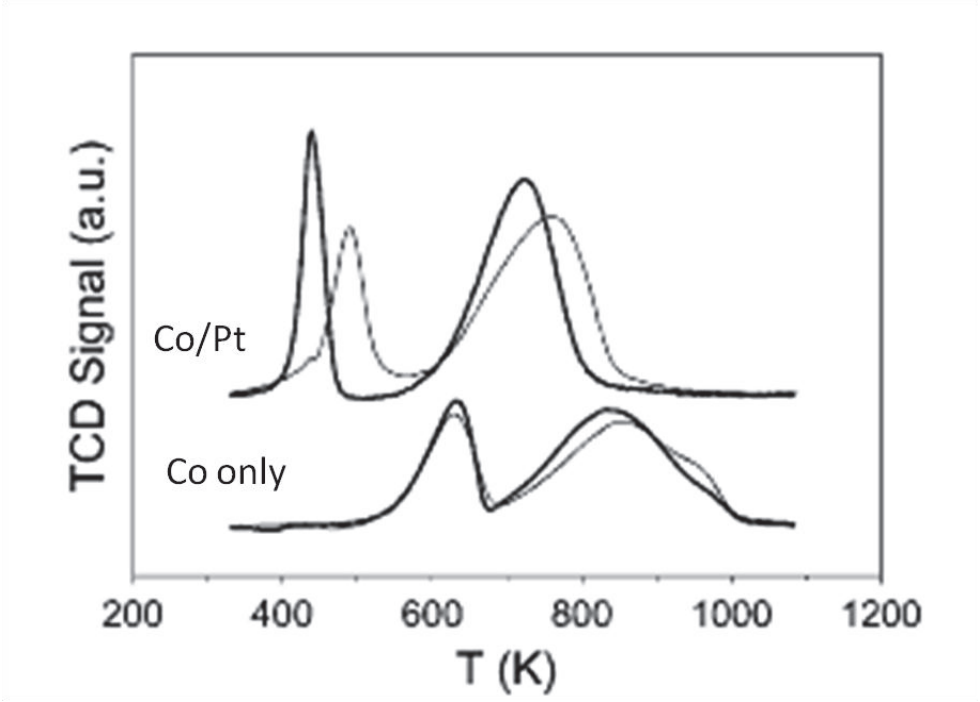

Figure 2-3. TPR profile comparison of unpromoted (Co only) and 0.5wt% promoted (Co/Pt) for 25wt% Co (bold) and 15wt% Co (thin) Al_2O_3 supported FT catalysts.(Jacobs, Das et al. 2002)

Large changes in peak shape due to addition of 0.4% Pt to 9% Co/Al_2O_3 are reported by Schanke et al.as shown in Figure 2-4. The first reduction peak is shifted from 327°C to a two peaks at 147°C and 177°C. A similar effect is observed with Pt addition to Co/Al_2O (Vada 1995). More typical than these bimodal effects is peak narrowing apparent from Figure 2-3 (Jacobs 2004; Jacobs, Ji et al. 2007).

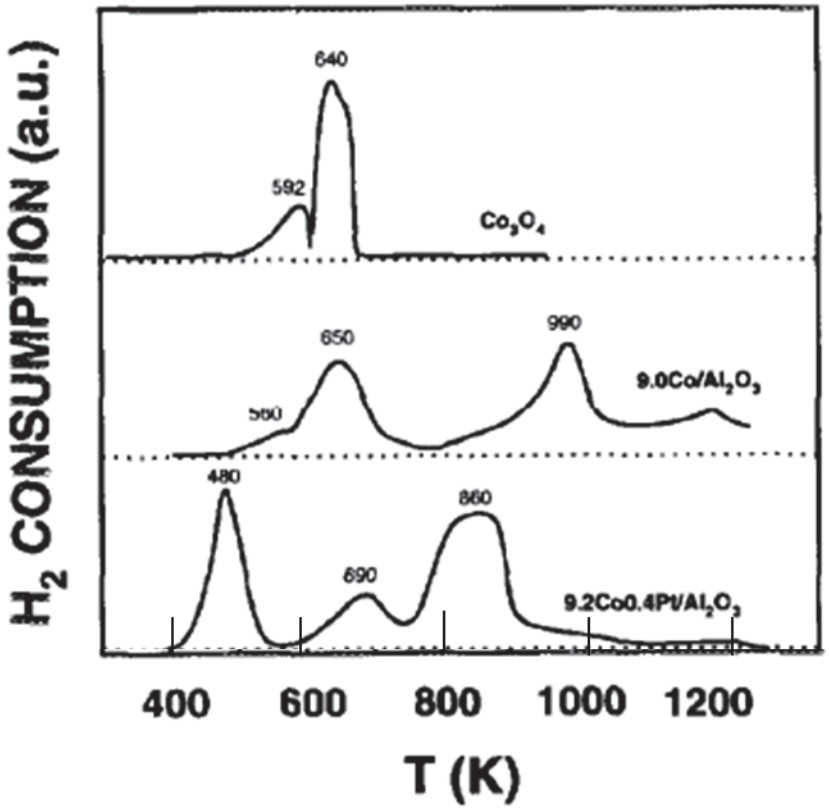

Figure 2-4. TPR of unsupported Co_3O_4 and Co/Al_2O_3 showing Pt promoters shift Co reduction peaks (Schanke, Vada et al. 1995)

Extent of reduction (EOR) , an important quantification of reducibility, is typically obtained from oxygen titration at 400^{o}C of a catalyst after reduction (Reuel and Bartholomew 1984). As with TPR profiles, comparisons of EOR between catalysts from different studies are more likely to be qualitative than quantitative due to the difficulty of isolating results from other variables that affect reducibility such as metal loading (shown by comparing the bold and thin lines in Figure 2-3), preparation variables, and reduction conditions.

Increases in EOR due to NM addition, when provided for a given catalyst type and Co loading, provide an effective quantification of improvements in reducibility. EOR increases of 30 absolute% (from 45% to 75%) have been found with 0.4-0.5wt% Pt addition (Schanke, Vada et

al. 1995; Jacobs, Das et al. 2002) as have much smaller changes such as the 6 absolute% increase (from 50% to 56%) with 0.2wt% Pt addition (Tsubaki and Fujimoto 2000). Kogelbauer found that adding 0.5 wt% Ru to 20% Co/Al_2O_3 increases EOR by 30 absolute% (from 58% to 88%) (Kogelbauer, Goodwin et al. 1996). In general, for reduction temperatures between 350°C and 450°C, NM promotion increases EOR by 33% to 80% relative to the unpromoted catalyst (Vada 1995; Das, Jacobs et al. 2003; Hosseini 2005; Chu, Chernavskii et al. 2007)

H_2 uptake, another gauge of reducibility, is the measurement of the amount of H_2 that chemisorbs on the reduced Co catalyst and with the assumption of 1 Co surface atom to 1 H adsorbed gives the Co surface atom density which is approximately proportional to the number of active sites (Co metal) on the surface. Jacobs et al.found that H_2 uptake increased from 66.9 μmols/g for 15wt% Co on Al_2O_3 to 140.6, 115.5 and 168.2 μmols/g with addition of 0.5wt% Pt, 1wt% Ru, and 1wt% Re respectively (Jacobs, Das et al. 2002). Two to three fold increases in H_2 uptakes as a result of NM addition are typical (Vada 1995; Tsubaki, Sun et al. 2001; Jacobs, Das et al. 2002).

2.3 NM Effects on Physical and Chemical Properties of Co Catalysts

In previous work it was observed that Co and NM loading, proximity of NMs to Co oxide phases, relative sizes of NM and Co oxide particles and spatial uniformity of NM and Co phases could significantly influence H_2 activation, H transport, and hence local reduction rate (Kobylinski 1978; Beuther, Kobylinski et al. 1986; Eri, Goodwin et al. 1989; Vada 1995; Mauldin 1999; Hosseini 2005; Chu, Chernavskii et al. 2007). Thus an understanding of the chemical and physical properties affected by NM type and depostion order are pertinent to this study.

Much of the work to understand the effects of Co and NM loadings is found in the patent literature, and the general concensus is that promotion effects are dependent on the relative NM and Co loadings (Beuther, Kobylinski et al. 1986; Mauldin and Varnado 2001; Jacobs, Ji et al. 2007). However, the effect of NMs on metal retention is limited (Prieto, Martinez et al. 2009). Studies related Co-NM proximity at the atomic scale and NM effects on particle size have received at least a little attention in the literature and are covered in the next two subsections. NM effects on spatial uniformity has received little attention, but a number of works detail pH effects on adsorption and thus spatial distribution. That NM promotion does not significantly affect surface area and pore structure of catalysts is largely consistent across the literature (Jacobs, Das et al. 2002). However, as noted earlier, Co surface area as measured by H_2 uptake typical increases mainly due to higher EOR with NM addition.

2.3.1 NM Chemical State/Bonding

Relatively recent literature reports studies which use XAFS and XANES methods to measure the chemical state and bonding of NM promoters. Pt bonds to Co following direct reduction (without calcination) at 400-450^{o}C (Guczi 2002) . In addition, Pt and Re reportedly bond with Co when the Co and NM precursors are calcined in the same step and then reduced at 350^{o}C (Pt) or 450^{o}C (Re) (Ronning 2001; Jacobs, Chaney et al. 2004). Ru's bonding is more controversial; i.e., observations in reduced catalysts of only Ru-Ru bonds (Bazin, Kovacs et al. 2003; Jacobs, Sarkar et al. 2008) as well as Ru-Co bonds (Iglesia 1993; Ma, Jacobs et al. 2011) have been reported.

2.3.2 Co Crystallite Size

Studies of Co crystallite size effects originated by the research groups of Bartholomew and Yermakov in the mid 1980s (Reuel and Bartholomew 1984; Lisitsyn, Golovin et al. 1985). Co crystallites below 6 nm (independent of support and preparation method) have been found less active (Barbier, Tuel et al. 2001; Bezemer, van Laak et al. 2004; Bezemer, Bitter et al. 2006; Martinez and Prieto 2007; Borg, Dietzel et al. 2008). This trend is not consistent across the literature, as others have shown that activity is unaffected by crystallite size (Johnson 1989). Given its possible effect on activity, it is important to understand the Co crystallite size effects of NM promotion.

Previous literature suggests that (1) Ru and Pt promoters do not significantly alter Co oxide crystallite sizes obtained during calcination compared to unpromoted Co catalysts (Li, Liu et al. 2006; Chu, Chernavskii et al. 2007; Jacobs, Ji et al. 2007; Karaca, Safonova et al. 2011) although (2) Re promotion reportedly causes formation of smaller Co oxide crystallites (Culross and Mauldin 2000; Mauldin and Varnado 2001; Borg, Hammer et al. 2009; Enger, Fossan et al. 2011). For example, Chu et al. showed that upon adding 1wt% Pt the Co_3O_4 crystallite size decreased by only 0.2 nm (to 9.3 from 9.5 nm) as estimated from XRD (Chu, Chernavskii et al. 2007). The smaller Co oxide crystallites resulting with Re promotion (typically in the range of 5-15% decreases) are thought to occur because Re oxide lowers Co ion mobility (Mauldin and Varnado 2001) thus preventing agglomeration during calcination. Nevertheless, Vada suggests that Co_3O_4 crystallite size is unaffected with Re promotion (19 nm) but deceases with Pt promotion (14 relative to 19 nm) (Vada 1995).

The effect of NM promoters on reduced Co crystallite size is complicated by a lack of consensus on how the reduction process affects Co crystallite size; findings vary between

reduced Co crystallites having no change, decrease, and increase in size relative to the corresponding calcined catalyst) (Borg, Hammer et al. 2009; Enger, Fossan et al. 2011; Park, Bae et al. 2011). Additionally, very few previous publications report direct measurements of crystallite size distribution (CSD) or average crystallite diameter (ACD) by TEM for reduced/ passivated catalysts; comparison of TEM measured CSDs for calcined and reduced catalysts are absent even from this literature (Reuel and Bartholomew 1984; Storsæter, Tøtdal et al. 2005; Li, Liu et al. 2006; Karaca, Safonova et al. 2011). Thus conclusions regarding NM effects on Co crystallite size are based upon estimates rather than measurements. Sun et al. estimated ACD from H_2 chemisorption and found that the ACD of reduced catalysts decreased in the following order: Co/Ru (13 nm) > Co (12 nm)>Co/Pt (4 nm). They also calculated ACD from TEM measurements of a limited number of particles and found qualitatively the same order, but quantitatively different values (6, 5, and 3 nm for Co/Ru, Co, and Co/Pt respectively). The agreement in order, but lower absolute values was also seen when Sun compared H_2 chemisorption and TEM derived crystallite sizes for unpromoted catalysts prepared by different methods (Sun, Fujimoto et al. 2003).

2.3.3 Co and NM Spatial Distribution

While the available literature does not directly tie NM addition to changes in metal spatial distribution, there has been significant work on the effects of pH on strength of adsorption and in some cases on the metal distribution (Heise and Schwarz 1985; Regalbuto 2007). Variations in spatial metal distribution, especially of the relative Co and NM distribution, are significant as proximity potentially influences promotion of Co reducibility—the major effect of NM addition (Iglesia 1993).

It is thus relevant to discuss how pH affects metal precursor adsorption to the support. First, it is important to understand that γ-Al_2O_3 has neutral OH groups on the surface at the point of zero charge (PZC), ~8. Exposure to solutions with a higher pH causes the surface groups to deprotonate to O^- . Exposure to solutions with a lower pH causes the surface to protonate to OH^{2+}. Figure 2-5 depicts this general concept and shows that of course the adsorption of either cations (pH>PZC) or anions (pH<PZC) is preferred after a change in the surface protonation. Thus during the impregnation of the support with NM, the pH of the deposition solution affects metal distribution by defining the surface charge and therewith the adsorption strength (Regalbuto 2007). As a result, uniform adsorption of a precursor on the support occurs at an optimal pH with its associated optimal surface charge, and optimal adsorption strength. If adsorption is too weak, the metal deposition profile will be dependent on drying rate and capillary forces which tend to create concentration gradients of the metal precursor. If adsorption is too strong and fast, the metal precursor will be adsorbed at pore inlets and a shell (or eggshell) of deposited metal will result. This effect can be mitigated by adding a salt, base, or acid to the solution. For example, Pt anions from chloroplatinic acid have been found to absorb very strongly in an eggshell profile on Al_2O_3 unless HCl, HNO_3, or inorganic nitrates are added to the impregnation solution thus loading the solution with anions which compete with the hexachloroplatinate for surface adsorption and allowing the Pt anions to penetrate deeper into the pellet and adsorb more uniformly (Heise and Schwarz 1985).

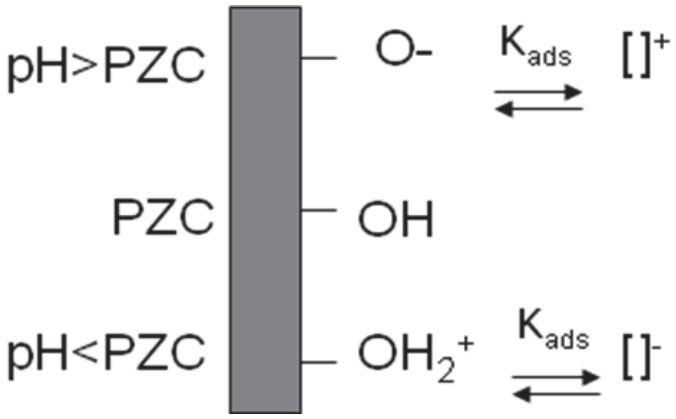

Figure 2-5. Point of zero charge

2.4 NM Effects on Activity/Selectivity and Stability of Cobalt Catalysts

Reducibility and Co crystallite size affect activity/selectivity and thus many studies, including several cited above, show changes (usually increases) in activity as a result of NM addition (although specific activity per catalytic site may increase or decrease slightly). Tsubaki found that turnover frequency (TOF), a measure of activity normalized by the number of available reduced Co sites, is affected by Ru and Pt promotion with TOF decreasing in the following order Co/Ru ($12.7x10^{-2}s^{-1}$) >Co ($9.3x10^{-2}s^{-1}$) >Co/Pt($4.2x10^{-2}s^{-1}$) during reactions at 513K, 145 psi , and a H_2:CO=2 (Tsubaki, Sun et al. 2001). The increase in activity with Ru addition was confirmed by Igelsia (at 473K, 290 psi, H_2:CO=2.05) with an increase of TOF from 3.9 to 6.4 $*10^{-4}$ s^{-1} when 0.14wt% Ru was added to 11.6wt%Co (Iglesia 1993). Vada et al. confirmed the lower TOF (at 493K, 14.5 psi, H_2:CO =7.3 and H_2:inert=1.1) with Pt promotion as well as Re promotion, i.e. TOFs of $20x10^{-3}$ s^{-1} and $18x10^{-3}$ s^{-1} respectively compared to $31x10^{-3}$ s^{-1} for the unpromoted catalyst (Vada 1995). Decrease in TOF with Pt promotion is not consistent in the literature, Diehl and Khodakov observed an increase in TOF at 513 K, 145 psi, and H_2:CO=2 for 0.2%Pt/10%Co/SiO_2 to 2.75 $x10^{-4}$ s^{-1} rather than 1.86 $x10^{-4}$ s^{-1} for the

unpromoted catalyst (Diehl and Khodakov 2009). Borg et al. showed that TOF was unaffected by Re promotion reporting both the Co/γ-Al_2O_3 and Co/Re/γ-Al_2O_3 catalysts as 52 x10^{-3} s^{-1} at 483K, 290 psi, H_2:CO=10 and H_2:inert= 2.2 (Borg, Froseth et al. 2007). Figure 2-6 depicts these values by normalizing the unpromoted (Co) catalyst TOF to a value of 1 for each study. From this, it is evident that the effect of NM on TOF is unclear and likely dependent on the type of NM. The inconsistencies in NMs effect on TOF is likely tied to variations in Co crystallite size as smaller (<6 nm) crystallites have been shown to be less active, see Figure 2-7 (Bezemer, Van Dillen et al. 2005; Bezemer, Bitter et al. 2006).

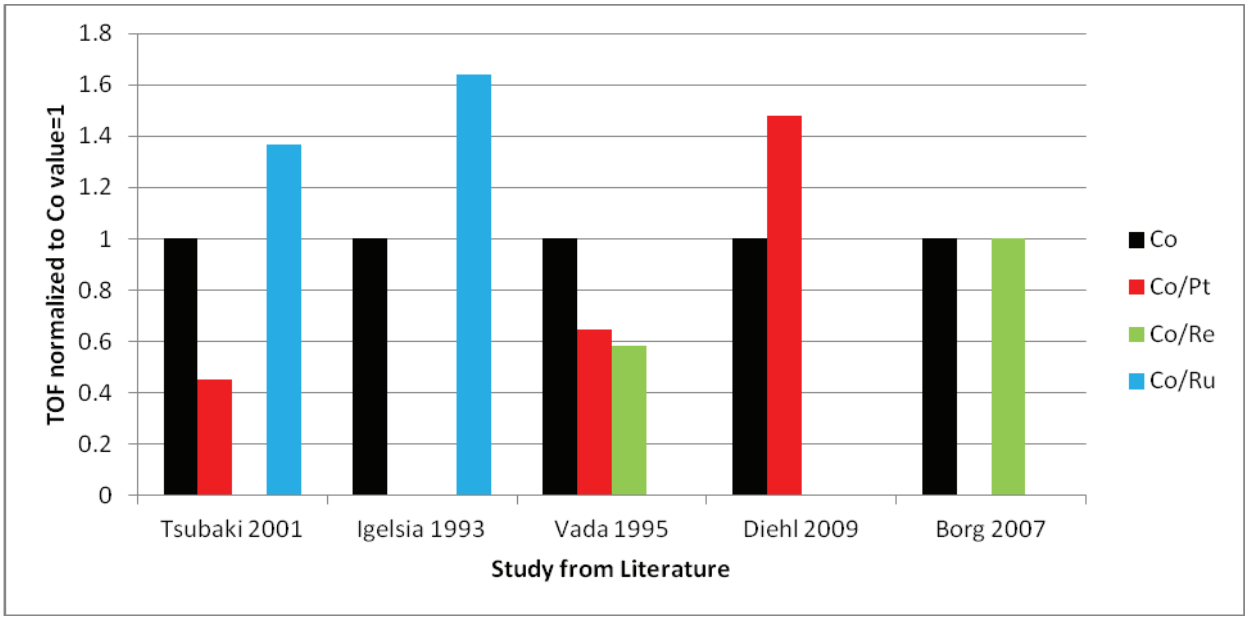

Figure 2-6. TOF normalized for unpromoted (Co) to have a value of 1 compared with promoted (Co/Pt, Co/Re, and Co/Ru) catalysts separated by study from literature

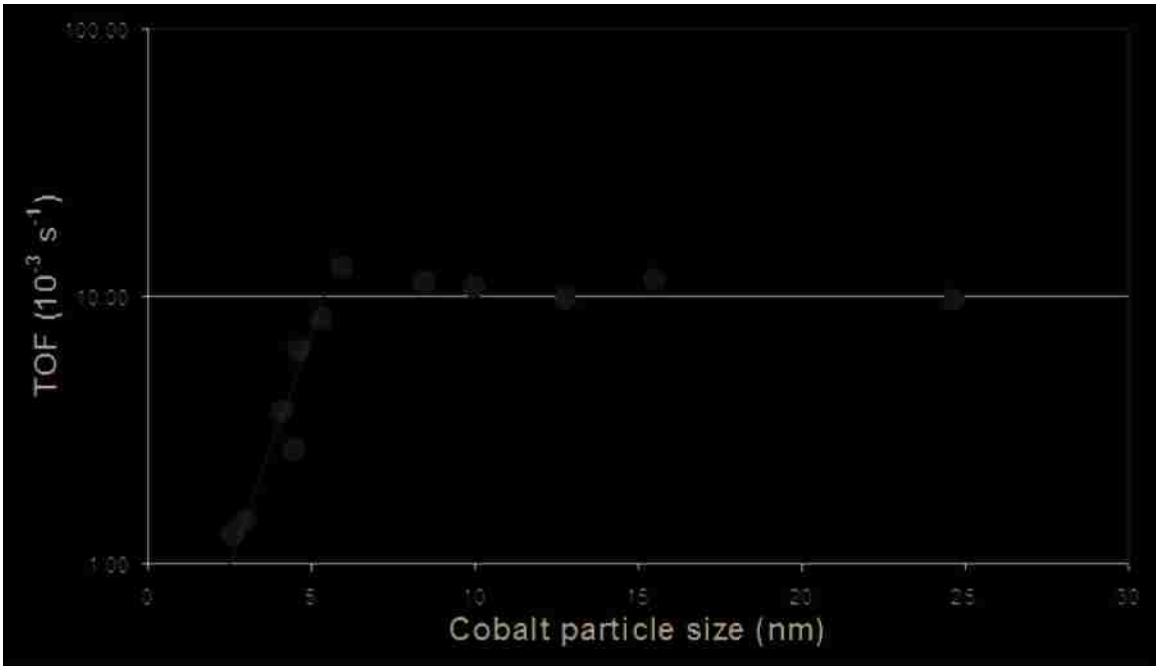

Figure 2-7. TOF as a function of reduce Co crystallite size for unpromoted (Co) (Bezemer, Van Dillen et al. 2005)

As previously mentioned, activity per gram is found to increase with NM promotion (Beuther, Kobylinski et al. 1986; Vada 1995; Mauldin and Varnado 2001). This increase in activity per gram is apparent even when TOF is constant. In the study from Borg et al.already mentioned addition of Re increased the mass-based activity from 1.6 to 2.7 μmols/g_{cat}/s (Borg, Froseth et al. 2007). Figure 2-8 shows the increase in rate as a function of Re addition. From this it is evident, that there is a plateau in activity with NM addition—after a Re/Co ratio of about 0.1 (1wt% Re on 11-12 wt% Co) additional Re does not further increase catalyst activity (Mauldin and Varnado 2001). As another example, a Gulf patent shows the rate increased from 49 to 102 mL of CO/g_{cat}-h for 20 wt% Co/Al_2O_3 supported FT catalyst with the addition of 0.05 wt% Ru. But when the Ru wt% was doubled to 0.10, the rate showed a plateau effect and increased only slightly (118 mL of CO/g_{cat}-h) (Beuther, Kobylinski et al. 1986).

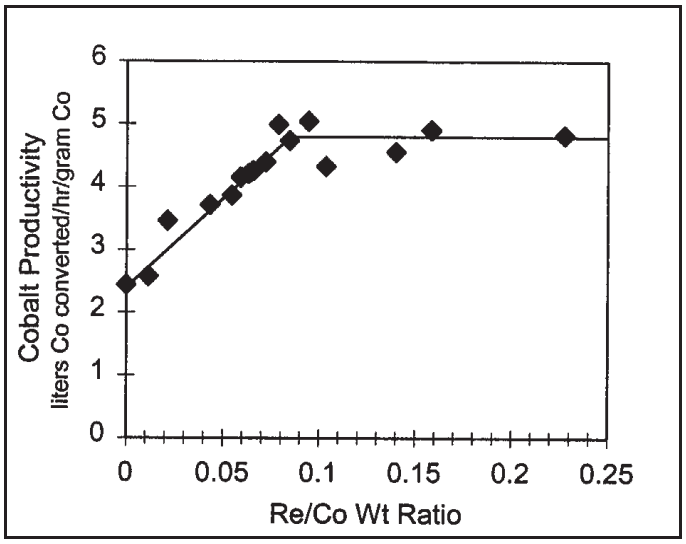

Figure 2-8: Re promotion plateau with 11-12% Co loading (Mauldin and Varnado 2001)

Generally C_{5+} selectivity increases and CH_4 selectivity decreases with NM addition (Iglesia 1993; Bartholomew and Farrauto 2006). Various observed trends have been reported. Tsubaki found that methane selectivity decreased in the following order: Co/Pt> Co≥Co/Ru. Increased methane and carbon dioxide selectivities companioned by a decrease in the desired C_{5+} selectivity with addition of NMs have been found by other groups (Xiao Shuzhang 2004; Chu, Chernavskii et al. 2007). Nevertheless, selectivity effects are not found in all studies; several have found that selectivity is unaffected by Re and Pt promotion (Vada 1995; Mauldin and Varnado 2001; Jacobs, Chaney et al. 2004). This lack of change is not clearly explained as NM generally increases EOR and thus dispersion and dispersion has been correlated with selectivity. In fact, transport restrictions due to higher site density and dispersion have been found to increase the residence time and readsorption probabilities of α−olefins and thus increase C_{5+} selectivity (Iglesia, Soled et al. 1992).

In relation to catalyst deactivation, studies have shown that NMs have a 'protective effect' by inhibiting Co site oxidation or carbon deposition during FT reactions (Iglesia 1997).

Ru and Pt have been found to overcome carbon deposition (Iglesia, Soled et al. 1988; Iglesia 1993; Huber and Barthlomew 2001). Pt has been shown to cut deactivation rates in half after reaction at 220^{o}C per 100 h (<1% X_{CO} drop for 0.1Pt/10Co rather than 2% X_{CO} drop for the unpromoted catalyst) (De Jong, Glezer et al. 1989). Even when carbon forms, NMs facilitate carbon gasification and thus enable in-situ rejuvenation (Beuther, Kobylinski et al. 1986; Eri, Goodwin et al. 1989; Eri, Goodwin et al. 1992). NM promotion also decreases the fraction of smaller Co crystallites that tend to be less stable and susceptible to sintering and reoxidation (Iglesia, Soled et al. 1988; Jacobs, Patterson et al. 2002).

2.5 Influence of Deposition Order

NMs can be deposited (impregnated) into the support by two main methods: (1) sequential deposition (seq-dep), where Co (or at least part of the total Co loading) is deposited after or (usually) before the NM or (2) co-deposition (co-dep), where Co (or at least part of the total Co loading) is deposited at the same time as the NM (Kobylinksi, 1986). In the case of this study and typically when seq-dep is performed, the Co is deposited first, and then the NM.

There is disagreement in literature regarding which deposition procedure is preferable. Beuther made catalysts by both co-dep and seq-dep (with or without calcinations between depositions) and concluded that neither deposition method is preferable when the inconvenience of an added step is ignored (Beuther, Kobylinski et al. 1986). Iglesia claimed that the calcination step is when surface oxides migrate allowing for intimate contact and thus suggested co-calcination to the NM oxide and Co oxide is required for effective reduction promotion, but that deposition order is not signficant (Iglesia 1993). Vada et al. found both Pt and Re promote reduction of Co even with seq-dep and calcination between deposition steps (Vada 1995). The

lack of consensus on the superiority of co-dep or seq-dep is made evident by Table 2-2, which shows that both co-dep and seq-dep (with and without calcination between the Co and NM depositions) preparation methods are used in NM promoted Co FT catalysts found in literature and patents.

Table 2-2. Order of deposition in literature

co-dep
(Morales, Grandjean et al. 2006)
(Chu, Chernavskii et al. 2007)
(Hosseini 2005)
(Eri, Goodwin et al. 1992)
(Khodakov, Girardon et al. 2007)
(Xiao and Qian 2008)
seq-dep (no calcinations between)
(Iglesia, Soled et al. 1988)
(Jacobs, Das et al. 2002; Jacobs, Chaney et al. 2004; Jacobs, Chaney et al. 2004; Jacobs, Sarkar et al. 2008)
(Eri, Goodwin et al. 1992)
seq-dep (calcinations between)
(Vada 1995)
(Beuther, Kibby et al. 1983; Beuther, Kibby et al. 1985)
(Xiao and Qian 2008)

2.6 Summary

A review of the literature on the effect of NM type (Pt, Re, or Ru) and deposition order (co-dep or seq-dep) in Co FT catalysts has been made. The predominate effect of NM addition is promotion of Co reduction. This is facilitated by close proximity of NMs to Co oxide phases and

high dispersion of both oxide phases, which in turn influence H_2 activation, H transport, and hence local reduction rate. A few studies address chemical state and bonding of NM atoms (with Co or other NM atoms), nm range proximity, and Co particle size. NMs are typical found in the zero valence state bonded to either Co or itself. There is not a general consensus on how NMs affect Co crystallite size. Micron and nanometer scale NM and Co spatial distributions in the support have received relatively little attention. However, the effects of pH and ion concentration during impregnation on metal precursor deposition have been investigated. While effective loadings of NM and Co have been addressed, studies of NM retention throughout preparation are also lacking. Increases in reducibility due to addition of NMs generally increases mass-based catalyst activity, while specific activity per catalytic site (TOF) may increase or decrease but only slightly. C_{5+} selectivity increases and methane selectivity decreases with addition of NM promoters and NMs have been found to increase stability by inhibiting deactivation due to oxidation and carbon deposition. Even with the many studies of NM promotion of Co FT catalysts, there is not a clear consensus on which type or deposition order is optimal.

3 Catalyst Preparation and Characterization Methods

3.1 Catalyst Preparation

The seq-dep catalysts of this study were prepared in five steps as depicted in Figure 3-1 and described in detail below:

Step 1: gamma alumina (γ-Al_2O_3) was stabilized by addition of lanthanum (La);

Steps 2, 3, and 4: Co was deposited by wet impregnation at 10, 20, and 25 nominal wt%;

Step 5: NM promoter was added in a final deposition step for a targeted NM/Co ratio of 0.007.

The co-dep catalysts were prepared by adding the NM promoter with Co in the 4th step. The details of the deposition order variation are given in Chapter 5 Effect of Deposition Order.

3.1.1 Support Treatment/Stablization

In Step 1, γ-Al_2O_3 support (Alfa Aesar item # 43858, ¼" rings, BET SA 174 $m^2 \cdot g^{-1}$, pore volume 0.802 $cm^3 \cdot g^{-1}$) was dried in air at 100°C for 2 h and calcined to 400°C for 2 h. The calcined support was impregnated with La using an aqueous chelated metal complex solution at constant pH of 5 using an acetic acid/acetate buffer (Van Dillen, Terorde et al. 2003). The chelating agent was Ethylenediaminetetraacetic acid (EDTA, Mallinckrodt Chemicals, 99.4%) and the La precursor was lanthanum nitrate ($La(NO_3)_3 \cdot 6H_2O$,Fisher Scientific, > 98% pure).

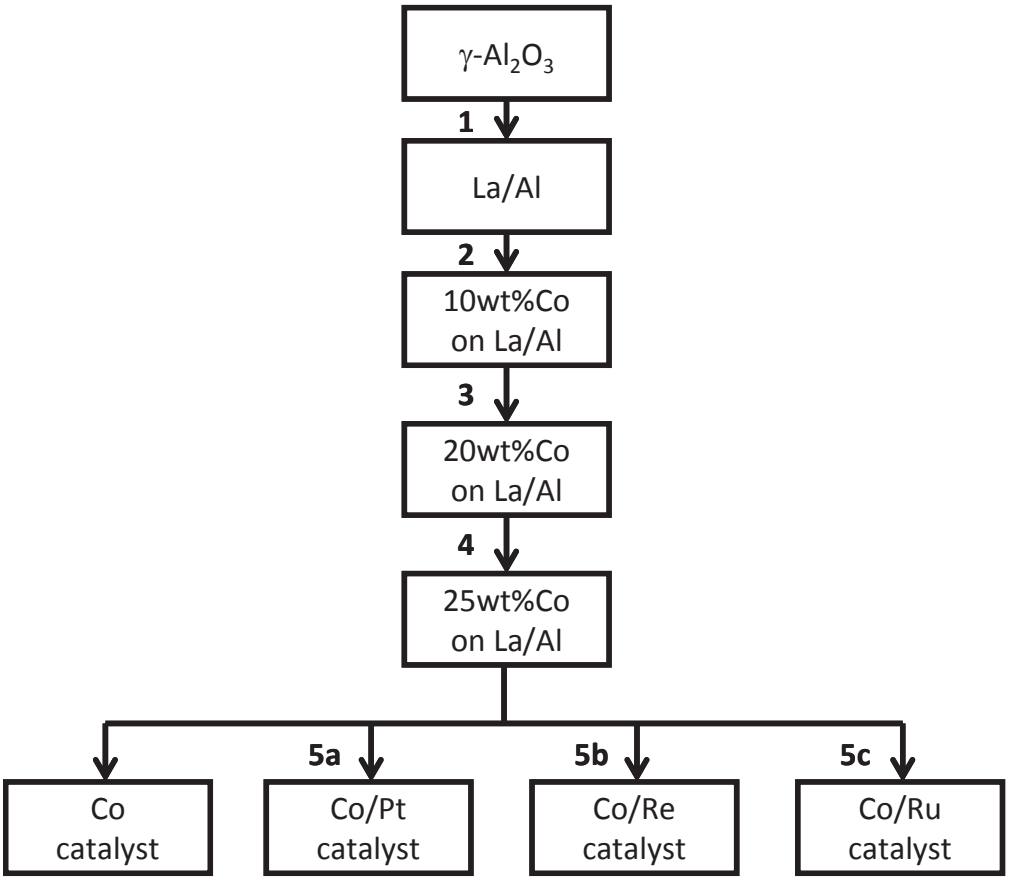

Figure 3-1. Schematic representation for the preparation of the unpromoted and sequentially deposited catalysts

Since the pH of the solution was lower than the PZC (Pinna 1998), the negatively charged La-EDTA complex strongly interacted with the positively charged oxide surface of the γ-Al_2O_3, Figure 2-5. The La-EDTA solution was poured onto buffer-submerged Al_2O_3 pellets and rotated in a rotary evaporator for 3-4 h after which the solution was poured off, and the pellets were washed and stirred in excess HPLC grade water for 30 minutes. This washing was repeated twice and then the pellets were dried under vacuum while rotating and heating first at 55°C for 4 h and then at 90^{o}C for 2 h. Next, the pellets were dried further and calcined in a quartz reactor in flowing air based on the following temperature-time profile designed from temperature-programmed oxidation (TPO) to maintain a low partial pressure of water, thus preventing

sintering: the sample was heated in air flowing 30 cm^3/g/min to (1) 100°C at 0.5°C·min^{-1} and held at 100°C for 1 h; (2) 120°C at 1°C·min^{-1} and held for 16 h; and (3) 700°C at 1°C·min^{-1} and held for 8 h.

3.1.2 Co/NM Deposition

For Steps 2, 3, and 4, Co was added to the support in three consecutive wet impregnation steps to obtain nominal Co loadings of 10, 20, and 25 wt% (calculated for the reduced catalyst) on the calcined La-stabilized support (La/Al). For the deposition solution, the amount of Co nitrate ($Co(NO_3)_2.6H_2O$, J. T. Baker 99.1%) to obtain those nominal loadings was dissolved in a volume of HPLC grade water corresponding to10% above incipient wetness. This solution was added to the catalyst pellets at 25°C and rotated in a rotary evaporator at 30 rpm for 10 h. This rotation without drying was optimized experimentally to give uniform Co deposition. The solvent was next removed slowly by evaporation at 55°C for 12 h—until the catalyst pellets appeared dry. After each deposition step, samples were further dried and calcined based on the following temperature-time profile established from TPO: the sample was heated in air flowing at 30 cm^3/g/min to (1) 100°C at 0.5°C·min^{-1} and held at 100°C for 2 h; (2) 120°C at 1°C·min^{-1} and held for 4 h; and (3) 250°C at 1°C·min^{-1} and held for 6 h.

After calcination of the 25 wt% Co catalyst from Step 4, the catalyst was split into four separate samples. In Step 5, NM promoter was added by a wet impregnation/evaporation technique similar to the Co addition using an aqueous solution containing the chloride salt of Pt (5a), Re (5b), or Ru (5c) to three samples targeting NM loadings of 0.3-0.6 wt% (a NM/Co molar ratio of 0.007); no promoter was added to the fourth sample. Each NM promoted sample was placed in the rotary evaporator for deposition, rotation, and drying using essentially the same method described for addition of Co to La/Al including the additional drying and calcination at

120°C and 250°C in a quartz reactor flow system. All catalysts were reduced in 10% flowing H_2 while heating to (1) 140°C at 1°C·min^{-1} and holding for 2 h; (2) 250°C at 0.5°C·min^{-1} and holding for 2 h; and (3) 360°C at 0.5°C·min^{-1} and holding for 6 h. The H_2 concentration was then increased to 100% and the sample was reduced at 360°C for an additional 10 h.

3.2 ICP

Inductively Coupled Plasma (ICP) measurements by a third party (Huffman Laboratories, Inc., Golden, Colorado) were made to determine Co and NM weight loadings in calcined catalyst samples. Duplicate samples of catalyst powder were digested in a mixture of HNO_3 and HCl, evaporated to near dryness, redigested in HNO_3 and HCl and diluted with water to a final matrix optimal for measurement. Co loading was determined by ICP atomic emission spectroscopy. NM loading was determined by ICP mass spectrometry using isotopes at 2 or 3 masses per NM. Reported experimental accuracy was ±10%.

3.3 BET

BET surface area, pore volume, and average pore size were measured by N_2 physisorption at -196°C using a Micromeritics TriStar 3000 automated system. The samples (0.15-0.25 g) were degassed overnight under atmospheric pressure at 120°C. Measurements were taken immediately after degassing. The total pore volume was calculated from the amount of vapor adsorbed at a relative pressure close to unity assuming that the pores are filled with the condensate in the liquid state. The pore size distribution curves were calculated from the desorption branches of the isotherms using the Barrett-Joyner-Halenda (BJH) formula (Barrett 1951).

3.4 TPR

TPR measurements were performed in a Mettler Thermogravimetric Analyzer (TGA)/ Differential Scanning Calorimeter (DSC) 1. Calcined catalysts (~10 mg) were placed in a platinum sample pan and pre-dried for 2 h in a flow of He at 200°C after which samples were cooled to room temperature. Once the weight stabilized, the catalysts were heated in 10% (v/v) H_2 in He from room temperature to 700°C at a heating rate of 3°C·min^{-1} and flowrate of 150 cm^3·min^{-1} (STP). Mass loss with time and derivative scans were obtained; from the latter scan two major peaks were typically observed, the first corresponding to the conversion of $Co_3O_4 \rightarrow CoO$ and the second corresponding to the conversion of $CoO \rightarrow Co$. To verify the assumed stoichiometry, TPR peak areas and ratios were calculated by fitting a modified Wiebull function. For each catalyst the TPR experiment as well as Wiebull function fitting, area, and ratio calculations were repeated.

3.5 Extent of Reduction

The extent of reduction (EOR) of reduced catalyst samples was determined by titration with O_2 in the same TGA in which the TPR spectra were obtained using a method adapted from Reuel and Bartholomew (Reuel and Bartholomew 1984). After 16 h reduction at 360^{o}C, the catalyst cell was purged with He at 340^{o}C (20°C below the reduction temperature), the sample temperature was then increased to 400°C and held for 1 h in flowing O_2. EOR was calculated from the weight gain of the sample which was presumably due to oxidation. It was assumed that during the reduction Co_3O_4 was first converted to CoO following which CoO was partially converted to Co^0. Thus, during oxidation of the reduced catalyst the O_2 uptake included moles required for conversion of fully reduced Co^0 to Co_3O_4 (Eq. 2) and partially reduced CoO to

Co_3O_4 (Eq. 3). This consideration is more comprehensive than most EOR calculations found in the literature. The calculation was done using the EXCEL solver to find the moles remaining as CoO after reduction by minimizing the sum square error between the measured moles of O($n_{O,measured}$) taken up during oxidation and the solved moles of O($n_{O,solved}$) based on the stoichiometry of the two steps involved.

$$3Co^0 + 2O_2 \rightarrow Co_3O_4 \quad (3\text{-}1)$$

$$6CoO + O_2 \rightarrow 2Co_3O_4 \quad (3\text{-}2)$$

The equations used in the calculation of EOR are given below:

$$n_{O,measured} = \frac{m_{cat,oxidized} - m_{cat,reduced}}{MW_O} \quad (3\text{-}3)$$

$$n_{O,solved} = \left(\frac{m_{catCo}}{MW_{Co}} - n_{CoO}\right) \cdot \frac{4}{3} + n_{CoO} \cdot \frac{1}{3} \quad (3\text{-}4)$$

$$EOR = \frac{\frac{m_{catCo}}{MW_{Co}} - n_{CoO}}{\frac{m_{catCo}}{MW_{Co}}} \quad (3\text{-}5)$$

where $m_{cat,oxidized}$ is the mass of catalyst after oxidation, $m_{cat,reduced}$ is the mass of catalyst after reduction, MW_O is the molecular weight of oxygen, m_{catCo} is the mass of Co in the sample (calculated based on ICP measurements), MW_{Co} is the molecular weight of Co, n_{CoO} is the moles of Co in the CoO form after reduction. The 4/3 and 1/3 are stoichiometric ratios (O/Co) for oxidation of Co^o and CoO to Co_3O_4 from Eqns. 2 and 3.

3.6 Hydrogen Uptake

A flow desorption method was used to measure H_2 uptakes in a custom flow system with a thermal conductivity detector (TCD) (see Figure 3-2) by a method adapted from that reported by Jones and Bartholomew (Jones and Bartholomew 1988). A catalyst sample of 0.20-0.40 g was placed in a quartz U-shape microreactor surrounded by a temperature-programmed furnace. The sample was reduced in situ in H_2 according to the same reduction profile described above (Section 3.1). Next, the sample was cooled and held at 340°C (20°C below the maximum reduction temperature) for 30 min while flowing Argon (Ar) to remove all hydrogen (gas phase, physisorbed H_2 and chemisorbed H atoms). H_2 chemisorption was carried out at 100°C while flowing 50% (v/v) H_2 in Ar for 60 min. Such conditions enabled rapid adsorption at near equilibrium, while adsorption at room temperature may require days or weeks to reach equilibrium. After completion of H_2 adsorption, the reactor was cooled using a dry ice/acetone mixture to -84°C, while continuing to flow H_2/Ar. Next, gas-phase H_2 and physisorbed hydrogen were removed with an Ar purge (12 cm^3/min) for 15 min or until the TCD signal returned to the baseline. After purging, H_2 was desorbed while increasing the sample temperature from -84 to 600°C at 20°C/min and measuring the concentration of desorbed H_2 by TCD. The TCD spectrum area was integrated to determine the moles of desorbed H_2 based on a calibration with known quantities of pulsed H_2. This procedure has been shown to accurately measure monolayer concentrations of adsorbed hydrogen: and, based on a known stoichiometry of 1H atom/Co surface atom, the number of Co surface atoms per gram of catalyst (Reuel and Bartholomew 1984; Barthlomew 1990). A diagram of the temperature schedule and steps of the process are shown in Figure 3-3.

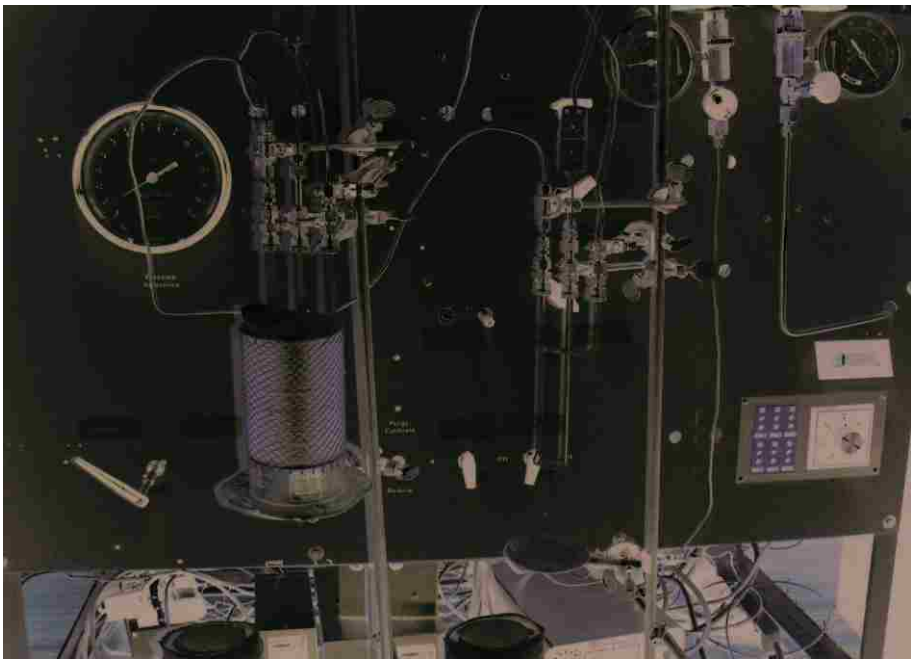

Figure 3-2. Schematic of H_2 chemisorption flow system, furnace, and micro reactor set-up

Co dispersion was calculated for each catalyst from H_2 uptake and EOR data using the following relationship (Barthlomew 1990; Bartholomew and Farrauto 2006):

$$\%D = 1.18\ \chi / EOR / W, \qquad (3\text{-}6)$$

where %D is the percentage dispersion of Co, χ is the H_2 uptake in μmole/g_{cat}, EOR (see Section 3.5) is the fraction of Co reduced to the metal, and W is the weight % of Co in the catalyst. Average Co crystallite diameter can be calculated from %D by the following equation and can be compared with measurements from TEM (Section 3.9):

$$d = \frac{94}{\%D} \qquad (3\text{-}7)$$

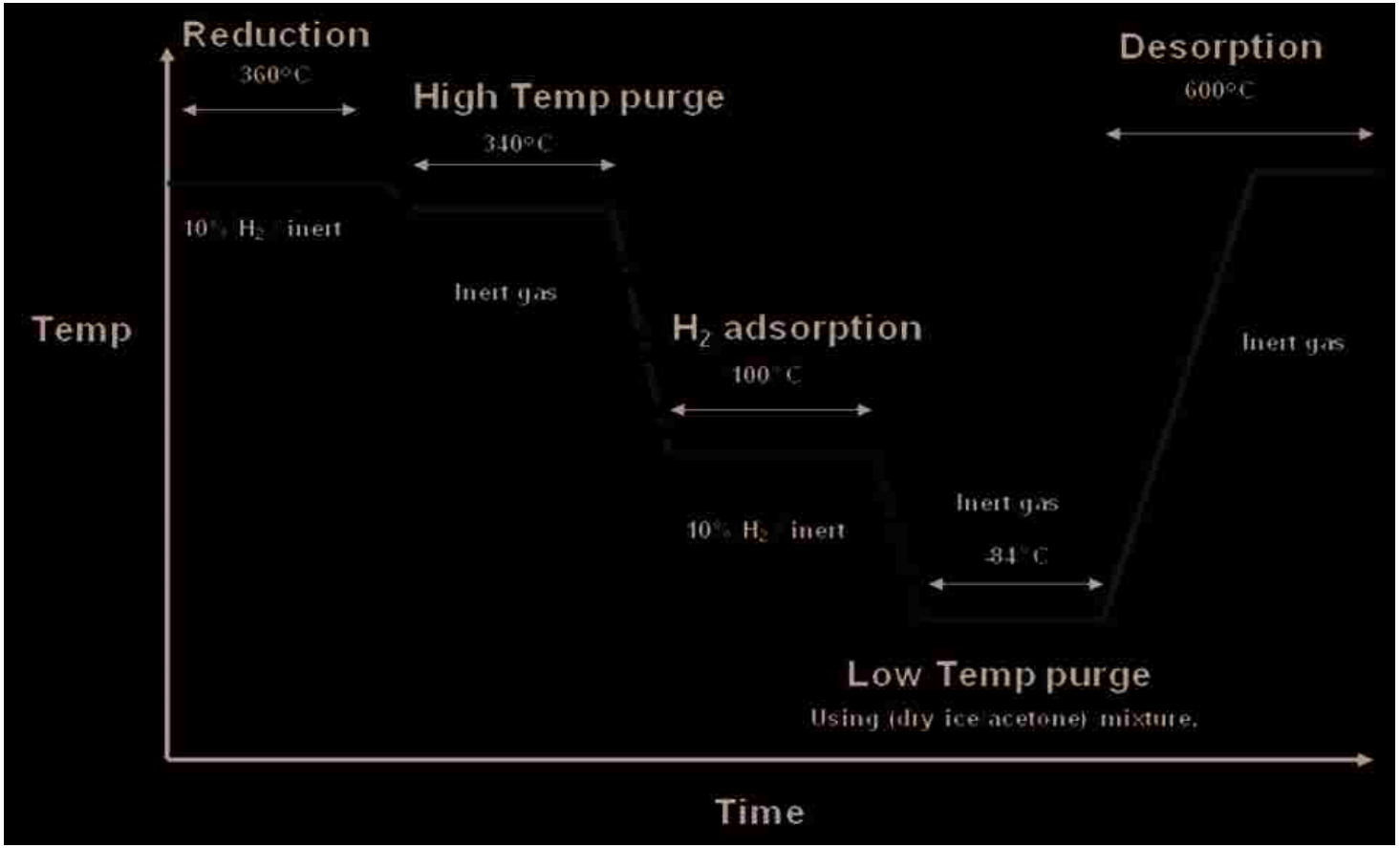

Figure 3-3. Diagram of H_2 chemisorption experiment temperatures and experiment steps

3.7 Microprobe

Microprobe scans of catalyst pellets were obtained to determine the metal distributions across the pellet. Catalyst pellets in the form of Raschig rings were embedded in epoxy resin mounts, allowed to harden, and then polished and coated with a thin layer of carbon to improve conductivity. An example of a prepared sample is shown in Figure 3-4.

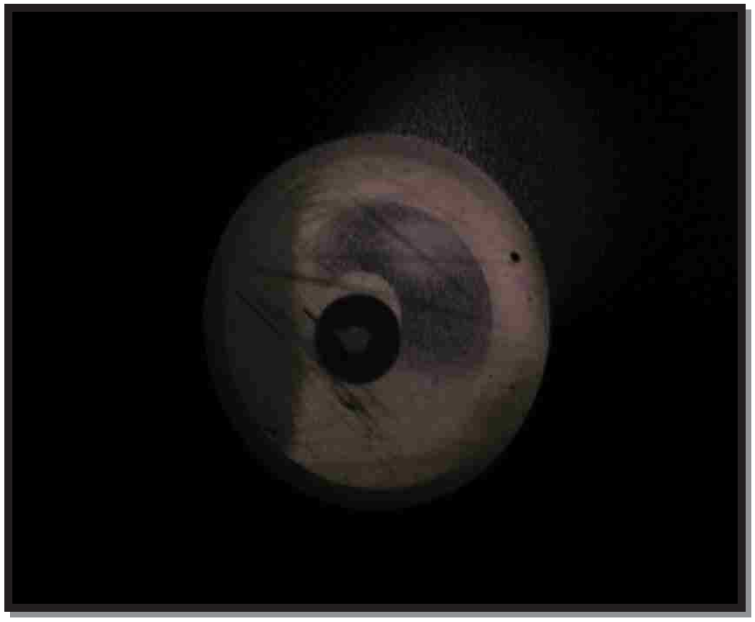

Figure 3-4. Prepared microprobe catalyst sample

A Cameca SX-50 electron microprobe was used to observe the distribution of elements across the catalyst pellet by bombarding the sample with electrons and detecting X-ray wavelengths characteristic of Co, La, Pt, Re, or Ru, using laser induced fluorescence (LIF) and positron emission tomography (PET) detectors. A diagram of this process is shown in Figure 3-5. The elements, detectors, and edges used are shown in Table 3-1.

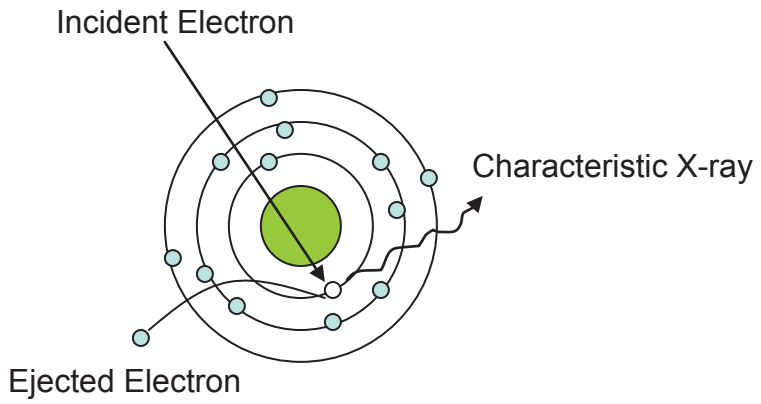

Figure 3-5. Diagram of process used to detected elements using microprobe analysis

Table 3-1. Element detector and edge information for microprobe.

Element	Detector	Edge
Co	LIF	K
La	PET	L
Pt	LIF	L
Re	LIF	L
Ru	PET	L

3.8 Scanning Electron Microscopy

SEM was used to look at the metal distributions with greater resolution. Catalyst pellets as prepared for microprobe (embedded in epoxy, polished, and carbon coated to prevent sample charging) were studied using a Phillips XL30 ESEM FEG. Line scans by x-ray Energy Dispersive Spectrometry (EDS) were performed to see the micron scale metal distribution across the pellet.

3.9 TEM

TEM measurements were made to obtain average crystallite diameter (ACD) and crystallite size distribution (CSD) of Co particles. Calcined and reduced/passivated catalyst samples were examined using an FEI Tecnai F20 TEM operated at 200 kV with a resolution of 0.24 nm. Catalysts were crushed into fine powder and put onto nickel grids. For each catalyst at least 10 TEM images were taken. Several hundred (400^{+}) Co crystallites were measured for each catalyst with Digital Micrograph software where the user identifies the Co particle edges and the software's standard tool uses the microscope calibration to give the particle diameter. The location of Co and Al_2O_3 phases in the samples were determined by EDS using an EDAM3 x-ray analyzer (probe diameter of ~3 nm). Surface mean ACD were calculated from the following equation,

$$d_{surfaceavg} = \frac{\sum_i d_i^3}{\sum_i d_i^2} \tag{3-8}$$

where d_i is measured diameter of each particle and d_{avg} is the surface averaged particle diameter (Mustard and Bartholomew 1981). Volume mean ACD were calculated from,

$$d_{volumeavg} = \frac{\sum_i d_i^4}{\sum_i d_i^3} \tag{3-9}$$

3.10 XAFS

Synchrotron XAFS experiments were performed to determine the oxidation state and bonding of the NMs. Pt L_{III}-edge, Re L_{III} edge, and Ru K-edge XAFS data were collected at Argonne National Laboratory's (Argonne, IL) Advanced Photon Source (APS) on the 10-ID

beamline. Calcined catalysts were crushed to a fine powder and pressed into self-supporting pellets in a stainless-steel sample holder. For reduced state experiments, this stainless-steel sample holder was placed in a quartz reactor and treated at 360°C or 400°C in a 4% (v/v) H_2/He mixture for 1 h, cooled, and purged with He. XAFS spectra analysis using *WinXAS* (Ressler 2008) included pre-edge background removal, adsorption edge normalization, and k^2-weighted Fourier transform data fits with standards and theoretical models to determine the bonding structure.

3.11 Fixed Bed Reactor Activity and Selectivity Tests

The activity and selectivity of each catalyst as a function of temperature, P_{H2}, and P_{CO} were measured in the BYU Catalysis Lab's fixed bed reactor system. Figure 3-6 is a photograph of the system and Figure 3-7 shows a schematic diagram of the experimental set-up. The fixed bed experiments were carried out in parallel stainless steel tubular flow microreactors, 0.6 cm inside diameter and 60 cm long, fitted with a ring to hold a metal mesh support, quartz glass wool, catalyst, and inert diluents material. Reactors were heated using a three-zone furnace with a separate controller for each zone. The catalyst bed consisted of 0.25 g of samples diluted in 2 g of white quartz sand (SiO_4, Sigma-Aldrich -50 +70 Mesh) as inert to avoid hot spots. A test was performed under the reaction conditions but without catalyst from which it was determined that the reactor and quartz sand had no activity. Prior to catalytic experiments, the samples were reduced *in-situ* according to the profile described in Section 3.1.2. The reactor was then cooled to the initial reaction temperature under He and H_2 flow. Catalytic behavior was studied at a total pressure of 21.5 bar with H_2/CO ratio of 4 (volume ratio) in the temperature range of 160-230°C. Bed temperature was measured by a type K (chromel-alumel) thermocouple placed

vertically in the reactor from the top. In the experiments a total flow (He, H_2 and CO/Ar) of approximately 60 $cm^3 \cdot min^{-1}$ was used, giving a GHSV (based on volume of catalyst) at STP of 10,000 h^{-1}. This flow was sufficient to keep the reactor operating in differential mode (conversion < 25%). These conditions are summarized in Table 3-2.

Table 3-2. Summary of typical reaction conditions

	Typical Reactor Condition
W_{cat}	0.25 g
F_{CO}	15.5 mol/h
T	160-230°C
P_{total}	21.5 bar (313 psi)
P_{H2}	8.7 bar (126 psi)
P_{CO}	2.1 bar (30 psi)
P_{He}	10.5 bar (153 psi)
SV	10000 hr^{-1}
X_{CO}	2-25%

The carbon monoxide cylinder contained 11.8% (v/v) of argon as an internal standard. Helium (49%) was used to minimize temperature gradients inside of the reactor. Inlet-gases were purified using deoxyo and zeolite traps; gas flow rates were regulated by mass flow controllers (Brooks Instruments 5850E series), and mixed in piping preceding reactor inlet. Reactor pressure was regulated by a Grove Valve & Regulator Co. backpressure regulator. Two high pressure condensation traps were placed in series to ensure the complete trapping of the liquid products. Heavier waxy products were collected as liquids in a hot trap at ~120°C, while lighter liquid products, including water, were collected in a cold trap at 0°C. Liquid/wax products were removed after the run from both traps. Non-condensed gases were expanded to 1.034 bar and analyzed online by gas chromatography using an Agilent 6890N. CO, CO_2, CH_4,

and H_2 gases were separated using a carbon supported, matrix 60/80 Carboxen-1000 stainless steel column (Supelco) and detected with a TCD.

Reported catalytic performance parameters were obtained after the catalyst had been stabilized—typically after about 50 h of operation at each temperature based on the criterion that the standard deviation of the GC CO and H_2 areas had stabilized to less than 10% of their average area for at least 6 h. Data were collected starting at low temperature and as temperature was increased stepwise until the conversion was above 25% for both reactors. In some cases data above 25% were collected for the more active of the two catalysts tested while waiting for the less active catalyst in one of the two reactors to reach 25% conversion. Data obtained above 25% conversion were reported for completeness, but these data were not used in the calculations of differential rates. The conversion, selectivity, and the turnover frequency (TOF) value in the Fischer-Tropsch synthesis were calculated using the equations that follow:

CO and H_2 fractional conversions:

$$X_{CO} = 1 - \frac{(CO/Ar)_{product}}{(CO/Ar)_{feed}} \tag{3-10}$$

$$X_{H_2} = 1 - \frac{(H_2/Ar)_{product}}{(H_2/Ar)_{feed}} \tag{3-11}$$

CH_4 Selectivity:

$$S_{CH_4} = \frac{100(CH_4/Ar)_{product}}{(CO/Ar)_{feed} X_{CO}} \tag{3-12}$$

Rates per gram catalysts

$$-r'_{CO} = \frac{X_{CO} * F^{o}_{CO}}{W_{cat}} \ , \tag{3-13}$$

Turn Over Frequency

$$TOF = \frac{-r'_{CO}}{2 * \chi} \ , \tag{3-14}$$

The k values for all rate data were calculated based on the power law expression reported by Ribeiro et al. (Ribeiro 1997):

$$-r'_{CO} = k * P^{0.7}_{H2} * P^{-0.2}_{CO} , \tag{3-15}$$

such that

$$k = \frac{-r'_{CO}}{P^{0.7}_{H2} * P^{-0.2}_{CO}} , \tag{3-16}$$

where P_{H2} is the average H_2 partial pressure and P_{CO} is the average CO partial pressure. The activation energy (E_A) was determined by Wolfram Mathematica's nonlinear regression of the k values based on the typical Arrhenius equation:

$$k = A * \exp(-E_A / R_g * T) , \tag{3-17}$$

where A (pre-exponential factor) and E_A are the parameters for the fit, R_g is the gas constant, and T is temperature in Kelvin. Linearized plots of log(k) vs. 1/T were also fit for comparison with the more traditional approach.

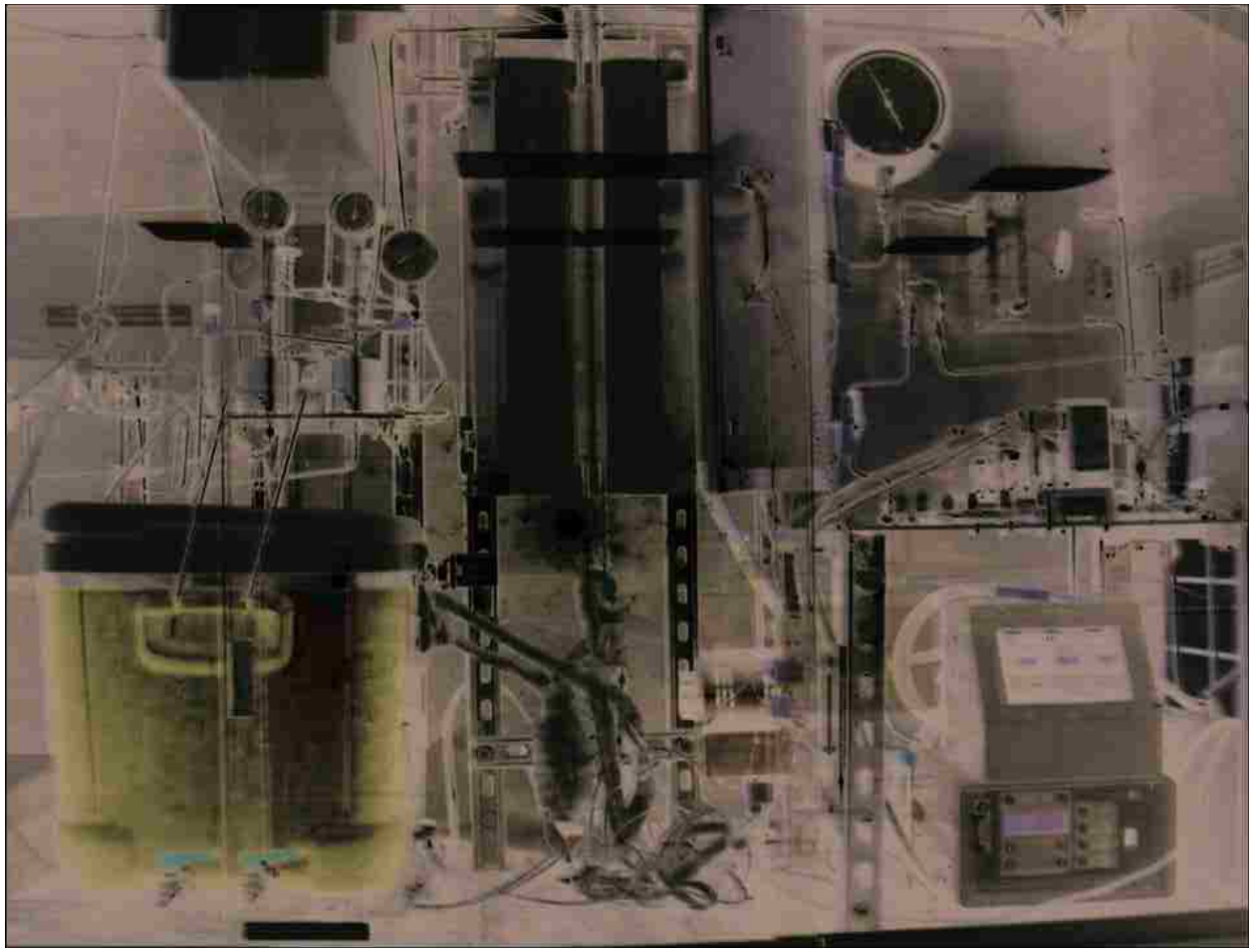

Figure 3-6: Photo of fixed bed reactor

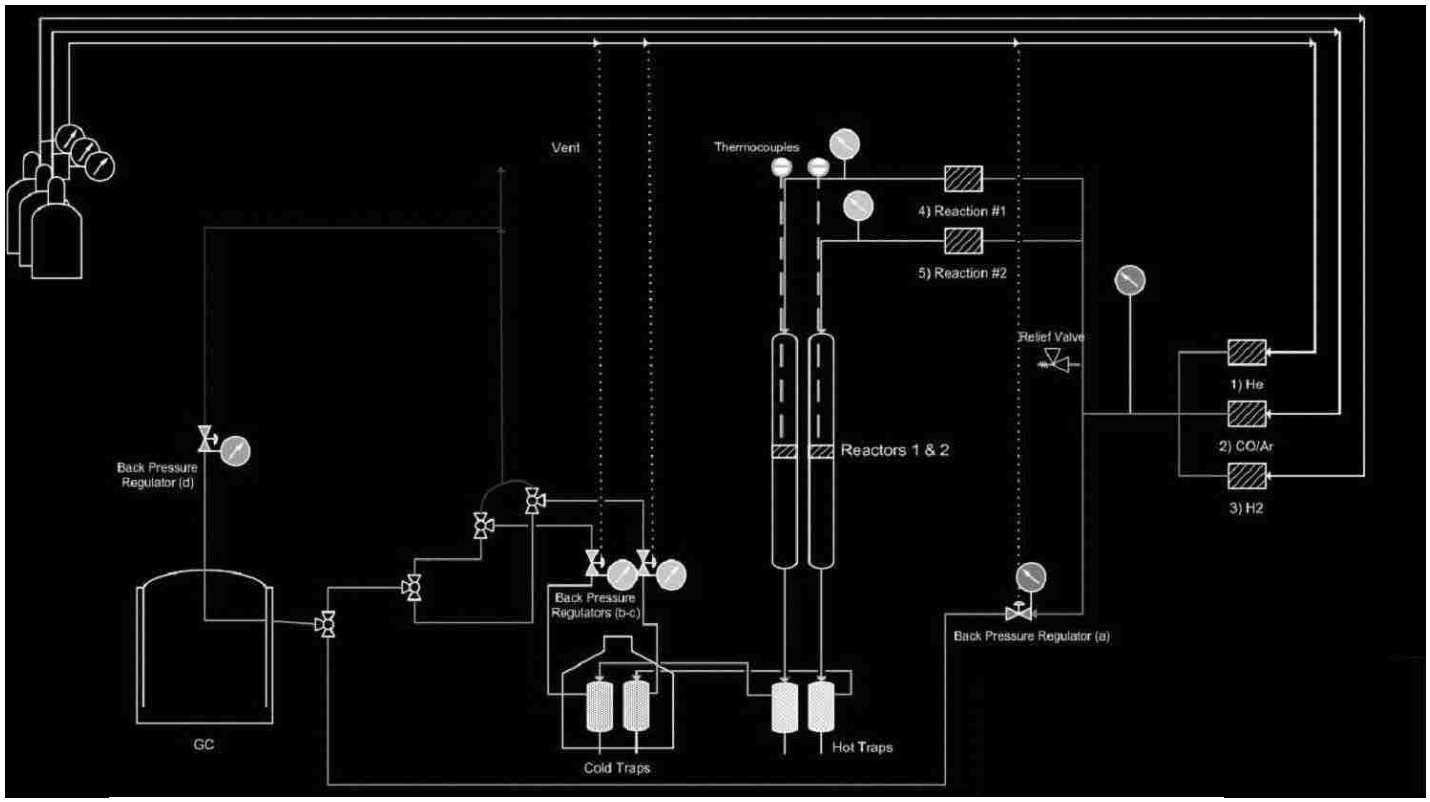

Figure 3-7: Schematic diagram of experimental set-up of the fixed bed reactor.

4 Effect of NM Addition

In order to understand effects of NM addition on physicochemical and catalytic properties, either Pt, Re, or Ru was added sequentially to the La-stabilized alumina supported Co FT catalyst as previously described. A comprehensive characterization of physicochemical, reducibility, and activity/selectivity properties was carried out for these four catalysts, including (1) BET measurements to determine surface area and pore size, (2) measurements by electron microprobe and scanning electron microscope (SEM) to determine spatial distribution of Co and NMs; (3) inductively coupled plasma (ICP)-atomic emission spectroscopy and mass spectroscopy to determine metal retention; (4) XAFS studies of Pt, Re, and Ru edges to observe the chemical state and bonding of NM atoms; and (5) transmission electron microscope (TEM) measurements of crystallite size of Co (oxide and metal) particles. Influences of these five factors on reducibility were investigated through the comparison of results from temperature programmed reduction (TPR), H_2 chemisorption, and extent of reduction (EOR) by O_2 titration measurements. The performance of the catalysts for FTS was evaluated by fixed bed experiments.

4.1 Physicochemical Properties

4.1.1 Surface Area and Pore Size

The ideal range of physical properties for Co FT catalysts was discussed on page 6 and of these properties surface area, pore volume, and pore diameter were measured by BET methods. Calcined catalyst surface areas ranged from 92-103 m^2/g. Pore volume and diameter also showed only minor variations with NM addition, i.e. 0.38-0.43 cm^3/g and 14.3-15.6 nm respectively. These results are consistent with the literature which shows that surface area, pore radius, and pore volume do not generally change with NM promotion (Jacobs, Das et al. 2002).

Table 4-1. BET measurements of surface area, pore volume, and pore diameter for calcined catalysts

Catalyst	Surface Area (m^2/g) ±5	Pore Volume (cm^3/g) ± 0.01	Pore Diameter (nm) ± 0.5
Co	103	0.43	15.0
Co/Pt-seq	98	0.40	15.2
Co/Re-seq	100	0.40	14.3
Co/Ru-seq	92	0.38	15.6

4.1.2 Co and Promoter Retention

Co and NM loadings were measured for duplicate samples of each calcined catalyst by ICP; the average concentrations for each catalyst are shown in Table 4-2. Co loadings ranging from 19.6 to 22.2 wt% are statistically the same as the target loading of 22.8 wt%. Pt and Re loadings were also within experimental error of the intended values, but the measured Ru concentration of

0.13 wt% indicates a statistically significant loss (54% of the targeted deposition quantity) during preparation.

Table 4-2. ICP measurements of Cobalt and noble metal loadings of calcined catalysts

Catalyst	Co wt% (nominal)[a]	Co wt% (actual)	NM wt% (nominal)[a]	NM wt% (actual)
Co	22.8	19.6	-	-
Co/Pt-seq	22.8	20.2	0.53	0.47
Co/Re-seq	22.8	21.0	0.50	0.64
Co/Ru-seq	22.8	22.2	0.27	0.13

a. For calcined catalysts, corresponding to 25 wt% Co and 0.007 NM/Co molar ratio of a fully reduced state.

4.1.3 Spatial Distribution of Co, La, and NMs

Electron microprobe wavelength dispersive X-ray spectroscopy scans of the La, Co, and NM distributions were conducted at different locations across representative pellets of each catalyst. The resulting images are shown in Figure 4-1. Spatially uniform concentrations of Co were observed qualitatively over a scale of several hundred microns in all four samples. Spatially uniform La concentrations were also observed for Co, Co/Pt, and Co/Re catalysts as well as the La/Al support. In the case of the Co/Ru catalyst, La was concentrated at the pellet edge. Additionally, Ru was similarly concentrated largely at the pellet edge.

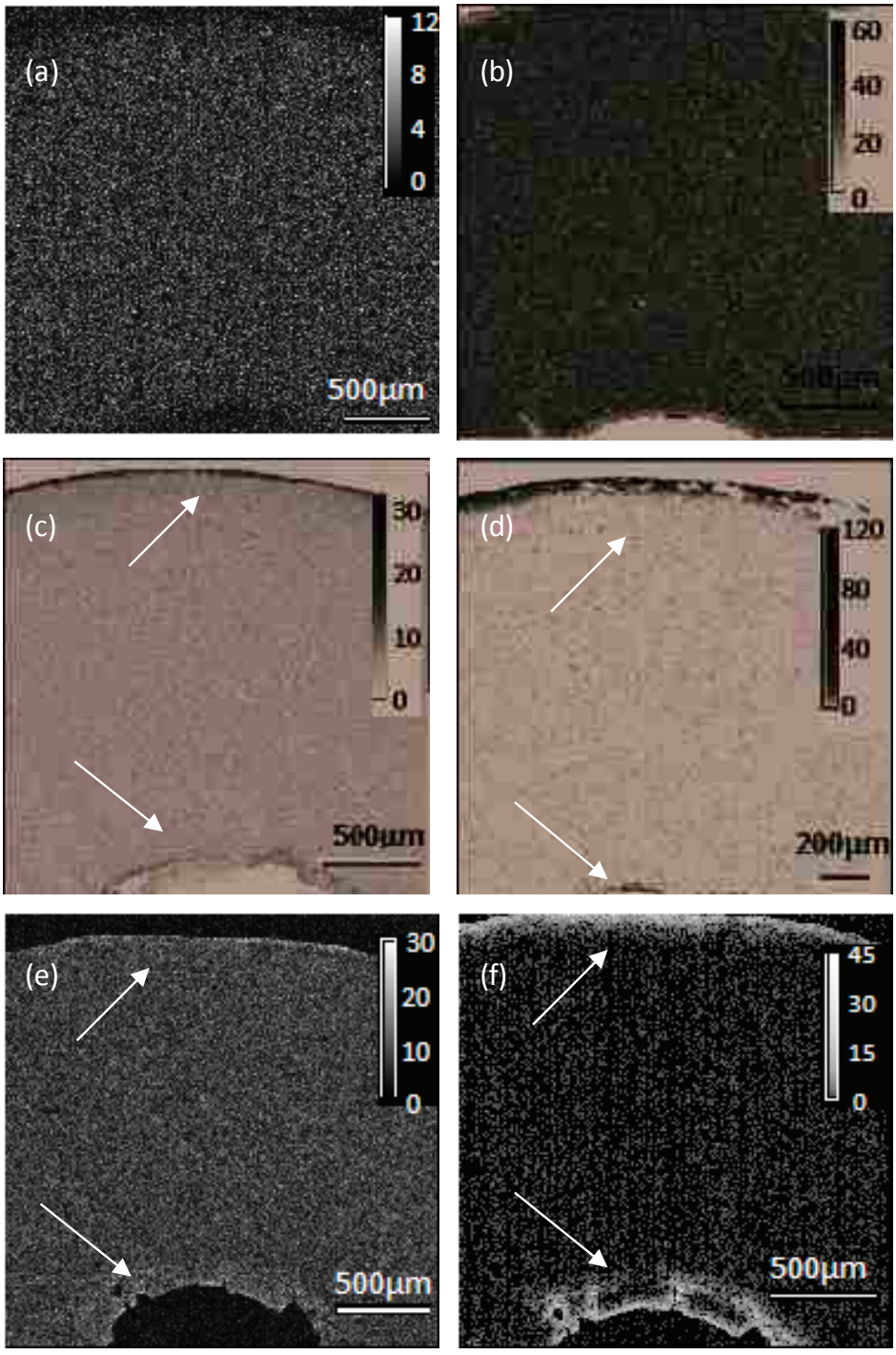

Figure 4-1. Microprobe images of metal distribution across representative catalyst pellets (a) La distribution for La stabilized support, representative also of calcined Co, Co/Pt-seq and Co/Re-seq catalysts after final calcination; (b) Co distribution for Co catalyst, representative of all four catalysts after final calcination; (c) La distribution for Co/Ru-seq catalysts after final calcination; (d) Ru distribution for Co/Ru-seq catalysts after final calcination; (e) La distribution for Co/Ru-seq catalysts after reduction; (f) Ru distribution for Co/Ru-seq catalysts after reduction

SEM was also used to investigate the metal distributions. Figure 4-2 shows an SEM analysis and image of Co/Ru. The edge portion of Co/Ru embedded in the epoxy resin was analyzed using SEM-EDS. Qualitatively there is a brighter edge (due to La and Ru concentration) in the sample.

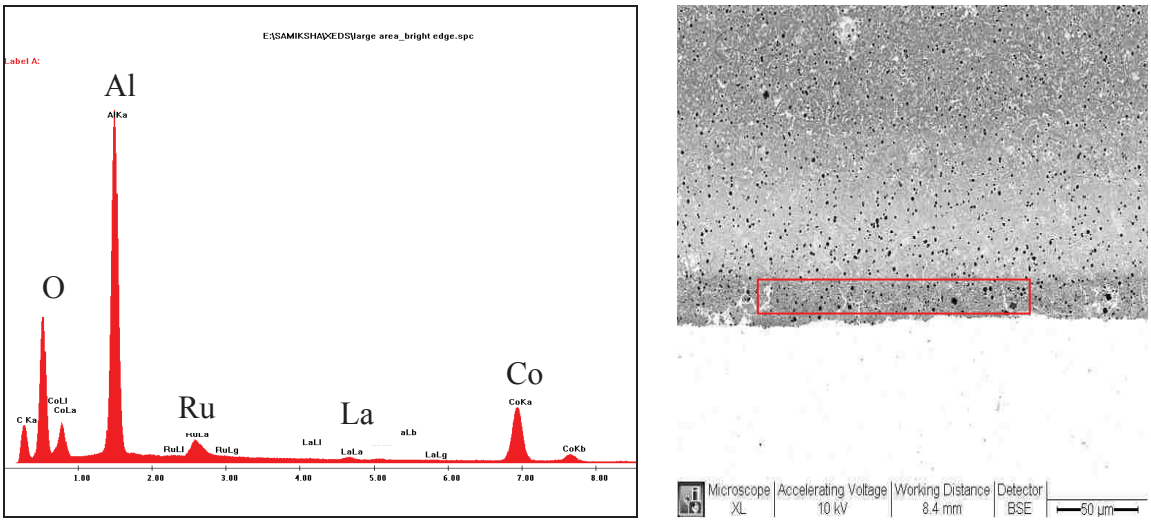

Figure 4-2. EDS Spectrum of analysis of large grey area at the edge portion of the Co/Ru-seq catalyst

The red boxed area of Figure 4-2 was analyzed by EDS and both Ru and La were detected (note: the heights of the peaks are indicative of concentration, but are also proportional to the weight of the element). EDS focused on a grey area (Figure 4-3) and on a bright spot (Figure 4-4) allowed for understanding of what elements were present in the center of the pellet. EDS of the grey area without a bright spot, Figure 4-3, shows high Al and O concentration and very little Co. EDS of the bright spot, Figure 4-4, shows a higher concentration of Co and O—probably the presence of Co_3O_4. In neither analyses (Figure 4-3 nor Figure 4-4) was Ru or La detected, which allows SEM to confirm the microprobe finding of higher La and Ru

concentration at the pellet edge. This undetectability was not because of a smaller area as confirmed by Figure 4-5—when a larger area was analyzed, but still no La or Ru was detected.

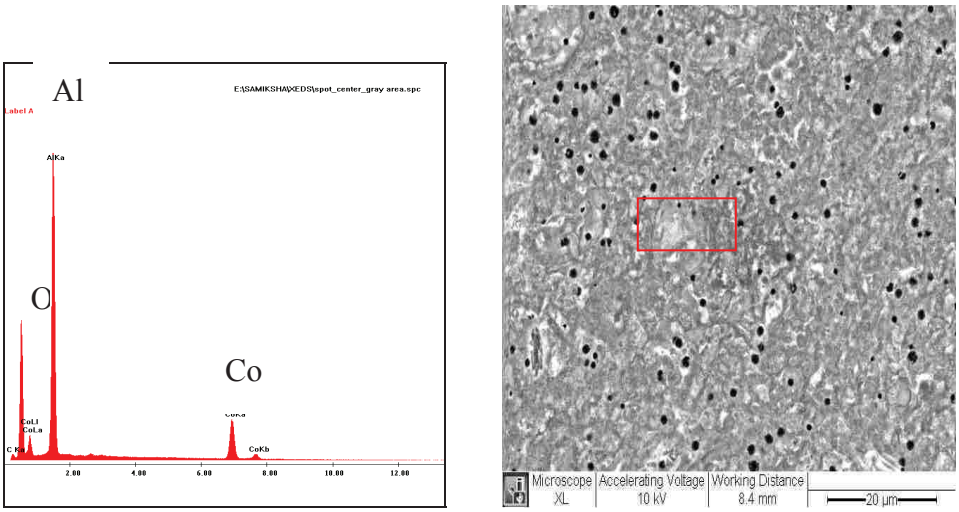

Figure 4-3. EDS Spectrum of analysis of central grey area (without white spot) of the Co/Ru-seq catalyst

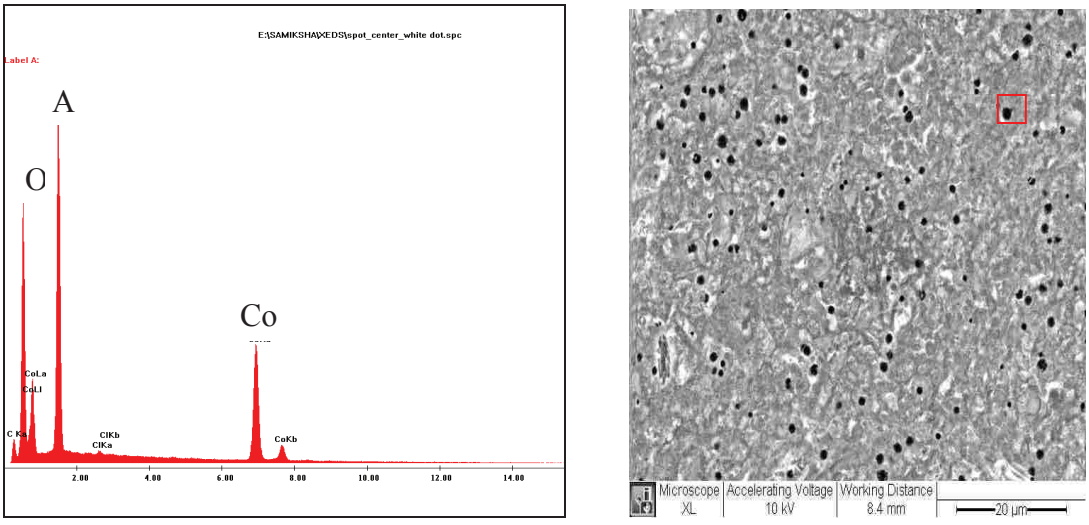

Figure 4-4. EDS Spectrum of analysis of bright spot at the center of the Co/Ru-seq catalyst

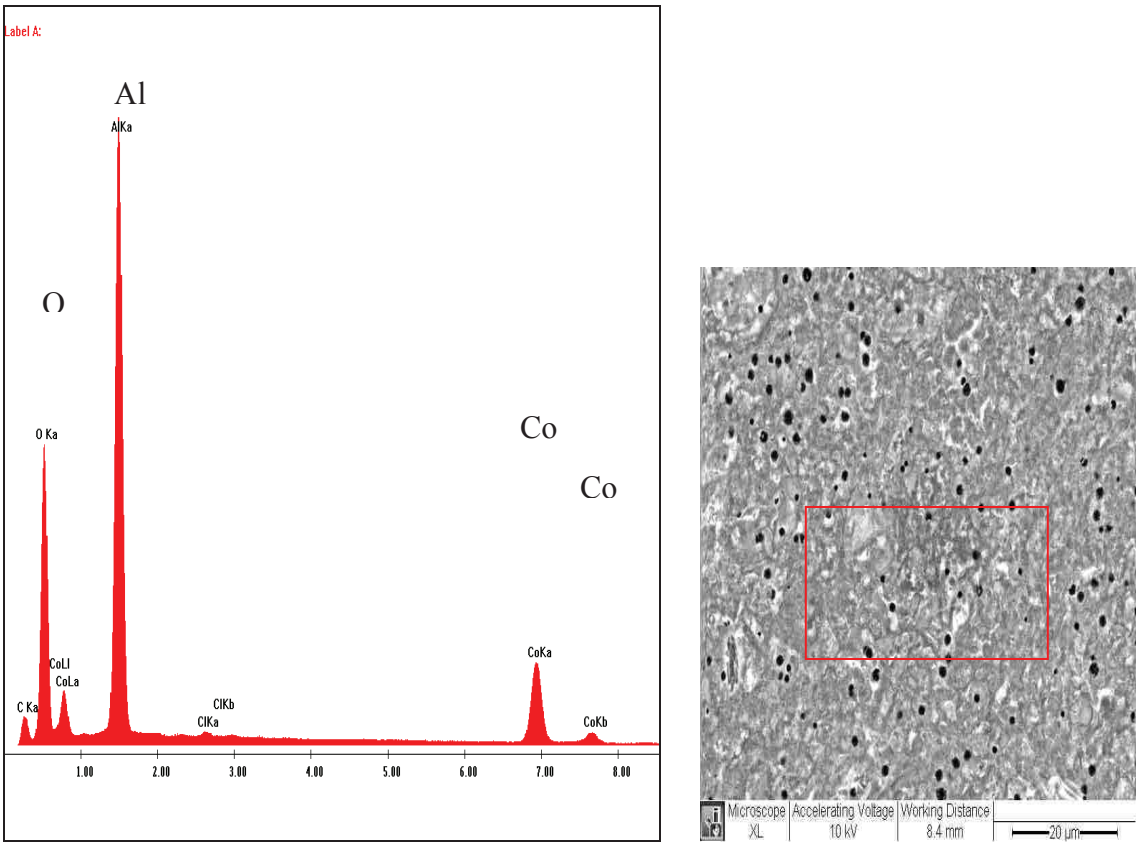

Figure 4-5. EDS Spectrum of the analysis of large area at the central portion of the Co/Ru-seq catalysts

Figure 4-6 shows an SEM image of the Co/Ru pellet focused on the surface edge. The red arrow is the line along which EDS was collected to study the Ru distribution, Figure 4-7. The data confirmed a substantially higher concentration at the pellet edge. While the concentration across the largest part of the pellet radius is much lower than at the edge, it is nearly constant and significant.

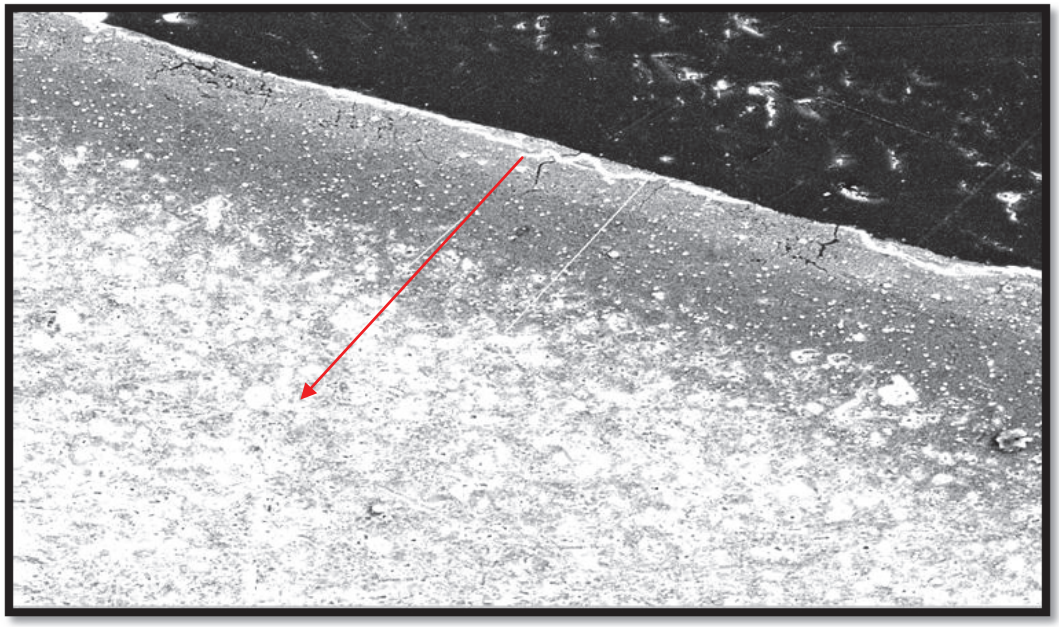

Figure 4-6. Co/Ru-seq pellet image from SEM with red arrow distinguishing where EDS line scan was performed

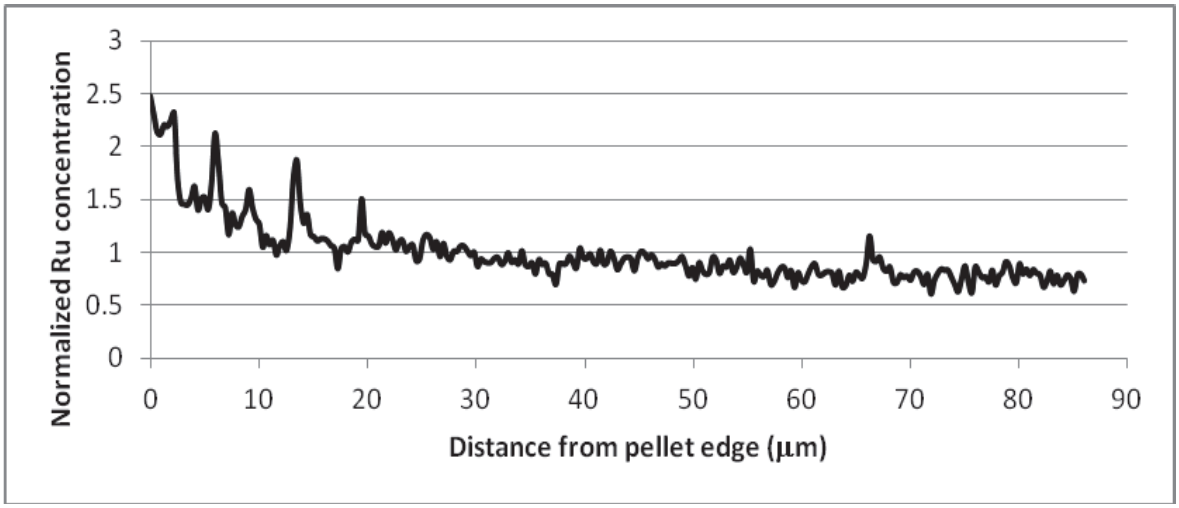

Figure 4-7. Normalized Ru concentration as a function of distance from edge of Co/Ru-seq catalyst pellet showing higher concentrations at pellet edge

4.1.4 Co Crystallite Size Distribution and Average Size

At least 10 transmission electron micrographs of each catalyst were taken both after final calcination and after 16 h reduction at 360°C followed by passivation. Representative micrographs are shown in Figure 4-8. Crystallite size distributions (CSDs) and average Co crystallite diameters (ACD) were determined from analysis of the TEM data and are summarized in Table 4-3 with histograms of diameter versus frequency in Figure 4-9. Both surface and volume mean ACDs of Co_3O_4 crystallites for the four calcined catalysts (Table 4-3) decrease as Co/Ru>Co/Pt>Co>Co/Re. After reduction the ACD of the Co/Ru catalyst decreased, while that of Co/Re increased.

Table 4-3. Average Co crystallite diameters (ACD) after calcination, and average diameters and distributions (CSD) after reduction determined from TEM images for the four catalysts of this study

	Calcined State		Reduced State[c]				
Catalyst	Surface ACD[a] (nm)	Volume ACD[b] (nm)	Surface ACD[a] (nm)	Volume ACD[b] (nm)	%<6 nm	%6-12 nm	%>12 nm
Co	5.1±1.2	5.6	4.7±1.5	5.7	83	17	0
Co/Pt-seq	9.2±2.8	10.7	8.0±2.2	8.8	29	69	2
Co/Re-seq	3.8±1.0	4.3	4.9±1.6	5.4	95	5	0
Co/Ru-seq	11.2±3.6	13.3	6.7±1.8	7.2	49	51	0

a. Surface ACD calculated from $d_{surfaceavg} = \frac{\sum_i d_i^3}{\sum_i d_i^2}$ **(3-8)**.

b. Volume ACD calculated from $d_{volumeavg} = \frac{\sum_i d_i^4}{\sum_i d_i^3}$ (3-9)

c. Extents of reduction to metallic Co range from 42% (Co) to 91% (Co/Pt) as shown in Table 4-6 after reduction at 360°C for 16 hr.

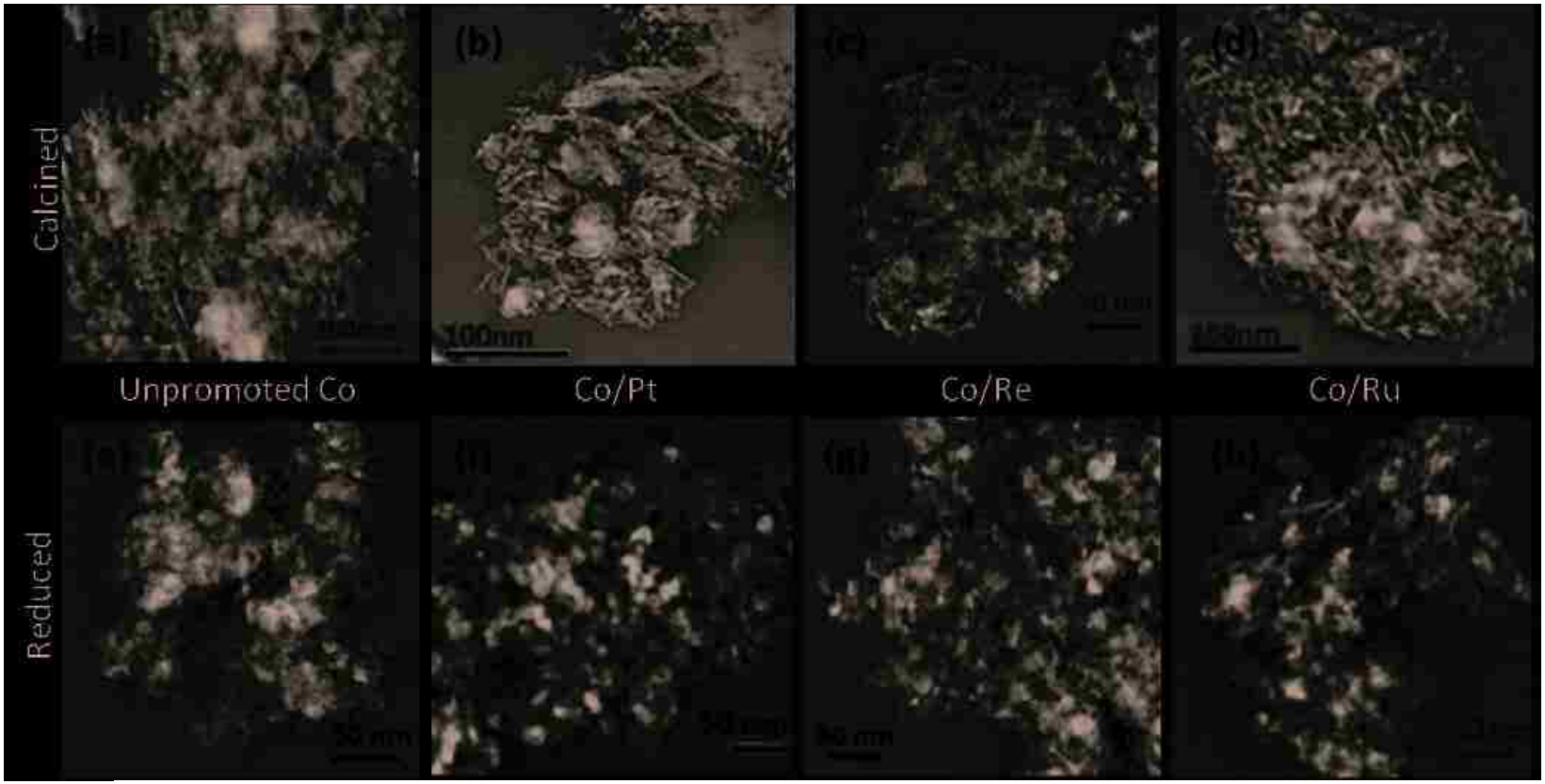

Figure 4-8. Representative transmission electron micrographs of the four catalysts in the calcined state (a) unpromoted Co, (b) Co/Pt-seq, (c) Co/Re-seq, and (d) Co/Ru-seq and their reduced state for (e) unpromoted Co, (f) Co/Pt-seq, (g) Co/Re-seq, and (h) Co/Ru-seq

Crystallite size distributions (CSDs) provide important insights not available from ACD data. Of particular interest are CSD data of reduced catalysts relative to the "ideal range" for Co FT catalysts of 6-12 nm (Borg, Dietzel et al. 2008; den Breejen, Radstake et al. 2009). From the CSD data given in Table 4-3 the majority of Co crystallites for the Co and Co/Re catalyst in the reduced state (83 and 95%, respectively) are smaller than 6 nm. This is a range considered undesirably small, since crystallites having diameters smaller than 6 nm are reportedly less active than those above 6 nm (Barbier, Tuel et al. 2001; Bezemer, van Laak et al. 2004; Bezemer, Bitter et al. 2006; Martinez and Prieto 2007; Borg, Dietzel et al. 2008). By contrast, the percentage of crystallites having diameters in the ideal range (6-12nm) is 69% for Co/Pt and 51% for Co/Ru. It is important to note that not all of the measured Co-containing particles in the reduced/passivated samples are Co metal; for example the percentage of Co reduced to the metal in the unpromoted Co catalyst is only 42%, while the remaining 58% is only partially reduced and likely present as CoO (see Table 4-6 for EOR's of all 4 catalysts). Crystallite size histograms (Figure 4-9) for calcined and reduced forms of the four catalysts show that (1) CSDs are relatively narrow for calcined and reduced forms of Co and Co/Re catalysts and relatively broad for Co/Pt and Co/Ru, and (2) CSDs for Co and Co/Ru are significantly shifted during reduction to smaller diameters, while the distribution for Co/Re shifts to slightly larger diameters and that of Co/Pt crystallites is relatively unchanged.

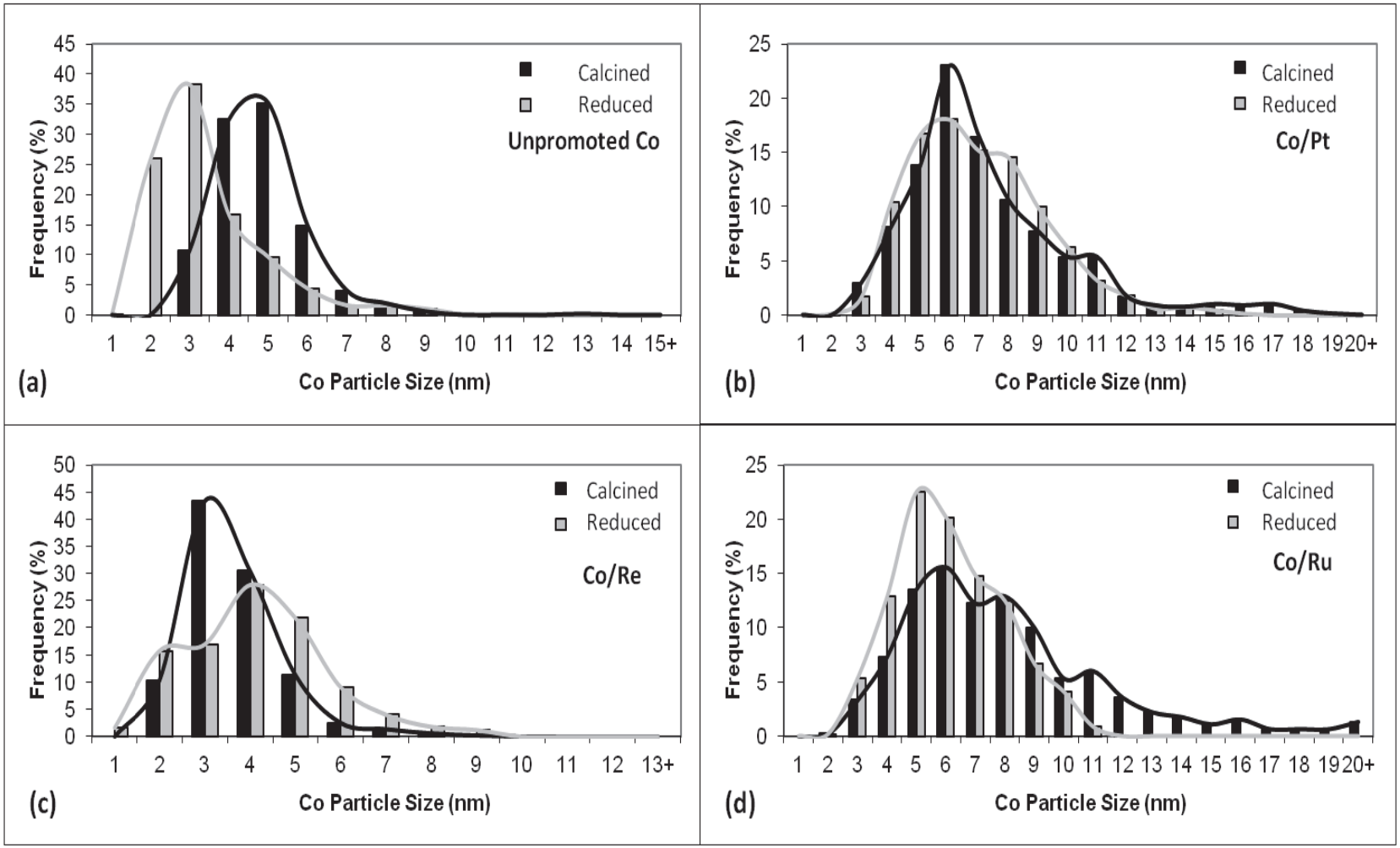

Figure 4-9. Histograms comparing Co crystallite diameter distributions (CSD) of calcined (black) and reduced/passivated (grey) for the (a) Co, (b) Co/Pt-seq, (c) Co/Re-seq, and (d) Co/Ru-seq catalysts

4.1.5 NM Chemical State and Bonding

The chemical state and atomic-scale bonding of Pt, Re, and Ru were investigated by XAFS after final calcination, and after 1 h of H_2 reduction treatment. The amount of Co in each oxidation state (Co_3O_4, CoO, and Co metal) after 1 h reduction at 360°C (and 400°C in the case of Pt) was determined in the TGA by O_2 titration in a separate set of experiments. The findings from both sets of experiments are summarized in Table 4-4. It should be emphasized that after reduction for 1 h at 360°C, the percentage of Co metal formed (EOR) is substantially higher for Co/Pt than for Co/Re or Co/Ru, i.e. 89% compared to 42 and 40% respectively. Note that under these conditions (1 h at 360°C) no Co metal was formed in the Co only catalyst.

Table 4-4. Summary of NM edge XAFS results and corresponding Co reducibility

Catalyst	Treatment[a]	Bonding Atoms	Bond Distance (Å)	Coord No.	% Co_3O_4[b]	%CoO[b]	%Co[b] (EOR)
Co	Calcined	-	-	-	100	-	-
	Reduced 360°C	-	-	-	11	89	-
Co/Pt-seq	Calcined	Pt-O	2.03	2.0	100	-	-
		Pt-Cl	2.31	4.0			
	Reduced 360°C	Pt-Co	2.56	6.1	-	11	89
	Reduced 400°C	Pt-Co	2.55	8.8	-	8	92
Co/Re-seq	Calcined	Re-O	1.76	4.2	100	-	-
	Reduced 360°C	Re-O	1.73	4.1	-	58	42
Co/Ru-seq	Calcined	Ru-O	1.94	6.2	100	-	-
	Reduced 360°C	Ru-Ru	2.66	8.8	-	60	40

a. Reduction at temperature shown for 1 h. b. determined by O_2 titration

Pt L_{III}-edge analysis of the calcined Co/Pt catalyst showed Pt^{4+}, but with some Cl neighbors unlike the standard PtO_2 structure of 6 O atoms at average distance 2.03 Å. XAFS of reduced Co/Pt catalyst showed Pt present as Pt^0. The change in the position of the magnitude and imaginary parts of the Fourier transform of the Pt/Co catalyst compared (Figure 4-10a) with bulk Pt metal indicates fewer bonding neighbors (6.1 vs 12) characteristic of surface Pt and shorter bond distances (2.6 vs 2.7Å). A theoretical model based on metallic bonding of Pt to Co fit the data well (see Figure 4-10b) (Jacobs, Chaney et al. 2004). An additional experiment at higher reduction temperature (400^{o}C) showed the fully reduced Pt atoms were still bonded only to Co, but with higher coordination, 8.8, and a bond distance of 2.55 Å.

The Re in the calcined Co/Re catalyst was found to be present as Re_2O_7 with no evidence of Re-Cl bonds. Reduction at 360^{o}C for 1 h was not sufficient to reduce Re; Re remained as Re_2O_7. Despite not undergoing Re reduction, the Re oxide in the Co/Re catalyst promoted Co reduction, i.e., for the Co/Re catalysts 42% and 58% of the original Co_3O_4 was reduced to Co^0 and CoO respectively; while, for the unpromoted Co catalyst none of the original Co_3O_4 was reduced to Co^o and 89% was reduced to CoO, while the remaining 11% was still present as Co_3O_4 (Table 4-4). This is particularly significant because while the difficulty of reducing Re oxide to the metal has been previously reported, facilitation of Co reduction without significant Re reduction is a new finding.

(a)

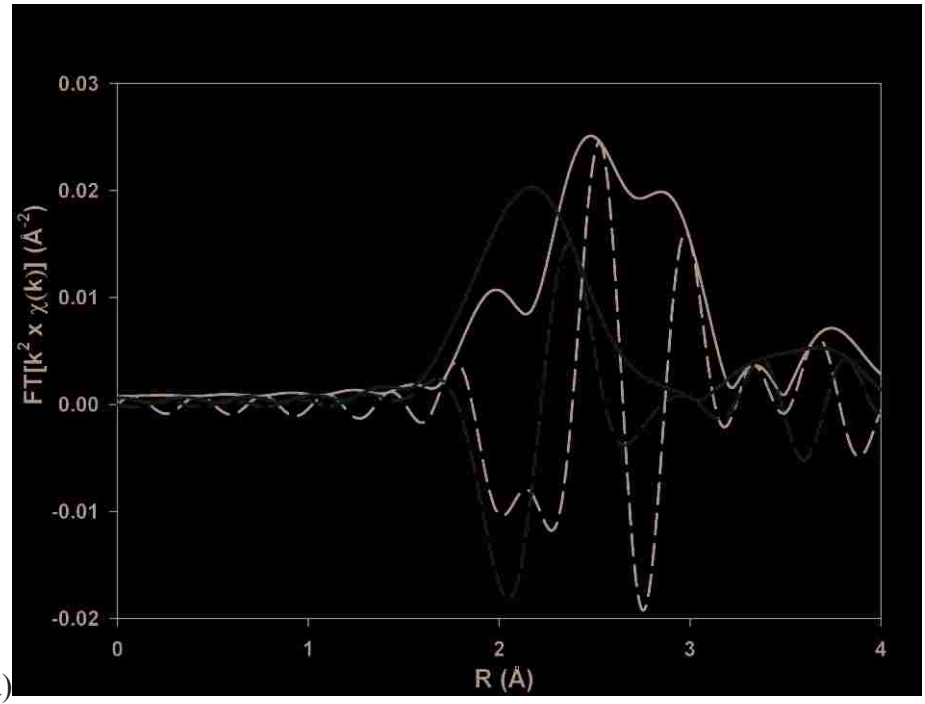

(b)

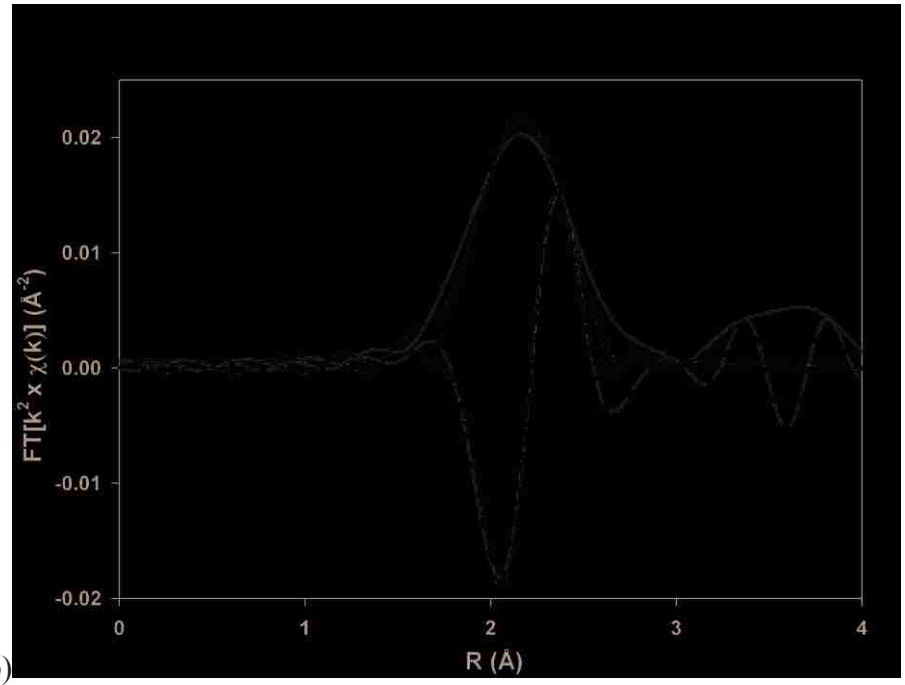

Figure 4-10. Comparison of the Fourier transform of the Pt L_{II} edge for the Pt/Co catalyst reduced at 360°C for 1 h in red: (a) Pt-Pt foil in black; (b) Pt-Co model in blue (k^2: Δk = 2.7-10.5 Å^{-1}: solid-magnitude of the Fourier transform and dotted-imaginary part of the Fourier transform)

XAFS analysis of the calcined Co/Ru catalyst showed that Ru was present as an oxide having a structure nearly identical to the bulk RuO_2 standard structure except for a slightly shorter bond distance (1.94 vs. 2.02 Å). After 1 h reduction at 360°C, RuO_2 was reduced to Ru^0 with a metallic structure also differing from the bulk metal, e.g. a slightly shorter bond distance than the Ru foil standard (i.e. a Ru-Ru bond length of 2.66 Å rather than 2.68 Å) as well as a peak at low R (~ 2 Å), Figure 4-11.

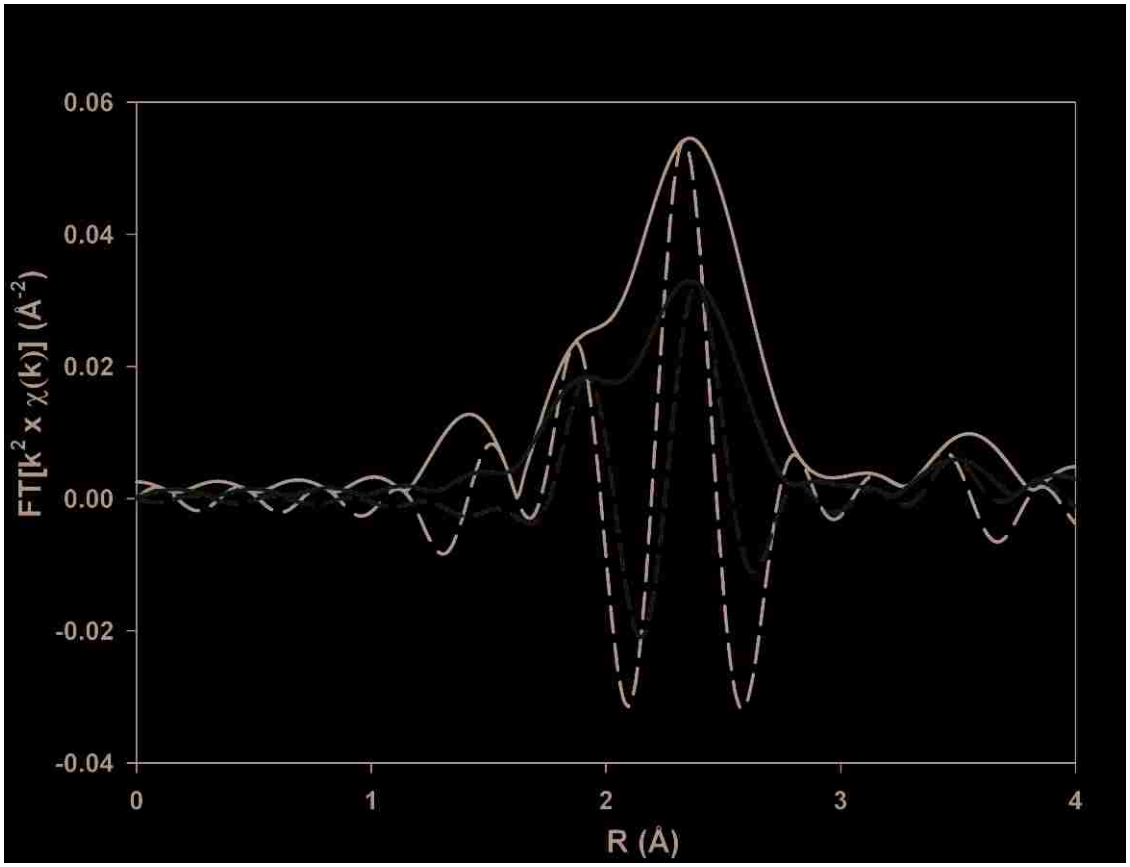

Figure 4-11. Comparison of the Fourier transform of the Ru K edge for the Ru/Co catalyst reduced at 360°C for 1 h in red, Ru-Ru foil in black (k^2: $\Delta k = 2.6 – 11.4$ Å^{-1}; solid-magnitude of the Fourier transform and dotted-imaginary part of the Fourier transform)

4.2 Co Reducibility

Reducibility of each catalyst was evaluated by TPR measurements to determine changes in reduction rate with temperature and peak temperatures of the two important solid-state conversion steps, $Co_3O_4 \rightarrow CoO$ and $CoO \rightarrow Co^0$. EOR by O_2 titration and number of active sites by H_2 chemisorption uptake were also determined.

4.2.1 TPR Profile

TPR derivative profiles (dw/dT, where w = catalyst weight) for each of the four catalysts are shown in Figure 4-12. The profile of all four catalysts includes two principal reduction peaks between 210°C and 700°C. Based on numerous previous TPR studies of supported Co, it is generally accepted that the two principal TPR peaks correspond to the two main steps of the Co reduction process—Co_3O_4 to CoO and CoO to Co metal (Brown, Cooper et al. 1982; Bechara, Balloy et al. 1999; Jacobs, Das et al. 2002). Peak temperatures of these two principal transitions are given for each catalyst in Figure 4-12.

The TPR peak positions for the unpromoted Co catalyst provide baseline reference points for comparing effects of NM promotion and are in excellent agreement with previous studies (Jacobs, Ji et al. 2007). The second peak is located well into the temperature range in which Co sintering rates are high confirming the need for NM promoters.

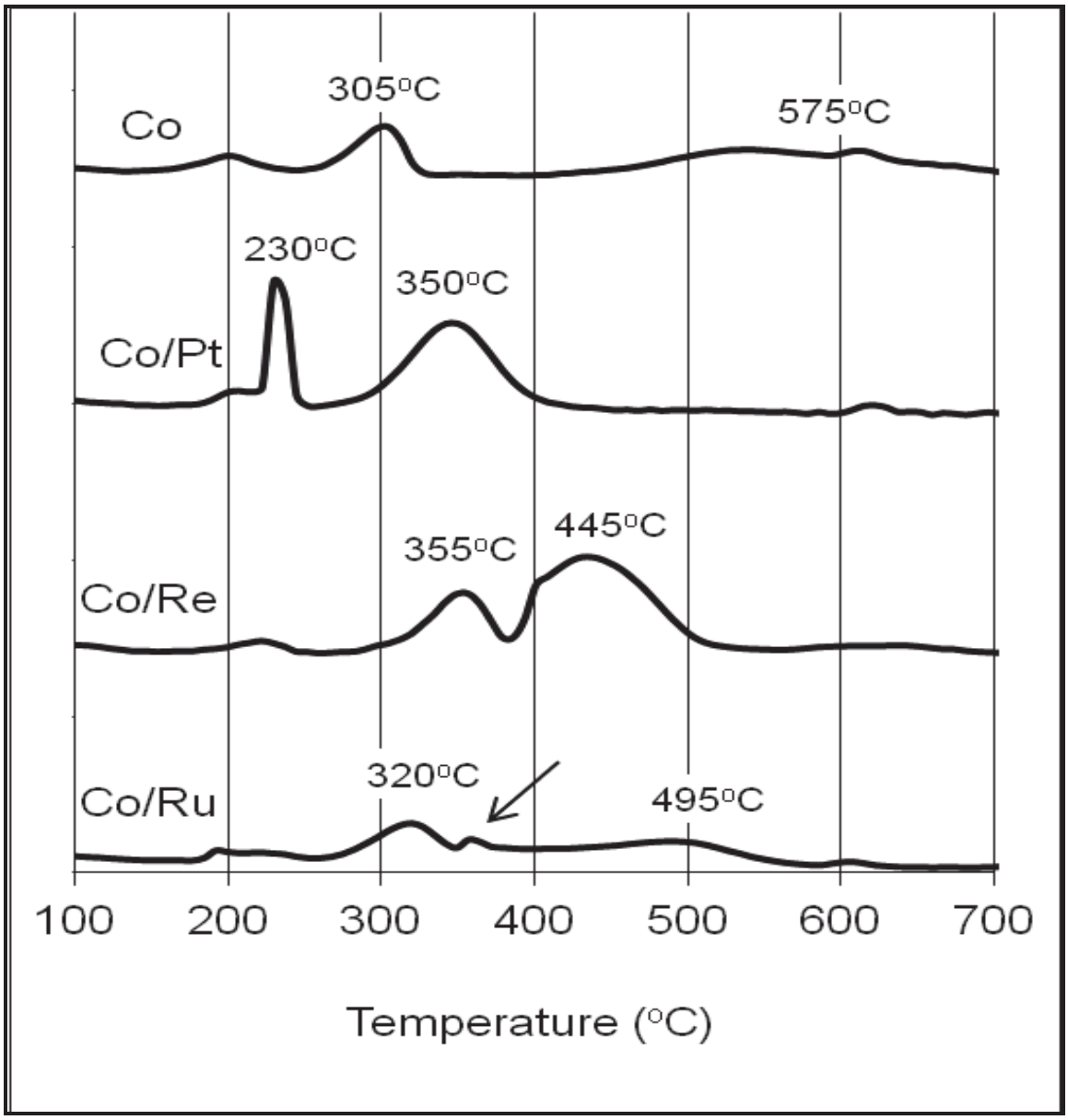

Figure 4-12. Temperature programmed reduction (TPR) derivative profiles

Differences in the TPR profiles indicate differences in NM promotion of Co reduction. The effect of Pt promotion (Figure 4-12) is to substantially shift both peaks to lower temperatures, i.e. Peak 1 is shifted from 305 to 230°C ($\Delta T = 75°C$) and Peak 2 is shifted even more significantly from 575 to 350°C ($\Delta T = 225°C$). These peak shifts are in qualitative agreement with previous

studies (Jacobs, Ji et al. 2007). It should be noted that quantitative differences in peak temperatures observed between this study and previous TPR studies are to be expected as peak temperatures are probably a function of catalyst composition (Co metal loading and NM/Co ratio) and catalyst preparation method. In addition to peak shifts, the widths of both peaks significantly decrease with the addition of Pt. Peak width, especially of the 2nd reduction peak is reported to decrease as the extent of Co interaction with the support decreases and similar narrowing with Pt addition has been seen previously (Jacobs 2004; Jacobs, Ji et al. 2007). It was observed in both this and other previous studies (Hilmen, Schanke et al. 1996; Mauldin and Varnado 2001; Ronning 2001; Jacobs, Chaney et al. 2004) that Re promotion causes a downward shift in temperature of the second reduction step only (CoO→Co); while the temperature of the first peak was increased by 50^{o}C, the downward shift of the second peak is 105^{o}C in this study. The higher temperature for the first reduction peak (355^{o}C rather than 305^{o}C) is more extreme, but qualitatively matches Shannon et al's (Shannon, Lok et al. 2007). Ru addition causes a downward shift of 80^{o}C in peak temperature for the second reduction step to 495^{o}C. It was observed in previous literature that Ru promotion also shifts the first reduction peak (for Co_3O_4→CoO) to lower temperatures (Kogelbauer, Goodwin et al. 1996; Jacobs, Chaney et al. 2004); however, in this study the first main reduction peak was about 15^{o}C higher than for the Co catalyst. Figure 4-12 shows that Ru promotion resulted in a small additional peak at ~350^{o}C (denoted with an arrow), between the two main reduction peaks.

Duplicate TPR runs were carried out for each catalyst from which the average peak areas as well as average and standard deviations of the peak area ratios were determined; these values are summarized in

Table 4-5. The stoichiometry of the reduction process steps ($Co_3O_4 \rightarrow CoO$ and $CoO \rightarrow Co$) predicts a ratio of 1 O atom lost in the second reduction step to 1/3 O atom lost in the first reduction step per Co atom. Thus, the ratio of the area of the second peak to that of the first peak should be 3.0. For both Co and Co/Pt catalysts the area ratio data are within one standard deviation of the proposed model. For Co/Re and Co/Ru, the ratio data, at 2.81 and 3.31, were slightly outside one standard deviation (but still within 10%) and the fits include consideration of bimodal effects as seen in previous studies (Schanke, Vada et al. 1995) and discussed later in this chapter.

Table 4-5. TPR peak areas and area ratios of two main TPR peaks in Figure 4-12; each area represents the average of two TPR experiments

Catalyst	$Co_3O_4 \rightarrow CoO$ Area	$CoO \rightarrow Co$ Area	Area Ratio ±std dev
Co	830	2560	3.08±0.09
Co/Pt-seq	979	2870	2.93±0.10
Co/Re-seq	975	2740	2.81±0.16
Co/Ru-seq	754	2490	3.31±0.24

In summary, of the three NMs studied, Pt is clearly the most effective reduction promoter in terms of larger shifts to lower peak temperatures, the narrow range over which the principal peaks occur, and near completion of reduction by 400^{o}C. The next most effective promoter is Re in view of a large downward shift of Peak 2 and near completion of reduction by 500^{o}C. Ru showed the smallest effect on reduction with reduction occurring over a broad temperature range (similar to the unpromoted Co catalyst) without completion until around 550-600^{o}C. However, it should be noted that while the same molar NM loading was targeted for each catalyst, the actual

Ru loading was significantly lower than the actual Pt and Re loadings and this undoubtedly affected the extent of Ru promotion of Co reducibility. Additionally, the TPR peak areas are consistent with, and offer strong corroborative evidence that the TPR reduction process steps are $Co_3O_4 \rightarrow CoO$ and $CoO \rightarrow Co$.

4.2.2 Extent of Co Reduction and Number of Active Sites

Average extents of reduction (EOR) measured by quantification of the mass gained during reoxidation of each reduced catalyst are listed in Table 4-6 ; the calculations assume oxidation to Co_3O_4 and take into consideration that the reduced state includes both Co and CoO. These EOR data align directly with predictions based on TPR peak temperatures and areas, Co/Pt > Co/Re > Co/Ru > Co. These data also show the significance of NM promotion resulting in 77-91% EOR for the promoted catalysts relative to an EOR of 42% for the unpromoted Co.

H_2 uptakes, Co dispersion, and estimates of Co crystallite diameter for the four catalysts reduced at the same conditions (16 h at 360^{o}C) are also shown in Table 4-6 . The H_2 uptakes were significantly higher for the NM promoted catalysts relative to the unpromoted Co as would be expected based on the substantially higher EORs. The Co dispersion (%D) values ranged from 10 to 20% with a trend of Co ≈ Co/Ru < Co/Pt < Co/Re. A higher dispersion and smaller predicted Co crystallite size for the Co/Re catalyst even when compared to the Co/Pt catalyst are consistent with the TEM measurement of Co crystallite diameter (Table 4-3) in spite of its slightly lower EOR relative to Co/Pt.

Table 4-6. Average values (and standard deviations) of H_2 uptake, extent of reduction (EOR), Co dispersion (D), and Co crystallite diameter (d) for the four catalysts of this study after reduction[a]

Catalyst	H_2 Uptake (μmols/g)	EOR (%)	%D [b]	d (nm) [c] from %D	d (nm)[d] from TEM
Co	65± 4	42± 6.4	9.6± 2.3	10.0±2.2	4.7±1.5
Co/Pt-seq	251± 14	91±11.1	16±3.3	5.9±1.1	8.0±2.2
Co/Re-seq	302± 17	83±5.2	20±2.6	4.6±0.6	4.9±1.6
Co/Ru-seq	150± 9	76±4.8	10±1.3	9.0±1.1	6.7±1.8

a. Reduction at 360°C and 1 atm for 16 hr.
b. See Eqn. 7.
c. d=94/%D
d. surface average

4.3 Activity/Selectivity Properties

The reaction conditions and basic activity/selectivity data (conversion, rate, and methane selectivity) for each catalyst are summarized in Table 4-7. These data were obtained in the fixed bed reactor after quantitative confirmation that the catalysts were at steady state (see Section 3.11) and assuming differential conditions. Each data point (row in Table 4-7) represents the average of at least 6 h of GC measurements.

Rate constant (k) values were determined using $k = \frac{-r'_{CO}}{P_{H2}^{0.7} * P_{CO}^{-0.2}}$, (3-16), for each data point in Table 4-7. The k values for data below 25% conversion were fit two different ways (nonlinear and linear regression) to determine E_A. These k and E_A values are given in Table 4-8. For each catalyst separately, the nonlinear fits (solid curves) are plotted with the data points in

Figure 4-13 and traditional Arrhenius linearized plots of log(k) vs 1/T are given in Figure 4-14. The solid line represents the nonlinear fit and the dashed lines represent the linear fit.

The data (Table 4-8) indicate that NM addition increases the activation energy. The Co and Co/Ru data and fits in Figure 4-14 and corresponding E_A values in Table 4-8 show that the differences between linear and nonlinear regression are sometimes negligible (as is especially the case for Co/Ru where the linear fit is indistinguishable from the nonlinear), but the Co/Pt and especially Co/Re plots show that linear fits weigh the low temperature data more heavily than the nonlinear fits resulting in a poor fit to the higher temperature data and indicating there can be a significant difference in the values obtained by the two regression methods. From the Co/Re catalyst, it is apparent that the nonlinear fit does a better job of aligning with the full data set.

To compare activity and selectivity at a standard set of conditions, the nearest data point to 200°C was normalized to 200°C, P_{CO} 2.1 bar (30 psia) and P_{H2} 9.0 bar (130 psia) for each catalyst. The resulting data are given in Table 4-9. The temperature adjustment was made using the nonlinear E_A values in Table 4-8 and the partial pressure adjustments were made using $-r'_{CO} = k * P_{H2}^{0.7} * P_{CO}^{-0.2}$, (3-15). Conversion is also included in Table 4-9 as an index to indicate which data were used from Table 4-7. The partial pressures were chosen as they are near the actual values (Table 4-7) and require only minor corrections. Surprisingly, the normalized $-r_{CO}$ values show that despite reduction promotion, NMs did not enhance activity on a per gram basis for these seq-dep catalysts. In fact, $-r_{CO}$ values follow the trend Co>Co/Pt>Co/Ru>Co/Re, but are all very close.

Table 4-7. Fixed bed reaction conditions and activity/selectivity data for 4 catalysts

Co only (w_{cat}= 0.258)						
Temp (^oC)	F_{CO} (mmol/hr)[b]	X_{CO}	$-r_{co}$ (mmol/g_{cat}.hr)[c]	P_{CO} avg (psi)	P_{H2} avg (psi)	S_{CH4}
157	15.93	2.2%	1.35	33	138	5.4%
167	15.93	4.0%	2.47	33	138	6.6%
179	15.93	7.2%	4.42	32	137	7.9%
189	15.93	12.5%	7.69	31	136	10.7%
201	15.93	19.9%	12.3	30	135	14.6%
Co only (w_{cat}= 0.253 g)[a]						
184	15.58	5.8%	3.66	32	138	-
204	15.58	18.3%	11.5	31	135	-
Co/Pt-seq (w_{cat} = 0.251 g)						
Temp (^oC)	F_{CO} (mmol/hr)[b]	X_{CO}	$-r_{co}$ (mmol/g_{cat}.hr)[c]	P_{CO} avg (psi)	P_{H2} avg (psi)	S_{CH4}
163	15.45	1.4%	0.83	33	138	12.8%
172	15.45	2.4%	1.46	33	138	13.1%
183	15.45	6.2%	3.8	32	138	12.3%
193	15.45	10.7%	6.57	32	137	17.8%
203	15.45	18.3%	11.27	31	135	21.9%
Co/Re-seq (w_{cat} = 0.251 g)						
Temp (^oC)	F_{CO} (mmol/hr)[b]	X_{CO}	$-r_{co}$ (mmol/g_{cat}.hr)[c]	P_{CO} avg (psi)	P_{H2} avg (psi)	S_{CH4}
159	15.45	0.5%	0.31	33	139	15.2%
169	15.45	1.4%	0.84	33	138	12.9%
179	15.45	3.1%	1.92	33	138	12.0%
189	15.45	6.6%	4.09	32	137	14.3%
200	15.45	12.0%	7.38	32	136	20.7%
209	15.45	18.1%	11.15	31	135	26.0%
Co/Ru-seq (w_{cat} = 0.251 g)						
Temp (^oC)	F_{CO} (mmol/hr)[b]	X_{CO}	$-r_{co}$ (mmol/g_{cat}.hr)[c]	P_{CO} avg (psi)	P_{H2} avg (psi)	S_{CH4}
191	15.47	8.3%	5.13	32	137	8.3%
196	15.47	10.9%	6.69	32	137	10.9%
206	15.47	20.2%	12.47	30	135	20.2%
221	15.47	41.2%	25.41	27	130	41.2%

[a]Two runs for Co only catalyst
[b]Initial Co molar flow rate
[c]Calculated using

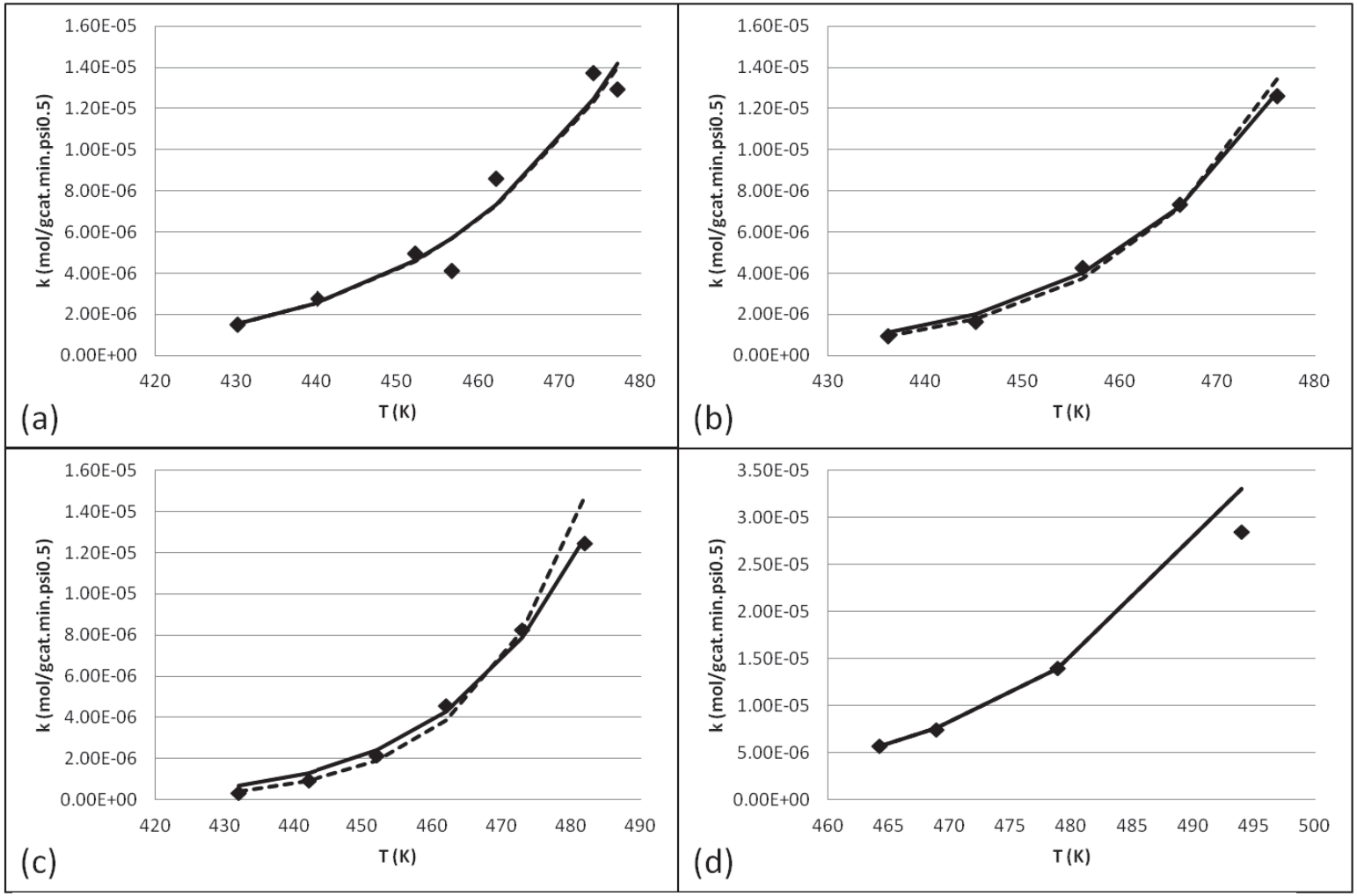

Figure 4-13. k vs T with nonlinear regression fit (solid curve) and linear regression fit (dashed curve) for (a) Co, (b) Co/Pt-seq, (c) Co/Re-seq, and (d) Co/Ru-seq catalysts

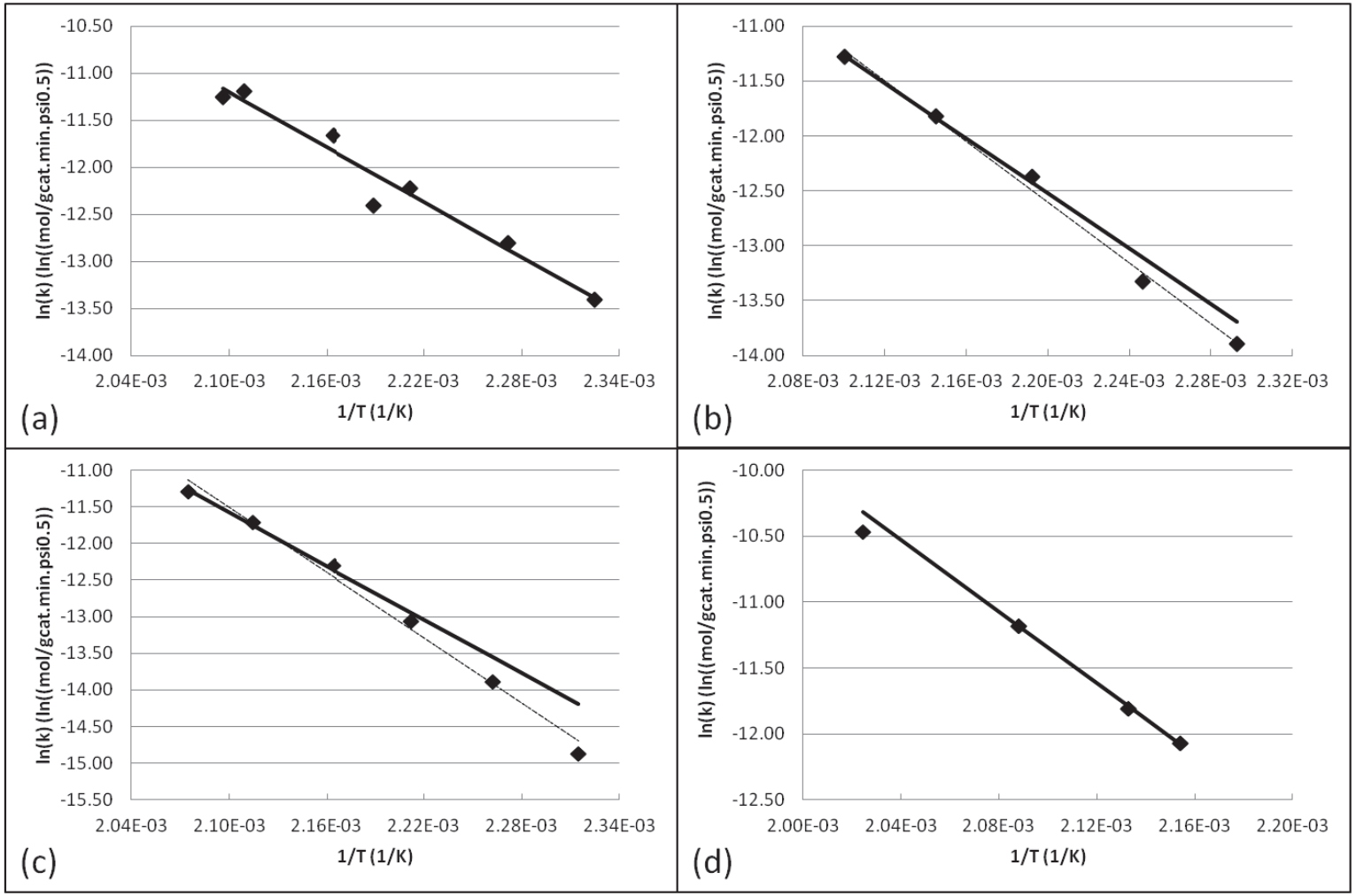

Figure 4-14. Linearization to ln(k) vs 1/T with nonlinear fit(solid line) and linear fit (dashed line) for (a) Co, (b) Co/Pt-seq (c) Co/Re-seq, and (d) Co/Ru-seq catalyst

Table 4-8. Apparent activation energies and preexponential factors from nonlinear and linear regression of fixed bed rate data with conversion below 25%

	E_A ($kJ \cdot mol^{-1}$)		A ($mol/g_{cat}.min.psi^{0.5}$)	
Catalyst	**Nonlinear**	**Linear**	**Nonlinear**	**Linear**
Co	78	80	4.6E+03	8.5E+03
Co/Pt-seq	105	115	4.1E+06	5.9E+07
Co/Re-seq	101	124	1.1E+06	3.9E+08
Co/Ru-seq	113	113	2.8E+07	2.8E+07

Table 4-9. Comparison of activity by normalizing to 200°C, P_{CO} of 2.1 bar (30 psia), and P_{H2} of 9.0 bar (130 psia)

Catalyst	X_{CO}[a]	$-r_{CO}$[b]	TOF[c] x 10^3	S_{CH4}
	(%)	($mmol \cdot g_{cat}^{-1} \cdot h^{-1}$)	(s^{-1})	(%)[a]
Co	19.90%	12.0	-	15%
Co/Pt-seq	18.30%	9.7	5.4	22%
Co/Re-seq	12.00%	7.6	3.5	21%
Co/Ru-seq	10.90%	8.8	8.2	22%

[a] from closest data point to 200°C

[b] adjusted to T=200°C, P_{CO}=2.1 bar (30 psia), P_{H2}=9.0 bar (130 psia) using A and E_A nonlinear fit of data

[c]TOF based on H_2 uptake after reduction(at the beginning of reaction) and neglect any further reduction of Co oxides to Co active sites with time on reaction stream.

4.4 Discussion

This chapter focuses on the chemistries of three commonly used NM promoters (Pt, Re, and Ru) and their effects on the chemical and physical properties of commercially relevant Co FT catalysts. The results of the present study are largely qualitatively consistent with those of previous studies addressing effects of relative concentrations of NM and Co on reduction rate as

a function of temperature and EOR to Co metal. The present study also provides new insights into other critical factors/issues which have received relatively little attention, i.e., (1) spatial distribution of NMs; (2) possible loss of NM during preparation; (3) the chemical state of each NM in the reduced Co catalyst; (4) the nature of bonding and coordination number of each NM with Co or itself; (5) influence of NM on Co CSD; and (6) the effects of Items 1-5 on Co reducibility and dispersion. The inclusion of factors 1, 2, and 5 in particular makes the present study the most comprehensive to date. This study is also one of only a few studies to report chemical and physical properties for commercially-relevant catalysts (in terms of composition and properties). The ensuing discussion will focus first on the critical aspects of NM distribution, retention, chemistry, and influence on CSD and second on their effects on Co dispersion, reducibility, and activity/selectivity.

4.4.1 Spatial Distribution, Retention, Chemical State, Bonding, and Coordination of NM Promoters and Their Influence on Co Crystallite Size

4.4.1.1 Spatial Distribution and Retention

First, it should be emphasized that current results (Figure 4-1and Figure 4-8) provide evidence that Co species concentrations are fairly uniform spatially with some clustering at the nm scale (from TEM) but highly uniform at the micron scale (from microprobe and SEM) in all four catalysts (Co, Co/Pt, Co/Re, and mostly Co/Ru) prepared by wet impregnation in a rotary evaporator. Given that the uniformity of Co concentration is essentially the same for all four catalysts of this study and that the NMs were added to batches of the unpromoted 25 wt% $Co/La/Al_2O_3$ catalyst, provides a valid basis for the comparison of NM promoter effects among these catalysts.

Secondly, it was not possible to ascertain the uniformity of the NM concentrations at the nanoscale, since NM concentrations were below the sensitivity of our STEM EDS experiments. However, SEM and electron microprobe results provide definitive evidence that Pt and Re were distributed uniformly at the micron scale, while Ru was largely concentrated at the edges of pellets with the La stabilizer in the alumina support. This was especially unexpected, given La's even distribution before Ru deposition. It should be emphasized, however, that while the Ru concentration was highest near the outer surface of the pellet, a measurable, low concentration of Ru was present throughout the catalyst also, as shown in Figure 4-7.

The fact that more than 50% of the Ru was lost during Co/Ru preparation is somewhat unexpected as the only other known report of Ru loss was for Ru-promoted Co FT catalysts using a different preparation technique (two step, incipient wetness, co-impregnation) and Ru precursor (nitrosyl nitrate) (Prieto, Martinez et al. 2009). It is hypothesized that this loss occurred via formation of highly volatile RuO_4 during drying or calcination. Indeed, RuO_4 is known to be formed and appear in the gas phase both during evaporation of a nitric acid solution containing Ru ions and by room temperature reaction of $Ru(OH)_3 \cdot nH_2O$ with F_2 or Cl_2 (Sakurai, Hinatsu et al. 1985). Since in the present study Ru was added by wet impregnation of the calcined Co catalyst with $RuCl_3$, the latter route involving reaction of Ru hydroxide with Cl_2 is more likely. Since XAFS experiments showed that at least part of the Ru in the calcined sample was RuO_2, such oxidation and volatilization does not appear to have affected all the Ru. The observation by XAFS of RuO_2 also shows that even though Ru and La were both concentrated at the pellet edge which suggests the possibility of the formation of $LaRuO_3$ (a very stable perovskite) (Labhestwar, Watanabe et al. 2003), $LaRuO_3$ was apparently *not* formed.

The observed sharp Ru concentration gradient is similar to a finding with a Co catalyst prepared by incipient wetness deposition (Delmon, Grange et al. 1978) but these two (this work and Delmon's work) studies are apparently unique and in the case of this study it is made more interesting when combined with the substantial Ru loss and similar La concentration gradient. Additional investigation is needed to further define the root causes of these problems, to improve Ru distribution and retention, and to determine the effect of Ru deposition on La distribution given the wide use of La oxide to stabilize Al_2O_3 supports against hydrothermal degradation.

4.4.1.2 Chemical State, Bonding, and Coordination of NM Promoters

4.4.1.2.1 Surface Bonding of Pt to Co

The appearance of a Pt-Co alloy in FT catalysts has been reported previously both after direct high temperature reduction (i.e. without calcination between the drying and reduction steps), and after calcination of Co and Pt precursors together (concurrently) followed by reduction (Guczi 2002; Jacobs, Chaney et al. 2004). The results of this study suggest another possible route to Pt-Co bond formation, i.e. via calcination of the Co and Pt precursors in *separate* steps under fairly mild conditions followed by reduction. It also adds insight into Pt-Co bimetallic formation. While both Pt and Co typically have a face-centered cubic structure and thus a coordination of 12, the Pt atoms after reduction for 1 h at 360^{o}C were coordinated to only 6.1 Co on average (Table 4-4), a coordination characteristic of Pt located at surface corner sites with Co neighbors as illustrated in Figure 4-15 at a site designated by C and consistent with previous suggestions (Jacobs, Chaney et al. 2004). After reduction at 400^{o}C, the Pt-Co coordination increases to 8.8—indicating a transition from a corner to a close packed surface planar site, as designated by P in Figure 4-15. This observation suggests significant Pt surface

mobility at relatively low reduction temperatures of 360-400^{o}C as a means for alloy formation at the surface of 6-12 nm diameter Co metal crystallites.

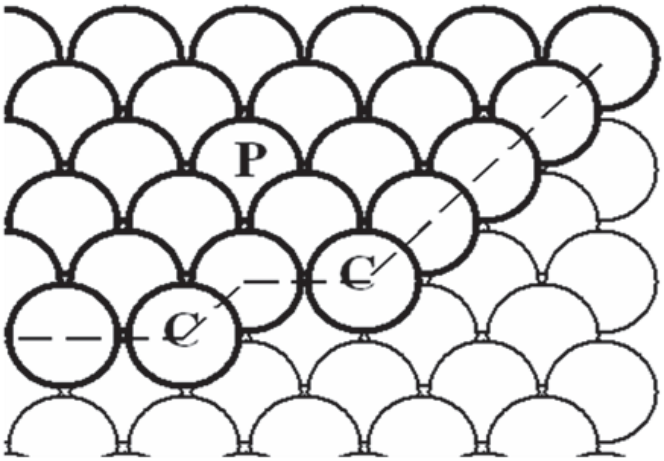

Figure 4-15. Model of Pt at corner sites, shown as (C), after 360oC reduction and Pt at surface closed packed planar sites, shown as (P), after 400oC reduction (courtesy of John Wiley (Bartholomew and Farrauto 2006))

4.4.1.2.2 Re Oxidation State

Ronning et al. found that after 1 h of reduction at 450^{o}C Re remained coordinated to oxygen with a decrease in coordination from 4.0 to 3.4(Ronning 2001). In this study after reduction for 1 h at 360^{o}C the coordination remained the same as in the calcined catalyst within experimental error, i.e., CN = 4.0. The lack of change observed in this study is significant and will be discussed in Section 4.4.2.2. Based on their XAFS data, Jacobs et al. suggested that Re bonds with Co during reduction for 10 h at 350^{o}C; however, their reported bond distance for Re-Co of 2.1 Å is not consistent with bonding of Re to Co, since the sum of Re and Co atomic radii of 1.37 Å and 1.25 Å is 2.6 Å (Jacobs, Chaney et al. 2004). Ronning et al. also observed that with a longer reduction time at 400^{o}C (6-12 h) Re-Co and Re-Re bonds are apparently formed with a reported bond radius of 2.53 Å for the Re-Co bonds (Ronning 2001). Thus, a long reduction

e.g.16 h at 360-400^{o}C could lead to Re reduction and formation of Re-Co bonds; this possibility might be explored in a future study.

4.4.1.2.3 Ru as a Separate Metal Phase

In a recent paper by Ma et al, XAFS data were reportedly consistent with formation of Ru-Co bonds for a Co catalyst having commercially relevant Co and Ru loadings (25wt% Co/0.27wt% Ru/Al2O3) after reduction for 10 h at 350^{o}C (Ma, Jacobs et al. 2011). That Ru-Co bonds had not been observed prior to this report (even by the same research group) (Bazin, Kovacs et al. 2003; Jacobs, Sarkar et al. 2008) was proposed to be an artifact of the high Ru loadings (2-4%) in prior studies. It was speculated that the XAFS signals for Ru-Ru bonds swamped out signals for Ru-Co bonds, if they existed for the high Ru loaded catalysts, as XAFS is a bulk signal. However, the XAFS results of the present study do not support that hypothesis; in fact only Ru-Ru bonding was observed in this study at even lower Ru loadings than the catalyst used by Ma et al. (Ma, Jacobs et al. 2011). While masking of Ru-Co bonds by more abundant Ru-Ru bonds even at the low Ru concentrations used in this study cannot be ruled out, differences in preparation including methods of impregnation, drying/calcination, reduction conditions, and in the chemistry of the Ru precursor may have contributed to the different observations of the two studies. One could speculate that the peak at low R in the radial distribution for Ru (Figure 4-11) is due to trace amounts of Ru-Co bonding. It is more likely, however, that this peak is due to a preponderance of small Ru clusters, since (1) the Fourier transform consists of only slightly shorter bond distances than for Ru foil; and (2) both the low R peak and contracted bond distance are characteristic of Ru nanoparticles of less than 3 nm (Miller 2006; Lei, Jelic et al. 2011).

4.4.1.3 Effects of NM and Reduction on Co Crystallite Diameters

Co CSD and ACD data presented in this study (see Table 4-3 and Figure 4-9) provide new insights regarding effects of promoters and reduction conditions on CSD, for both calcined and reduced catalysts. Very few previous publications report direct measurements of CSD or ACD by TEM (Reuel and Bartholomew 1984; Storsæter, Tøtdal et al. 2005; Li, Liu et al. 2006; Karaca, Safonova et al. 2011), and *comparison* of calcined and reduced-catalyst TEM-measured CSDs are apparently absent in available literature, although previous works by Ruckenstein and Hu as well as Saib et al. have made such comparison in redispersion studies of unpromoted model Co/alumina and Co/silica catalysts using TEM (Ruckenstein and Hu 1986; Saib, Moodley et al. 2010).

Previous studies of conventional supported FT catalysts indicate that with a few exceptions Ru and Pt promoters do not significantly alter Co oxide particle sizes obtained during calcination compared to unpromoted Co catalysts (Li, Liu et al. 2006; Chu, Chernavskii et al. 2007; Jacobs, Ji et al. 2007; Karaca, Safonova et al. 2011), though it is consistently reported that Re promotion causes formation of smaller Co oxide particles during calcination (Mauldin and Varnado 2001; Borg, Hammer et al. 2009; Enger, Fossan et al. 2011). Smaller Co oxide crystallites are thought to occur in Co/Re catalysts because Re oxide lowers Co ion mobility (Mauldin and Varnado 2001) thus preventing agglomeration during calcination. The results of this study align with this hypothesis, since addition of Re to a sample of the calcined unpromoted catalyst followed by calcination (a thermal treatment that typical results in agglomeration) resulted in Co oxide crystallites for the Co/Re catalyst of a statistically similar size to the unpromoted Co. By contrast, in calcined Co/Pt and Co/Ru catalysts, Co oxide crystallites were

observed to be statistically larger than in the unpromoted catalyst, indicating agglomeration during the additional calcination step.

Previous literature contains widely varying estimates of ACD from H_2 chemisorption and XRD for reduced catalysts relative to those for calcined catalysts suggesting reduction may increase, decrease, or not affect ACD (Borg, Hammer et al. 2009; Enger, Fossan et al. 2011; Park, Bae et al. 2011). Shrinkage in crystallite sizes during reduction is expected from a decrease in molar volume due to loss of O atoms. For a catalyst with 100% of the Co_3O_4 particles reduced to Co metal, a 25% decrease in crystallite diameter would be expected (Schanke, Vada et al. 1995). Figure 4-16 shows the predicted crystallite size decrease for each catalyst taking into account the measured EOR compared with the actual percent changes in volume mean ACD from the TEM measurements given in Table 4-3. For example, the Co/Pt catalyst, since 91% of the cobalt oxide is reduced to the metal and a 23% decrease was predicted for O loss (0.91*0.25). The actual 18% decrease in volume mean ACD for the Co/Pt catalyst is consistent with that prediction. For the Co/Ru catalyst, the observed decrease in volume mean ACD of 46% and shift of the CSD during are greater than the decrease molar volume change and EOR predict, 19%, and are likewise consistent with the splitting of thin oxide film into smaller crystallites during reduction.

This splitting mechanism has been observed in TEM studies of redispersion of base metals, including Co, on model alumina and silica surfaces, in which sintered catalysts were treated in O_2 at high temperatures causing transformation of the 3D metal crystallites to thin toroidal or spheroidal oxide films occupying a large area. During subsequent reduction, each of these films is split into small 3D hemispherical metal clusters (Ruckenstein and Hu 1986; Barthlomew 1993). This phenomenon can be explained in terms of nanoscale surface chemistry.

Co oxide, which has a lower interfacial free energy than reduced Co metal, readily wets the alumina surface forming Co oxide rafts or films; spreading of the oxide on the surface is also facilitated by a strong chemical oxide-oxide interaction. During reduction, the Co oxide film breaks apart into small metal crystallites which retract (ball up) to form 3D spheres or hemispheres. These small metal crystallites, due to their relative high surface energy, do not wet the support to a large extent nor do they interact strongly with the alumina support (Ruckenstein and Hu 1986).

The change in volume mean ACD during reduction for the Co/Re catalyst follows a trend opposite to Co/Pt and Co/Ru, Figure 4-16. The Co/Re volume mean Co ACD increases 26% with reduction (while O volume loss and EOR predict a decrease of 21%) suggesting that either crystallite agglomeration or Ostwald ripening occurs during reduction (Barthlomew 1993). The volume mean ACD for the Co catalyst also increased (2%) when a (11%) decrease was predicted based O loss.

Of the previous studies reporting TEM measurements of supported Co ACD, the study by Reuel and Bartholomew (Reuel and Bartholomew 1984), Sun et al.(Sun, Fujimoto et al. 2003) and this study provide data comparing values of surface mean ACD from TEM with estimates of crystallite size determined from H2 chemisorption. ACD determined from TEM in this study for the reduced unpromoted catalyst is only 4.7 nm (Table 4 3), while that from H2 chemistorption was estimated to be 10.0 nm (Table 4 6). This discrepancy may be explained as follows. Because it was not practically possible to distinguish between Co metal and Co oxide crystallites by TEM and since the unpromoted catalyst has such a low EOR (42%, Table 4 6), it is likely that a large fraction of the smaller, more difficult to reduce, crystallites observed by TEM were Co oxide rather than Co metal sites and thus unlikely to adsorb H2. TEM/chemisorption agreement was

better in the previous study (Reuel and Bartholomew 1984), i.e., ACD values from TEM vs. H2 chemisorption were 11 vs. 9.7 nm and 14 vs. 14 nm for 10 and 15% Co catalysts, respectively; however, the previous results may not be quantitatively comparable to those of this study, since the two catalysts of Reuel and Bartholomew were of significantly lower Co loading, contained no La oxide stabilizer, and were reduced at a higher temperature (400oC compared to 360oC in this study). A similar but smaller difference between surface mean ACD values from TEM and H2 chemisorption for the reduced Co/Ru catalyst, 9.0 vs. 6.7 nm, is probably also explained in part by incomplete reduction of small crystallites of Co oxide (EOR of 76%). In addition, large Co crystallites in Co/Ru observable both by SEM and TEM could have biased the CSD to large crystallite size. (Scans of unpromoted catalyst did not show such agglomerates.) Both of these are similar to Sun et al's work showing smaller measured TEM ACD than predicted from H2 chemisortion (Sun, Fujimoto et al. 2003). For the Co/Pt catalyst the difference between crystallite diameter estimated from TEM and H2 uptake is reversed (8.0 vs 5.9 nm). Given the high reducibility of the Co/Pt catalyst (EOR of 91%) it is likely that reduced Co particles below TEM measurement resolution (< 2 nm) could have chemisorbed a significant fraction of the total H2 uptake. For Co/Re estimates of crystallite diameter from TEM and chemisorptions (4.9 vs 4.6 nm) are in very good agreement indicating that the crystallites in the TEM images are representative of the reduced crystallites in the catalyst.

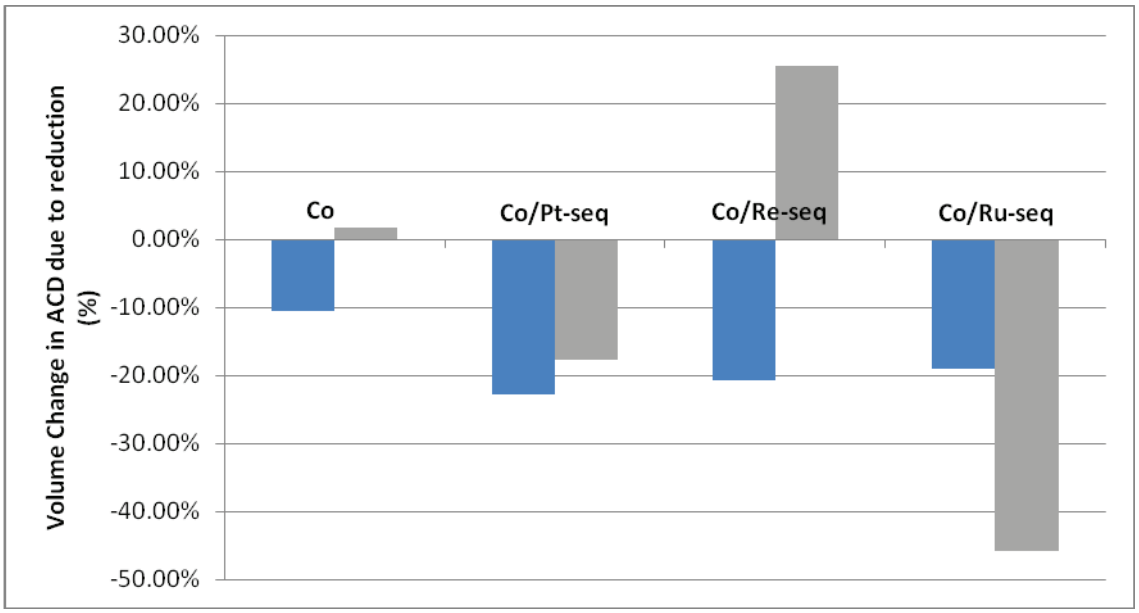

Figure 4-16. Comparison of predicted (blue) % change in volume mean ACD and actual (gray) % change volume mean ACD due to reduction

4.4.2 Effects of NM promoters on Co Reducibility

Despite differences in spatial distribution, NM oxidation state, and bonding, all three NMs substantially improved Co reducibility as determined from both TPR and EOR. In fact the magnitude of the increases in EOR observed due to NM promotion in this study of 80 to 120% (see Table 4-6) exceed the typical 33 to 80% increases reported in the literature after reduction at temperatures between 350^{o}C and 450^{o}C (Vada 1995; Das, Jacobs et al. 2003; Hosseini 2005; Chu, Chernavskii et al. 2007).

4.4.2.1 Pt, the Most Effective Reduction Promoter

The combination of Co/Pt TPR profiles showing the most significant peak narrowing and shifts to lower temperatures (Figure 4-12) as well as the highest EOR value of the four catalysts

(Table 4-6) indicates that Pt is the most effective promoter for improving the reduction of Co. The fact that Pt edge XAFS data show direct Pt-Co bond formation (Table 4-4 and Figure 4-10) combined with the favorable TPR and EOR results suggests that the proximity of Co and Pt and the mobility of Pt atoms or clusters to form a Pt-Co surface bimetallic at mild reducing conditions are responsible for this highly effective promotion of Co reducibility by Pt. While Co-Pt bimetallic formation is not a new finding (Guczi 2002; Jacobs, Chaney et al. 2004), the increased integration of Pt into Co surface layers or onto sites of higher coordination with further reduction (400^{o}C compared to 360^{o}C) is a new finding and suggests facile surface mobility of Pt metal atoms or clusters as the mechanism for surface bimetallic formation.

4.4.2.2 Re Oxide, an Effective Reduction Promoter

XAFS and EOR results for Co/Re after reduction at 360^{o}C for 1 h show that Re is not reduced but rather remains in the form of the perrhenate (Re_2O_7): yet the reduction of Co in Co/Re is efficiently promoted (Table 4-4). Previous studies have shown reduction promotion when Re-Co bonds form (Ronning 2001; Jacobs, Chaney et al. 2004) as well as after simply mixing and gently grinding Co/Al_2O_3 and Re/Al_2O_3 together (Hilmen, Schanke et al. 1996). However, the observation in the present study of Co reduction promotion during reduction for only 1 h at 360^{o}C without detectable reduction of the Re_2O_7 within limits of experimental error is quite unexpected. If a small fraction of Re_2O_7 had been reduced, it would follow that small numbers of Re metal sites, significantly lower in concentration than currently used in commercially representative catalysts, would be sufficient for Co reduction promotion; however, this seems unlikely given the amount of prior research which indicates that optimal amounts of

Re promoter are in the range used in this study. The mechanism by which Re_2O_7 promotes reduction is unclear and warrants further study.

A close look at the Co/Re TPR profile reveals a shoulder on the 2nd peak at 400°C (Figure 4-12). Given the area of this shoulder and its position, it could correspond to a fraction of smaller Co_3O_4 crystallites that are not readily reduced until a temperature just below that at which most of the CoO crystallites are reduced to Co metal. Indeed, the ratio of the area of the 2nd main peak (excluding that of the shoulder) to that of the 1st main peak plus that of the shoulder of 2.8 agrees closely with the stoichiometric prediction of 3 (see Table 4-3). The hypothesis that the shoulder is due to reduction of smaller Co_3O_4 crystallites is supported by the abundance of 2 and 3 nm crystallites measured from TEM in the calcined sample (see Table 4-3).

4.4.2.3 Ru promotes Co Reduction Even With Issues of Significant Loss and Poor Spatial Distribution

Despite the significant loss of Ru metal and its poor spatial distribution, Ru nevertheless significantly improved reducibility, i.e. increased EOR to 77% compared to 42% for the unpromoted Co, and H_2 uptake to 150 μmol/g compared to 65μmols/g. The fact that the Ru promoted catalyst produced three distinguishable reduction peaks in the TPR may be due to the nonuniform Ru distribution. It is hypothesized that Ru at a relatively high concentration near the pellet edge reduces first initiating H_2 dissociation/spillover to reduce nearby Co_3O_4 which apparently leads to the broadening of the small 200°C peak (relative to the other three catalysts), Figure 4-12. At higher temperatures some bulk Co_3O_4 (not near the Ru concentrated pellet edge) reduces to CoO resulting in the first main peak at 320°C (at effectively the same temperature as

the unpromoted catalyst). It is hypothesized that the small intermediate peak is due to CoO crystallites having greater proximity to Ru crystallites (probably close to the pellet edges) thus facilitating their reduction to Co metal at a lower temperature. Finally at a relatively high temperature, reduced Co crystallites facilitate hydrogen spillover and reduction of CoO throughout the pellet near which Ru is present only at low concentrations giving the 2nd main peak (495°C). This hypothesis is substantiated by good agreement between the measured and stoichiometrically predicted peak area ratio (Table 4-5) resulting from assignment of the Co_3O_4 → CoO transition to the first main peak and the CoO→Co transition to both intermediate and 2nd main peaks. It also provides an explanation for the absence of promotion expected for the first main TPR peak.

4.4.3 Effects on Activity

Despite significant increases in reducibility and even in the number of active sites (as measured by H_2 uptake), NM addition did not result in higher catalyst activity per gram; in fact the activity was slightly lower than for the unpromoted catalyst. Figure 4-17 shows that the k value 90% confidence intervals overlap for the unpromoted, Co/Pt-seq, and Co/Ru-seq catalyst such that the only difference of activity that can be made with 90% confidence is that the unpromoted is more active than the Co/Re-seq catalyst. Nevertheless, the fact that differences are not statistically significant does not mean that they are the same.

Deactivation was probably not the culprit, because effects of carbon deposition should be very low at a 4:1 H_2:CO ratio; moreover no detectable drop in activity was observed when returning the catalyst to standard test conditions during several days on stream. The significantly higher H_2 uptakes for NM promoted catalysts relative to the unpromoted catalyst

would not necessarily be expected to result in higher activity if the higher H_2 uptake was due to reduction of crystallites smaller than about 2 nm (which were not observed by TEM) as they could chemisorb substantial amounts of H_2 but would contribute negligibly to activity. The low activity of the Co/Re catalyst considering its high H_2 uptake (compared to the other promoted catalysts as well as the unpromoted catalyst) is consistent with this hypothesis as the measured CSD shows an abundance of small crystallites—95% of the Co crystallites below 6 nm increasing the likelihood of crystallites smaller than the practical TEM detection. Additionally, the high reducibility and difference between H_2 uptake-estimated and TEM-measured reduced Co crystallite diameters for the Co/Pt catalyst was already shown to suggest reduced Co crystallites below 2 nm (Section 4.4.1.3). The possibility of support H_2 spillover which is increased by finely dispersed NM sites adds another source of discrepancy between the activity suggested by the high H_2 uptake and the measured activity during fixed bed reaction

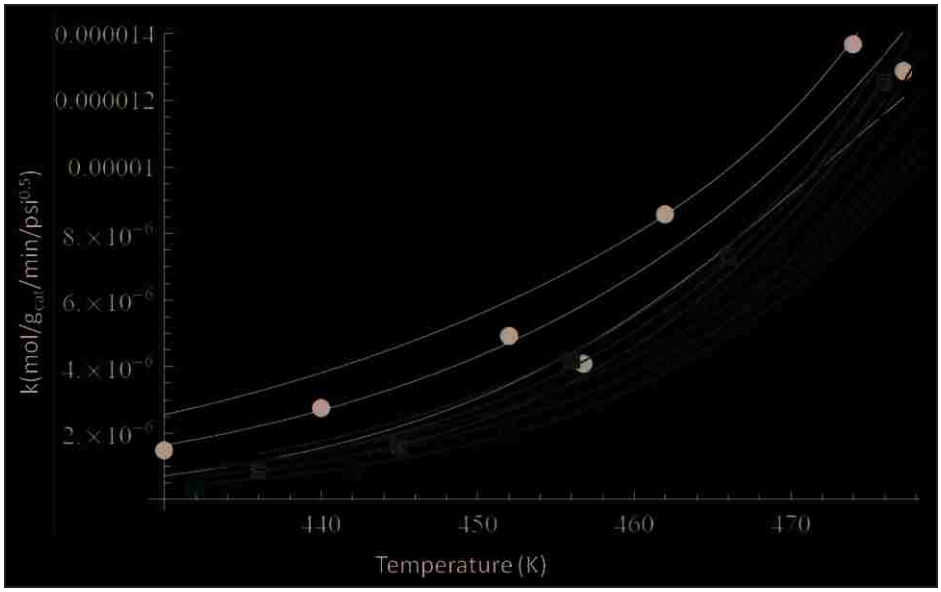

Figure 4-17. k as a function of temperature for the unpromoted (black), Co/Pt-seq (red), Co/Re-seq (green), and Co/Ru-seq (blue) with the nonlinear fit as the center line and the 90% confidence interval for the fit as the outer lines for each catalyst

4.5 Conclusions

From a comprehensive study of the effects of NM type on (i) metal retention, (ii) spatial distribution of NM and Co phases, (iii) NM bonding and oxidation state, and (iv) Co crystallite size and the subsequent effects of these properties on Co reducibility, dispersion, and FT activity/selectivity a number of significant, new observations were made forming the basis for the following conclusions:

1. Co retention was statistically similar for all four catalysts and within experimental error of the quantity added during preparation. NM retention was complete for Pt and Re relative to quantities added during preparation; by contrast about 50% of the Ru initially added was lost during catalyst preparation including impregnation, drying and calcination procedures.
2. Co was uniformly distributed spatially in all four Co catalysts. NM distribution varied dramatically, i.e. Pt and Re were uniformly distributed across pellets while Ru was largely concentrated at the pellet edge. La incorporated in the support was distributed uniformly across pellets for Co, Co/Pt, and Co/Re catalysts; however, in the Co/Ru catalyst, La was concentrated at the pellet edge.
3. About 70 and 50% of crystallite diameters in Co/Pt and Co/Ru catalysts, respectively, reduced at 360^{o}C were in range of 6-12 nm. By contrast, 83 and 95% of Co metal crystallite diameters in Co and Co/Re catalysts reduced at 360^{o}C were observed to be below 6 nm.

4. XAFS measurements following mild reduction (1 h in 4%H_2 at 360^{o}C) of Co/Pt, Co/Ru, and Co/Re catalysts indicate the formation of surface bimetallic Pt-Co bonds, a separate Ru metal phase, and unreduced Re_2O_7 respectively.
5. Despite the substantially different chemical states and bonding in Pt, Re, and Ru promoted Co catalysts, all three promoter types facilitate Co reduction after only 1 hr at 360^{o}C. This was particularly surprising for the unreduced Re_2O_7.
6. Of the three NM promoters studied, Pt best facilitates reduction of Co as indicated by TPR and EOR measurements.
7. The TPR peak areas are consistent with, and offer strong corroborative evidence that the reduction process steps are $Co_3O_4 \rightarrow CoO$ and $CoO \rightarrow Co$.
8. The Co/Re catalyst had the highest H_2 uptake (Co/Re > Co/Pt > Co/Ru > Co); thus Re is the most efficient of the three promoters in facilitating a high dispersion of Co.
9. The fit of Co/Re catalyst activity is statistically lower than the unpromoted catalyst. The Ru and Pt promoted catalysts made by sequential deposition are slightly less active per gram than the unpromoted catalyst, but this difference is not statistically significant.

5 Effect of Deposition Order

As noted in Chapter 2, there is little agreement from the previous literature regarding preferred methods for adding NM promoters to Co catalysts. Thus, the objective of the work described in this chapter was to understand the effects of the order of NM addition on Co catalyst properties and performance.

NM-promoted 25% Co/La/Al_2O_3 catalysts were prepared by a three-step (co-deposition) or four-step (sequential-deposition) wet impregnation. The distinguishing steps of these two processes, co-deposition (co-dep) and sequential-deposition (seq-dep), are depicted in Figure 5-1 and Figure 5-2.The first two steps in both deposition techniques were the same—Co nitrate impregnations to 10wt% and 20wt% Co, each followed by drying in a rotary evaporator followed by drying and calcination in flowing air. The third step of the co-dep process included simultaneous addition of sufficient Co nitrate to reach a total of 25wt% Co and NM (as the chloride salt) (Figure 5-1). The seq-dep process included a third step in which Co nitrate was added to reach a total of 25wt% Co and fourth step to deposit the NM (as the chloride salt) (Figure 5-2). The latter preparation method was used in the preparation of the four catalysts described in Chapter 4.

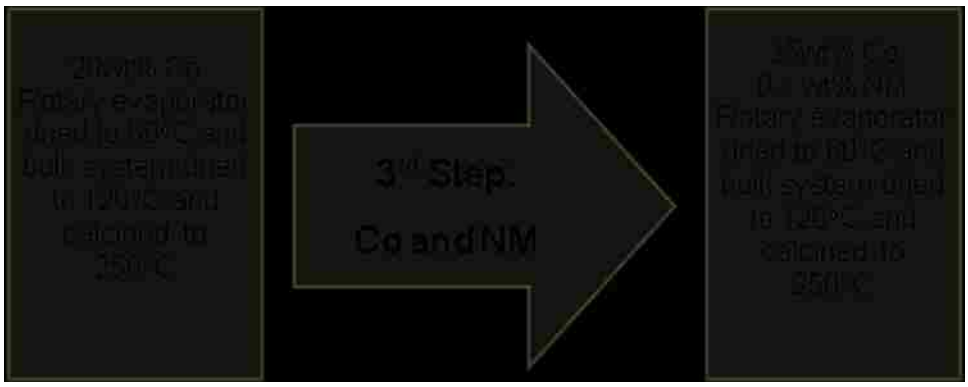

Figure 5-1. Depiction of co-dep 3rd step

Figure 5-2. Depiction of seq-dep 3rd and 4th steps.

The differences between seq-dep and co-dep are that seq-dep included separate depositions for the final Co deposition and the NM deposition as well as three additional thermal treatments between those two depositions: (1) rotary evaporator drying to 60°C, (2) bulk drying to 120°C, and (3) calcination to 250°C which happened between the deposition of Co and the deposition of NM.

While these differences were a consequence of the timing of NM addition, an investigation to separate the effects of the variation of thermal treatment between the seq-dep and co-dep was

performed. This was done by preparing Ru promoted catalyst by two additional seq-dep procedures as illustrated in Table 5-1. The two procedures varied by the drying used between the final Co and the NM depositions as shown in columns 2-4. (1) The first procedure was more like co-dep with only a drying at 60°C in the rotary evaporator (denoted by RE only) between the last Co deposition and the NM deposition. (2) The second procedure was more like seq-dep with both drying at 60°C in the rotary evaporator and bulk system drying to 120°C in flowing air (denoted by RE and 120). After each drying procedure, Ru chloride was added by either wet impregnation (denoted by Aq) or "dry" impregnation to incipient wetness (denoted by IW). Thus, the following four seq-dep catalysts were added to the investigation: Co/Ru-RE only, Co/ Ru-RE /120, Co/Ru- IW RE only, and Co/Ru-IW RE/120.

To determine if the Ru containg precursor affected the significance of variations in deposition order, one additional Ru promoted catalyst was made (making the total 7) using a nitrosyl nitrate rather than chloride precursor by the standard seq-dep procedure, Figure 5-2. Thus while the main objective of this chapter was to investigate the effects of deposition order, this chapter also includes results and discussion of effects of thermal treatments and NM precursor as they relate back to the main objective.

Comprehensive characterization of physicochemical, reducibility, activity/selectivity properties of the three co-dep/seq-dep pairs (promoted with Pt, Re, and Ru) were carried out using the same methods used in Chapter 4. It should be noted that the results for the Co-only and seq-dep were reported and discussed in Chapter 4 but are included here for purpose of comparisons.

Table 5-1. Summary of variations in drying and impregnation method for one catalyst prepared by co-deposition and 5 catalysts prepared by sequential deposition

		Treatments between 3rd and 4th Deposition Step				
Catalyst	Metals in 3rd Deposition Step	Rotary Evaporator Drying	Bulk Drying to 120°C	Bulk Calcination to 250°C	Metals in 4th Deposition Step	Amount of Solvent in 4th Deposition
Co/Ru-co	Co and Ru	N/A				
Co/Ru-AQ RE only	Co	X			Ru	wet
Co/Ru-AQ RE/120	Co	X	X		Ru	wet
Co/Ru-IW RE only	Co	X			Ru	incipient wetness
Co/Ru-IW RE/120	Co	X	X		Ru	incipient wetness
Co/Ru-seq	Co	X	X	X	Ru	wet

5.1 Chemical and Physical Properties

5.1.1 Surface Area and Pore Size Distribution

Surface area and pore properties for each catalyst (Co, Co/Pt-co, Co/Pt-seq, Co/Re-co, Co/Re-seq, Co/Ru-co, and Co/Ru-seq) are listed in Table 5-2. As expected from literature and the seq-dep data (Section 4.1.1), deposition order does not significantly affect the surface area, pore volume, or pore diameter (Jacobs, Das et al. 2002). While there are slight differences, the differences are inside the 95% confidence interval.

Table 5-2.BET measurements of surface area, pore volume, and pore diameter data for deposition order comparison

Catalyst	Surface Area (m^2/g) ±5	Pore Volume (cm^3/g) ± 0.01	Pore Diameter (nm) ± 0.5
Co	103	0.43	15.0
Co/Pt-co	99	0.4	15
Co/Pt-seq	98	0.4	15.2
Co/Re-co	96	0.41	15.4
Co/Re-seq	100	0.4	14.3
Co/Ru-co	102	0.41	14.9
Co/Ru-seq	92	0.38	15.6

5.1.2 Co and NM Retention

Co and NM loadings were measured for duplicate samples of each calcined catalyst by ICP; the average concentrations for each catalyst are shown in Table 5-3. Co loadings do not show a deposition order trend and are all statistically the same as the target loading of 22.9 wt%. Pt and Re loadings are also within experimental error of the intended values for both deposition orders. Ru, however, did show a significant deposition order trend with much lower loadings due to substantial loss of 85% for co-dep compared to a still significant yet lower loss of 53% for seq-dep. For the additional Ru seq-dep catalysts which investigate thermal treatment differences, the data are consistent with a trend of greater loss for those dried only in the rotary evaporator (results are similar to the co-dep catalyst) compared to those dried in both the rotary evaporator and to 120^{o}C in a flow system (results are closer to seq-dep) (see Table 5-4). It is further evident from Table 5-4 that catalysts prepared by wet Ru deposition suffer a greater loss of Ru than those prepared by dry Ru deposition and that the Ru promoted seq-dep catalyst prepared using the nitrosyl nitrate precursor has much higher retention (76%) of Ru relative to that prepared from the chloride, (Co/Ru-seq) (46%).

Table 5-3. Metal loading for deposition order comparison

Catalyst	Co			NM		
	Nominal wt%	Actual wt%	% Lost	Nominal wt%	Actual wt%	% Lost
Co	22.9	19.63	14%	N/A	N/A	N/A
Co/Pt-co	22.9	20.58	10%	0.53	0.46	13%
Co/Pt-seq	22.9	20.24	12%	0.53	0.47	12%
Co/Re-co	22.9	21.82	5%	0.5	0.59	0%
Co/Re-seq	22.9	21.02	8%	0.5	0.64	0%
Co/Ru-co	22.9	22.06	4%	0.27	0.04	85%
Co/Ru-seq	22.9	22.24	3%	0.27	0.13	54%

Table 5-4. Ru loading for deposition order, thermal treatment, and precursor chemistry comparison (all seq-dep except for the first sample)

Catalyst	Ru	
	Actual wt%	% Lost
Co/Ru-co	0.04	85%
Co/Ru-Aq-RE	0.00	100%
Co/Ru-Aq-RE/120	0.05	83%
Co/Ru-IW-RE	0.02	92%
Co/Ru-IW-RE/120	0.09	68%
Co/Ru-seq	0.13	54%
Co/Ru(nitrate)-seq	0.20	24%

5.1.3 Spatial Distribution of Co, La, and NMs

Electron microprobe scans showed all metals were uniformly distributed (Co, La, and NM) for all 3 co-dep NM catalysts. The even distributions of La and Ru for the Co/Ru-co catalyst signal a deposition order trend—Ru and La are concentrated at the pellet edge with seq-dep, but not co-dep.

Differences in spatial uniformity at the micron scale were observed for the Ru promoted catalysts investigating thermal treatment variations. Thus a Ru gradient results when RE/120 drying is done between the 3rd Co deposition and the Ru deposition, but it is not seen when only RE drying is done between those depositions (see Figure 5-3 b and d compared with a and c). This gradient is more extreme with incipient wetness than wet deposition (Figure 5-3 d compared to b). The La distributions for these catalyst show the opposite trend, i.e. RE only drying results in a greater concentration gradient than RE/120 drying moreover when Ru is added by a wet deposition the gradient is exacerbated , see Figure 5-4 a and c compared with b and d.

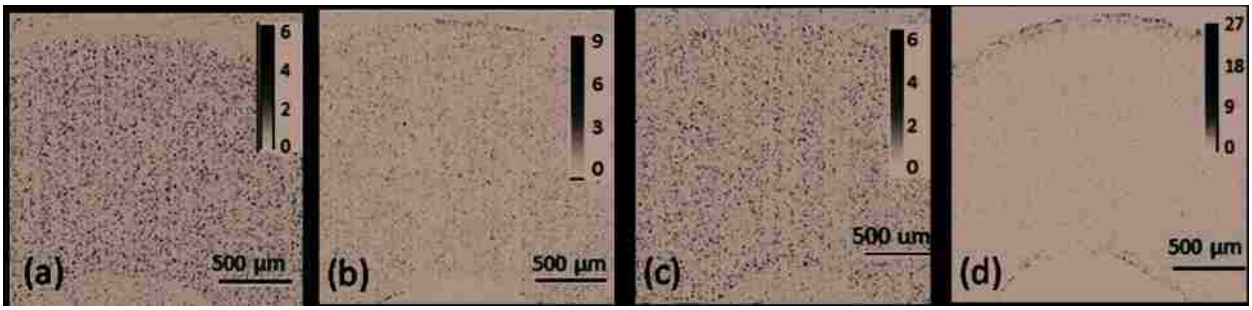

Figure 5-3. Microprobe images of Ru distribution for the thermal treatment investigation catalysts (a)Co/Ru-AQ RE only, (b) Co/Ru-AQ RE/120, (c) Co/Ru-IW RE only, and (d) Co/Ru-IW RE/120

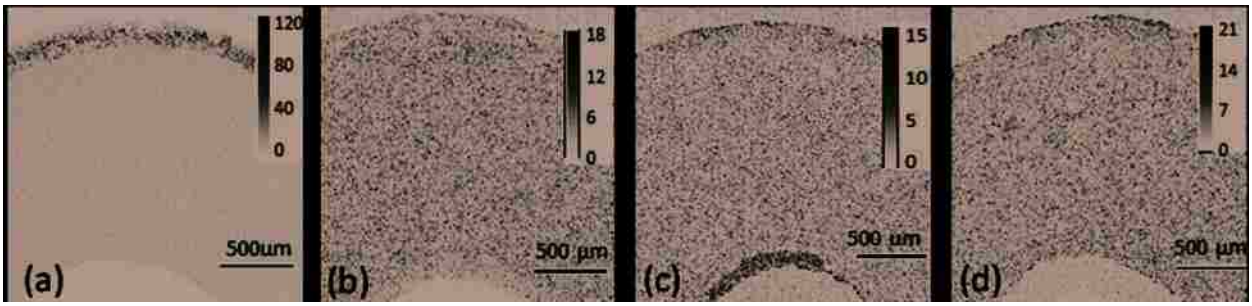

Figure 5-4. Microprobe images of La distribution for the thermal treatment investigation catalysts (a) Co/Ru-AQ RE only, (b) Co/Ru-AQ RE/120, (c) Co/Ru-IW RE only, and (d) Co/Ru-IW RE/120

5.1.4 Co Crystallite Size

TEM images were collected for the catalysts after calcination and after reduction/passivation. ACD's and CSD based on measurements of Co crystallites after calcination are given in Table 5-5. Larger oxide crystallites are observed for the Pt and Re promoted co-dep catalysts than corresponding seq-dep catalysts. Similarly larger oxide cyrstallites are observed for the calcined co-dep catalysts (Co/Ru included) than that for the unpromoted catalyst. Thus, the addition of NM (even without an extra calcination step) results in larger Co oxide particles except in the case of Co/Re-seq.

The crystallite sizes after 16 h reduction at 360°C and passivation are given in Table 5-6. The co-dep catalysts ACD is smaller than the seq-dep catalyst for all three NMs, but especially with Pt and Ru as the promoter. This shift to smaller crystallites results in nearly all the particles being below 6nm.

The deposition order effect on the CSD after reduction are portrayed through histograms in Figure 5-5 as well as the percentages within each range given in Table 5-6. The data show a definite trend to smaller particles with co-dep compared to seq-dep. This trend is especially apparent for the Ru and Pt promoted catalysts.

Table 5-5. Average Co crystallite diameters (ACD) and average diameters and distributions (CSD) after calcination determined from TEM images

Catalyst	Surface ACD[a] (nm)	Volume ACD[b] (nm)	%<6nm	%6-12 nm	%>12nm
Co	5.1±1.2	5.6	78	21	1
Co/Pt-co	13.6±4.4	17.5	30	57	13
Co/Pt-seq	9.2±2.8	10.7	25	70	5
Co/Re-co	6.1±2.1	7.5	67	33	0
Co/Re-seq	3.8±1.0	4.3	95	5	0
Co/Ru-co	10.3±3.3	11.8	22	63	15
Co/Ru-seq	11.2±3.6	13.3	24	66	10

a. Surface ACD calculated from $d_{surfaceavg} = \frac{\sum_i d_i^3}{\sum_i d_i^2}$ (3-8).

b. Volume ACD calculated from $d_{volumeavg} = \frac{\sum_i d_i^4}{\sum_i d_i^3}$ (3-9)

Table 5-6. Average Co crystallite diameters (ACD) and average diameters and distributions (CSD) after reduction/passivation[a] determined from TEM images

Catalyst	Surface Avg[b] d (nm)	Volume Avg[c] d (nm)	%<6nm	%6-12 nm	%>12nm
Co	4.7±1.5	5.7	83	17	0
Co/Pt-co	4.3±1.3	4.8	91	9	0
Co/Pt-seq	8.0±2.2	8.8	26	72	3
Co/Re-co	4.2±1.1	4.5	92	8	0
Co/Re-seq	4.9±1.6	5.4	62	38	0
Co/Ru-co	4.1±1.2	4.6	92	8	0
Co/Ru-seq	6.7±1.8	7.2	49	51	0

a. Extents of reduction to metallic Co range from 42% (Co) to 91% (Co/Pt) as shown in Table 4-6 after reduction at 360°C for 16 hr.

b. Surface ACD calculated from $d_{surfaceavg} = \frac{\sum_i d_i^3}{\sum_i d_i^2}$ (3-8).

c. Volume ACD calculated from $d_{volumeavg} = \frac{\sum_i d_i^4}{\sum_i d_i^3}$ (3-9)

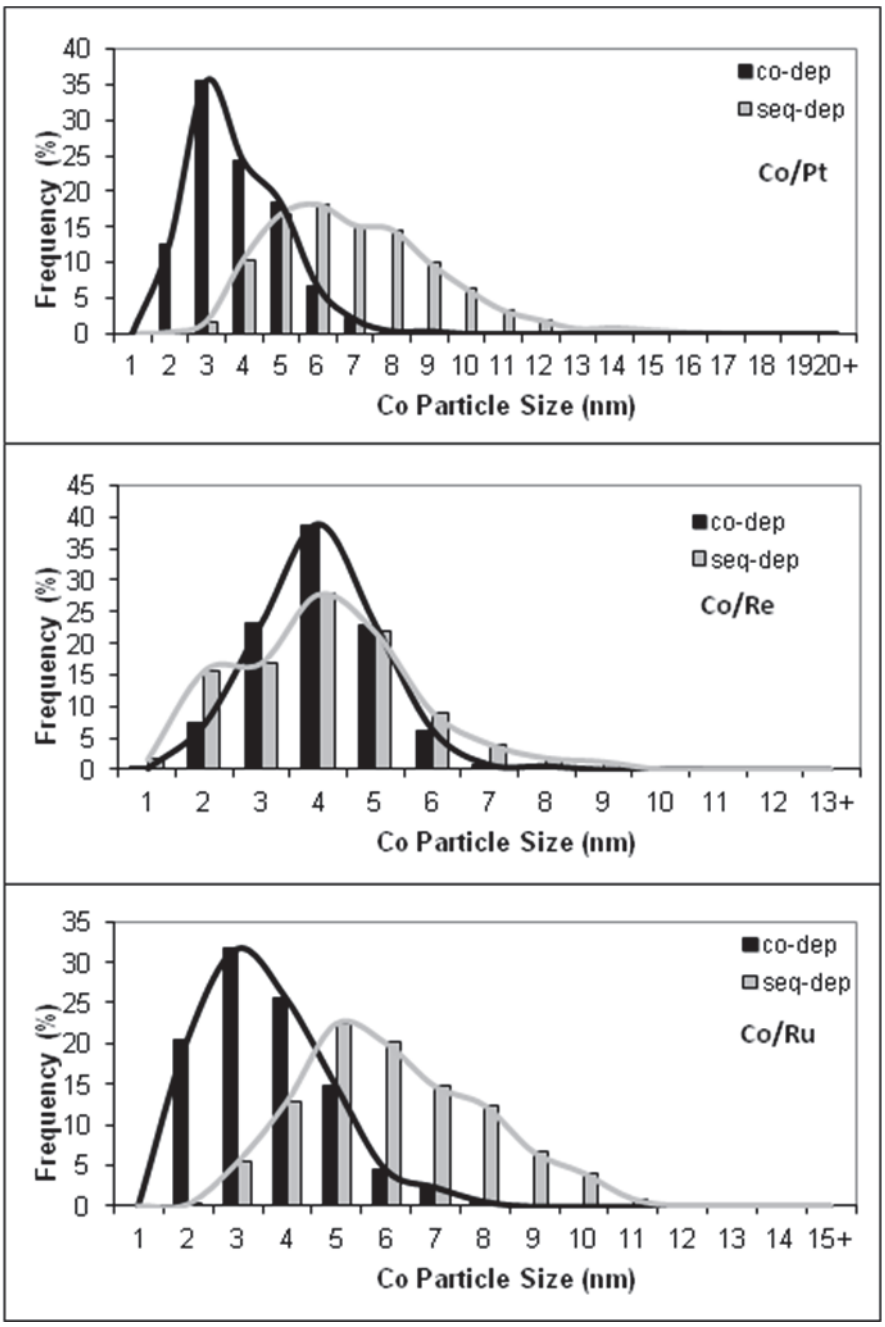

Figure 5-5. Histogram comparing Co crystallite diameter distributions after reduction of co-dep (black) and seq-dep (grey) Co/Pt (a) , Co/Re (b), and Co/Ru (c) catalysts.

5.1.5 NM Chemical State and Bonding after Calcinations and Reduction

The NM edge XAFS results after final calcination, and after 1 h of H_2 reduction as well as the O_2 titration TGA results of the amount of Co in each oxidation state (Co_3O_4, CoO, and Co metal) after a 1 h H_2 reduction are given in Table 5-7. There is not a notable difference in NM chemical state or atomic-scale bonding between deposition orders. Pt, Ru, and Re promotion resulted in the formation of surface bimetallic Pt-Co bonds, Ru-Ru metal bonds, and Re-O bonds (characteristic of unreduced Re oxide) respectively. An additional Co/Re-co experiment after 400^{o}C reduction rather than 360^{o}C does provide evidence of Re reducibility (from Re_2O_7 to ReO_2).

The Co oxidation state information provided in Table 5-7 to show promotion of Co reduction which companioned the NM chemical state and bonding provides a glimpse into the deposition order effect on reducibility to be discussed in the next section. The order of Co reducibility after 1 h of reduction at 360^{o}C was Co/Pt-seq>Co/Pt-co>Co/Re-co>Co/Re-seq.

5.1 Reducibility

5.1.1 TPR

Figure 5-6 shows the reduction profiles and peak temperatures from TPR experiments for Re, Pt, and Ru promoted catalysts prepared by both co-dep and seq-dep methods. The temperature of the final reduction peak shows the clearest deposition order effect, i.e., co-dep(especially with Ru and Re as the promoter) shifts this peak to a lower temperature (by 40 and 30^{o}C, respectively). Co/ Pt is the least affected by desposition order showing no deposition order effect for the first peak tempearature and only 10^{o}C for the second peak.

Table 5-7. Summary of NM edge XAFS results and corresponding Co reducibility

Catalyst	Treatment[a]	Bonding Atoms	Bond Distance (Å)	Coord No.	% Co_3O_4[b]	%CoO[b]	%Co[b] (EOR)
Co/Pt-co	Calcined	similar to Co/Pt-seq			100	-	-
	Reduced 360°C	Pt-Co	2.56	5.8	-	27	73
	Reduced 400°C	Pt-Co	2.55	8.8	-	19	81
Co/Pt-seq	Calcined	Pt-O	2.03	2	100	-	-
		Pt-Cl	2.31	4			
	Reduced 360°C	Pt-Co	2.56	6.1	-	11	89
	Reduced 400°C	Pt-Co	2.55	8.8	-	8	92
Co/Re-co	Reduced 360°C	Re-O	1.72	4.2	-	49	51
	Reduced 400°C	XANES matches ReO_2			-	26	74
Co/Re-seq	Calcined	Re-O	1.76	4.2	100	-	-
	Reduced 360°C	Re-O	1.73	4.1	-	58	42
Co/Ru-seq	Calcined	Ru-O	1.94	6.2	100	-	-
	Reduced 360°C	Ru-Ru	2.66	8.8	-	60	40

a. Reductions were for 1 h

b. determined by O_2 titration

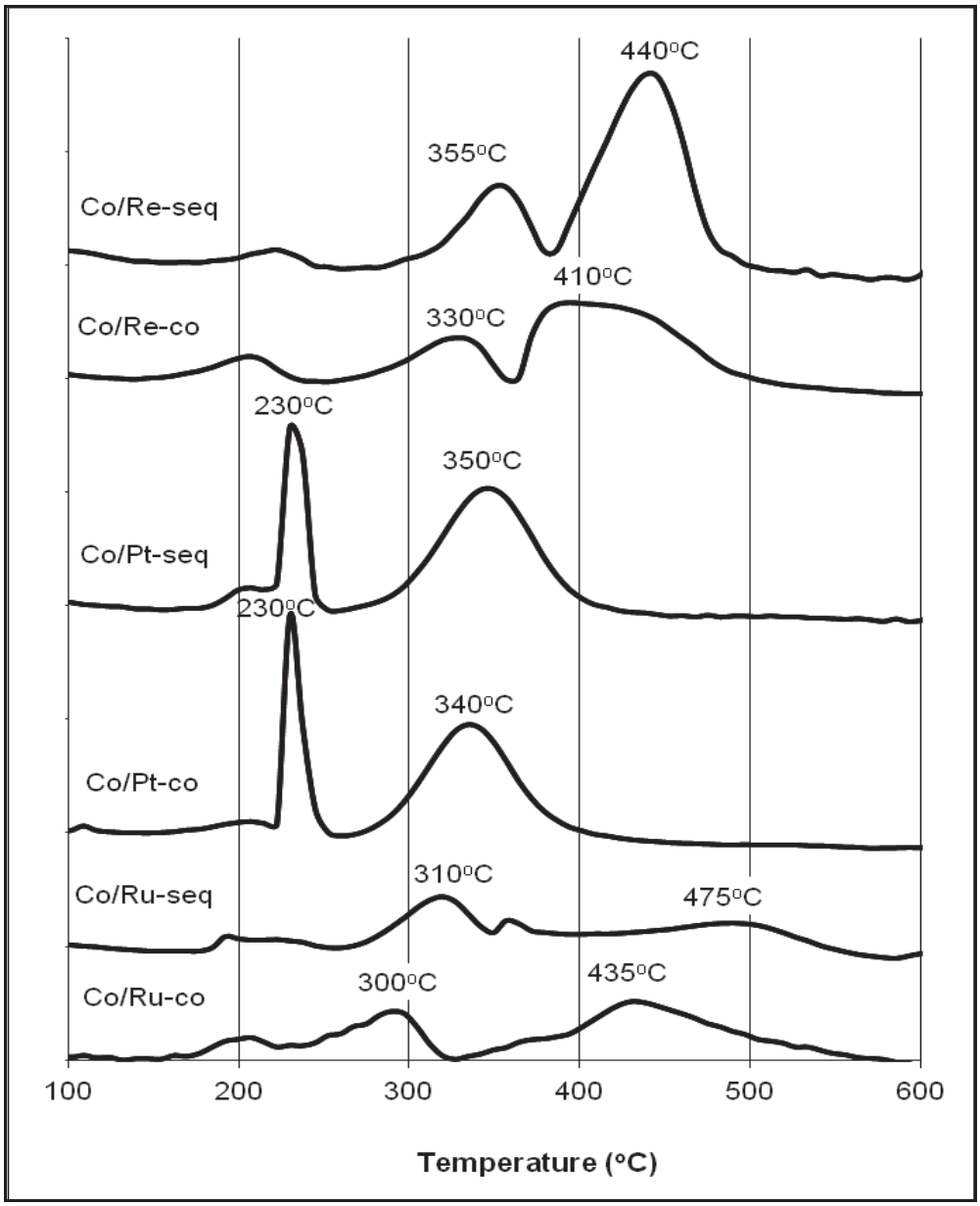

Figure 5-6. Reduction profiles for deposition order comparison

5.1.2 Extent of Reduction, Number of Active Sites and Dispersion

EOR was determined by O_2 titration after 16 h of reduction at 360°C and the results are shown in Table 5-8. For the co-dep catalysts, the EORs decrease in the order Co/Pt-co≥Co/Re-co>Co/Ru-co. This ranking is expected and the same as was seen with seq-dep, except the

difference between Co/Pt-co and Co/Re-co is less extreme. It is surprising however considering the modest differences in the TPR peak temperatures and lower Peak 2 temperatures for the co-dep catalysts, that the EORs for the co-dep catalyst are substantially lower than those for the seq-dep catalysts. Nevertheless, the TPR data are obtained over a relatively short period of time, while EOR data reflect the result of a much longer and more severe reduction (over 16 h and during 10 of those hours flowing 100% H_2). Give the more server reduction period before EOR measurements and the much smaller ACD for the co-dep catalysts, their lower EOR are likely a result of smaller crystallites which are known to be resistant to reduction (see Table 5-6).

The H_2 uptakes (also in Table 5-8) of Pt and Ru promoted catalysts are higher for co-dep than for seq-dep, since the former contain smaller Co crystallites with higher overall Co surface areas (despite lower EORs). These values were used to determine %D, which range from 10 to 20%. For all three co-dep catalysts the %D was ~20%. For the Co and Co/Ru-seq catalysts %D was ~10% and Co/Pt-seq was ~16%. Thus, Co dispersions for the Co/Ru co-dep preparations are twice those for seq-dep and ~50% higher for Co/Pt co-dep versus seq-dep preparation..

Table 5-8. H_2 Uptake, EOR, %D, and estimated d

Catalyst	H_2 Uptake (μmol/g)	EOR (%)	%D	d (nm)
Co	65	42	9.6	9.97
Co/Pt-co	297	77	22.0	4.27
Co/Pt-seq	251	91	16.1	5.87
Co/Re-co	268	74	19.5	4.82
Co/Re-seq	302	84	20.4	4.63
Co/Ru-co	219	62	19.0	4.95
Co/Ru-seq	150	77	10.4	9.1

5.2 Activity/Selectivity

The reaction conditions and basic activity/selectivity data (conversion, rate, and methane selectivity) for the co-dep catalysts are given in Table 5-9. Similar data for the seq-dep and unpromoted catalysts are given in Table 4-7. These data were obtained in the fixed bed reactor after quantitative confirmation of steady state as described in the fixed bed method section (page 36) and assume differential reactor conditions. Each data point (row in Table 5-9) represents the average of 6 h worth of GC measurements.

Rate constant (k) values were determined using $k = \frac{-r'_{CO}}{P_{H2}^{0.7} * P_{CO}^{-0.2}}$, (3-16), for each data point in Table 5-9. The k values for data below 25% conversion were fit two different ways (nonlinear and linear regression) to determine activation energy ($E_{A)}$. These k and E_A values for these regressions are given in Table 5-10 and the nonlinear (solid curves) and linear (dashed) fits are plotted with the data points in Figure 5-8. Traditional Arrhenius linearized plots of ln(k) vs 1/T are given in Figure 5-9 where again the solid line represents the nonlinear fit and the dashed lines (which are not always distinguishable due to the similarity of the fit) represent the linear fit .The data in Table 5-10 and also in Figure 5-7 show that the co-dep catalysts all have nearly equal (Re) or lower (Ru and Pt) nonlinear fit E_A values than their corresponding seq-dep catalysts. In the case of Pt, the E_A for co-dep is lower even than the unpromoted catalyst.

Table 5-9. Fixed bed reaction conditions and activity/selectivity data for 3 co-dep catalysts

Co/Pt-co (w_{cat} = 0.258 g)						
Temp (^oC)	F_{CO} (mmol/hr)[b]	X_{CO}	$-r_{co}$ (mmol/g_{cat}.hr)[c]	P_{CO} avg (psi)	P_{H2} avg (psi)	S_{CH4}
164	15.87	7.73%	4.77	32	137	3.0%
173	15.87	11.16%	6.88	32	136	4.9%
184	15.87	16.61%	10.24	31	135	9.2%
194	15.87	25.52%	15.74	30	133	13.9%
Co/Pt-co (w_{cat} = 0.250g[a])						
200	21.83	23.64%	20.64	36	146	13.5%
185	21.83	13.51%	11.80	38	148	7.9%
170	11.30	9.90%	4.47	39	149	11.5%
Co/Re-co (w_{cat} = 0.258 g)						
Temp (^oC)	F_{CO} (mmol/hr)[a]	X_{CO}	$-r_{co}$ (mmol/g_{cat}.hr)[b]	P_{CO} avg (psi)	P_{H2} avg (psi)	S_{CH4}
162	15.87	2.87%	1.77	33	138	6.0%
172	15.87	4.98%	3.07	33	138	7.0%
182	15.87	10.78%	6.65	32	137	10.5%
192	15.87	18.30%	11.28	31	135	14.8%
203	15.87	27.29%	16.83	29	133	20.8%
213	15.87	40.31%	24.86	27	130	29.4%
Co/Ru-co (w_{cat} = 0.252 g)						
Temp (^oC)	F_{CO} (mmol/hr)[a]	X_{CO}	$-r_{co}$ (mmol/g_{cat}.hr)[b]	P_{CO} avg (psi)	P_{H2} avg (psi)	S_{CH4}
187	15.50	9.41%	5.81	32	137	12.9%
193	15.50	12.52%	7.72	31	136	15.1%
198	15.50	17.17%	10.59	31	135	18.1%
203	15.50	31.01%	19.13	29	132	29.0%
Co/Ru-co (w_{cat} = 0.250 g[a])						
170	5.85	6.84%	1.59	39	149	13.7%
185	14.34	7.62%	4.35	39	149	7.3%
200	14.34	15.94%	9.10	38	148	15.9%

[a] Two runs

[b] Initial CO molar flow rate

[c] Calculated using $-r'_{CO} = \frac{X_{CO} * F^o_{CO}}{W_{cat}}$, (3-13)

Table 5-10. E_A values from nonlinear and linear regression

	E_A ($kJ \cdot mol^{-1}$)		A ($mol/g_{cat}.min.psi^{0.5}$)	
Catalyst	**Nonlinear**	**Linear**	**Nonlinear**	**Linear**
Co	78	80	4.6E+03	8.5E+03
Co/Pt-co	73	74	2.5E+03	3.6E+03
Co/Pt-seq	105	115	4.1E+06	5.9E+07
Co/Re-co	104	107	6.4E+06	1.2E+07
Co/Re-seq	101	124	1.1E+06	3.9E+08
Co/Ru-co	90.1	110	10.0E+04	2.0E+07
Co/Ru-seq	113	113	2.8E+07	2.8E+07

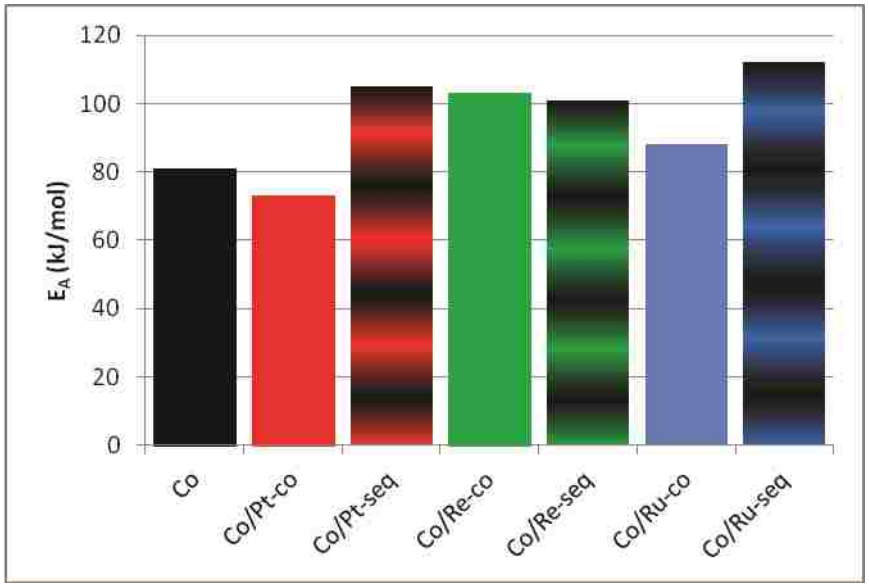

Figure 5-7. E_A for each catalyst

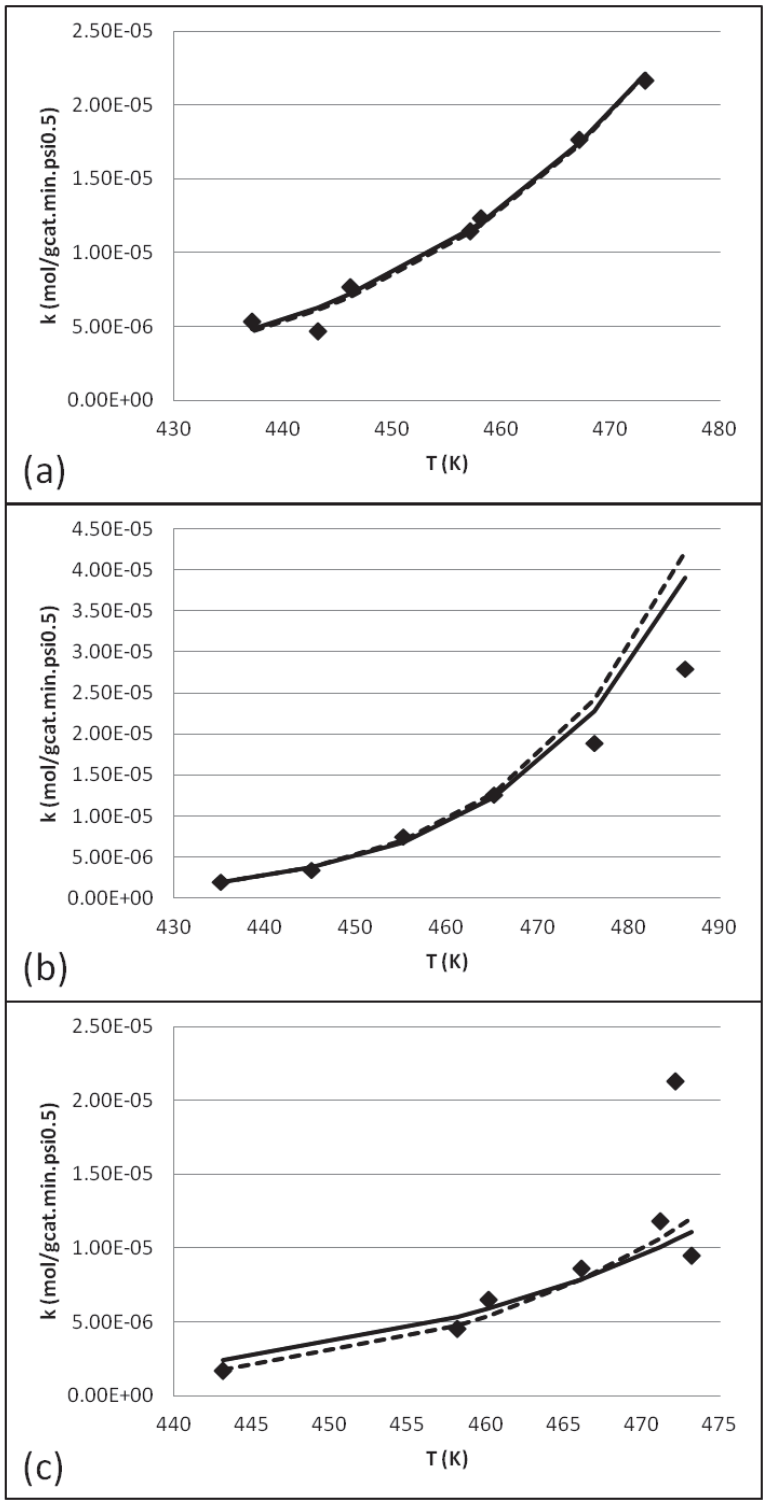

Figure 5-8. Rate constant versus temperature with nonlinear regression fit as solid curve and linear regression fit as dashed curve for (a) Co/Pt-co, (b) Co/Re-co, and (c) Co/Ru-co catalysts

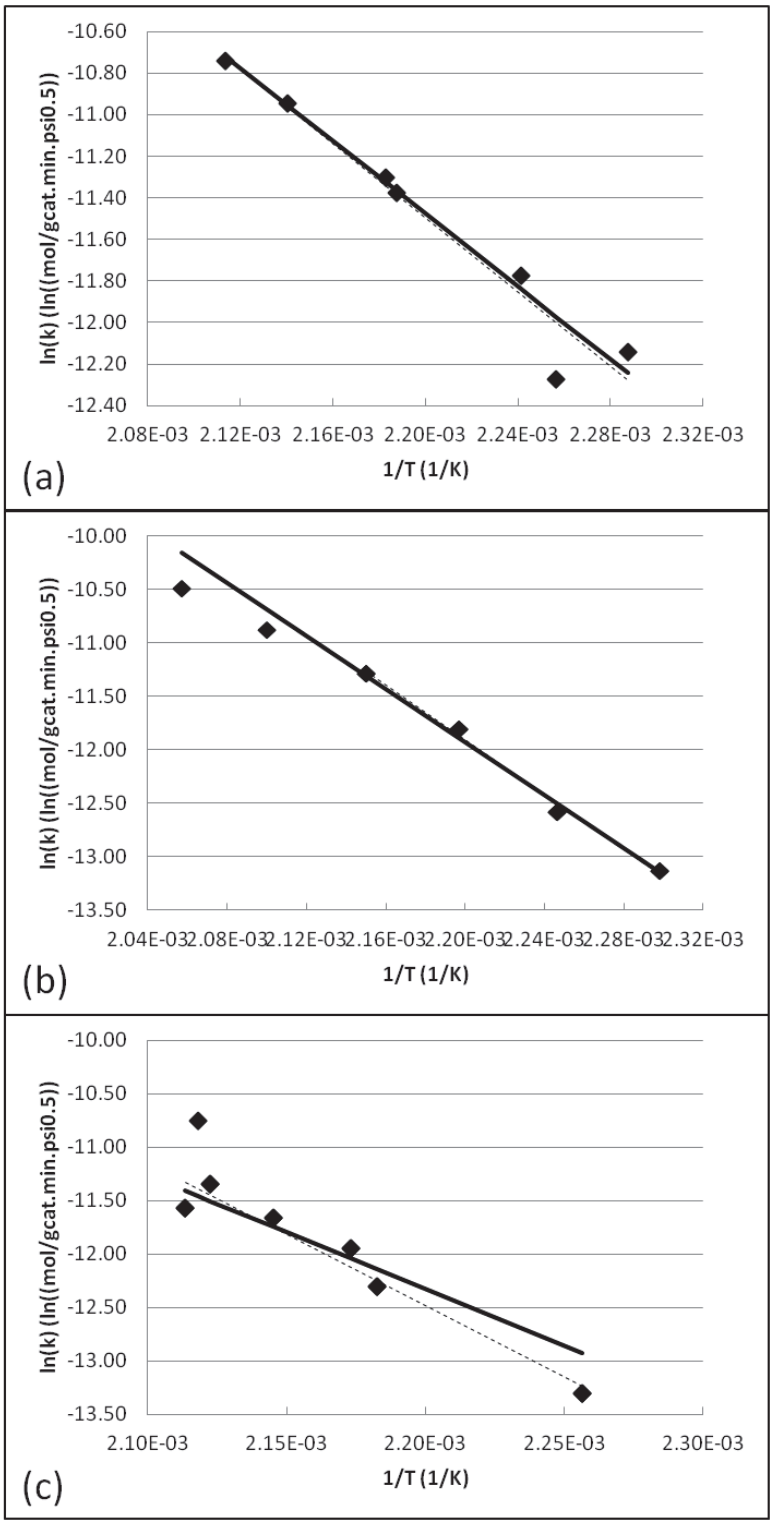

Figure 5-9. Linearization to ln(k) vs 1/T with the nonlinear fit (solid line) and linear fit (dashed line) for (a) Co/Pt-co, (b) Co/Re-co, and (c) Co/Ru-co catalysts

To compare activity and selectivity data at a standard set of conditions, the nearest data point to 200°C for each catalyst was normalized to 200°C, P_{CO} of 2.1 bar (30 psia), and P_{H2} of 9.0 bar (130 psia) and the resulting rate data are given in Table 5-11. The temperature adjustment was made using the nonlinear E_A values in Table 5-10 and partial pressure adjustments were made using $-r'_{CO} = k * P_{H2}^{0.7} * P_{CO}^{-0.2}$, (3-15). Conversion is also given as an index to which data were used from Table 5-9and Table 4-7. [It should be noted that the alternate and somewhat common way of normalizing data to a given temperature is by using an E_A of 100 kJ/mol (Ribeiro 1997). The–r_{CO} given in Table 5-11 (using the nonlinear fit A and E_A) are within 0.3 $mmol \cdot g_{cat}^{-1} \cdot h^{-1}$ to the values generated using 100kJ/mol except in the case of Co where the 100kJ/mol approximation yields 11.4 (the data point being at 200°C for Co/Pt-co allowed for the normalization to require only P_{CO} and P_{H2} adjustments).] An examination of the normalized –r_{CO} values shows that deposition order's affect on rate is significant, Co/Pt-co>Co/Re-co>Co≥Co/Ru-co≥Co/Pt-seq≥Co/Ru-seq≥Co/Re-seq. After normalization, the co-dep catalysts are all more active than all the seq-dep catalysts. This activity trend is made particularly apparent by Figure 5-10. The figure also shows that the Co catalyst was actually more active than the Co/Ru-co as a function of temperature under the fixed bed conditions of this study and that the Co catalyst was as active as the Co/Re-co catalyst below 170°C. Thus it is just the Pt promoted catalysts that shows a deposition order trend such that the co-dep>unpromoted>seq-dep across the entire temperature range. Re promotion does show this trend for all temperatures above 170°C and the co-dep catalysts are always more active than the corresponding seq-dep. Table 5-11 shows TOF data which indicate the same deposition order trend as the rate values—co-dep > corresponding seq-dep catalyst. Table 5-11 also specifies the

methane selectivity values for each catalyst. The co-dep are lower than seq-dep with Ru and Pt promotion, but the same with Re.

Table 5-11. Comparison of activity by normalizing to 200°C, P_{CO} of 2.1 bar (30 psia), and P_{H2} of 9.0 bar (130 psia)

Catalyst	X_{CO}[a]	$-r_{CO}$[b]	TOF[c] x 10^3	S_{CH4}
	(%)	(mmol·g_{cat}^{-1}·h^{-1})	(s^{-1})	(%)[a]
Co	19.9%	12.0	-	15%
Co/Pt-co	23.6%	19.8	9.23	14%
Co/Pt-seq	18.3%	9.7	5.37	22%
Co/Re-co[d]	18.3%	18.1	9.34	21%
Co/Re-seq	12.0%	7.6	3.47	21%
Co/Ru-co[e]	17.2%	11.8	7.51	18%
Co/Ru-seq	10.9%	8.8	8.17	22%

[a] from closest data point to 200°C
[b] adjusted to T=200°C, P_{CO}=30 psia, P_{H2}=130 psia using A and E_A nonlinear fit of data
[c]TOF based on H_2 uptake after reduction(at the beginning of reaction) and neglect any further reduction of Co oxides to Co active sites with time on reaction stream.
[d]data point at 192°C used to predict activity (X_{CO}, $-r_{CO}$, and TOF) , but data point 203°C though above 25% conversion is likely more representative of methane selectivity (S_{CH4})
[e]data point at 198°C most representative of expected activity at 200°C

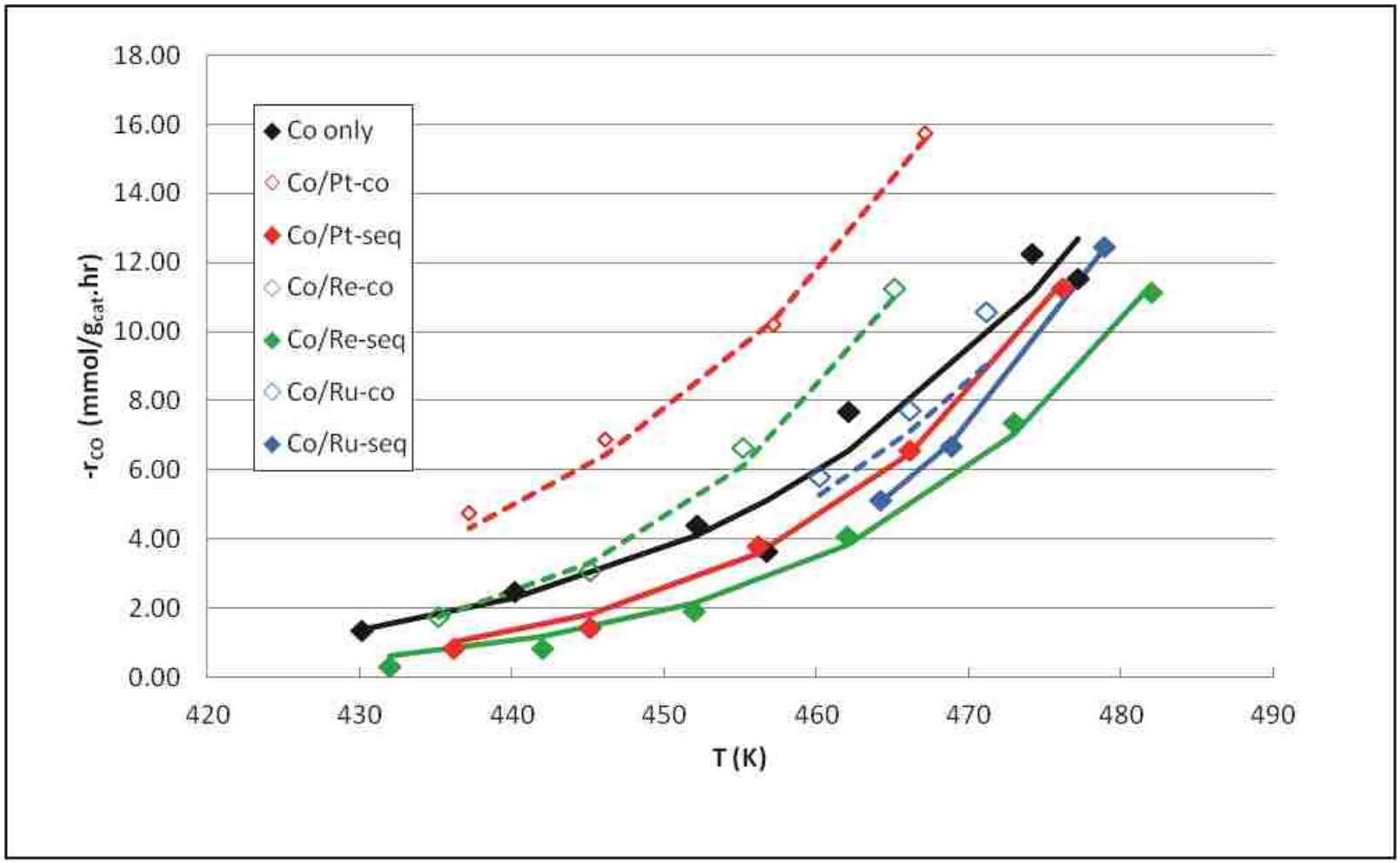

Figure 5-10. Rate as a function of temperature showing data with initial condition of P_{CO} of 30 psia and P_{H2} of 126 psia

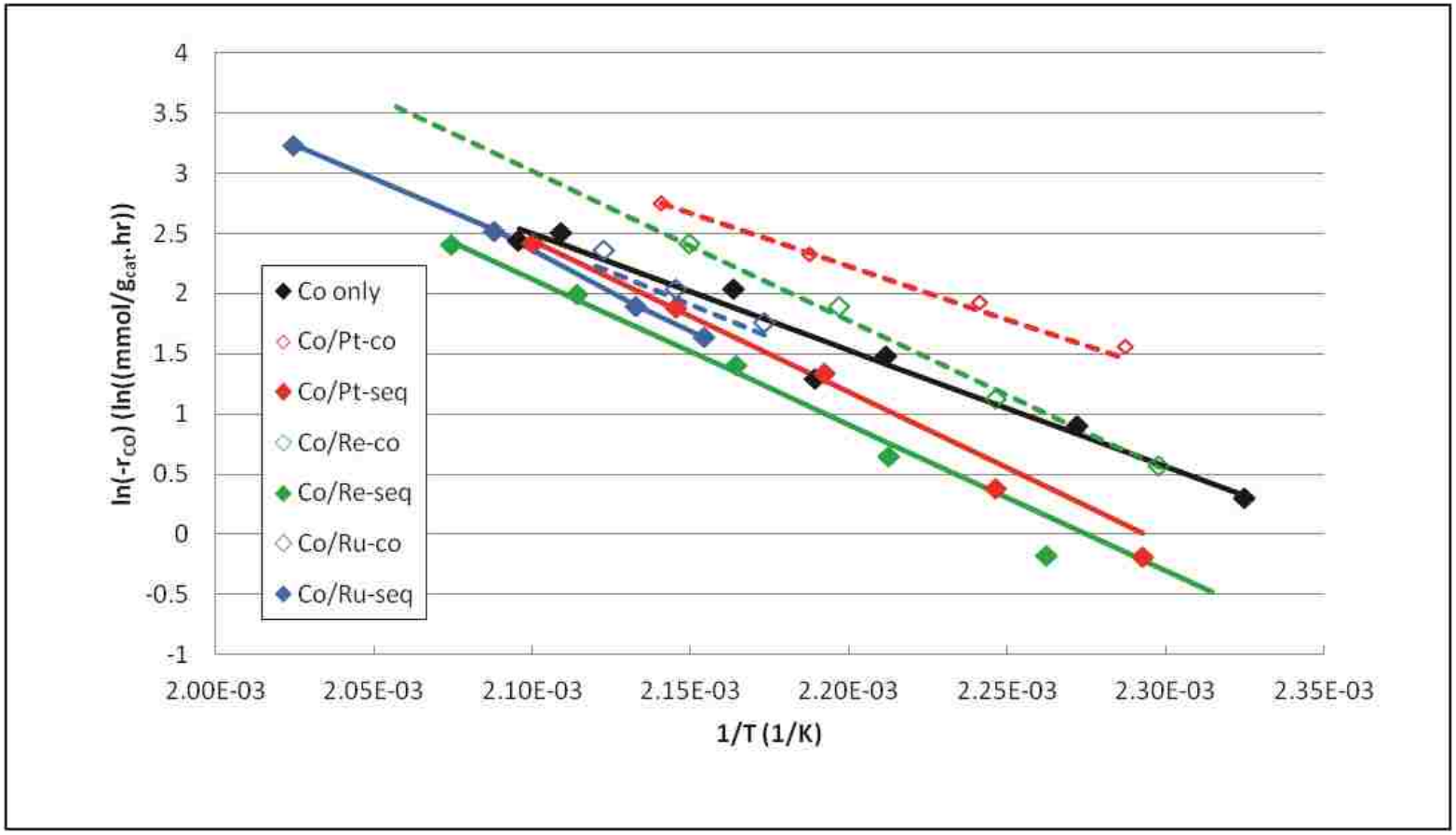

Figure 5-11.a Linearization to ln(rate) vs 1/T showing data with initial condition of P_{CO} of 30 psia and P_{H2} of 126 psia

5.3 Discussion

While the results presented in this chapter are qualitatively consistent with literature they also provide fresh new insights into the effect of deposition order (including the related effects of thermal treatments and NM precursor) on the properties and performances of Co FT catalysts. In the ensuing discussion of these results, it will be demonstrated that catalyst properties most greatly influenced by these variations in preparation procedure include (1) Ru retention; (2) Ru and La distribution; (3) Co crystallite size; (4) Co reducibility; and (5) catalyst activity.

5.3.1 Ru Retention

The results of chemical analysis provide direct evidence of substantial Ru losses during drying and calcination treatments (see Table 5-3 and Table 5-4). Moreover substantial losses for co-dep and seq-dep (Table 5-3) are correlated with deposition order; a greater loss (of 85%) with co-deposition occurs relative to that (53%) for sequential deposition. This greater loss for co-deposition is consistent with the hypothesized loss of volatile RuO_4 via (1) its formation in a nitric acid solution created by Co nitrate hydrolysis and containing Ru ions; and/or (2) by room temperature reaction of $Ru(OH)_3 \cdot nH_2O$ with Cl ions as discussed in Section 4.4.1.1. Since during co-dep, Co nitrate is added with the Ru chloride both nitric acid and chlorine routes are likely with co-dep and thus greater RuO_4 formation would be expected than with seq-dep in which the calcination of Co nitrate to an oxide happens before Ru deposition; thus only the chlorine route to RuO_4 formation is likely.

Results for catalysts prepared with variations in drying and impregnation provide further insight into Ru loss during. Figure 5-12 shows the Ru retention (%) for the Co/Ru-co, Co/Ru-IW-RE/120, and Co/Ru-seq catalysts. When dried in RE to 60^{o}C and then to 120^{o}C in flowing air

before sequential incipient wetness impregnation of Ru chloride (Co/Ru-IW-RE/120, center bar in Figure 5-12), 32% of the Ru was retained rather than to 15% for co-dep and 46% for seq-dep (60^{o}C and 120^{o}C drying as well as calcination to 250^{o}C between Co and Ru depositions). This suggests that the nitric acid route to RuO_4 occurs partially during concurrent 120^{o}C drying and partially during concurrent calcination. When only RE drying was done between the final Co deposition and the incipient wetness Ru deposition (Co/Ru-IW-RE), Ru loss was statistically equivalent to that of the co-dep catalyst and shows that RE drying between depositions does not facilitate Ru retention. The two thermal treatment variation catalysts which used wet Ru deposition (Co/Ru-Aq-RE and Co/Ru-Aq-RE/120) have Ru loss as extreme as or greater than the co-dep catalyst likely due to redissolving of Co nitrate and hydrolysis which lowers pH, thus facilitating the nitric acid route to RuO_4 formation). ICP data for the Co/Ru(N)-seq catalyst shows the best retention (76%). Thus Ru loss can be at least partially overcome by choosing a precursor that avoids oxidation by the chlorine route. In addition, Ru is retained by doing a 120^{o}C drying or even better 250^{o}C calcination after the final Co deposition and before Ru deposition.

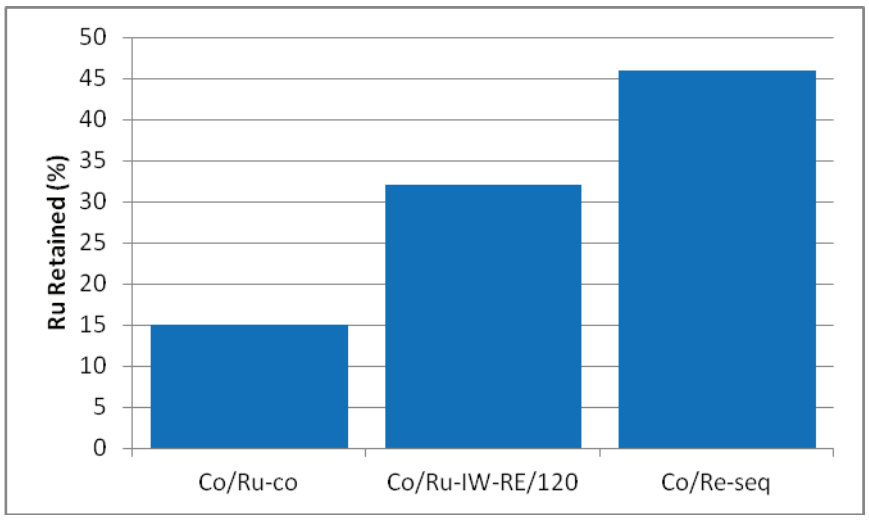

Figure 5-12. NM addition and thermal treatment effect on Ru retention (%)

5.3.1 Ru and La Distribution

SEM and electron microprobe data show that Ru and La concentrate at the pellet edge with seq-dep but not co-dep of Ru. This observation suggests that the Ru and La concentration gradients are a result of exposure to the Ru only deposition solution and literature provides likely explanations for the mechanisms of both Ru and La gradient formation with exposure aqueous $RuCl_3$ deposition.

(1) Ru has been shown to precipitate from $RuCl_3$ solutions when the pH is rapidly increased (Delmon, Grange et al. 1978). When the $RuCl_3$ solution was poured over the 25wt% Co γ-Al_2O_3 pellets its pH was below the point of zero charge for the γ-Al_2O_3 (Pinna 1998) and the surface OH groups gained H^+ from the deposition solution thus increasing the solution pH causing precipitation of Ru from solution. Delmon et al. showed that this precipitated Ru does not always uniformly distribute across the catalyst (Delmon, Grange et al. 1978).

The initial strong acid exposure likely resulted in the La gradient as (1) strongly adsorbed La has been shown to desorb and redistribute as a result of exposure to a strong acid(Zhai and Chen 2011).; moreover the La was uniformly distributed before exposure to the acidic deposition solution. In fact, La redistribution and concentration at the pellet edge (as in this study) in the presence of a strong acid, e.g. $H_2C_2O_4$ has been observed (Zhai and Chen 2011).

The thermal treatment variation catalysts provide two more pieces to the puzzle of understanding these gradients. (1) The La gradient is observed in the seq-dep catalysts that were only dried in the RE after the final Co deposition and before the Ru deposition while the Ru gradient is observed only in the seq-dep catalyst which was dried in the RE and thereafter in flowing air at 120^{o}C. These observations demonstrate that the Ru and La gradients are not connected by causation and. This conclusion is consistent with the prediction based on the lack of bonding proximity of Ru and La in the XAFS results. (2)That incipient wetness impregnation of Ru by sequential deposition causes a more extreme Ru gradient is consistent Murrell and Yates work and with the hypothesis that the Ru gradient is due to Ru precipitation from the pH increase and then Ru deposition at the pellet edge. Indeed Murrell and Yates showed that Ru precipitates from solution and deposits with a more extreme concentration gradient (Ru was only found in the outer 1/3 shell of the catalysts) when a quasi-incipient wetness preparation, while with wet deposition the Ru non-uniformity was less extreme (Delmon, Grange et al. 1978).

5.3.2 Co Crystallite Size

The Co oxide crystallite sizes for the Re and Pt promoted catalysts are larger for the co-dep than seq-dep. These differences in the Co oxide crystallite size are likely tied to variations in protonation of hydroxide groups on the Al_2O_3 surface with the pH of the deposition solution and

thus different strengths of Co adsorption (Regalbuto 2007). It is hypothesized that the pH of the co-dep solution of NM and Co results in protonation of the Al_2O_3 hydroxide groups (due to acidity) such that stronger oxide-oxide bonds form during the co-calcination. While it is reasonable to suppose that the Al_2O_3 surface would be completely covered with Co oxide after calcination at 20wt% (before the Co and NM co-deposition), the TEM EDS scans of the calcined final catalysts show Co oxide crystallites as well as blank Al_2O_3 suggesting that after calcination of the 20wt% Co deposition there would be available Al_2O_3 and thus locations for this Al_2O_3 hydroxide group protonation. This hypothesis is consistent with the tailing from the CSD above about 7 nm size after calcination , as shown in Figure 5-14 (black distribution), because stronger bonds would result in Co oxide crystallites that spread further (into thin rafts) on the Al_2O_3 surface. Additionally the disappearance of this tailing with reduction (also shown in Figure 5-14 by comparing the black and grey distributions) is consistent as these thin rafts are more likely to break apart and/or more extremely ball-up rather than just shrink due to molar volume decreases when O is lost by reduction to Co metal, especially since Co metal has higher surface energy and weaker interactions with the Al_2O_3 support (Ruckenstein and Hu 1986; Barthlomew 1993). In fact the decrease in volume mean ACD for all co-dep catalysts was more extreme than the corresponding seq-dep catalysts (and expectation), see Figure 5-13. This is particularly significant for Re promotion as the seq-dep catalyst actually showed Co crystallite growth with reduction.

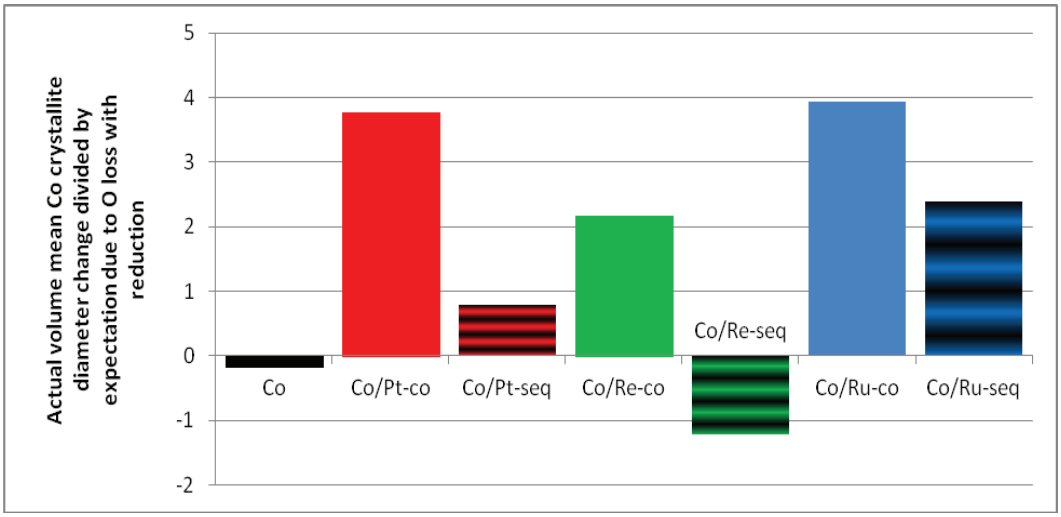

Figure 5-13. Comparison of actual volume mean Co crystallite diameter change divided by expectation due to O loss with reduction

An unexpected crystallite size result is that all three co-dep catalysts have surface averaged ACD's of 4.2±0.1 nm and nearly the same as the unpromoted (4.7nm) despite significantly different Co oxide ACD (6.1 to 13.6 nm). Additionally, the CSD of the co-dep catalysts are very similar, Figure 5-14, after reduction (though slightly shifted in the case of Co/Re-co). This sameness and repeatability of co-dep catalyst Co crystallites size suggests the opportunity to tune to optimal size and justifies additional examination to optimize the crystallite size and study the relationship between the calcined and reduced state. In addition, the agreement between the H_2 chemisorption predicted and TEM measured Co crystallite diameters shows promise.

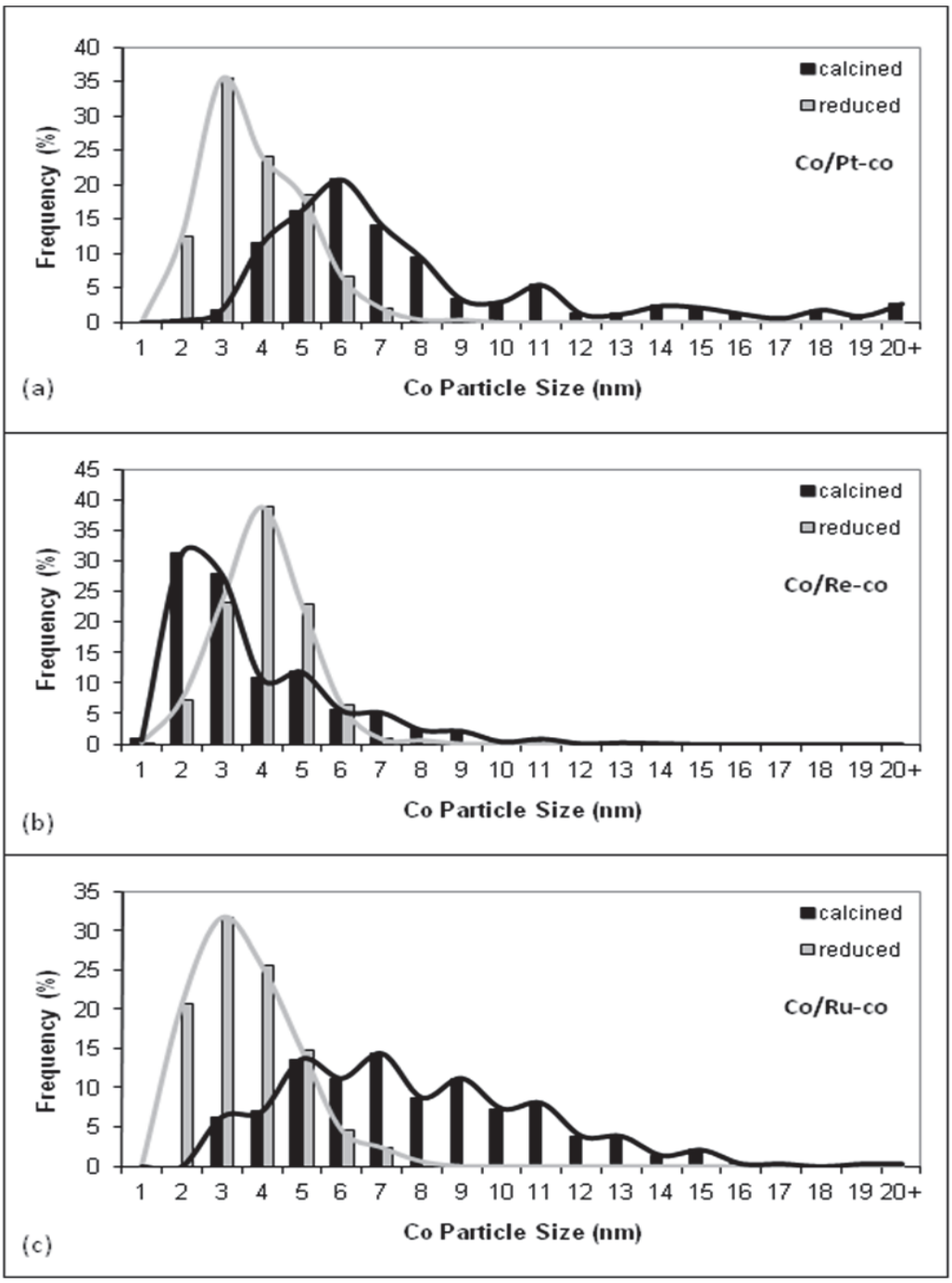

Figure 5-14. Histogram comparing Co crystallite diameter distributions after calcination (black) and reduction (grey) Co/Pt-co (a) , Co/Re-co (b), and Co/Ru-co (c) catalysts.

5.3.3 Reducibility

The second main TPR profile peaks of the co-dep (especially Ru and Re promoted) catalysts are shifted to lower reduction temperatures than the corresponding seq-dep catalysts by 10-40^{o}C. This is consistent with the research of Iglesia which states that calcination of NM and Co precursors together increases intimate contact between the NM and Co in the final catalyst and thus reduction promotion (Iglesia 1993). The TPR of the Pt pomoted catalysts shows only slight differences between co-dep and seq-dep suggesting that Pt's ability to further promote Co reduction is minimal when co-deposited. This is likely a result of the formation of direct Pt-Co bonds even with seq-dep and no notable increase in the NM-Co contact suggested by Iglesia and thus no notable increase in Pt's ability to promote Co reduction. Thus, while the TPR profiles illustrate that co-dep catalysts are more reducible than seq-dep, the significance of the deposition order effect on TPR behavior is NM type dependent.

The deposition order effect on reducibility in terms of EOR is opposite—the co-dep catalysts have lower EOR by 10-15% (Table 5-8) than the corresponding seq-dep catalysts. The smaller Co crystallites seen after reduction with co-dep compared to seq-dep provide a clear explanation—the lower EORs are likely a result of forming smaller CoO crystallites during the $Co_3O_4 \rightarrow CoO$ step, because literature shows that more highly dispersed (smaller) crystallites interact more strongly with the support and have lower EOR (Reuel and Bartholomew 1984). The fraction of crytallites below 6 nm is plotted versus EOR in Figure 5-15 and illustrates this correlation of lower EOR resulting when particles below 6 nm are more abundant.

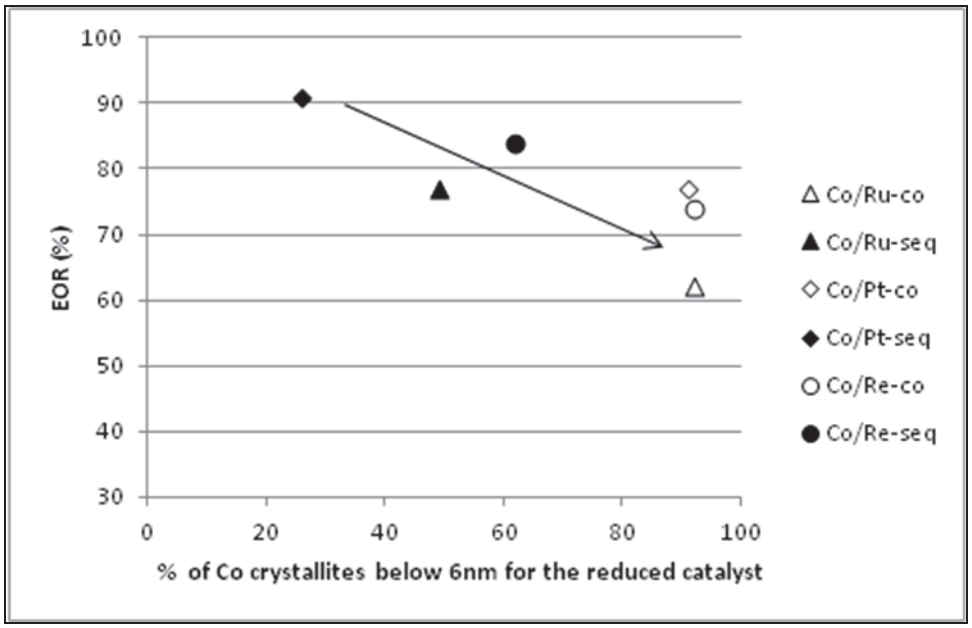

Figure 5-15. Plot of EOR as a function of % of reduced catalyst Co crystallites below 6 nm showing a decrease in reducibility with an increase in abundance of small particles

The Co dispersion (%D) data showed that the Co metal for all three co-dep catalysts and even Co/Re-seq is twice (~20%) as dispersed as the Co metal in the unpromoted, and Co/Ru-seq catalysts (~10%) and 50% more dispersed than the Co/Pt-seq catalyst. Thus, Co dispersion increase due to NM addition (Khodakov, Chu et al. 2007) requires co-dep if Ru and is more extreme by co-dep if Pt are used as the promoter, but happens to the same extent with either deposition order for Re.

5.3.4 Activity

The data given in Section 5.2 show that the all co-dep catalysts are more active per gram than cooresponding seq-dep catalysts by 35-135%, see Figure 5-19. For the Co/Pt (Figure 5-16) and Co/Re (Figure 5-17) catalysts the depostiion order difference in activity is statistically significant—the 90% confidence intervals do not overlap. The difference for the Co/Ru

catalysts is not statisically significant, Figure 5-18. In the case of Co/Pt, the co-dep catalysts is statisically more active than the unpromoted catalyst by 65%, Figure 5-16. It is possible that the extreme loss of Ru is hindering the same trend from being apparent for Ru when co-deposted, though the increase activity with 0.1wt% Ru shown in a Gulf patent suggests is more than poor retention that affected Ru ability to promote FTS activity (Beuther, Kobylinski et al. 1986). The increased activity per gram with co-dep fits with the higher H_2 uptake measurements of active sites compared to the seq-dep catalysts for Ru promotion—showing a higher activity due to more active sites. Additionally, it fits with Khodakov's suggestion that higher activity has been attributed to increased dispersion not just increased reducibility, because Co/Pt-co and Co/Ru-co have higher dispersion than the unpromoted as well as corresponding seq-dep catalysts (Khodakov, Chu et al. 2007).

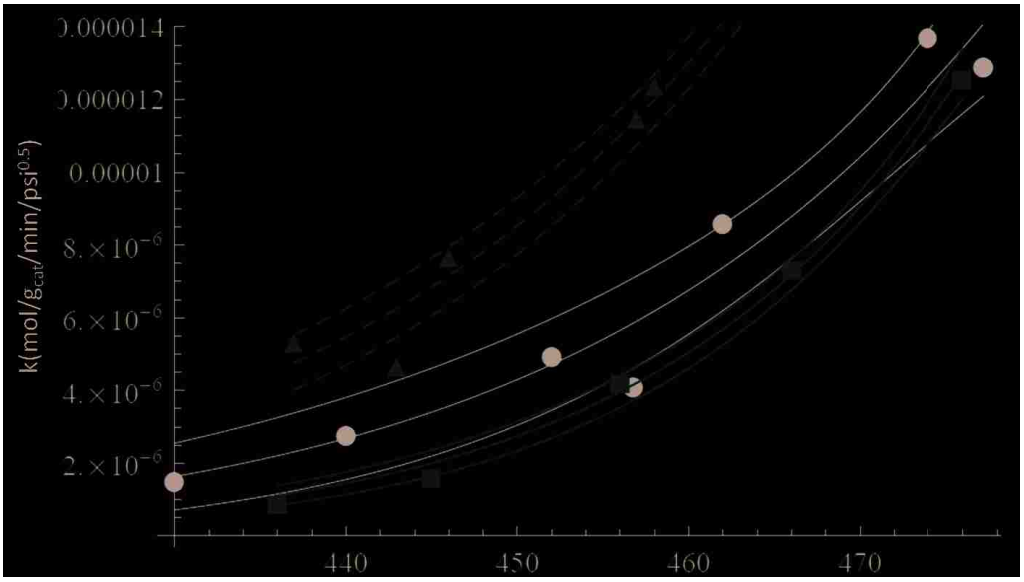

Figure 5-16. k as a function of temperature for Co/Pt-seq (red, solid), Co/Pt-co (red, dashed), and Co only (black) catalysts with the nonlinear fit as the center line and the 90% confidence interval for the fit as the outer lines for each catalyst

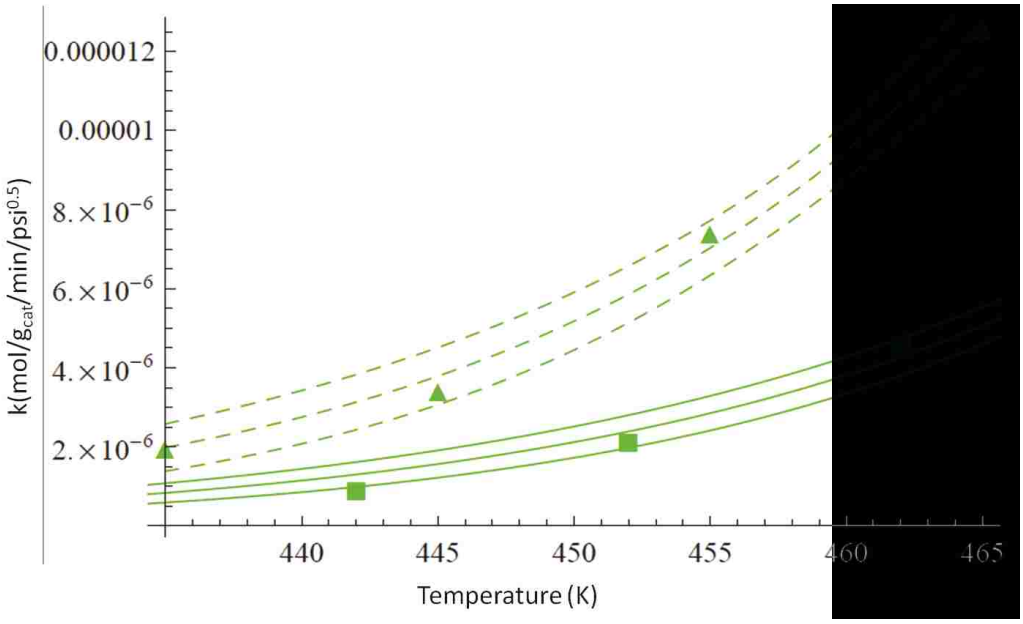

Figure 5-17. k as a function of temperature for Co/Re-seq (solid) and Co/Re-co (dashed) catalysts with the nonlinear fit as the center line and the 90% confidence interval for the fit as the outer lines for each catalyst

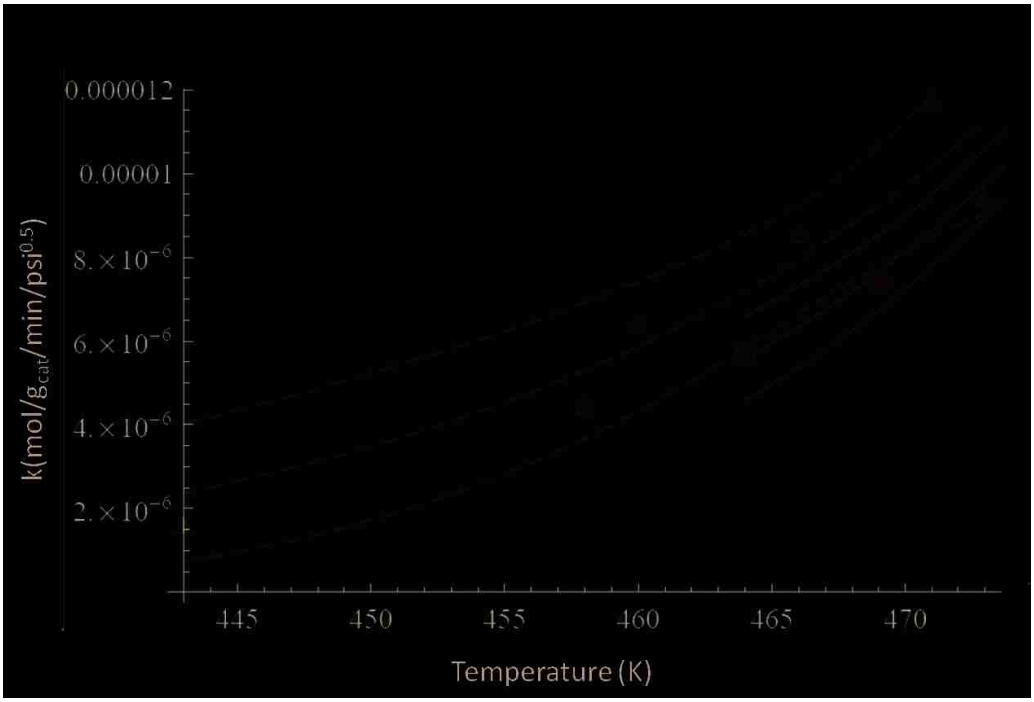

Figure 5-18. k as a function of temperature for Co/Ru-seq (solid) and Co/Ru-co (dashed) catalysts with the nonlinear fit as the center line and the 90% confidence interval for the fit as the outer lines for each catalyst

Table 5-12. Rate and turn over frequency extrapolated to typical reaction conditions (50% conversion, 20 atm, 200°C and 2:1 H_2:CO) along with H_2 uptake and TEM measured surface averaged crystallite diameter for comparison

Catalyst	H_2 Uptake (μmol/g)	Surface Avg d (nm)	$-r_{CO}$ ($mmol \cdot g_{cat}^{-1} \cdot h^{-1}$)[a]	TOF x 10^3 (s^{-1})[a]
Co	65	4.7±1.5	8.1	-
Co/Pt-co	297	4.3±1.3	15	7.01
Co/Pt-seq	251	8.0±2.2	7.3	4.06
Co/Re-co	268	4.2±1.1	13.1	6.78
Co/Re-seq	302	4.9±1.6	5.4	2.47
Co/Ru-co	219	4.1±1.2	7.5	4.78
Co/Ru-seq	150	6.7±1.8	6.7	6.19

[a]Turnover frequency in molecules of CO converted per catalytic site per second and conversion rate calculated at 50% CO conversion, 20 bar, H_2:CO=2 (P_{CO}=48.3 psi and P_{H2}=96.7 psi)

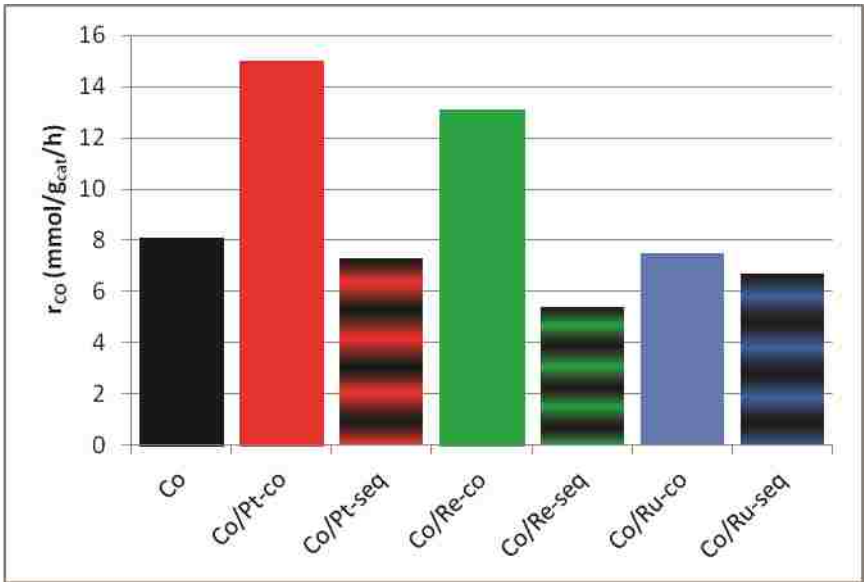

Figure 5-19. Rate at 50% conversion, 20 bar, H_2:CO = 2 (P_{CO} = 48.3 psi and P_{H2} =96.7 psi)

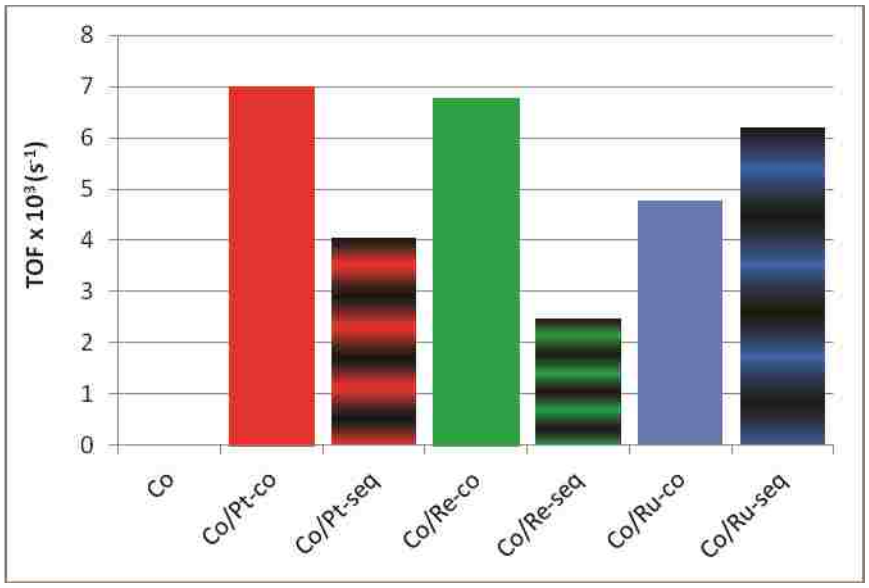

Figure 5-20. TOF at 50% conversion, 20 bar, H_2:CO = 2 (P_{CO} = 48.3 psi and P_{H2} =96.7 psi)

With Re and Pt promotion, the co-dep catalysts have higher TOF than their corresponding seq-dep catalysts, Figure 5-20. Thus the increased activity is not due to higher abundance of active sites (especially since in the case of Re the co-dep catalyst has a lower H_2 uptake), but rather a greater activity per site. The higher TOF for Co/Pt-co is somewhat surprising as the ACD is only 4.3nm with 91% <6nm compared to 8.0 nm with 26% < 6 nm for Co/Pt-seq, because literature shows that crystallites below 6nm have lower TOF (Bezemer, Van Dillen et al. 2005; Bezemer, Bitter et al. 2006). This difference suggests Bezemer's results for unpromoted Co catalysts apparently do not extent to our study of *promoted* Co catalysts, but they did apply when only comparing seq-dep catalysts amongst themselves (Section 4.4.3). Their explanation for the decrease in TOF with a decrease in particle size is suggested to be blockage of edge and corner sites with irreversibly adsorbed CO as well as lower intrinsic activity to the planar sites (den Breejen, Radstake et al. 2009). It is possible that either one or both of these

mechanisms of lower TOF are in some way overcome by NM addition, but also that the particle size effect is not general. The 'protective effect' of inhibiting carbon deposition during FT reactions seen by Iglesia (Iglesia 1997) suggests that NMs may hinder blockage of the edge and corner sites. In addition, it is also possible that La is influencing CO dissociation and thus allowing for increased TOF as La has been shown to enhance CO dissociation in NM systems (Kildemo, Ramsvik et al. 2002). The results of this study indicate that either the 6-12 nm "ideal" range for Co crystallite is not applicable as Johnson et al.'s work showed Co hydrogenation is crystallite size insensitive (Johnson 1989; Johnson 1991), or the differences based on particle size are in some way overcome by other differences resulting from promotion (NM and La) and variation in NM deposition order. It is likely that differences in %D and EOR are also affecting the TOF. Figure 5-21 shows the TOF as a function of EOR and Figure 5-22 shows the TOF as a function of %D. The TOF of the co-dep catalyst increase with EOR until around 70% EOR where there is a plateau effect matching the finding for Johnson et al. Alternatively the TOF of the seq-dep catalyst match the decrease with %D expected based on the same work (Johnson 1989).

The lower methane selectivity for Pt and Ru when co-deposited shows evidence of significant promoter effects to another generally accepted crystallite size trend that smaller particles resulting in higher methane selectivity, because the Co/Pt-co and Co/Ru-co catalysts has smaller crystallites and lower methane selectivity than their sequentially-deposited counterparts. This offers confirming evidence that NM addition and deposition order variation affect the applicability of generally accepted Co crystallite size activity/selectivity effects.

It should be noted that comparison of fresh catalyst characterizations of EOR, %D, and Co crystallite size with properties after 50^{+} h of reaction may not show the expected trends as

catalysts were probably further reduced during reaction and hence EOR, %D, and Co crystallite size would be different for the aged catalysts. In addition, there are possible errors in H_2 chemisorption uptakes (and thus %D) due to probable spillover from the support (Harrison and Hecker 2012).

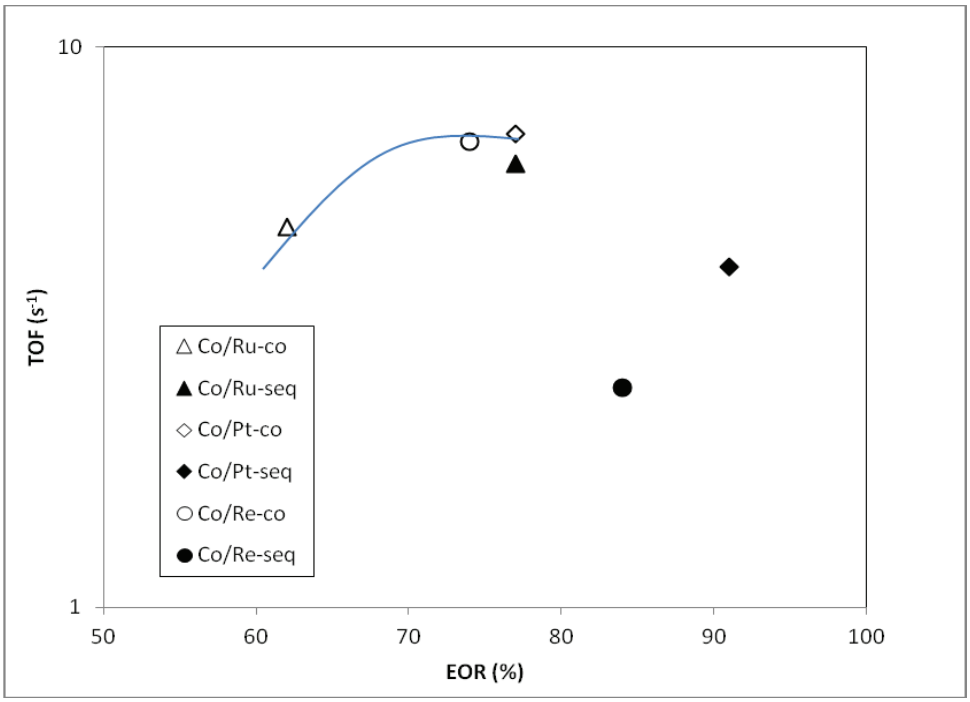

Figure 5-21. TOF at 50% conversion, 20 bar, H_2:CO = 2 (P_{CO} = 48.3 psi and P_{H2} =96.7 psi) as a function of EOR

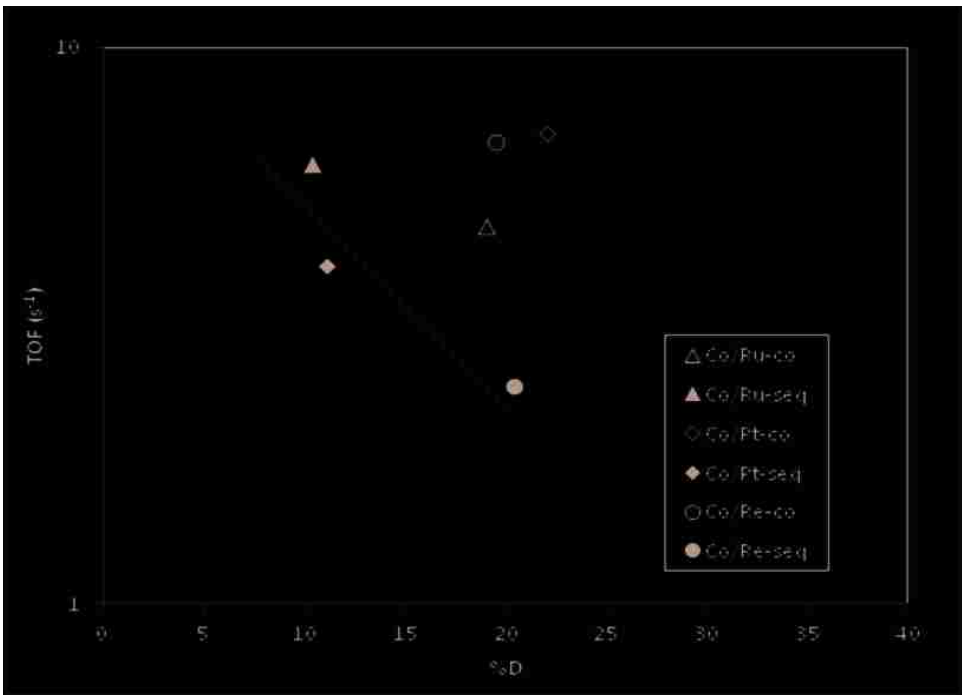

Figure 5-22. TOF at 50% conversion, 20 bar, H_2:CO = 2 (P_{CO} = 48.3 psi and P_{H2} =96.7 psi) as a function of %D

5.4 Conclusions

The effects of NM deposition order on (i) metal retention, (ii) spatial distribution of NM and Co phases, (iii) NM bonding and oxidation state, and (iv) Co crystallite size and the subsequent effects of these properties on Co reducibility and activity were investigated. The results of these studies are consistent with the following main conclusions.

1. The Ru promoted catalysts lost significant amounts of Ru. This loss was more extreme with co-dep (85%) than seq-dep (53%). Retentions for the other NM's (Pt and Re) and Co were good (statistically negligible loss).
2. Unlike the poor La and Ru spatial distribution seen with Co/Ru-seq, the Co/Ru-co catalysts showed uniform distribution of all metals. Co, Pt, and Re were always

distributed uniformly. La was also uniform in the unpromoted, Pt, and Re promoted catalysts.

3. The co-deposition method produced catalysts with smaller Co crystallites than the seq-dep method and nearly all Co crystallites' diameters were <6 nm after reduction at 360^{o}C. In fact all three co-deposited catalysts had a surface averaged ACD of 4.1- 4.3 nm compared to the values of 8.0, 6.7, and 4.9 nm for Co/Pt-seq, Co/Ru-seq, and Co/Re-seq, respectively.
4. The predominant NM bonding following mild reduction (1 h in 4%H_2 at 360^{o}C) did not show a deposition order effect as measured by XAFS. Pt, Ru, and Re promotion by both deposition orders resulted in the formation of surface bimetallic Pt-Co bonds, Ru-Ru metal bonds, and Re-O bonds (characteristic of unreduced Re oxide) respectively.
5. The temperature required for reduction of the calcined catalysts to Co metal is lower for co-dep catalysts than seq-dep for all NMs by 10-40^{o}C, as seen by downward shifts in the temperatures of the second main peak in the TPR profiles.
6. Extents of reduction for the co-dep catalysts are lower than seq-dep.
7. The CO depletion rates per gram for the Pt and Re co-dep catalyst are statistically higher than their corresponding seq-dep catalysts. When normalized to typical reaction conditions, they are higher by 140, and 100% for Re, and Pt, respectively. The small difference with Ru (co-dep only 20% more active than seq-dep when normalized to typical reaction conditions, which is not statistically different) is likely due to extremely poor Ru retention with co-deposition.
8. With Pt and Re promotion, the TOF of the co-dep catalysts are higher than the seq-dep catalysts by 70-80%.

9. In the case of Pt the TOF of the co-dep catalyst is higher even with a surface averaged ACD of only 4.3 nm and 91% < 6 nm compared to 8.0 nm and 26% < 6 nm for the seq-dep, which indicates that either the 6-12 nm "ideal" range for Co crystallite is not quantitatively applicable likely due to differences in %D and EOR which also affect the TOF.
10. The methane selectivities of the co-deposited catalysts were lower or the same as their sequentially-deposited counterparts.
11. The lower methane selectivity for Pt and Ru when co-deposited shows evidence of significant promoter effects to the generally accepted crystallite size trend of smaller particles resulting in higher methane selectivity, because the Co/Pt-co and Co/Ru-co catalysts has smaller crystallites and lower methane selectivity than their sequentially-deposited counterparts. This offers confirming evidence that NM addition and deposition order variation affect the applicability of generally accepted Co crystallite size activity/selectivity effects.
12. The co-dep Pt catalyst is statistically more active than the unpromoted catalyst while its corresponding seq-dep catalyst counterpart is less active.

6 Summary, Conclusions and Recommendations

6.1 Introduction

This work has investigated the effects of NM choice and deposition order on alumina supported Cobalt Fischer Tropsch catalysts. This chapter is organized as follows: First a summary of the observations and results from this study are presented similarly to previous chapters (physical and chemical properties, reducibility, and activity/selectivity). Then, a list of the main conclusions is shown. Finally the recommendations for further study are given.

6.2 Summary of Observations and Results

Deposition order and NM choice have different impacts on the catalyst properties as summarized by the ranges shown in Table 6-1 for physical/chemical properties, Table 6-2 for reducibility properties, and Table 6-3 for activity/selectively properties. For the NM choice column, the range shown in each box is between Pt, Ru, and Re for either co-dep or seq-dep (whichever showed the largest range between the 3NMs). For the deposition order column, the range is between co-dep and seq-dep for either Pt, Re, or Ru (whichever showed the largest range). In the cases where the impact is statistically negligible, S/N is designated in the table

along with the property value. For example, Co weight loading ranges from 20.2 wt% (Co/Pt-seq) to 22.2 wt% (Co/Ru-seq) when the NM is varied, but this difference is statistically negligible, thus the table lists S/N and 20.2 -22.2 (seq).

6.2.1 Physical and Chemical Properties

The physical and chemical properties examined in this study include BET surface area and pore size, metal loadings (retention), metal distribution, Co crystallite size (oxide and metal), and NM bonding structure. These properties are given in Table 6-1. The BET surface area and pore size as well as the Co weight loading and distribution did not show any statistical effects of NM choice or deposition order. The other properties did show NM choice and/or deposition order effects.

The NM retention and loading only showed differences with Ru as the promoter. Pt and Re retention and distribution were within experimental error of the target and uniform, for both deposition orders. Ru, on the other hand, was poorly retained and showed a deposition order trend with 53% loss when sequentially-deposited and 85% loss with co-deposition. Additionally, for the Co/Ru-seq, Ru and La were concentrated at the pellet edge. In contrast, for Co/Ru-co both L and Ru were uniformly distributed. In fact, La was also uniformly distributed in the 5 other (Co only, Re and Pt promoted) catalysts.

Table 6-1.Impact of NM NM choice and deposition order on physical/chemical. Largest range for each category are shown.

Property	NM Choice Range	Deposition Order Range
BET Surface Area (m^2/g)	S/N 96 - 102 (co-dep)	S/N 92 - 102 (Ru)
BET Pore Volume (cm^3/g)	S/N 0.38 - 0.40 (seq-dep)	S/N 0.38 - 0.41 (Ru)
BET Pore Diameter (nm)	S/N 14.3 - 15.6 (seq-dep)	S/N 14.3 - 15.4 (Re)
Co Weight Loading (wt%)	S/N 20.2 – 22.2 (seq-dep)	S/N 21.0 - 21.8 wt (Re)
Noble Metal Retention[a] (%)	15 - 100 (co-dep)	15 - 47 (Ru)
Co Distribution	S/N uniform (all)	S/N uniform (all)
NM Distribution	concentrated at edge – uniform (seq-dep)	concentrated at edge – uniform (Ru)
La Distribution	concentrated at edge – uniform (seq-dep)	concentrated at edge – uniform (Ru)
Calcined Co ACD (nm) measured by TEM	3.8 - 11.2 (seq-dep)	3.8 - 6.1 (Re)
Reduced Co ACD (nm) measured by TEM	4.9 - 8.0 (seq-dep)	4.3 – 8.0 (Pt)
Reduced Co ACD (nm) estimated from H_2uptake	4.6 – 9.1 (seq-dep)	5.0 – 9.1 (Ru)
Reduced Co CSD (% 6-12 nm) measured by TEM	38 – 72 (seq-dep)	9 – 72 (Pt)
NM Bonding	Pt-Co, Ru-Ru, Re_2O_7 (co-dep and seq-dep)	S/N Pt-Co, Ru-Ru, Re_2O_7 (Each NM has same bonding with both deposition orders)

[a]NM comparison based on % of target, because target wt% different for each NM.

Co crystallite size measured by TEM also showed variations with NM and deposition order. The Co oxide particle size varied drastically by NM type (3.8-11.2 nm) and deposition order (3.8-6.1 nm). The larger Co oxide particles resulting with co-deposition suggest that the variation in deposition solution pH by the addition of a NM precursor protonates the Al_2O_3

surface OH groups resulting in stronger oxide-oxide bonds between the Co and support and causing the Co oxides to spread into thin rafts on the support surface. This idea is consistent with the disappearance of the crystallite size distribution (CSD) large particle tailing and the apparent balling up or breaking apart of thin Co oxide rafts of the Ru and Pt promoted co-deposited catalyst with reduction to Co metal. In fact, the co-deposited catalysts *all* have smaller reduced Co particles than their corresponding sequentially-deposited catalysts with an average crystallite diameter of 4.1-4.3 nm. Approximately 92% of the crystallites are below 6 nm when any of the three NMs was co-deposited with only 8% in the "ideal" 6-12 nm range. For Pt and Ru sequential-deposition, 72 and 51% respectively were between 6-12 nm.

Estimates of reduced Co crystallite diameters from H_2 chemisorption agreed outstandingly with TEM measurements varying for the co-deposited catalysts. The H_2 uptake estimate of crystallite size for the unpromoted (10.0 nm) was more than 100% different than the TEM measured (4.7 nm) probably due to the TEM measurement including unreduced CoO (58%).

XAFS results of the NM edge showed a strong NM type effect, but no influence of deposition order. Pt forms direct bonds with Co and further reduction provides evidence of Pt mobility into the Co structure. After only 1 hr of reduction at 360^{o}C Pt is coordinated to ~6 Co atoms and after 1 hr at 400^{o}C the coordination is ~9. Ru remains in a separate metal phase after reduction even at low loadings counter to the recently published evidence of Ru-Co bimetallic (Ma, Jacobs et al. 2011). Re apparently remains Re_2O_7 for the main condition studied (1 h 360^{o}C reduction). Only when reduced at 400^{o}C for 1 hr rather than 360^{o}C does Re reduces to ReO_2. Even when Re remained as Re_2O_7 it promoted Co reduction very well giving 42% reduced to Co

metal compared to *none* for the unpromoted catalyst. The lack of Re reduction shows that Re's ability to promote Co reduction does not require bulk reduction of Re_2O_7—a new finding.

6.2.2 Reducibility Properties

The reducibility properties included in this study were TPR profile, H_2 uptake, extent of reduction, and dispersion. These properties are given in Table 6-2. By all measures, NM addition resulted in promotion of Co reducibility.

Table 6-2.Impact of NM NM choice and deposition order on reducibility. Largest range for each category are shown.

Property	NM Choice Range	Deposition Order Range
$Co_3O_4 \rightarrow CoO$ Reduction Peak Temperature (^oC)	230 - 355 (seq-dep)	330– 355 (Re)
$CoO \rightarrow Co$ Reduction Peak Temperature (^oC)	350 – 475 (seq-dep)	435 – 475 (Ru)
Extent of Reduction (%)	77 – 91 (seq-dep)	62 – 77 (Ru)
H_2 Uptake (μmols/g)	150 – 302 (seq-dep)	150 – 219 (Ru)
Dispersion (%)	10.4 – 20.4 (seq-dep)	10.4 – 19.0 (Ru)

The co-deposited catalysts showed lower TPR peak temperatures than the seq-deposited catalysts. This deposition order effect was less extreme than the NM choice effect as final peak temperatures followed the trend Co/Pt-co<Co/Pt-seq<Co/Re-co<Co/Re-seq<Co/Ru-co<Co/Ru-seq. The Ru catalyst showed another effect with sequential-deposition—the TPR profile showed a small intermediate peak likely due to the nonuniform Ru distribution. TPR peak areas were consistent with, and offer strong corroborative evidence that the reduction process steps are

Co_3O_4 →CoO and CoO→Co. The EOR trend also showed both TPR profile and particle size effects in that the smaller co-deposited catalysts' Co particles were less reducible so the sequentially-deposited catalysts had higher EOR than the co-deposited catalysts. The EOR ranking was Co/Pt-seq>Co/Re-seq>Co/Ru-seq=Co/Pt-co>Co/Re-co>Co/Ru-co>Co.

H_2 uptake was clearly higher with co-dep when Ru was the promoter. Pt and Re showed a much smaller deposition order effect (~30 μmols/g). The unpromoted catalyst %D was ~10%. For all three co-dep catalysts the %D was ~20%. For the Co/Ru-seq catalysts %D was ~10%, Co/Pt-seq ~16%, and the Co/Re-seq was 20%. Thus, Pt and Re give significantly increased dispersion compared to the unpromoted with either deposition order, but co-deposition is required for Ru to result in increased %D.

6.2.3 Activity and Selectivity Properties

Fischer Tropsch activity/selectivity was studied by fixed bed reaction and the ranges of these properties are given in Table 6-3. Co/Pt-co was the most active of all the catalysts.

Table 6-3.Impact of NM choice and deposition order on activity/selectivity. Largest range for each category are shown.

Property	NM Choice Range	Deposition Order Range
E_A (kJ/mol)	69[a] – 102 (co-dep)	69[a] – 105 (Pt)
$\mathbf{-r_{CO}\ (mmol \cdot g_{cat}^{-1} \cdot h^{-1})^b}$	11.5 – 21.5 (co-dep)	9.4 – 21.5 (Pt)
TOF $x10^3$ $(s^{-1})^b$	3.31 – 7.62 (seq-dep)	5.19 – 9.98 (Pt)
S_{CH4} (%)	14 – 21 (co-dep)	14 – 22 (Pt)

[a]E_A Appendix
[b]T=200°C, P_{CO}=2.1 bar (30 psia), P_{H2}=9.0 bar (130 psia) using A and E_A nonlinear fit of data

The activities of the sequentially-deposited catalysts were surprisingly lower than that of the unpromoted catalyst. The co-deposited catalysts were more active than their sequentially deposited counterparts. In the case of Pt promotion, the deposition order effect was co-deposition > unpromoted>sequential-deposition. The NM effect was Co/Pt>Co/Re>Co/Ru when co-deposited and Co/Pt≥Co/Ru≥Co/Re when sequentially-deposited. With Pt and Re promotion, the TOF of the co-deposited catalyst are ~2X higher than their sequentially-deposited counterparts. This is very significant and suggests that the co-deposition of NM increases the activity per site. In the case of Pt the TOF of the co-dep catalyst is higher even with a surface averaged ACD of only 4.3 nm and 91% < 6 nm compared to 8.0 nm and 26% < 6 nm for the seq-dep, which indicates that either the 6-12 nm "ideal" range for Co crystallite is not applicable as Johnson et al.'s work showed Co hydrogenation is crystallite size insensitive (Johnson 1989; Johnson 1991), or the differences based on particle size are in some way overcome by other differences resulting from promotion (NM and La) and variation in NM deposition order. It is likely that differences in %D and EOR are also affecting the TOF. The lower methane selectivity for Pt and Ru when co-deposited shows evidence of significant promoter effects to another generally accepted crystallite size trend that smaller particles resulting in higher methane selectivity, because the Co/Pt-co and Co/Ru-co catalysts has smaller crystallites and lower methane selectivity than their sequentially-deposited counterparts. This offers confirming evidence that NM addition and deposition order variation affect the applicability of generally accepted Co crystallite size activity/selectivity effects.

6.3 Main Conclusions

The main conclusions for this study are shown below in 26 statements. The most significant conclusions are bolded.

1. BET surface area and pore size were not affected by NM type or deposition order.
2. Retention and distribution of Co, Pt, and Re were not affected by NM type or deposition order.
3. **Ru retention is problematic and deposition order dependent**. With co-deposition only 15% of the targeted Ru is retained (0.04 wt%), while with sequential-deposition 46% is retained (0.13 wt%). This retention can apparently be improved by using a nitrosyl nitrate rather than chloride Ru precursor.
4. Ru distribution is deposition order dependent—uniform with co-deposition and concentrated at the pellet edge with sequential-deposition. The La distribution is also affected by Ru sequential-deposition as La in that case is concentrated at the pellet edge. Ru co-deposition gives uniform La distribution; it remains uniform like the unpromoted catalyst as well as Pt or Re promoted catalysts by both deposition orders.
5. Reduced Co crystallite size shows no NM effect when the NM is co-deposited. The ACD for all 3 catalysts are between 4.1 and 4.3nm and ~92% of the crystallites are < 6nm.
6. The co-deposited catalysts all have smaller reduced Co crystallite size than their corresponding sequentially-deposited catalysts. Reduced Co crystallite size is affected by deposition order for Pt and Ru. Smaller particles (~92% < 6nm) result with co-deposition than (72 and 51%, respectively) sequential-deposition.
7. Estimates of reduced Co crystallite diameters from H_2 chemisorption agreed very well with TEM measurements for the co-deposited catalysts.

8. **Pt forms direct bonds with Co for both co-deposition and sequential deposition.** This has not been seen in the literature before for catalysts with calcination between Co and Pt deposition.
9. Further reduction provides evidence of Pt mobility into the Co structure as the Pt coordination to Co increased from ~6 to ~9.
10. **Ru remains in a separate metal phase after reduction even at low loadings.** This is contrary to the most recent theory that Ru bonds directly to Co and that this bonding is only apparent at low loadings.
11. **Re's ability to promote Co reduction does not require bulk reduction of Re**. Re remained as Re_2O_7 and still promoted Co reduction well (e.g. 42% reduced to Co metal compared to *none* for the unpromoted catalyst).
12. The predominant NM bonding following mild reduction did not show a deposition order effect as measured by XAFS.
13. By all measures of reducibility (TPR, EOR, H_2 uptake), all NM promoted catalysts were more reducible than the unpromoted catalyst.
14. The TPR peak areas are consistent with, and offer strong corroborative evidence that the stoichiometry of the reduction process steps are $Co_3O_4 \rightarrow CoO$ and $CoO \rightarrow Co$
15. The co-deposited catalysts have lower TPR peak temperatures than their corresponding sequentially-deposited catalysts; there is a clear deposition order trend.
16. The NM choice effect on Co reducibility measured from TPR was stronger than the deposition order trend. Both Pt promoted catalysts have lower TPR peak temperatures than both Re promoted catalysts, which are lower than both Ru promoted catalysts.

17. The EOR showed a significant deposition order trend of higher reducibility for sequential-deposition than co-deposition. This may be due to the smaller co-deposited catalysts Co crystallites interacting with the support more strongly.
18. The NM type affect on EOR, while weaker than that of deposition order still showed the trend of Pt> Re>Ru to give an overall EOR trend of Co/Pt-seq>Co/Re-seq>Co/Ru-seq=Co/Pt-co>Co/Re-co>Co/Ru-co>Co.
19. The Co/Pt-co was the most active of all the catalysts both on rate per mass and TOF basis.
20. **The activities per gram of the Co/Re-seq catalyst were statistically lower than the unpromoted catalysts.** Additionally, the Co/Pt-seq and Co/Ru-seq activities were lower, but that difference was not statistically significant**.**
21. **The co-deposited Re and Pt catalysts were statistically more active than their corresponding sequentially-deposited catalysts**. Their TOFs are ~2-3 times higher. The Ru difference was not statistically significant, but showed the same trend of co-deposition resulting in higher activity than sequential-deposition.
22. **The NM choice effect on FT activity was Co/Pt>Co/Re>Co/Ru when co-deposited.**
23. **The 6-12 nm "ideal" range for Co crystallite is not applicable** as evidenced by the higher TOF with smaller ACD and more crystallites <6 nm when comparing Co/Pt-co with Co/Pt-seq. This could be because either, as Johnson et al.'s work showed, Co hydrogenation is crystallite size insensitive (Johnson 1989; Johnson 1991), the differences based on particle size are in some way overcome by other differences resulting from promotion (NM and La) and variation in NM deposition order, or that differences in %D and EOR are also affecting the TOF.

24. The methane selectivities of the co-deposited catalysts were lower or the same as their sequentially-deposited counterparts.
25. The co-deposited catalysts all have statistically the same (Re) or lower E_A (Ru and Pt) values than their corresponding sequentially-deposited catalysts. In the case of Pt, the E_A for co-dep is lower even than the unpromoted catalyst and is suspiciously low.

6.4 Recommendations

The recommendations for further work based on these main findings are:

1. Study the Ru loss during drying and calcination. This could be done by drying and calcining the wet catalysts immediately after Ru deposition while measuring which gases come off by mass spectroscopy.
2. Investigate the Pt-Co bimetallic formation and Pt mobility into Co by insitu XAFS of the Pt edge while reducing for 1 hr at 360^{o}C and 400^{o}C.
3. Further the understanding of Co reduction promotion without reduction of Re_2O_7 to Re for hydrogen spillover. This could be done by insitu XAFS of the Re edge and Co edges of the Co/Re catalyst and the Co edge of the unpromoted catalyst while reducing at 360^{o}C for 1 hr.
4. Study the variations in Ru and La spatial distribution. It is suggested to start this study by trying nonaqueous or pH buffered aqueous Ru deposition for the Co/Ru-seq catalyst to eliminate Ru precipitation
5. Study differences in Co crystallite size and Ru loss when preparing a co-deposition of Ru using the nitrosyl nitrate rather than chloride precursor.

6. Explore the tuneability of Co crystallite size with co-deposition. Supports with a different pore size or changing the Co loading would probably result in a different average Co crystallite size.
7. Investigate the lower activity of the sequentially-deposited NM promoted catalysts compared with the unpromoted catalyst.
8. Look into the suspiciously low activation energy of the Pt co-deposited catalyst.
9. Determine the rate law and P_{H2} and P_{CO} dependencies. This can be done by doing fixed bed experiments at various H_2:CO ratios and taking care to have a few experiments with constant P_{CO} or P_{H2} while studying the other (P_{H2} or P_{CO}) dependency.
10. Investigate if the high S_{CH4} can be lowered by decreasing the H_2:CO to typical conditions (2 rather than 4).
11. Test if the catalyst stability is a function of NM or deposition order.
12. Prepare a catalyst with some NM co-deposited in the final Co deposition and some sequentially-deposited to determine how the deposition order effects combine.

7 References

Administration, U. S. E. I. (2012). "International Energy Statistics." Retrieved 10 May 2012, 2012.

Barbier, A., A. Tuel, et al. (2001). "Characterization and Catalytic Behavior of Co/SiO_2 Catalysts: Influence of Disperson in Fischer Tropsch Reaction." Journal of Catalysis **200**(1): 106-116.

Barrett, E. P. J., Leslie G.; Halenda, Paul P. (1951). "The determination of pore volume and area distributions in porous substances. I. Computations from nitrogen isotherms." Journal of the American Chemical Society(73): 8.

Barthlomew, C. H. (1990). "Hydrogen adsorption on supported cobalt, iron, and nickel." Catalysis Letters **7**(1-4): 27-51.

Barthlomew, C. H., Ed. (1993). Model Catalyst Studies of Supported Metal Sintering and Redispersion Kinetics in Catalysis, A Specialist Periodical Report. London, Royal Society of Chemistry.

Bartholomew, C. H. (2003). History of Cobalt Catalyst Design for FTS. National Spring Meeting of the American Institute of Chemical Engineers, New Orleans.

Bartholomew, C. H. and R. J. Farrauto (2006). Fundamentals of Industrial Catalytic Processes, John Wiley & Sons, Inc.

Bazin, D., I. Kovacs, et al. (2003). "Ru-Co/NaY bimetallic catalysts: in situ EXAFS study at Co K- and Ru K- adsorption edges." Applied Catalysis A-General **242**: 179-186.

Bechara, R., D. Balloy, et al. (1999). "Influence of the Characteristics of γ-Aluminas on the Dispersion and the Reducibility of Supported Cobalt Catalysts." Chemistry of Materials **11**(7): 1703-1711.

Beuther, H., C. L. Kibby, et al. (1983). Fluid Bed Catalyst for Synthesis Gas Conversion and Utilization Thereof for Preparation of Diesel Fuel. United States, Gulf Research & Development Company**:** 8.

Beuther, H., C. L. Kibby, et al. (1985). Fluid Bed Catalyst for Synthesis Gas Conversion and Utilization Thereof for Preparation of Diesel Fuels. United States, Gulf Research and Development**:** 5.

Beuther, H., T. P. Kobylinski, et al. (1986). Synthesis Gas Conversion Using Ruthenium-Promoted Cobalt Catalyst. United States, Gulf Research and Development Company**:** 7.

Bezemer, G., J. H. Bitter, et al. (2006). "Cobalt Particle Size Effects in the Fischer-Tropsch reaction Studied with Carbon Nanofiber Supported Catalysts." Journal of American Chemical Society **128**(12): 3956-3964.

Bezemer, G. I., A. van Laak, et al. (2004). "Cobalt supported on carbon nanofibers- A promising novel Fischer-Tropsch catalyst." Studies in Surface Science and Catalysis **147**: 259-264.

Bezemer, G. L., A. J. Van Dillen, et al. (2005). Cobalt on Carbon Nanofiber Catalysts for the study of Cobalt Particle-Size Effects in Fischer-Tropsch Catalysis. North American Catalysis Society Meeting Philadelphia, PA.

Borg, O., P. D. C. Dietzel, et al. (2008). "Fischer-Tropsch synthesis: Cobalt particle size and support effects on intrinsic activity and product distribution." Journal of Catalysis **259**(2): 161-164.

Borg, O., V. Froseth, et al. (2007). "Fischer-Tropsch synthesis. Recent studies on the relation between the properties of supported cobalt catalysts and the activity and selectivity." Studies in Surface Science and Catalysis **167**: 117-122.

Borg, O., N. Hammer, et al. (2009). "Fischer-Tropsch synthesis over un-promoted and Re-promted g-Al2O3 supported cobalt catalysts with different pore sizes." Catalysis Today **142**: 70-77.

Brown, R., M. E. Cooper, et al. (1982). "Temperature Programmed Reduction of Alumina-Supported Iron, Cobalt, and Nickel Bimetallic Catalysts." Applied Catalysis **3**: 177-186.

Chu, W., P. A. Chernavskii, et al. (2007). "Cobalt species in promoted cobalt alumina-supported Fischer-Tropsch catalysts." Journal of Catalysis **252**: 215-230.

Culross, C. C. and C. H. Mauldin (1998). Preparation of High Activity Catalysts. United States of America.

Culross, C. C. and C. H. Mauldin (2000). Preparation of High Activity Catlysts; The catalysts and their use. U. S. Patent, Exxon Research and Engineering Company.

Das, T. K., G. Jacobs, et al. (2003). "Fisher-Tropsch synthesis: chacterization and catalytic properties of rhenium promoted cobalt alumina catalysts." Fuel **82**: 805-815.

De Jong, K. P., J. H. E. Glezer, et al. (1989). Supported Metal Catalyst and the Use Thereof. U. S. Patent. United States, Shell Oil Company, Houston, Texas.

Delmon, B., P. Grange, et al., Eds. (1978). Preparation of Catalysts II: Scientific Bases for the Preparation of Heterogeneous Catalysts : Proceedings of the Second International Symposium. Amsterdam, The Netherlands, Elsevier Scientific Publishing Company.

den Breejen, J. P., P. B. Radstake, et al. (2009). "On the Origin of the Cobalt Particle Size Effects in Fischer-Tropsch Catalysis." Journal of American Chemical Society **131**: 7197-7203.

Diehl, F. and A. Y. Khodakov (2009). "Promotion of Cobalt Fischer-Tropsch Catalysts with Noble Metals: a Review " Oil & Gas Science and Technology - Rev. IFP **64**(1): 11-24.

Enger, B. C., **A.-L. Fossan**, et al. (2011). "Modified alumina as catalyst support for cobalt in the Fischer-Tropsch Synthesis." Journal of Catalysis **284**: 9-22.

Eri, S., J. J. G. Goodwin, et al. (1989). Catalyst for Production of Hydrocarbons. United States, Den Norske Stats Olijelskap A.S., Norway.

Eri, S., J. J. G. Goodwin, et al. (1989). Fischer-Tropsch catalyst containing cobalt and rhenium for production of hydrocarbons. United States of America. **4801573**.

Eri, S., J. J. G. Goodwin, et al. (1992). Process using a supported catalyst for hydrocarbono synthesis. United States of America, Den, Norske Stats Olijeselskap A.S.

Eri, S., J. J. G. Goodwin, et al. (1992). Supported catalyst for Hydrocarbon Synthesis. United States.

Girardon, J. S., A. Constant-Griboval, et al. (2005). "Optimization of the pretreatment procedure in the design of cobalt silica supported Fischer-Tropsch catalysts." Catalysis Today **106**(1-4): 161-165.

Guczi, L. B., D.; Kovacs, I.; Borko, L.; Schay, Z.; Lynch, J.; Parent, P.; Lafon, C.; Stefler, G.; Koppany, Zs.; Sajo, I. (2002). "Structure of Pt-Co/Al2O3 and Pt-Co/NaY Bimetallic Catalysts: Characterization by In Situ EXAFS, TPR, XPS and by Activity in Co (Carbon Monoxide) Hydrogenation. ." Topics in Catalysis **20**(1-4): 129-139.

Hargreaves, S. (2012) "Turning Natural Gas into Diesel Fuel." CNN Money.

Harrison, L. and W. Hecker (2012). Discussion on H_2 spillover in Cobalt standard catalyst. K. Cook. Provo, UT.

Heise, M. S. and J. A. Schwarz (1985). "Preparation of Metal Distributions within Catalyst Supports." Journal of Colliod and Interface Science **107**(1): 237-243.

Hilmen, A. M., D. Schanke, et al. (1996). "TPR Study of the mechanism of rhenium promotion of alumina-supported cobalt Fischer-Tropsch catalyst." Catalysis Letters **38**: 143-147.

Hosseini, S. A. (2005). "Evaluation of Ru-promoted Co/l Al2O3 catalyst in Fischer-Tropsch sythesis in a CSTR." Catalysis Communications **6**: 233-240.

Huber, G. and C. H. Barthlomew (2001). "Pt-promotion of Co/SiO_2 Fischer-Tropsch Synthesis Catalyts." Studies in Surface Science and Catalysis **136**: 283-288.

Iglesia, E. (1993). "Review: Design, Synthesis, and Use of Cobalt-Based Fischer-Tropsch Synthesis Catalysts." Applied Catalysis **161**: 59-78.

Iglesia, E. (1997). "Design, synthesis, and use of cobalt-based Fischer-Tropsch synthesis catalysts." Applied Catalysis A: General **161**: 59-78.

Iglesia, E., S. L. Soled, et al. (1988). Cobalt-Ruthenium Catalyst for Fischer-Tropsch Synthesis and Process for Their Preparation. U. S. Patent. United States, Exxon Research and Engineering Company. **1:** 10.

Iglesia, E., S. L. Soled, et al. (1992). "Fischer-Tropsch synthesis on cobalt and ruthenium. Metal dispersion and support effects on reaction rate and selectivity." Journal of Catalysis **137**(1): 212-224.

Iglesia, E. S., Stuart L.; Fiato, Rocco A.; Via, Grayson H. (1993). "Bimetallic synergy in cobalt-ruthenium Fischer-Tropsch synthesis catalysts. ." Journal of Catalysis **143**(2): 345-368.

Jacobs, G., J. A. Chaney, et al. (2004). "Fischer-Tropsch synthesis: study of the promotion of Re on the reduction property of Co/Al2O3 catalysts by in situ EXAFS/XANES of Co K and Re LIII edges and XPS. ." Applied Catalysis A: General **264**: 203-212.

Jacobs, G., J. A. Chaney, et al. (2004). "Fischer-Tropsch synthesis: study of the promotion of Pt on the reduction property of Co/Al_2O_3 catalyst by in situ EXAFS of Co K and Pt L_{III} edges and XPS." Journal of Synchroton Rad. **11**: 414-422.

Jacobs, G., T. K. Das, et al. (2002). "Fischer Tropsch Synthesis: support, loading, and promoter effects on the reducibility of cobalt catalyst." Applied Catalysis A: General **233**: 263-281.

Jacobs, G., Y. Ji, et al. (2007). "Fischer-Tropsch synthesis: Temperature programmed EXAFS/XANES investigation of the influence of support type, cobalt loading, and noble metal promoter addition to the reduction behavior of cobalt oxide particles. ." Applied Catalysis A: General **333**(2): 177-191.

Jacobs, G., Y. Ji, et al. (2007). "Fischer-Tropsch synthesis: Temperature programmed EXAFS/XANES investigation of the influence of support type, cobalt loading, and noble metal promoter addition to the reduction behavior of cobalt oxide particles. ." Applied Catalysis A: General **333**(2): 177-191.

Jacobs, G., P. Patterson, M., et al. (2002). "Fischer-Tropsch synthesis:deactivation of noble metal promoted Co/Al_2O_3 catalysts." Applied Catalysis A-General **233**: 215-226.

Jacobs, G., A. Sarkar, et al. (2008). "Fischer-Tropsch Synthesis: Assessment of the Ripening of Cobalt Clusters and Mixing between Co and Ru Promoter via Oxidation-Reduction-Cycles over Lower Co-Loaded Ru-Co/Al2O3 Catalysts." Ind. Eng. Chem. Res. **47**: 672-680.

Jacobs, G. C., John A.; Patterson, Patricia M.; Das, Tapan K.; Maillot, Julie C.; Davis, Burtron H. (2004). "Fischer-Tropsch synthesis: study of the promotion of Pt on the reduction property of Co/Al2O3 catalysts by in situ EXAFS of Co K and Pt LIII edges and XPS. ." Journal of Synchrotron Radiation **11**(5): 414-422.

Johnson, B. G. (1989). The role of surface structure in carbon-monoxide hydrogenation on cobalt catalysts. Chemical Engineering. Provo, UT, Brigham Young University. **PhD:** 149.

Johnson, B. G. B., Calvin H.; Goodman, D. Wayne. (1991). "Role of surface structure and dispersion in carbon monoxide hydrogenation on cobalt. ." Journal of Catalysis **128**(1): 231-247.

Jones, R. D. and C. H. Bartholomew (1988). "Improved flow technique for measurement of hydrogen chemisorption on metal catalysts." Applied Catalysis **39**: 77-88.

Karaca, H., O. V. Safonova, et al. (2011). "Structure and catalytic performace of Pt-promoted alumina-supported cobalt catalysts under realistic conditions of Fischer-Tropsch synthesis." Journal of Catalysis **277**: 14-26.

Khodakov, A. Y., W. Chu, et al. (2007). "Advances in the Development of Novel Cobalt Fischer-Tropsch Catalysts for Synthesis of Long-Chain Hydrocarbons and Clean Fuels." Chemical Review **107**: 1692-1744.

Khodakov, A. Y., J. S. Girardon, et al. (2007). Effect of calcination and promotion with noble metals on the structure and catalytic performance of cobalt silcia and alumina supported Fischer-Tropsch catalysts: A comparative study. North American Catalysis Society 20th North American Meeting, Houston, TX.

Kildemo, M., T. Ramsvik, et al. (2002). "Study of Co adsorption on La-Rh(100) surface alloys." Surface Science **497**: 254-268.

Kobylinski, T. P. (1978). Conversion of Synthesis Gas Using A Cobalt-Ruthenium Catalyst. United States of America, Gulf Research and Development**:** 6.

Kogelbauer, A., J. J. G. Goodwin, et al. (1996). "Ruthenium Promotion of Co/Al2O3Fischer-Tropsch Catalysts." Journal of Catalysis **160**(1): 125-133.

Labhestwar, N. K., A. Watanabe, et al. (2003). "New improved sytheses of $LaRuO_3$ perovskites and their applications in environmental catalysis." Applied Catalysis B: Environmental **40**(1): 21-30.

Lei, Y., J. Jelic, et al. (2011). "Effect of Particle Size and Adsorbates on the L3, L2 and L1 X-Ray Absorption Near Edge Structure of Supported Pt Nanoparticles." Topics in Catalysis **54**(5-7): 334-348.

Li, P., J. Liu, et al. (2006). "In situ synthesis and characterization of Ru promoted Co/Al_2O_3 Fischer-Tropsch catalysts." Applied Catalysis **307**: 212-221.

Lisitsyn, A. S., A. V. Golovin, et al. (1985). "Properties of catalysts perpared by pyrolysis of dicobalt octacarbonyl on silica containing surface titanium ions." Journal of Catalysis **95**(2): 527-538.

Ma, W. P., G. Jacobs, et al. (2011). "Fischer-Tropsch Synthesis: Influence of CO Conversion of Selectivities, H_2/CO Usage, Ratios, and Catalyst Stability for a Ru Promoted Co/Al_2O_3 Catalyst Using a Slurry Phase Reactor." Topics in Catalysis **54**: 757-767.

Martinez, A. and G. Prieto (2007). "Breaking the dispersion-reducibility dependence in oxide-supported cobalt nanoparticles." Journal of Catalysis **245**(2): 470-476.

Mauldin, C. H. (1999). Preparation of High Activity Catalysts the Catalysts and Their Use. United States of America, Exxon Research and Engineering Company**:** 8.

Mauldin, C. H. and D. E. Varnado (2001). "Rhenium as a promoter of titania-supported cobalt Fischer-Tropsch catalysts." Studies in Surface Science and Catalysis **136**(Natural Gas Conversion VI): 417-422.

Miller, J. (2006). "The Effect of Gold Particle Size on the Au-Au Bond Distance and Reactivity Towards Oxygen in
Supported Catalysts." Journal of Catalysis **240**(2): 222-234.

Morales, F., D. Grandjean, et al. (2006). "X-ray Absorption Spectroscopy of Mn/Co/TiO2 Fischer−Tropsch Catalysts: Relationships between Preparation Method, Molecular Structure, and Catalyst Performance." The Journal of Physical Chemistry B **110**(17): 8626-8639.

Morales, F. and B. M. Weckhuysen, Eds. (2006). Promotion Effects in Co-based Fischer-Tropsch Catalysis. Catalysis.

Mustard, D. G. and C. H. Bartholomew (1981). "Determination of metal crystallite size and morphology in supported nickle catalysts." Journal of Catalysis **67**(1): 186-206.

Park, S.-J., J. W. Bae, et al. (2011). "Deactivation behaviors of Pt or Ru promoted $Co/P\text{-}Al_2O_3$ catalyst during slurry-phase Fischer-Tropsch synthesis." Catalysis Communications **12**: 539-543.

Pinna, F. (1998). "Supported metal catalysts preparation." Catalysis Today **41**(1-3): 129-137.

Prieto, G., A. Martinez, et al. (2009). "Cobalt supported on morphologically tailored SBA-15 mesostructures: The impact of pore length on metal dispersion and catalytic activity in Fischer-Tropsch synthesis." Applied Catalysis **367**: 146-156.

Regalbuto, J., Ed. (2007). Catalyst Preparation: Science and Engineering. Boca Raton, FL, CRC Press.

Ressler, T. (2008). WinXAS 3.2.

Reuel, R. C. and C. H. Bartholomew (1984). "Effects of support and dispersion on the CO hydrogenation activity/selectivity properties of cobalt." Journal of Catalysis **85**(1): 78-88.

Ribeiro, F. W., A.; Bartholomew, C.; and Somorjai, G. (1997). "Reproducibility of Turnover Rates in Heterogeneous Metal Catalysis: Compilation of Data and Guidelines for Data Analysis." Catalysis Review Science and Engineering **39**.

Ronning, M. N., David G.; Holmen, Anders (2001). "In situ EXAFS study of the bimetallic interaction in a rhenium-promoted alumina-supported cobalt Fischer-Tropsch catalyst." Catalysis Letters **72**(3-4): 141-146.

Ruckenstein, E. and X. D. Hu (1986). "The Effect of Steam on Supported Metal Catalysts." Journal of Catalysis **100**: 1-16.

Saib, A. M., D. J. Moodley, et al. (2010). "Fundamental understanding of deactivation and regeneration of cobalt Fischer-Tropsch synthesis catalysts." Catalysis Today **154**: 271-282.

Sakurai, T., Y. Hinatsu, et al. (1985). "Adsorption of ruthenium tetraoxide on metal surfaces." Journal of Physical Chemistry **89**(10): 1892-1896.

Schanke, D., S. Vada, et al. (1995). "Study of Pt-Promoted Cobalt CO Hydrogenation Catalysts." Journal of Catalysis **156**(1): 85-95.

Sexton, B. A., A. E. Hughes, et al. (1986). "An XPS and TPR Study of the Reduction of Promoted Cobalt-Kieselguhr Fischer-Tropsch Catalysts." Journal of Catalysis **97**: 390-406.

Shannon, M. D., C. M. Lok, et al. (2007). "Imaging promoter atoms in Fischer-Tropsch cobalt catalysts by aberration-corrected scanning transmission electron micropscopy." Journal of Catalysis **249**: 41-51.

Shell. (2012). "Gas to Liquids." Future of Energy Retrieved July 5, 2012, 2012.

Storsæter, S., B. Tøtdal, et al. (2005). "Characterization of alumina-, silica-, and titania-supported cobalt
Fischer–Tropsch catalysts." Journal of Catalysis **236**: 139-152.

Sun, S., K. Fujimoto, et al. (2003). "A highly active and stable Fischer-Tropsch synthesis cobalt/silica catalyst with bimodal cobalt particle distribution." Catalysis Communications **4**(8): 361-364.

Tsubaki, N., S. Sun, et al. (2001). "Different Functions of the Noble Metals Added to Cobalt Catalysts for Fischer-Tropsch Synthesis." Journal of Catalysis **199**: 236-246.

Tsubaki, S. S. and K. Fujimoto (2000). "Promotional Effect of Noble Metal to Co-based Fischer-Tropsch Catalysts Prepared from Mixed Cobalt Salts." Catalysis Letters **29**(2): 176-177.

Tullo, A. H. (2011). "Natural Gas Sasol proposes gas-to-liquids plant for Louisiana." Chemical and Engineering News **89**(39): 9.

Vada, S. H., A.; Aadnanes, E.; Schanke, D.; Holmen, A. (1995). "Fischer-Tropsch synthesis on supported cobalt catalysts promoted by platinum and rhenium." Topics in Catalysis **2**(1).

Van Berge, P. J., J. Van De Loosdrecht, et al. (2008). Cobalt Catalyst. United States of America.

Van Dillen, A. J., R. J. A. M. Terorde, et al. (2003). "Synthesis of supported catalysts by impregnation and drying using aqueous chelated metal complexes." Journal of Catalysis **216**(1-2): 257-264.

Viswanathan, B. and R. Gopalakrishnan (1986). "Effect of Support and Promoter in Fischer-Tropsch Cobalt Catalysts." Journal of Catalysis **99**: 342-348.

Xiao Shuzhang, L. Z., Zhou Guoguang, Xu Zuhui (2004). "Modification effect of cerium in gas hydrogenation of acrylonitrile over Pd/Al2O3 catalysts." Chemical research and application **6**(1): 82-.

Xiao, T. and Y. Qian (2008). Promoted carbide-based Fischer-Tropsch catalyst, method for its preparation and uses therof. W. I. P. Organization, Oxford Catalysts Limited.

Zhai, Q.-Z. and L.-G. Chen (2011). "Adsorptive Performance of Nanoscale α-Al_2O_3 Towards La(III)." Asian Journal of Chemistry **23**(9): 3975-3978.

APPENDIX A BET

For each catalyst, the BET data are given as well as the pore size distributions. The BET SA and mezopore V_{pore} directly from the report file along with the volume density function calculation of mezopore d_{pavg} are given on the left along with other report file and calculated values. The distributions are given on the right.

The excel versions of each of these files is included as part of the electronic Appendix (available from Dr. Hecker, hecker@byu.edu , or the BYU Chemical Engineering Department). In the folder, BET where:

1.xls=Co/Ru-co

2.xls=Co/Pt-co

3.xls=Co/Ru-seq

4.xls=Co/Pt-seq

5.xls=Co only

6.xls=Co/Re-co

7.xls=Co/Re-se

Date:	1/21/2010	
Sample:	Co Only	
Technician:	Krikor Hagopian	
Source File (Name.RPT):	C:\Documents and Settings\jhortor	
Save As (Path\Name.xls):		
BET DATA (From Report File)		
BET SA:	103	m^2/g
Mezopore d_{pavg}:	16.0	nm
Mezopore V_{pore}:	0.412	cm^3/g
BJH A_{pore}:	117	m^2/g
BJH V_{pore}:	0.417	cm^3/g
Micropore SA:	8	m^2/g
Micropore V_{pore}:	0.0	cm^3/g
Direct Calculation		
Mezopore d_{pavg}:	18.208	nm
Mezopore SA:	129.1	m^2/g
Mezopore V_{pore}:	0.427	cm^3/g
Volume Density Function Calculation		
Mezopore d_{pavg}:	14.953	nm
Standard Deviation σ_g:	2.893	nm
Log-normal Mean μ_{ln}:	2.0	
Log-normal SD σ_{ln}:	0.4	

Mezopore range is r^p > 1.5 nm

$_g$ denotes geometric calculation

$_{ln}$ denotes log-normal distribution

C. Chu, et al. 'Pore-size Distribution of Copper Oxide-Alumina Catalysts,' J. Chem. Eng. Data 16(3), 1971, 327-331.

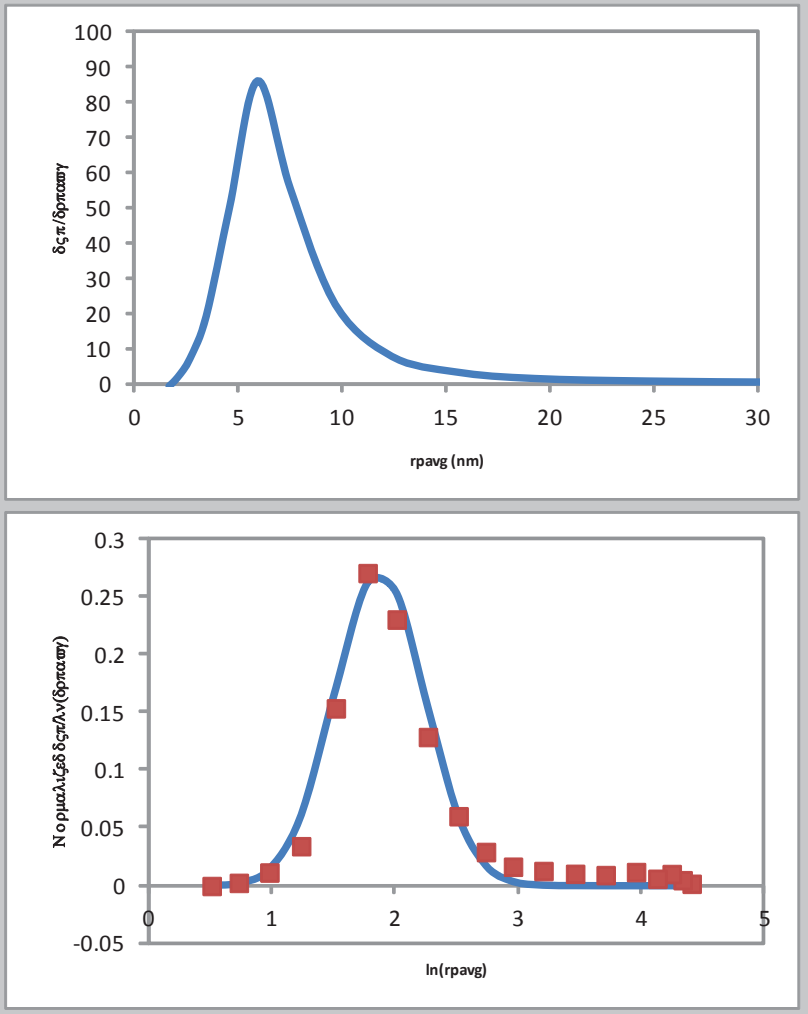

Figure 1. BET surface area and pore size for Unpromoted catalyst

Date:	1/20/2010	
Sample:	Co/Ru-seq	
Technician:	Krikor Hagopian	
Source File (Name.RPT):	C:\Documents and Settings\jhorton5\M	
Save As (Path\Name.xls):		
BET DATA (From Report File)		
BET SA:	100	m^2/g
Mezopore d_{pavg}:	15.7	nm
Mezopore V_{pore}:	0.393	cm^3/g
BJH A_{pore}:	113	m^2/g
BJH V_{pore}:	0.397	cm^3/g
Micropore SA:	7	m^2/g
Micropore V_{pore}:	0.0	cm^3/g
Direct Calculation		
Mezopore d_{pavg}:	18.166	nm
Mezopore SA:	121.6	m^2/g
Mezopore V_{pore}:	0.404	cm^3/g
Volume Density Function Calculation		
Mezopore d_{pavg}:	15.101	nm
Standard Deviation σ_g:	2.885	nm
Log-normal Mean μ_{ln}:	2.0	
Log-normal SD σ_{ln}:	0.4	

Mezopore range is $r^p > 1.5$ nm

$_g$ denotes geometric calculation

$_{ln}$ denotes log-normal distribution

C. Chu, et al. 'Pore-size Distribution of Copper Oxide-Alumina Catalysts,' J. Chem. Eng. Data 16(3), 1971, 327-331.

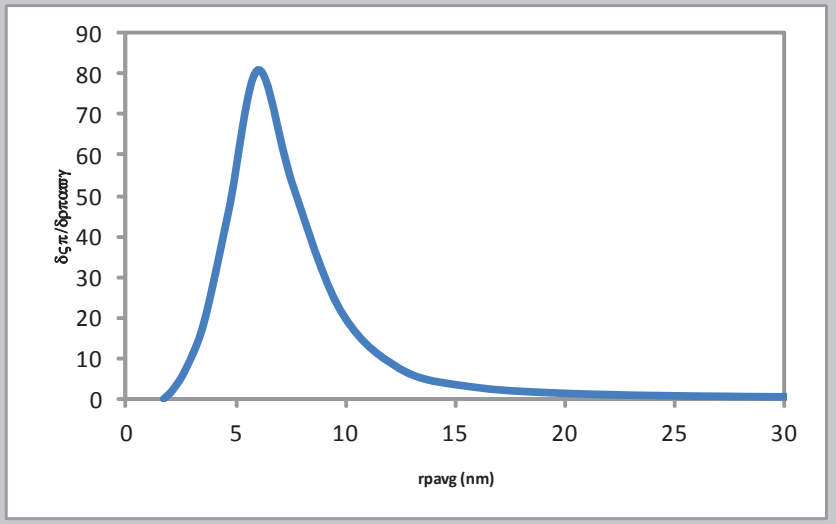

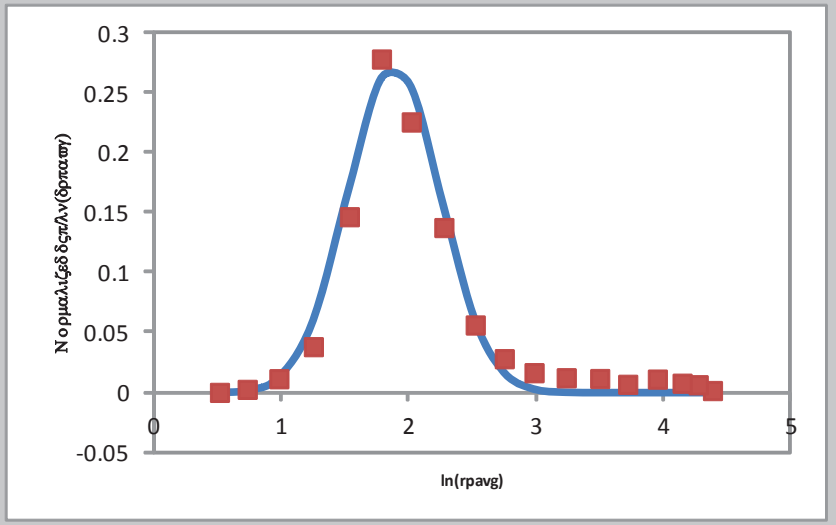

Figure 2. BET surface area and pore size for Co/Ru-seq catalyst

Date:	1/20/2010	
Sample:	Co/Ru-co	
Technician:	Krikor Hagopian	
Source File (Name.RPT):	C:\Documents and Settings\jhorton5\My	
Save As (Path\Name.xls):		
BET DATA (From Report File)		
BET SA:	102	m^2/g
Mezopore d_{pavg}:	15.6	nm
Mezopore V_{pore}:	0.401	cm^3/g
BJH A_{pore}:	116	m^2/g
BJH V_{pore}:	0.404	cm^3/g
Micropore SA:	7	m^2/g
Micropore V_{pore}:	0.0	cm^3/g
Direct Calculation		
Mezopore d_{pavg}:	17.964	nm
Mezopore SA:	124.8	m^2/g
Mezopore V_{pore}:	0.411	cm^3/g
Volume Density Function Calculation		
Mezopore d_{pavg}:	14.913	nm
Standard Deviation σ_g:	2.901	nm
Log-normal Mean μ_{ln}:	2.0	
Log-normal SD σ_{ln}:	0.4	

Mezopore range is $r^p > 1.5$ nm

$_g$ denotes geometric calculation

$_{ln}$ denotes log-normal distribution

C. Chu, et al. 'Pore-size Distribution of Copper Oxide-Alumina Catalysts,' J. Chem. Eng. Data 16(3), 1971, 327-331.

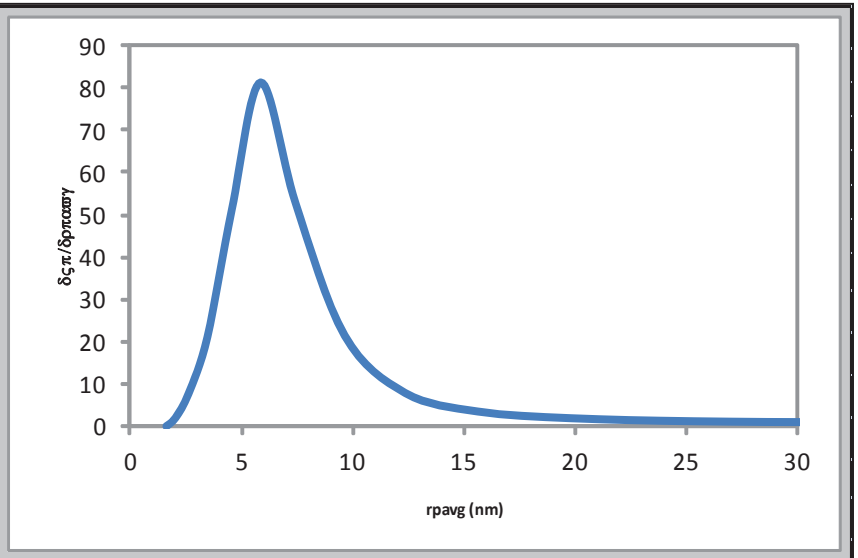

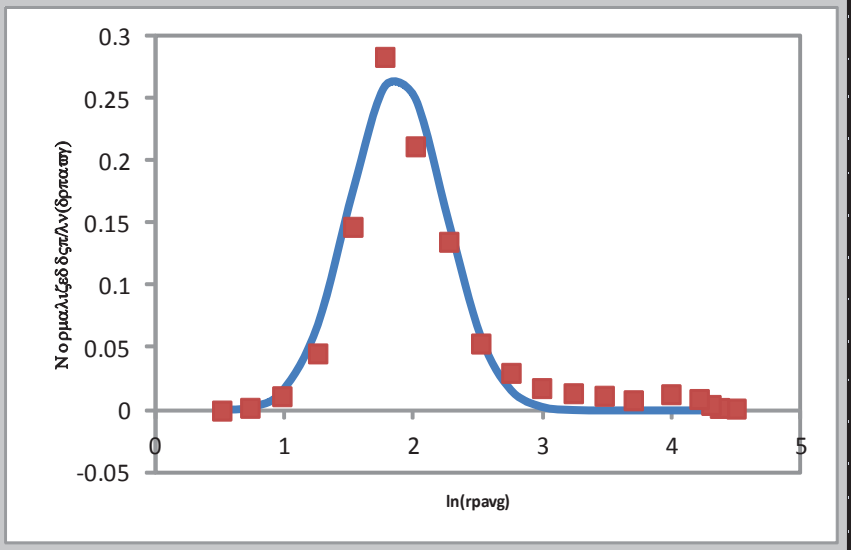

Figure 2. BET surface area and pore size for Co/Ru-co catalyst

Date:	1/20/2010	
Sample:	Co/Pt-co	
Technician:	Krikor Hagopian	
Source File (Name.RPT):	C:\Documents and Settings\jhorton5	
Save As (Path\Name.xls):		
BET DATA (From Report File)		
BET SA:	102	m^2/g
Mezopore d_{pavg}:	15.6	nm
Mezopore V_{pore}:	0.398	cm^3/g
BJH A_{pore}:	115	m^2/g
BJH V_{pore}:	0.401	cm^3/g
Micropore SA:	6	m^2/g
Micropore V_{pore}:	0.0	cm^3/g
Direct Calculation		
Mezopore d_{pavg}:	18.218	nm
Mezopore SA:	123.5	m^2/g
Mezopore V_{pore}:	0.409	cm^3/g
Volume Density Function Calculation		
Mezopore d_{pavg}:	14.919	nm
Standard Deviation σ_g:	2.887	nm
Log-normal Mean μ_{ln}:	2.0	
Log-normal SD σ_{ln}:	0.4	

Mezopore range is $r^p > 1.5$ nm

$_g$ denotes geometric calculation

$_{ln}$ denotes log-normal distribution

C. Chu, et al. 'Pore-size Distribution of Copper Oxide-Alumina Catalysts,' J. Chem. Eng. Data 16(3), 1971, 327-331.

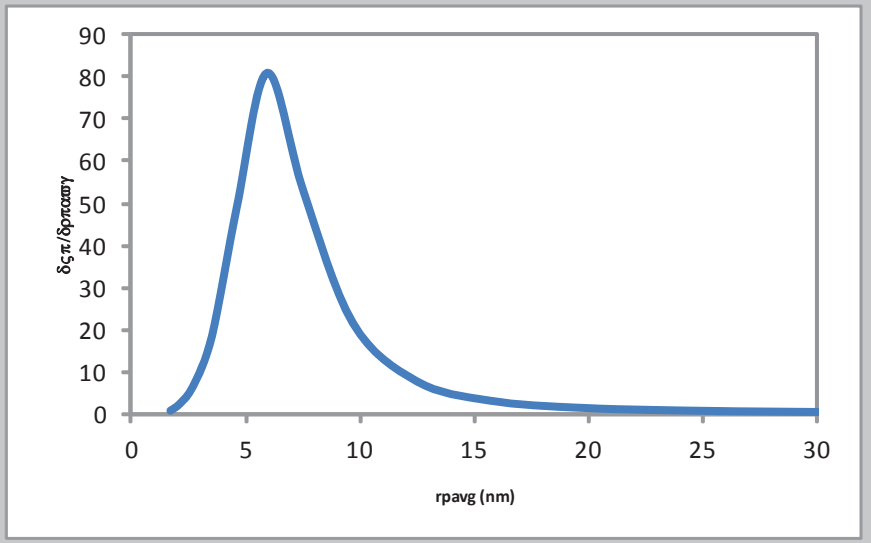

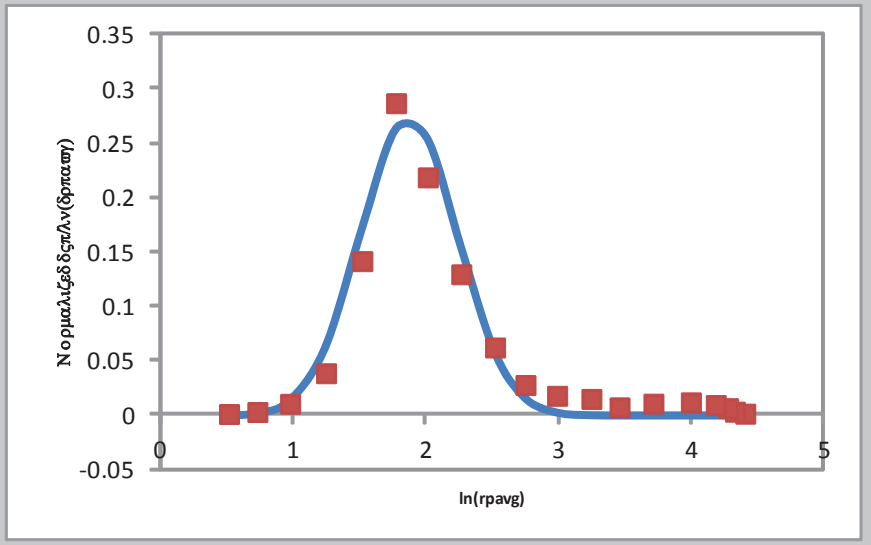

Figure 3. BET surface area and pore size for Co/Pt-co catalyst

Date:	3/3/2010	
Sample:	Co/Re-seq	
Technician:	Krikor Hagopian	
Source File (Name.RPT):	C:\Kari\Kinetics Research\BET\done\	
Save As (Path\Name.xls):		
BET DATA (From Report File)		
BET SA:	100	m^2/g
Mezopore d_{pavg}:	15.3	nm
Mezopore V_{pore}:	0.382	cm^3/g
BJH A_{pore}:	114	m^2/g
BJH V_{pore}:	0.386	cm^3/g
Micropore SA:		m^2/g
Micropore V_{pore}:	6.3	cm^3/g
Direct Calculation		
Mezopore d_{pavg}:	17.481	nm
Mezopore SA:	123.5	m^2/g
Mezopore V_{pore}:	0.395	cm^3/g
Volume Density Function Calculation		
Mezopore d_{pavg}:	14.328	nm
Standard Deviation σ_g:	2.874	nm
Log-normal Mean μ_{ln}:	2.0	
Log-normal SD σ_{ln}:	0.4	

Mezopore range is $r^p > 1.5$ nm

$_g$ denotes geometric calculation

$_{ln}$ denotes log-normal distribution

C. Chu, et al. 'Pore-size Distribution of Copper Oxide-Alumina Catalysts,' J. Chem. Eng. Data 16(3), 1971, 327-331.

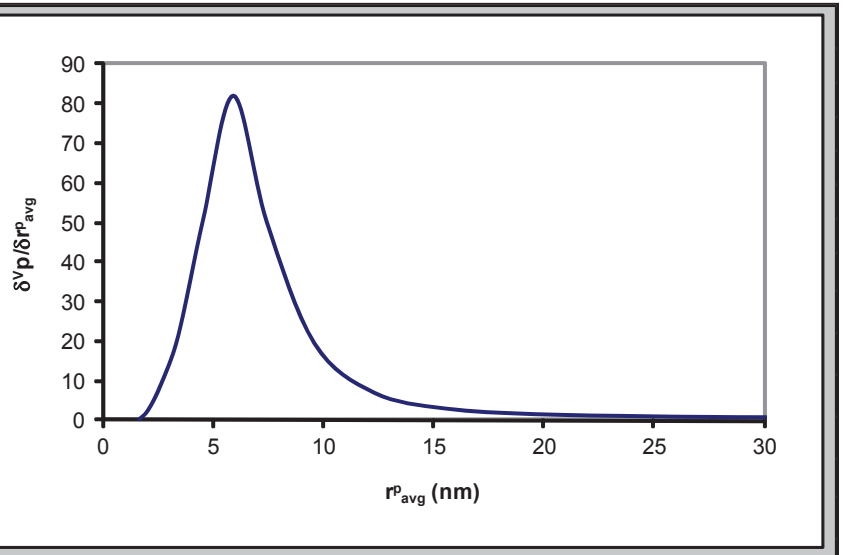

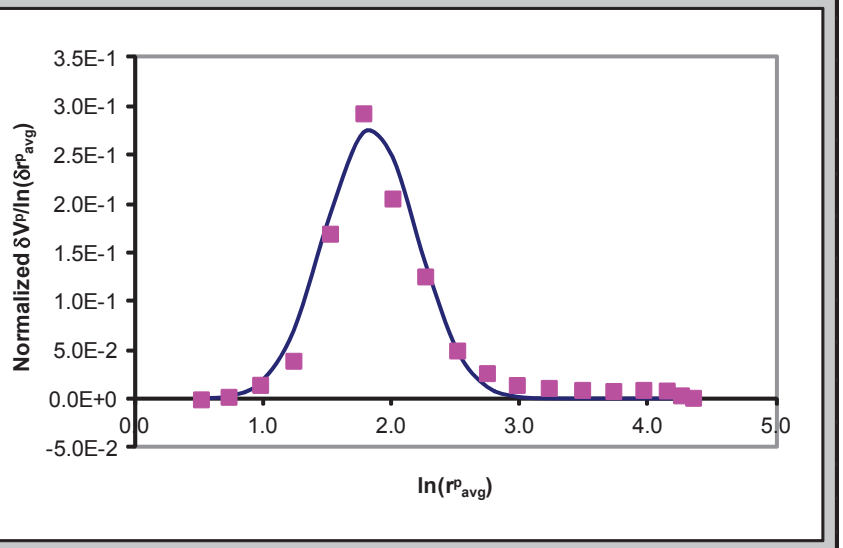

Figure 4. BET surface area and pore size for Co/Re-seq catalyst

Date:	3/2/2010	
Sample:	Co/Re-co	
Technician:	Krikor Hagopian	
Source File (Name.RPT):	C:\Kari\Kinetics Research\BET\	
Save As (Path\Name.xls):		
BET DATA (From Report File)		
BET SA:	96	m^2/g
Mezopore d_{pavg}:	16.4	nm
Mezopore V_{pore}:	0.396	cm^3/g
BJH A_{pore}:	110	m^2/g
BJH V_{pore}:	0.401	cm^3/g
Micropore SA:		m^2/g
Micropore V_{pore}:	5.3	cm^3/g
Direct Calculation		
Mezopore d_{pavg}:	18.957	nm
Mezopore SA:	119.7	m^2/g
Mezopore V_{pore}:	0.410	cm^3/g
Volume Density Function Calculation		
Mezopore d_{pavg}:	15.433	nm
Standard Deviation σ_g:	2.882	nm
Log-normal Mean μ_{ln}:	2.0	
Log-normal SD σ_{ln}:	0.4	

Mezopore range is $r^p > 1.5$ nm

$_g$ denotes geometric calculation

$_{ln}$ denotes log-normal distribution

C. Chu, et al. 'Pore-size Distribution of Copper Oxide-Alumina Catalysts,' J. Chem. Eng. Data 16(3), 1971, 327-331.

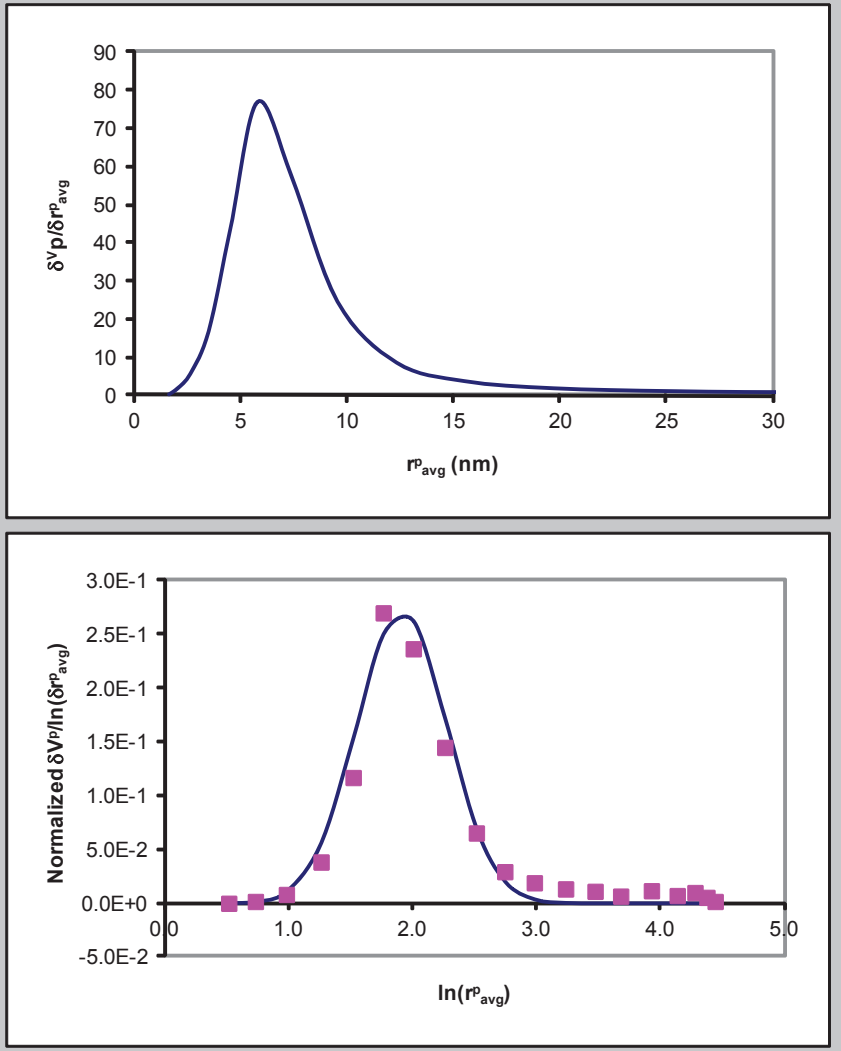

Figure 5. BET surface area and pore size for Co/Re-co catalyst

APPENDIX B METAL DISTRIBUTION

For each catalyst as well as the blank support, the microprobe scans for each element that were not already included in the dissertation are shown.

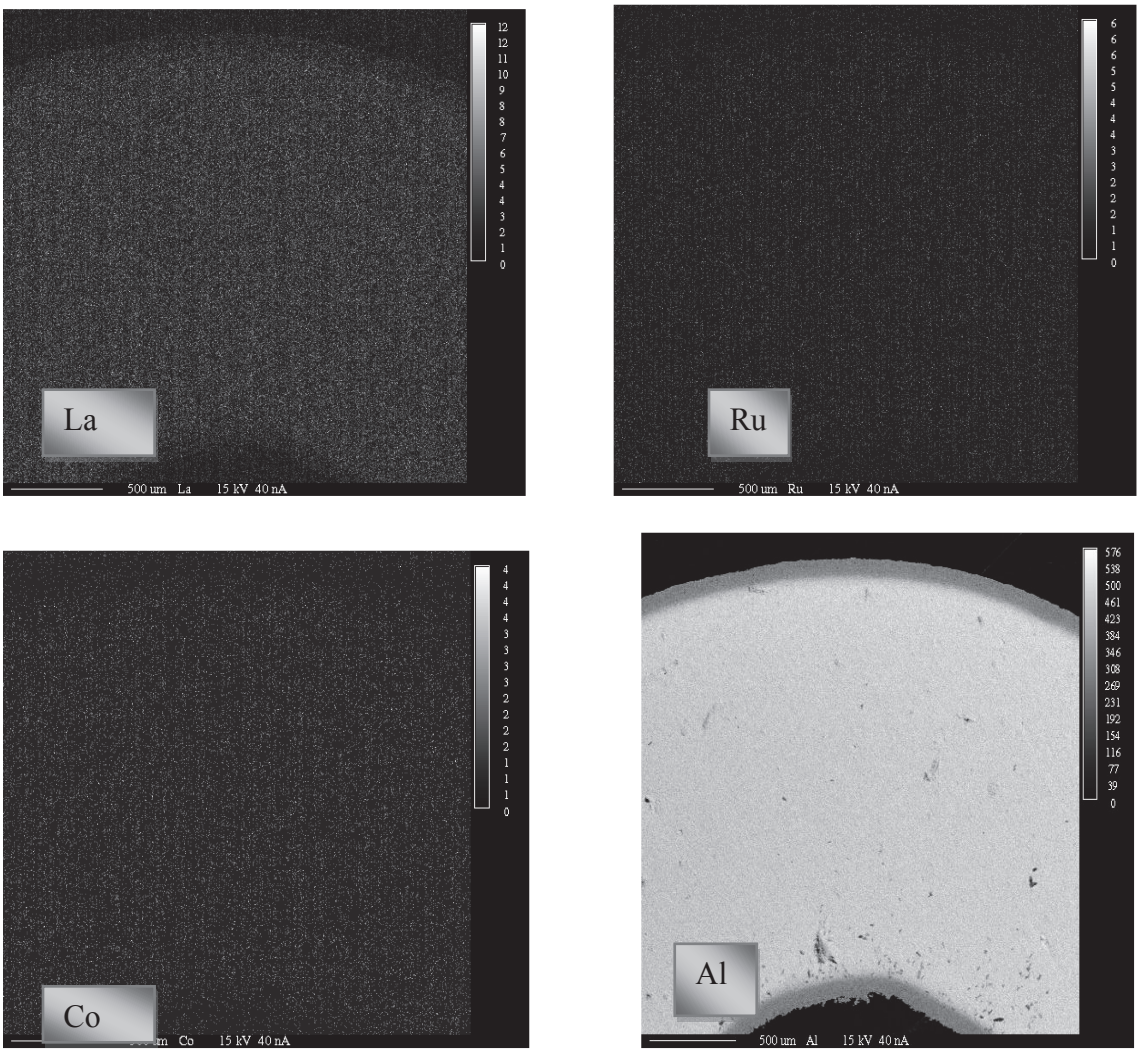

Figure 1. La, Ru, Co, and Al metal distributions for the unpromoted catalyst

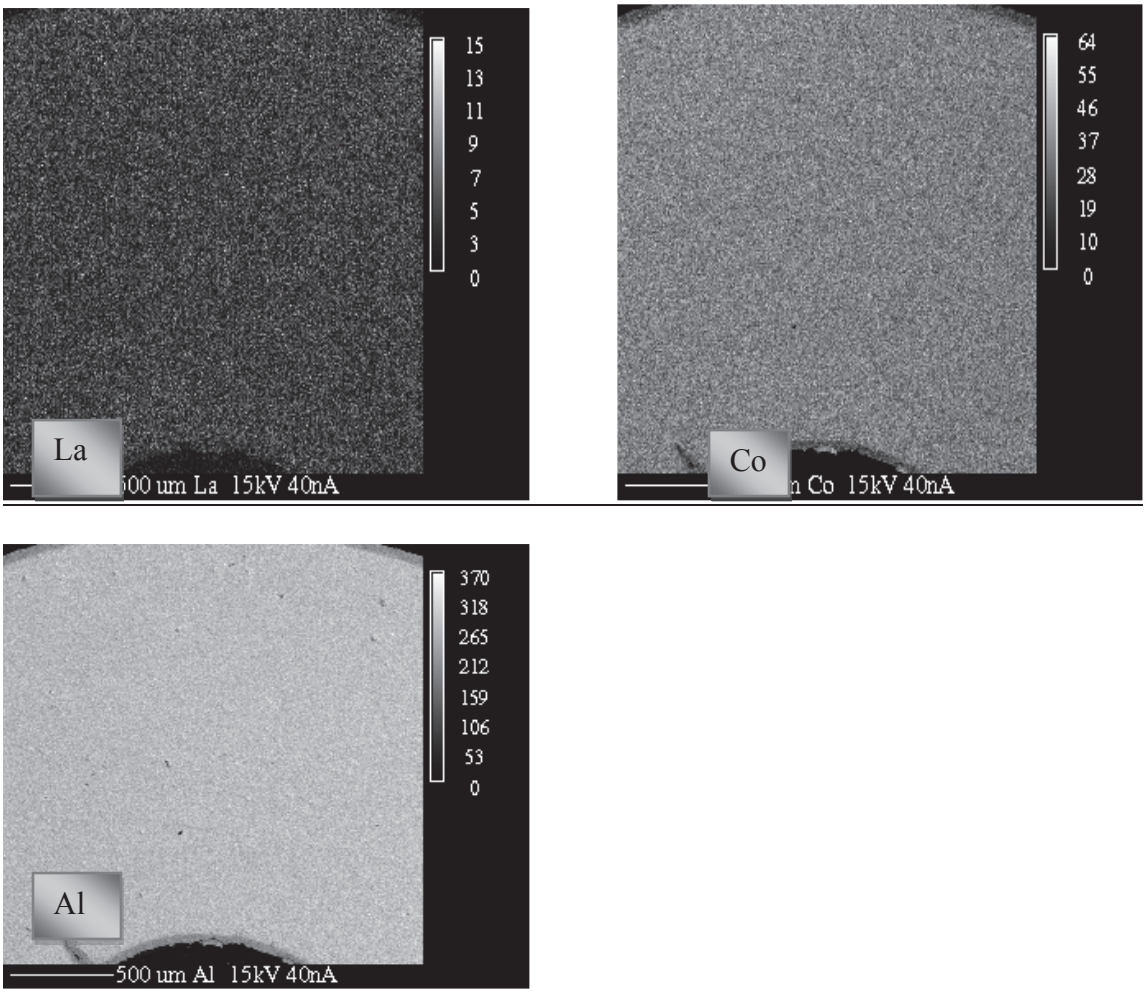

Figure 2. La, Co, and Al metal distributions for the unpromoted catalyst

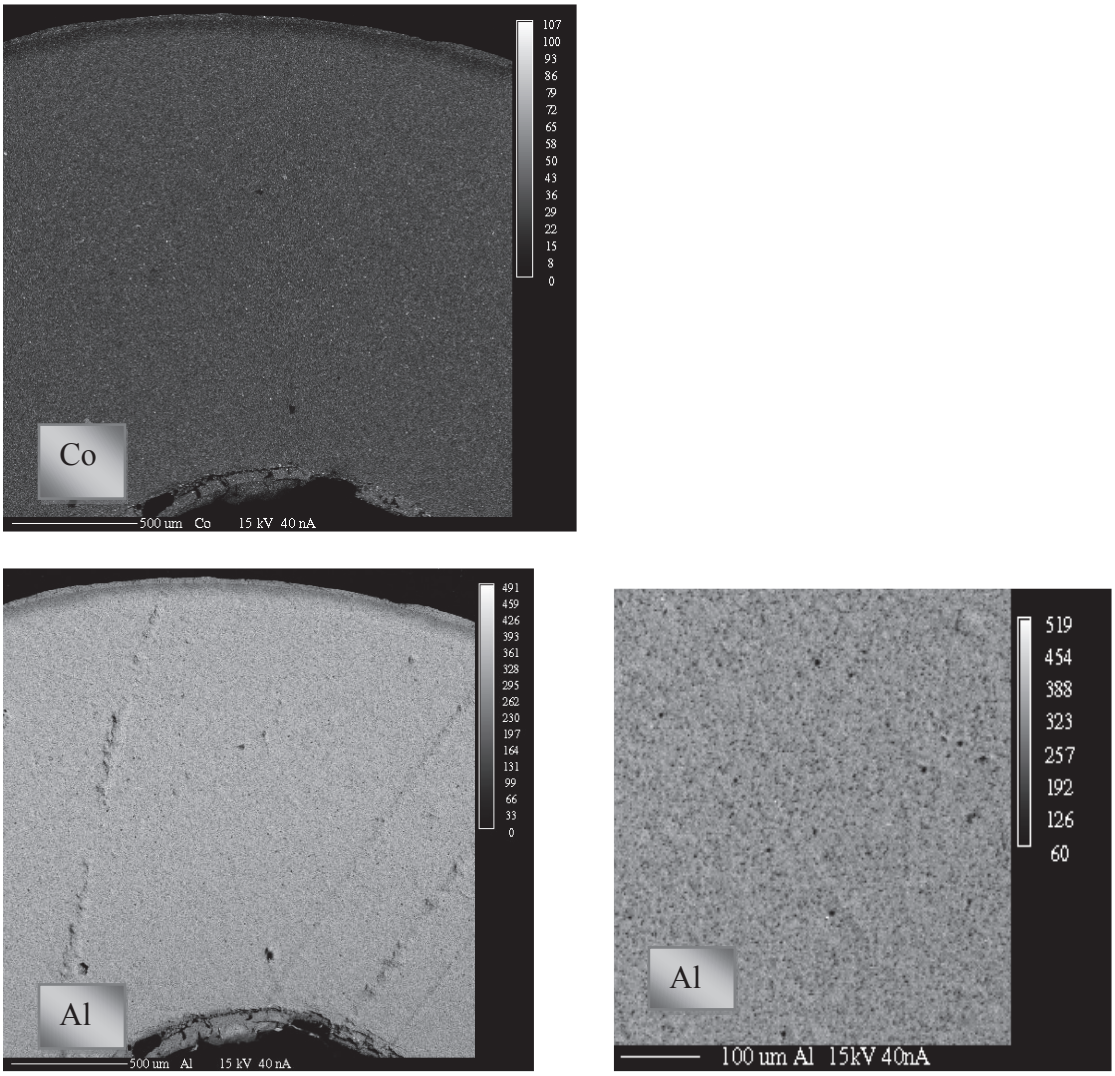

Figure 3. Co and Al Metal Distributions for the Co/Ru-seq catalyst

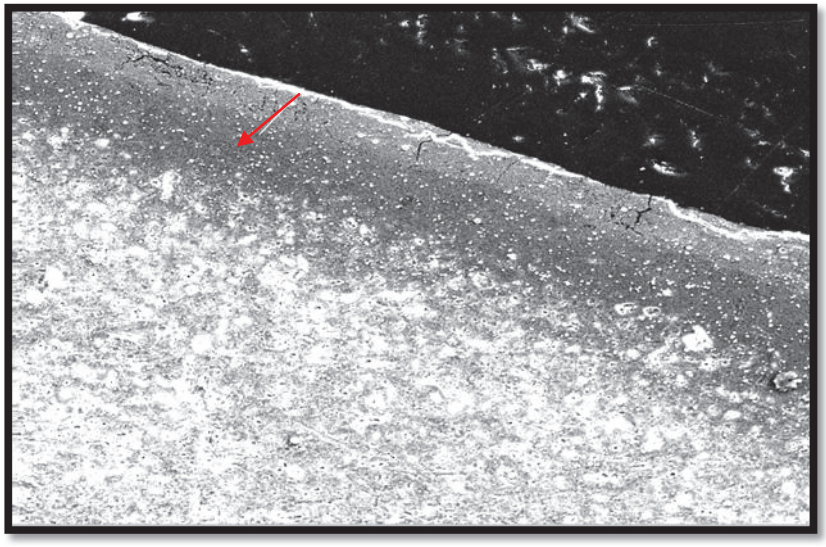

Figure 4. Linescan from edge towards the first dark layer of Co/Ru-seq catalyst

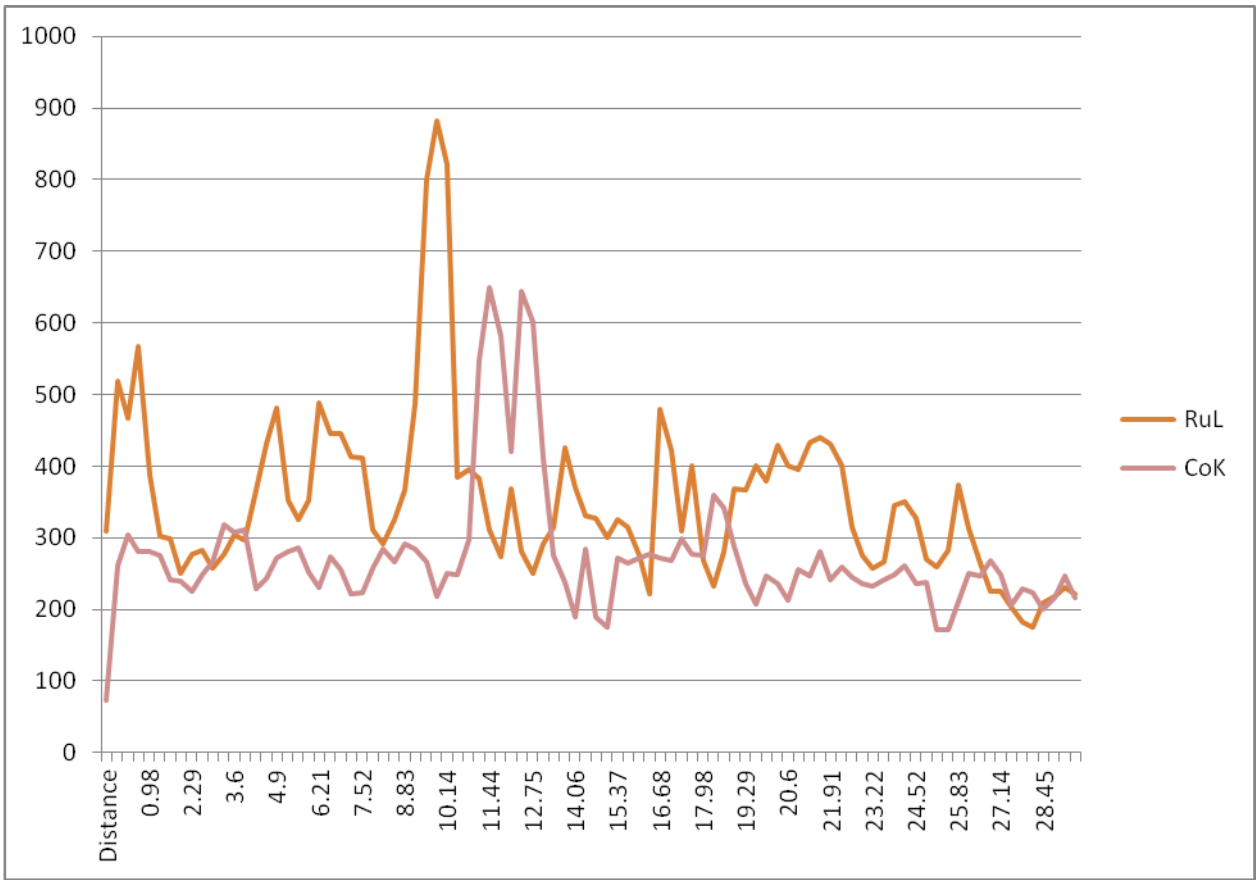

Figure 5. when counts plotted vs distance, higher count of Ruthenium found at the edge than the darker (epoxy) layer of Co/Ru-seq catalyst

Sample 1: SEM Line scans

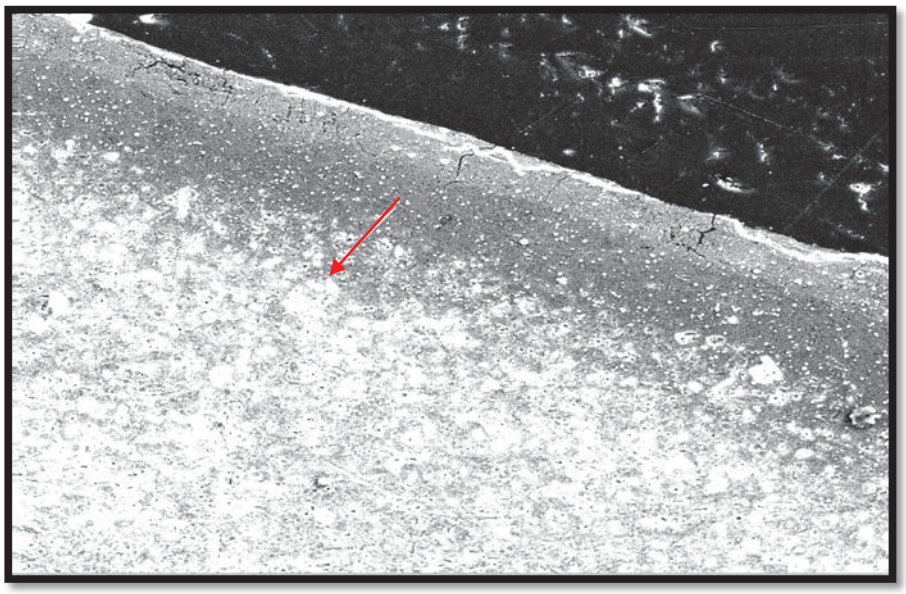

Figure 6. Linescan from dark (epoxy) layer towards the center of Co/Ru-seq catalyst

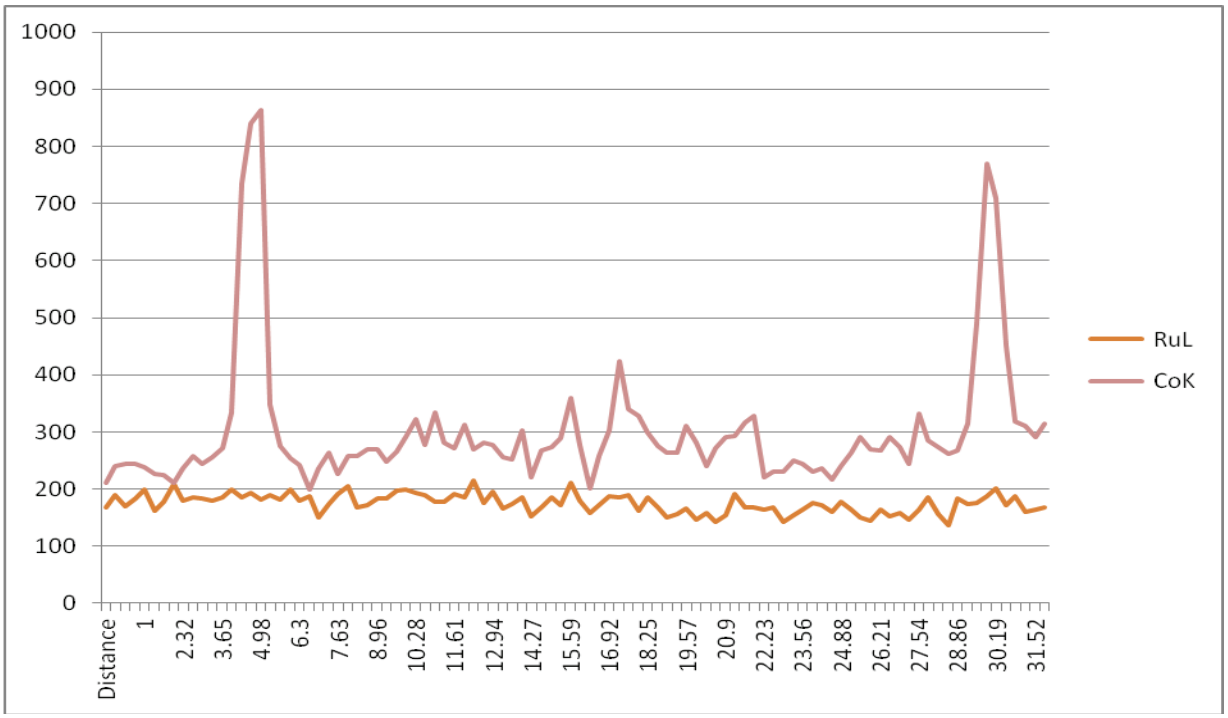

Figure 7. when counts plotted vs distance, Ruthenium count is really low of Co/Ru-seq catalyst Co/Pt-seq

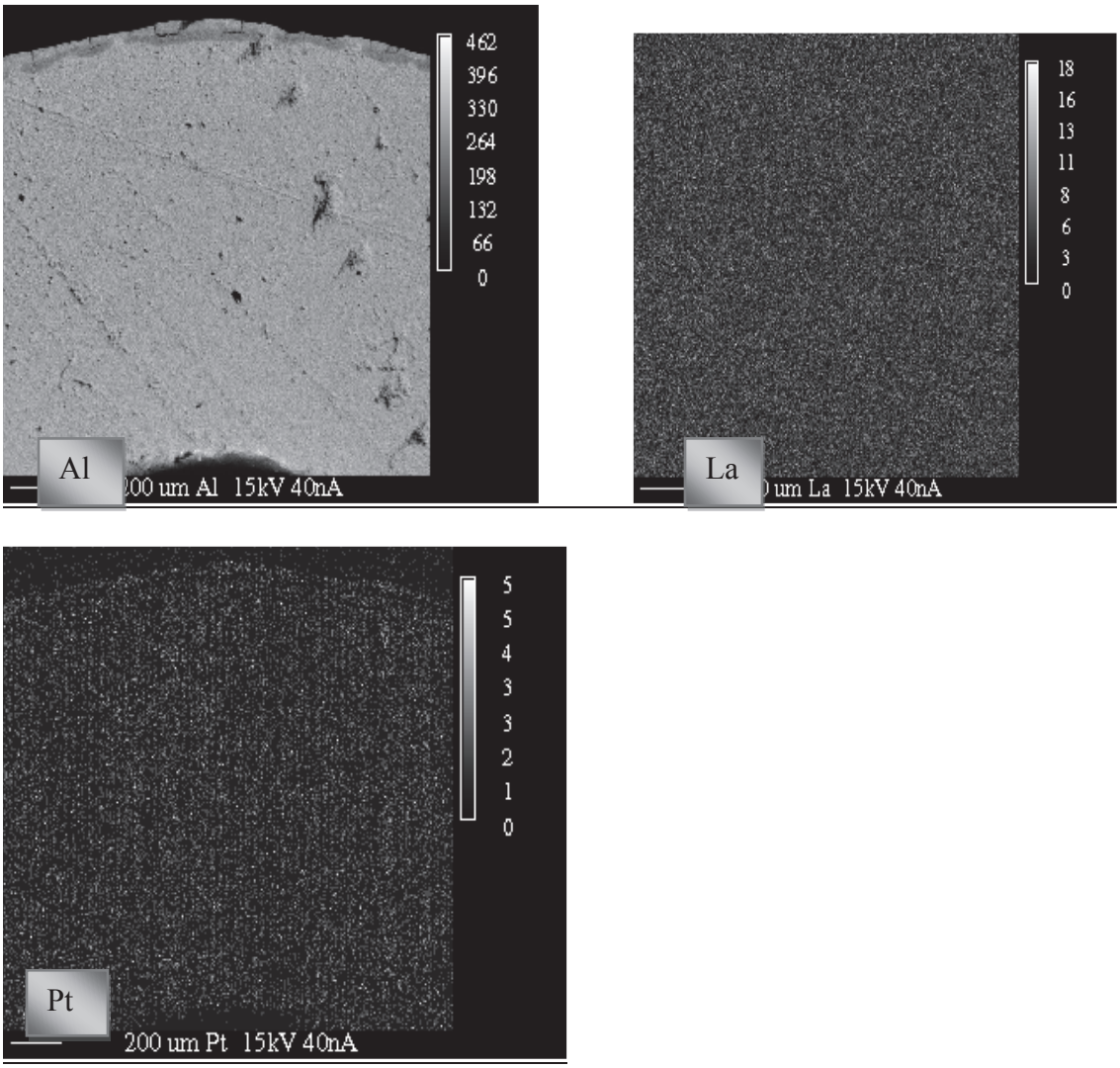

Figure 8. Co, La, and Pt metal distributions for the Co/Pt-seq catalyst

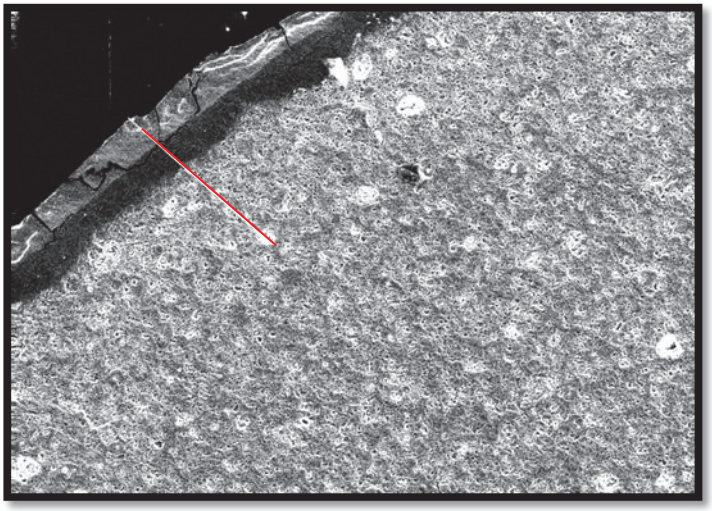

Figure 9. Linescan from edge to the center for the Co/Pt-seq catalyst

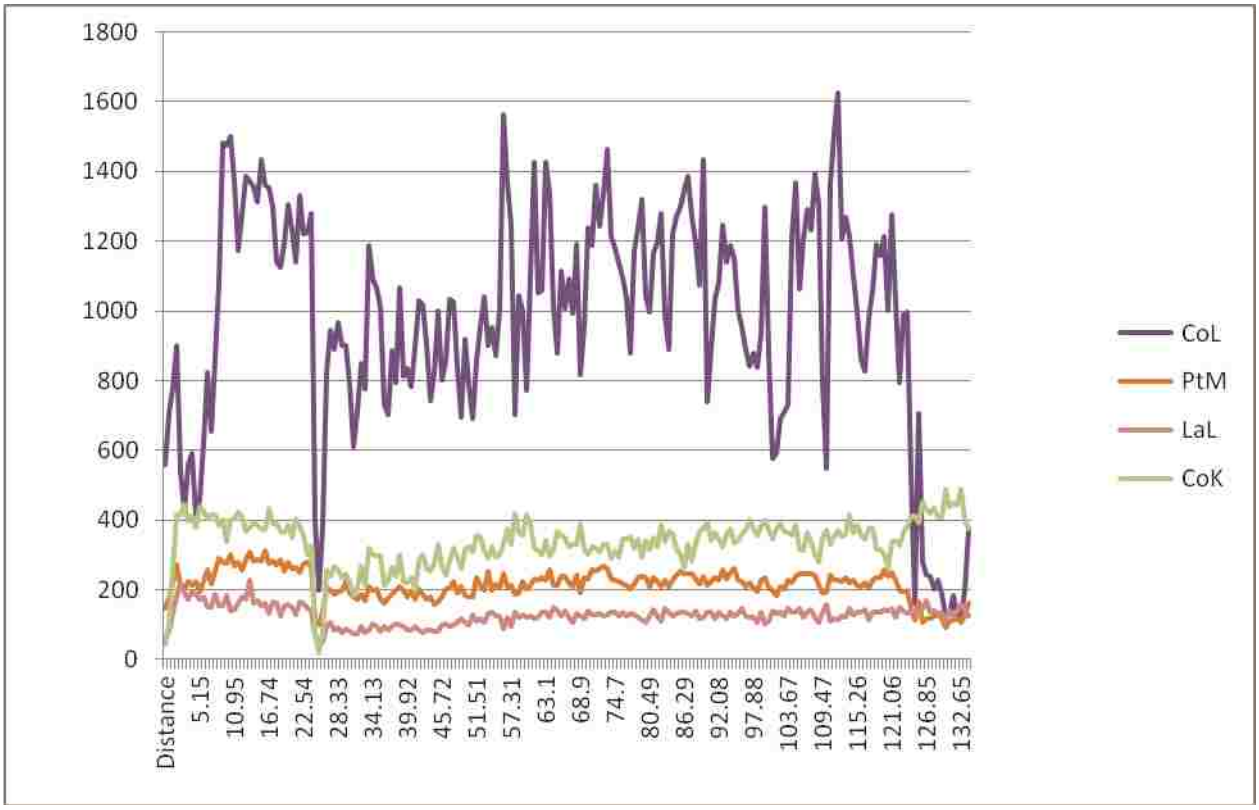

Figure 10. Co, Pt, and La counts from linescan from edge to the center for the Co/Pt-seq catalyst

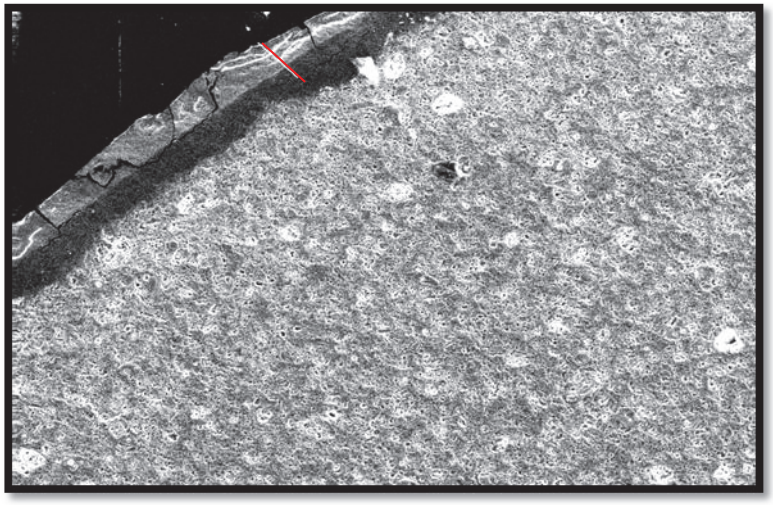

Figure 11. linescan from bright to dark edge for the Co/Pt-seq catalyst

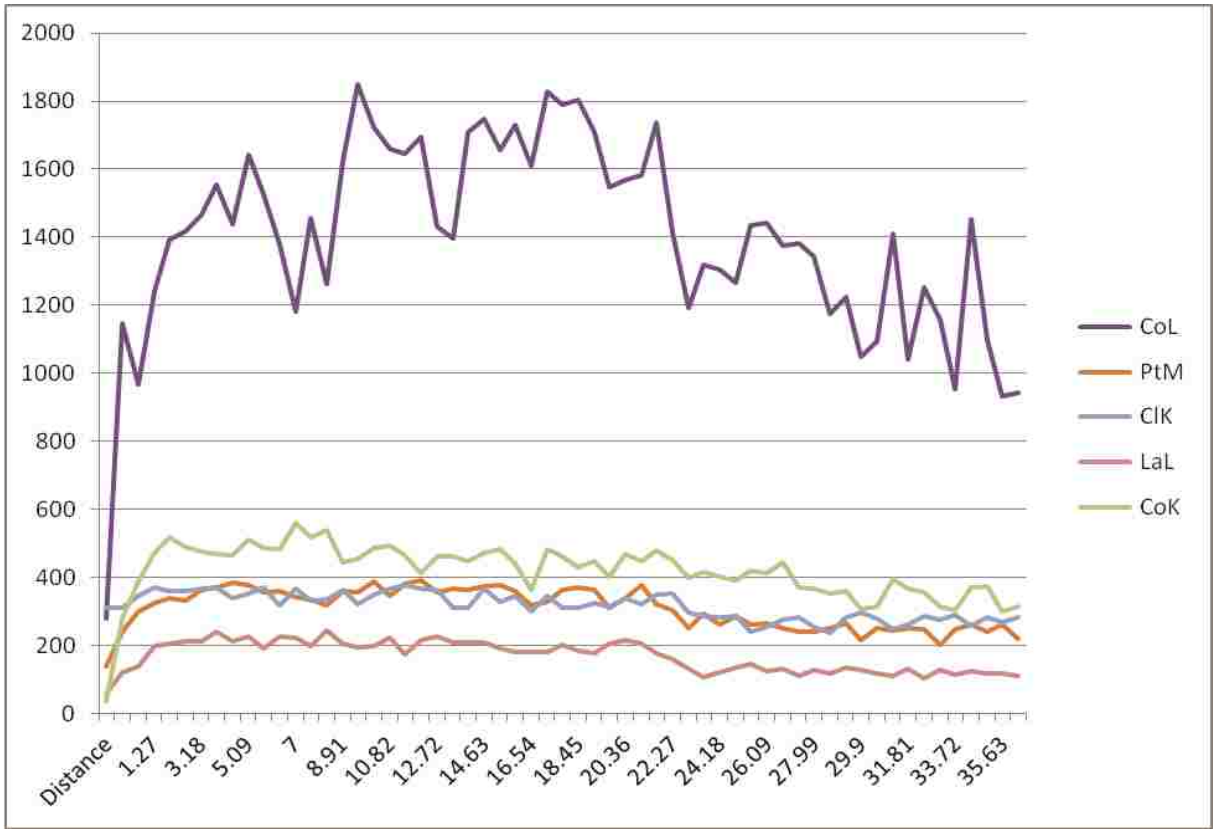

Figure 12.Co, Pt, O, and La counts from linescan from bright to dark edge for the Co/Pt-seq catalyst

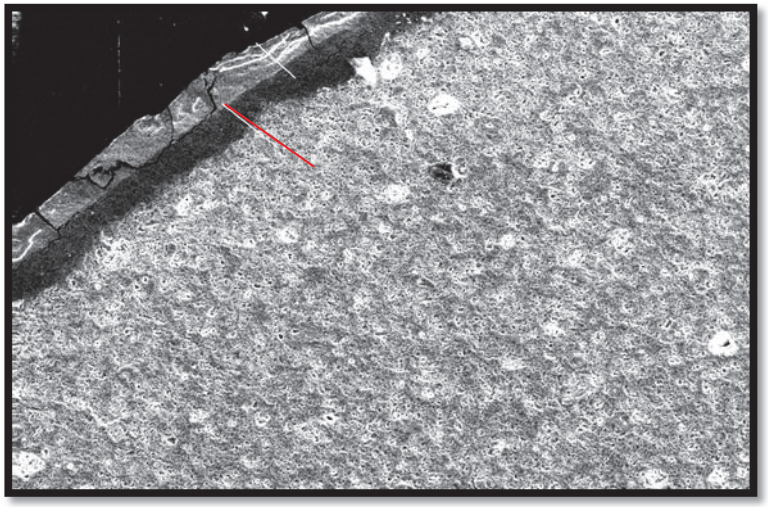

Figure 13. linescan from dark edge to center for the Co/Pt-seq catalyst

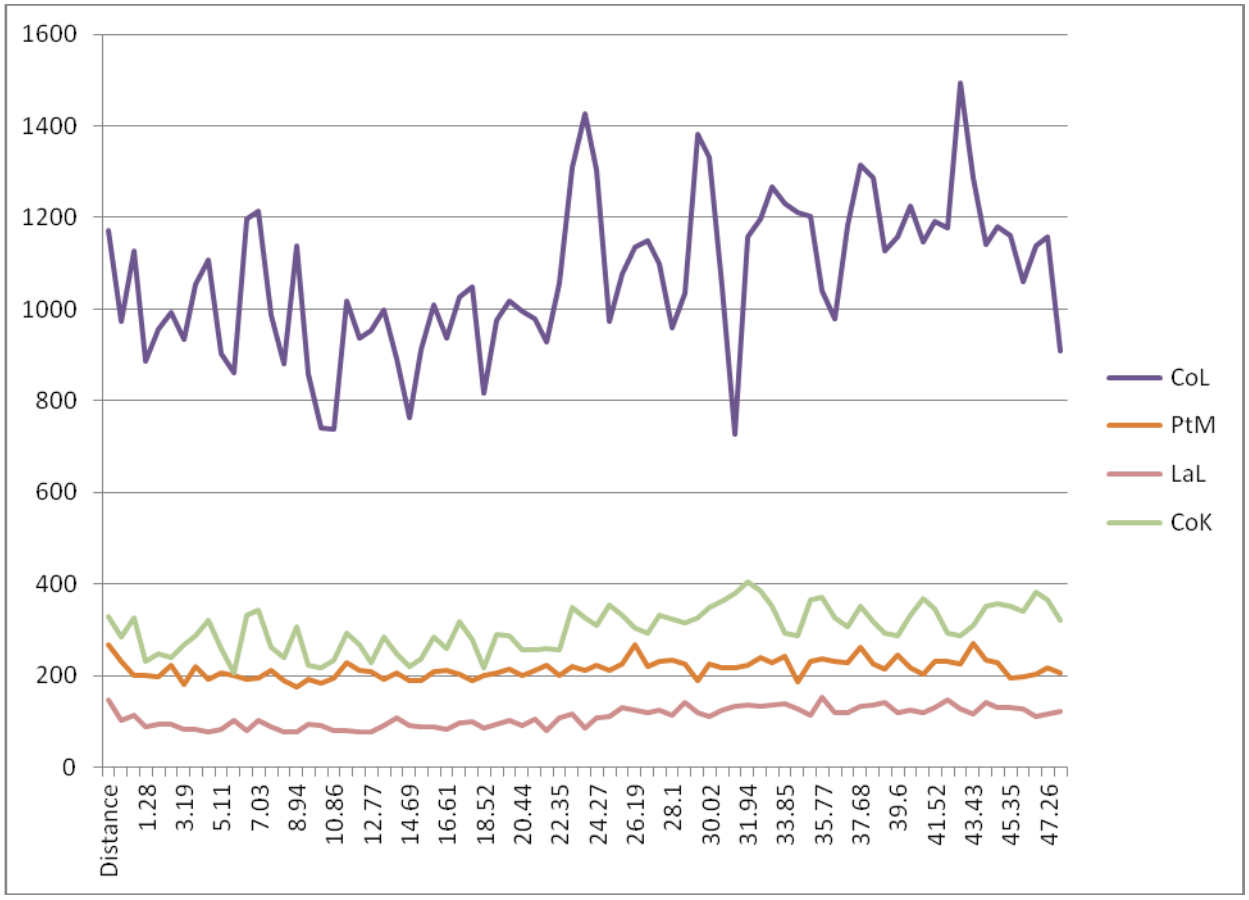

Figure 14. Co, Pt and La counts from the linescan from dark edge to center for the Co/Pt-seq catalyst

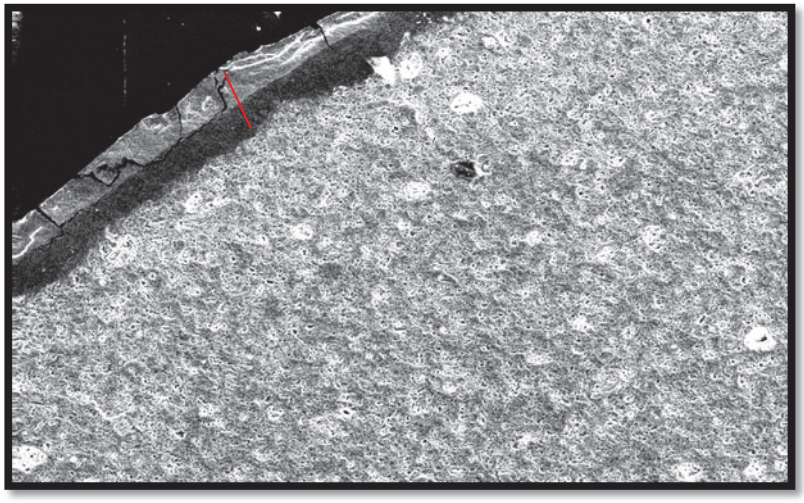

Figure 15. linescan of a white chunk for Co/Pt-seq catalyst

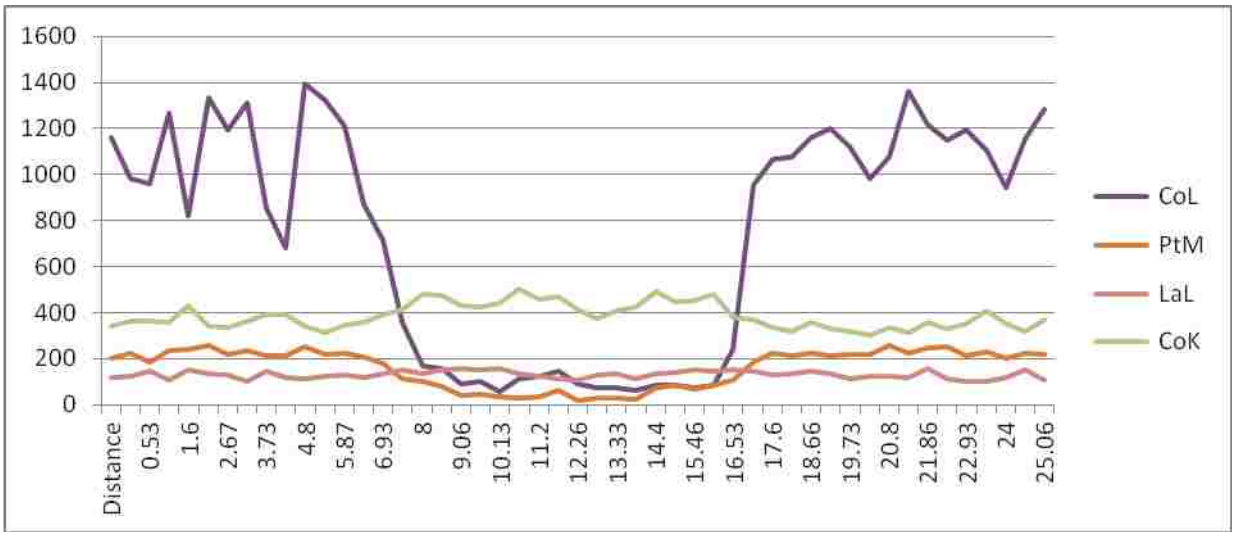

Figure 16. Co, Pt, and La counts from the linescan of a white chunk for Co/Pt-seq catalyst

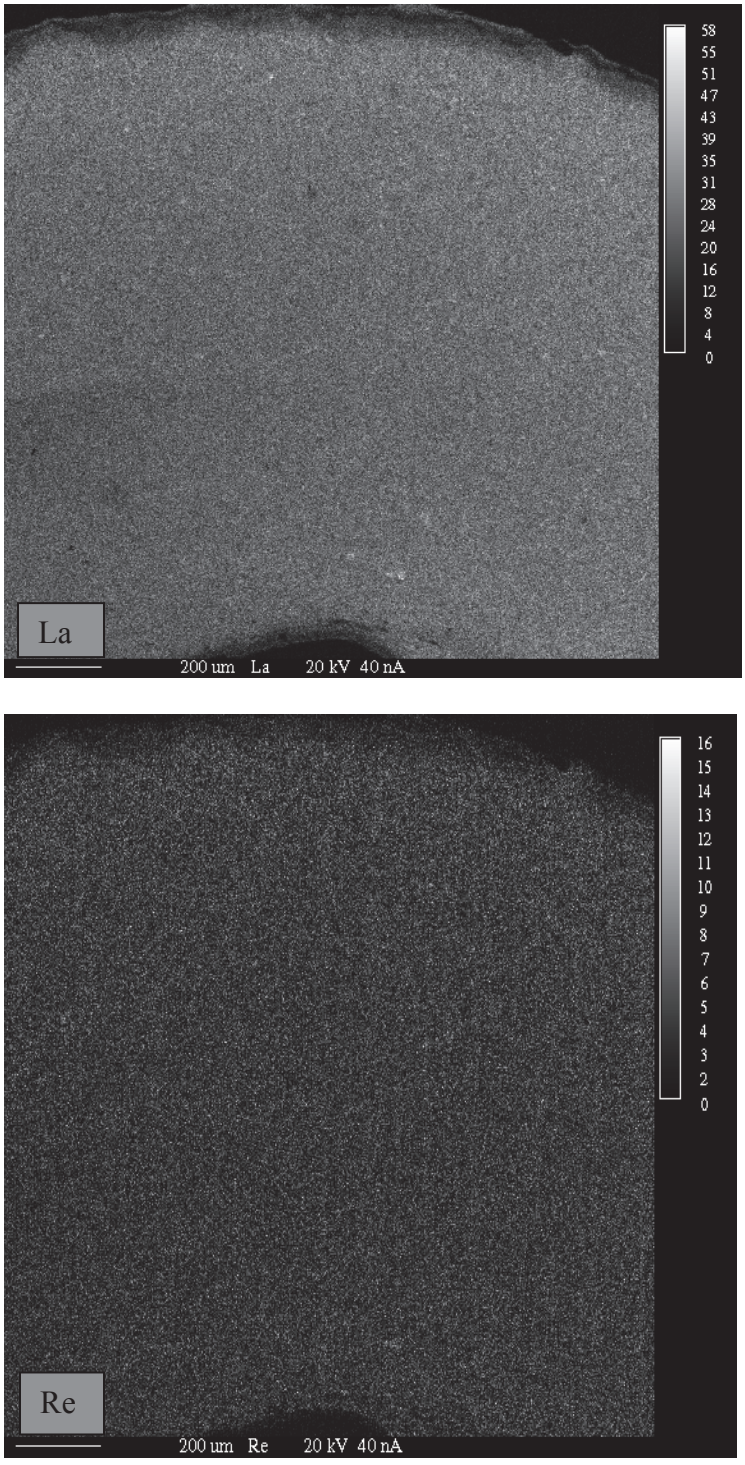

Figure 17. La and Re metal distributions for the Co/Re-seq catalyst

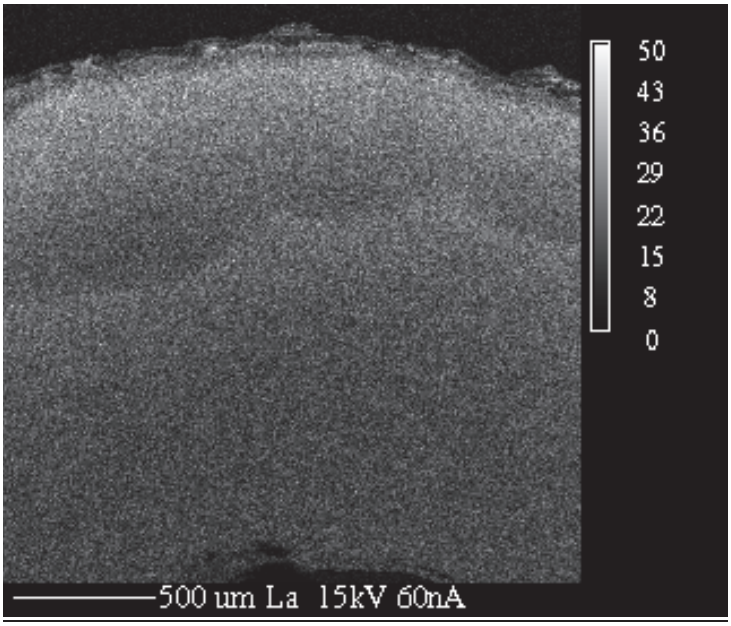

Figure 18. La metal distributions for the Co/Ru-co catalyst

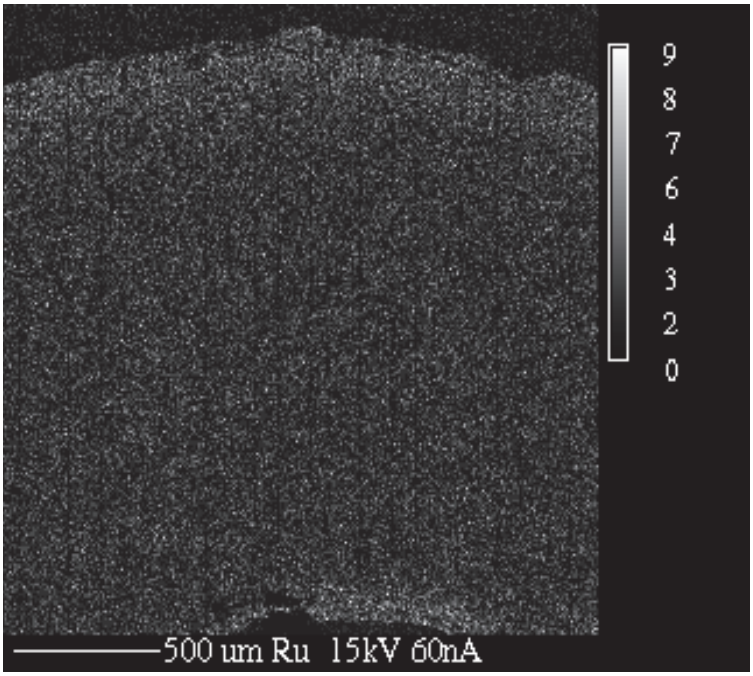

Figure 19. Ru metal distributions for the Co/Ru-co catalyst

APPENDIX C COBALT CRYSTALLITE SIZE

A representative TEM image of each catalyst is included below. For each catalyst, the microscope image files with the calibration of size as well as the excel files with all the measured particle sizes are included as part of the electronic Appendix (available from Dr. Hecker, hecker@byu.edu , or the BYU Chemical Engineering Department) in the folder TEM.

Co only

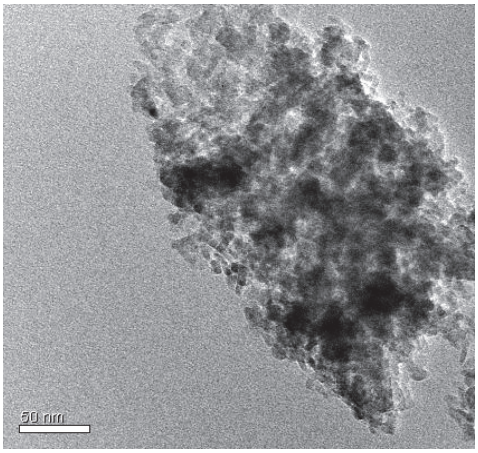

Co/Ru-seq

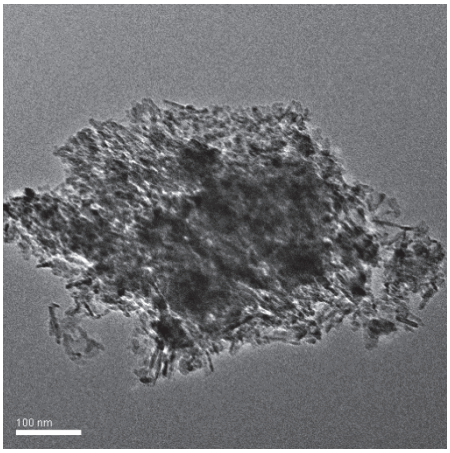

Co/Pt-seq

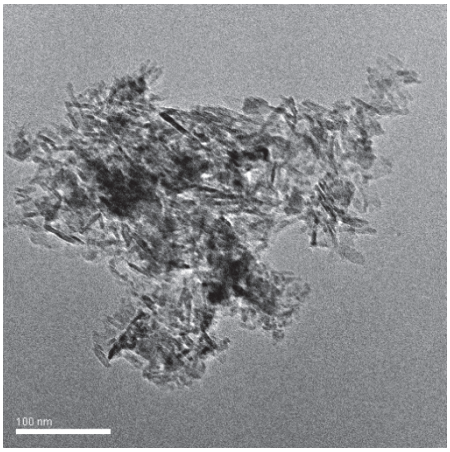

Co/Re-seq

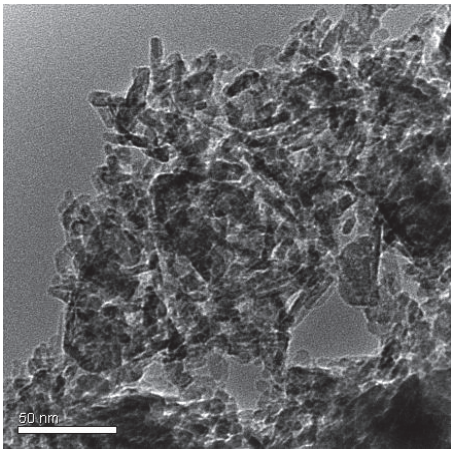

Figure 1. Representative TEM Images for the unpromoted and seq-dep catalysts

Co/Re-co

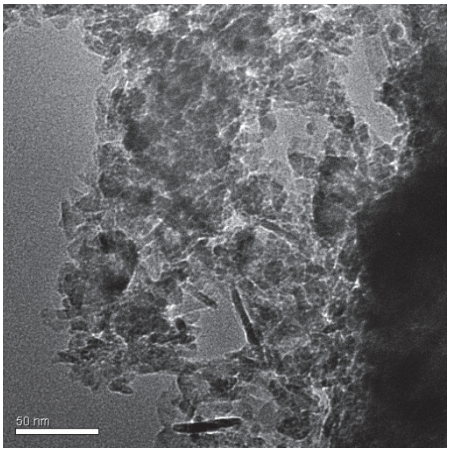

Co/Ru-co

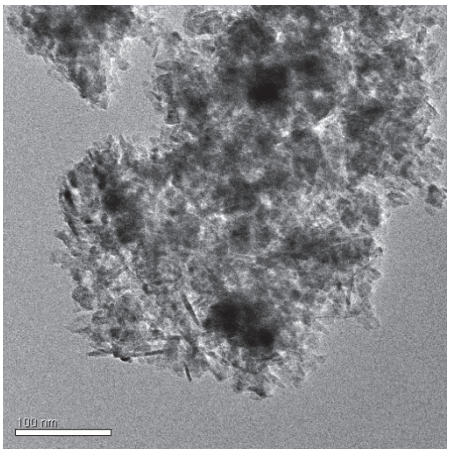

Co/Pt-co

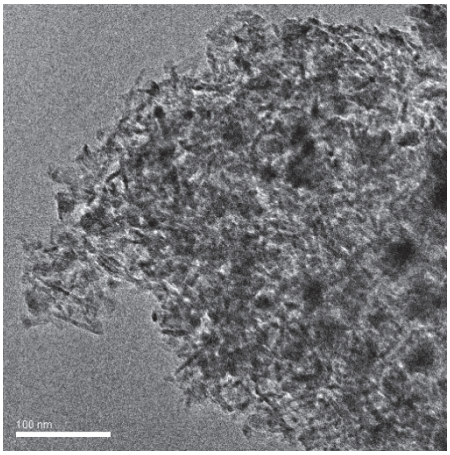

Figure 2. Representative TEM Images for the co-dep catalysts

APPENDIX D XAFS

For each catalyst, the XAFS data of normalized adsorption as a function of energy is plotted. The complete XAFS calcined as well as reduced (360^{o}C and in some cases 400^{o}C) data files are included as part of the electronic Appendix (available from Dr. Hecker, hecker@byu.edu , or the BYU Chemical Engineering Department) in the XAFS folder.

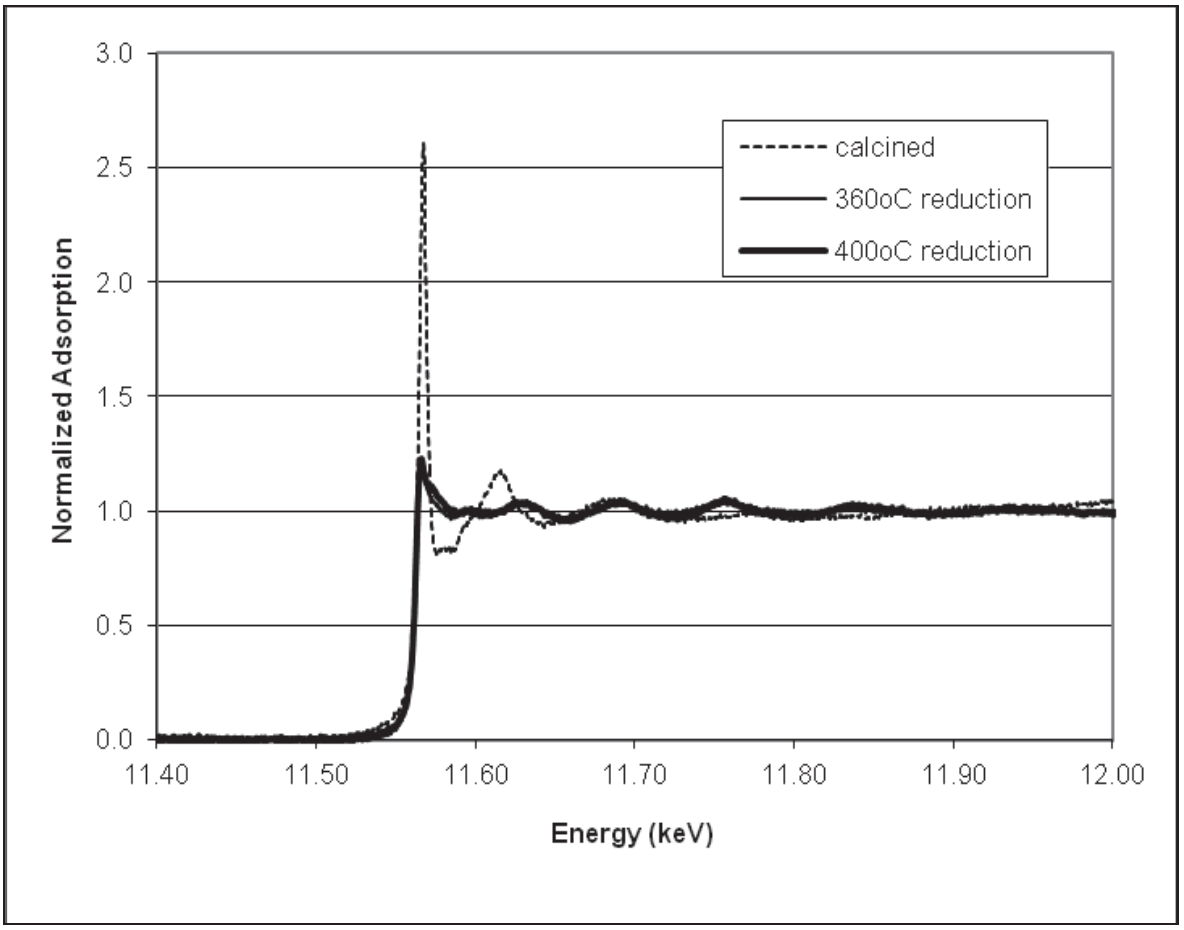

Figure 1. Normalized XAFS adsorption edge for Co/Pt-co catalyst

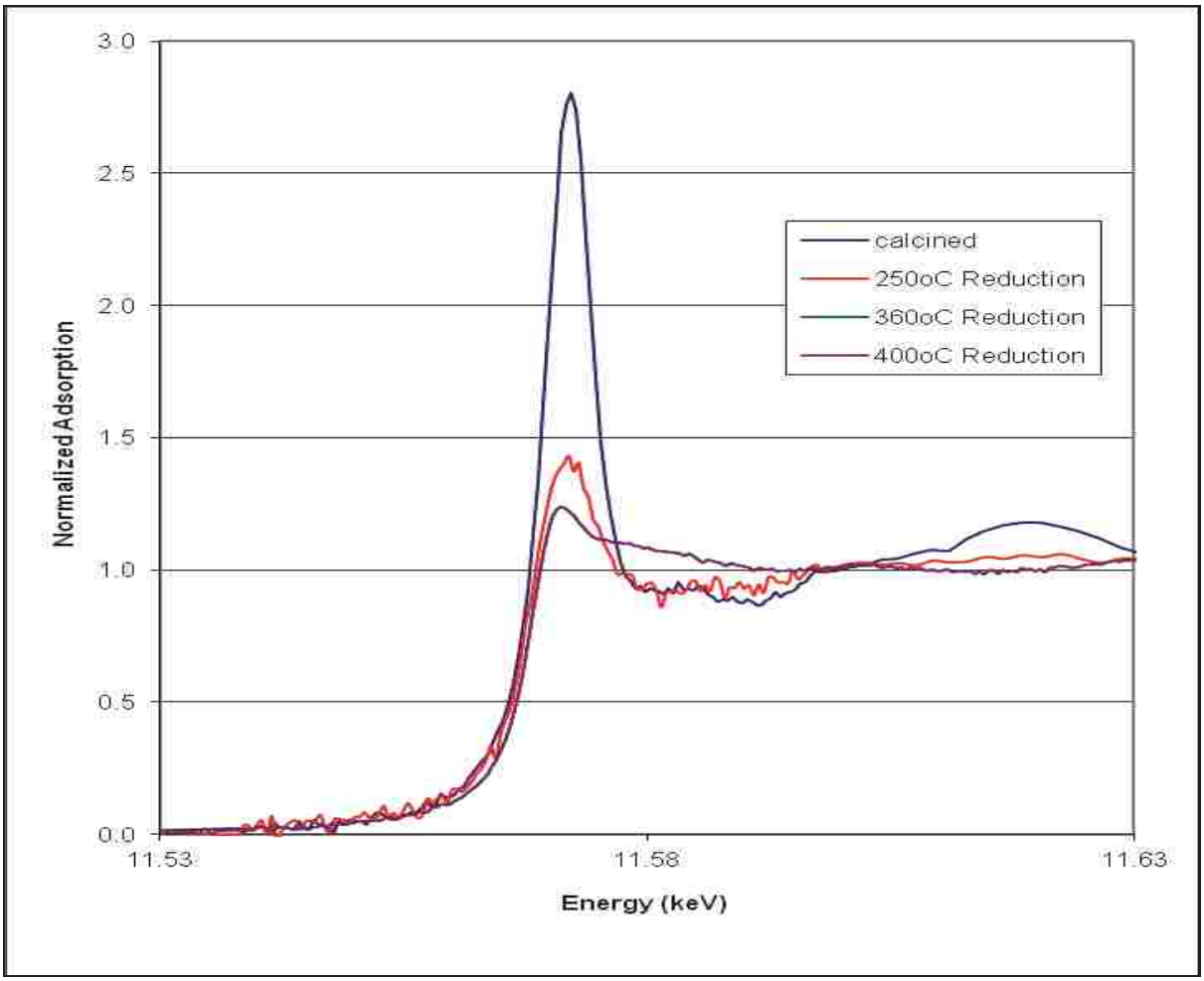

Figure 2. Normalized XAFS adsorption edge for Co/Pt-seq catalyst

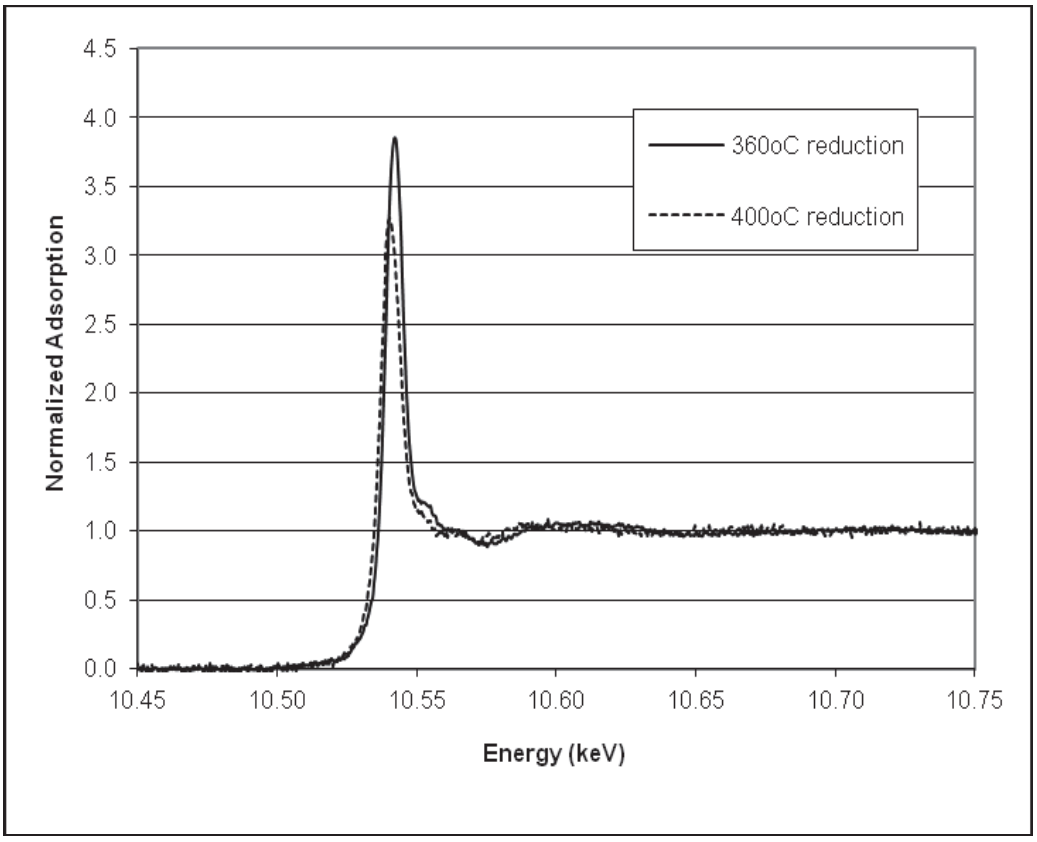

Figure 3. Normalized XAFS adsorption edge for Co/Re-co catalyst

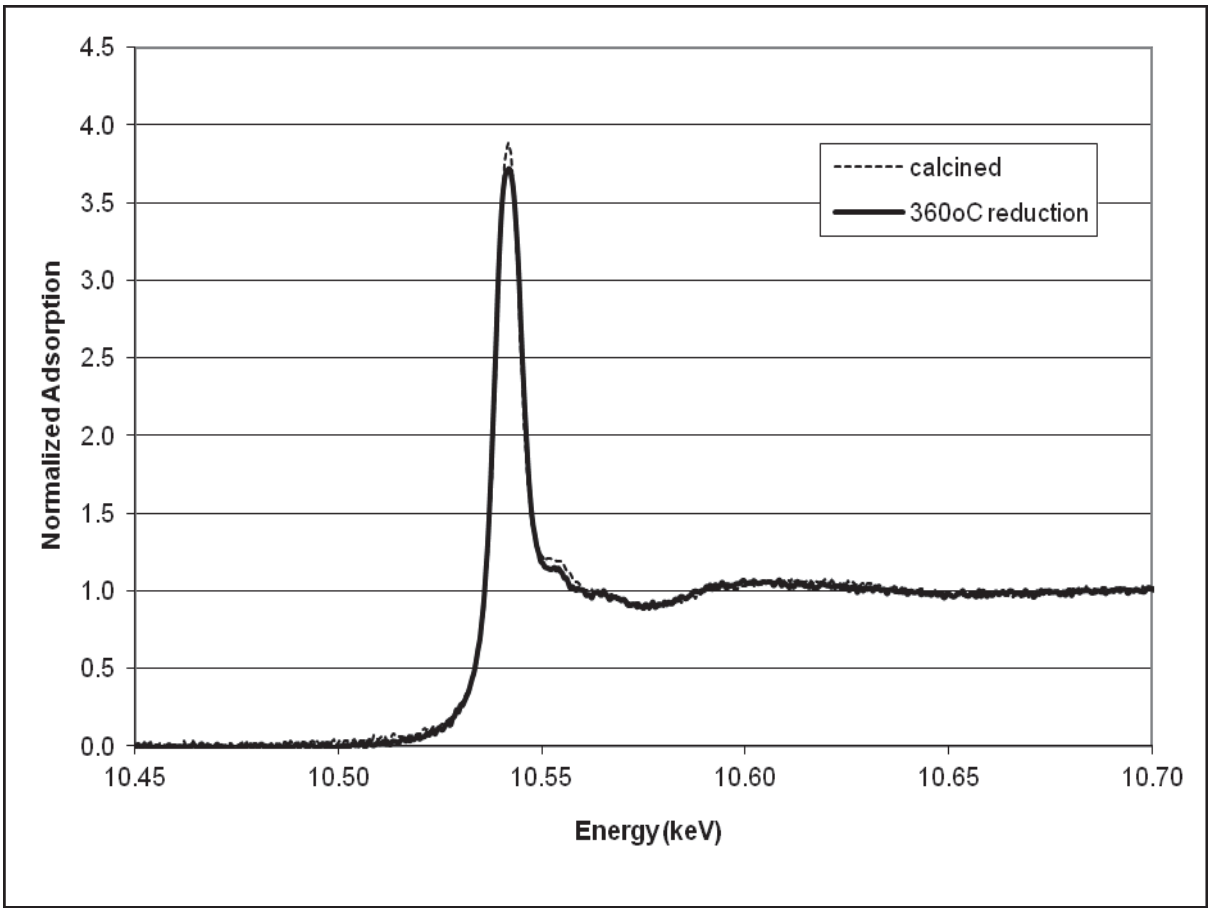

Figure 4. Normalized XAFS adsorption edge for Co/Re-seq catalyst

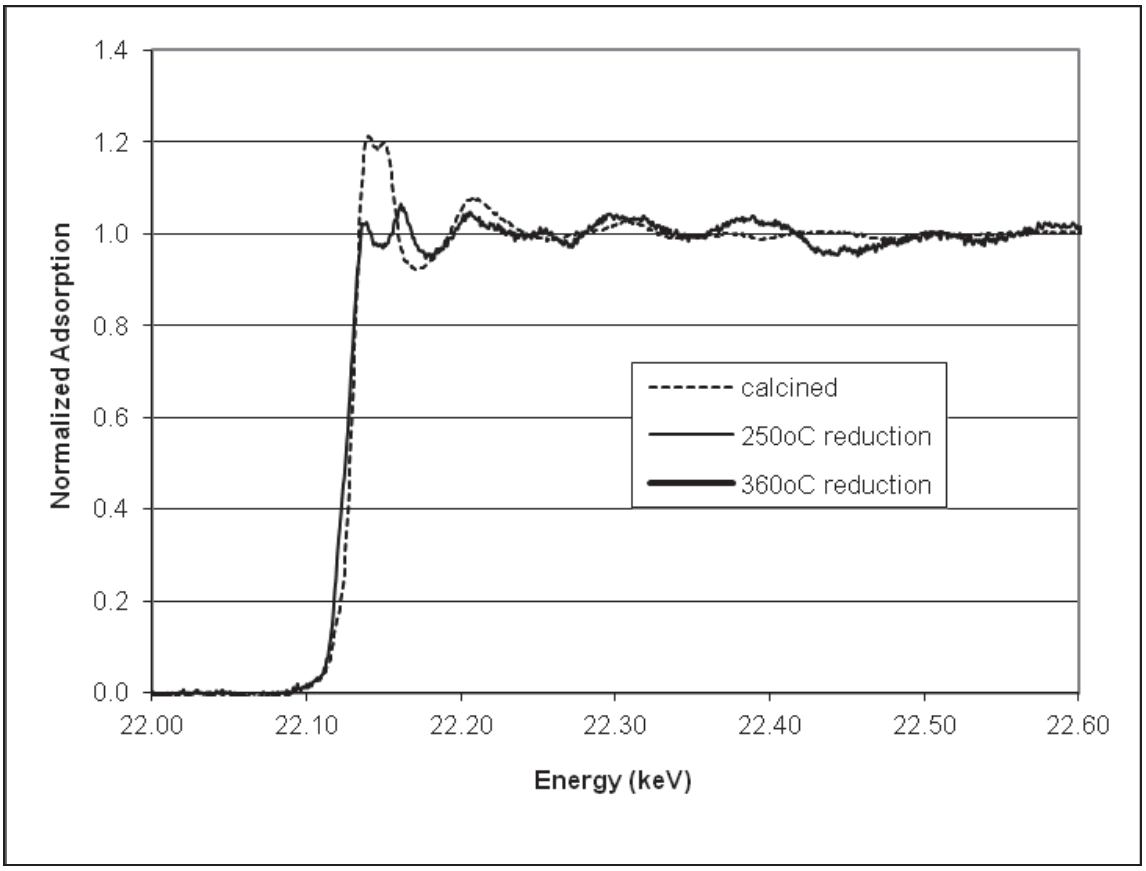

Figure 5. Normalized XAFS adsorption edge for Co/Ru-seq catalyst

APPENDIX E REDUCIBILITY

For each catalyst, the temperature programmed reduction and extent of reduction data are included as part of the electronic Appendix (available from Dr. Hecker, hecker@byu.edu , or the BYU Chemical Engineering Department) in the Reducibility folder.

The TPR folder includes TGA data files of temperature, percentage of weight, and original catalyst mass.

The EOR folder includes TGA data files of temperature, percentage of weight, and original catalyst mass as well as EOR calculator files showing the calculation extent of reduction from this data.

APPENDIX F H_2 CHEMISORPTION

For each catalyst, desorption curve and temperature ramp are plotted as a function of time. The excel versions of each of these files with the data and plots are included as part of the electronic Appendix (available from Dr. Hecker, hecker@byu.edu , or the BYU Chemical Engineering Department). In the folder, H_2 chemisorption where:

1.xls=Co/Ru-co

2.xls=Co/Pt-co

3.xls=Co/Ru-seq

4.xls=Co/Pt-seq

5.xls=Co only

6.xls=Co/Re-co

7.xls=Co/Re-seq

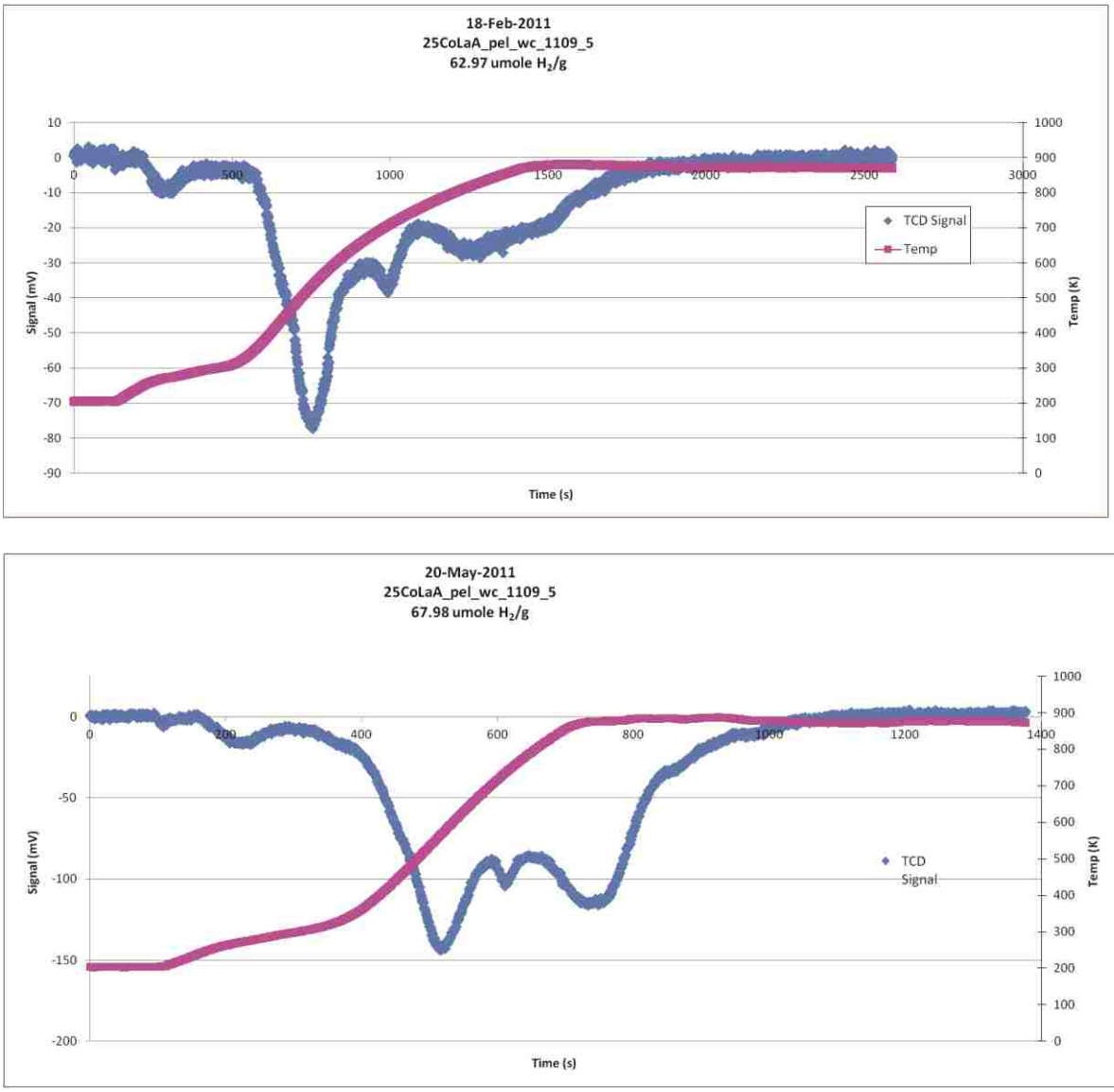

Figure 1. H_2 desorption curves for the unpromoted catalyst

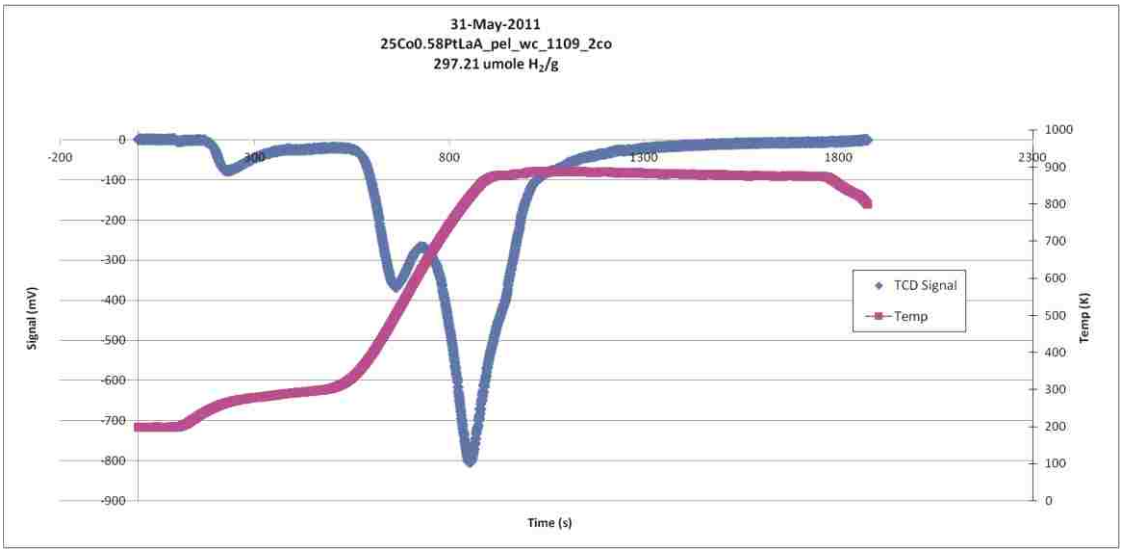

Figure 2. H_2 desorption curve for the Co/Pt-co catalyst

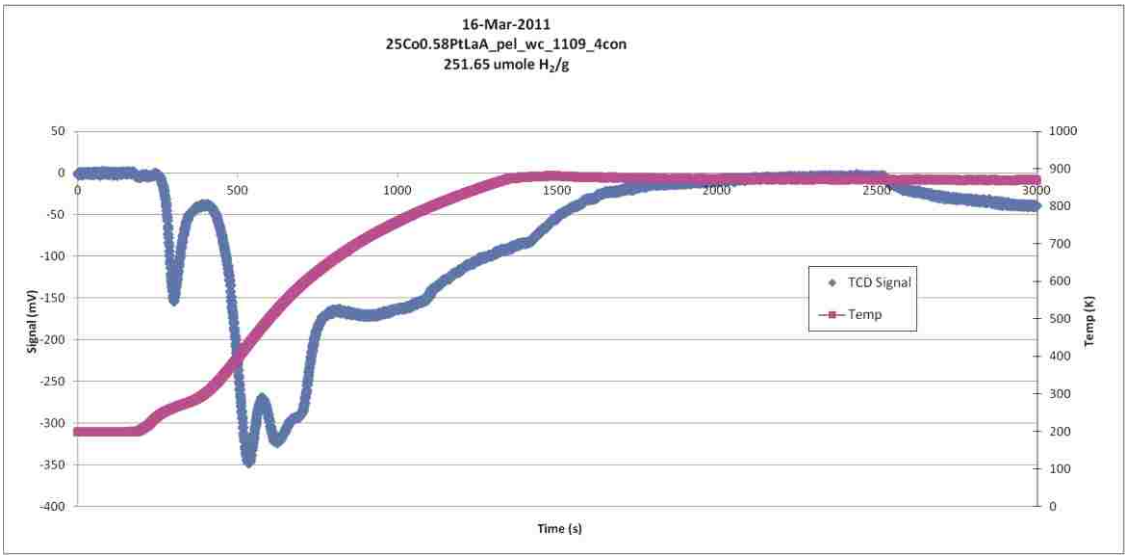

Figure 3. H_2 desorption curve for the Co/Pt-seq catalyst

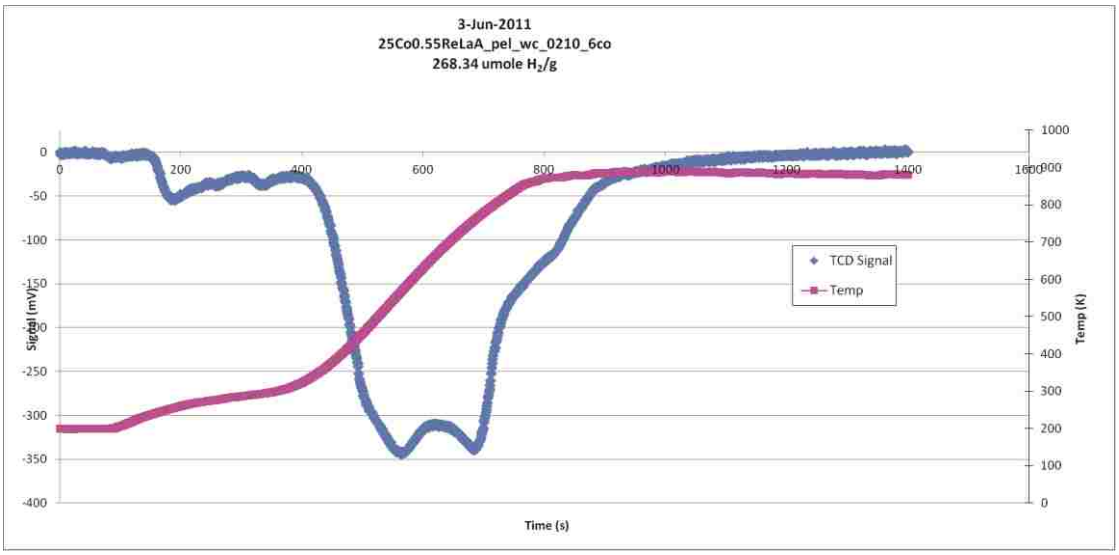

Figure 4. H_2 desorption curve for the Co/Re-co catalyst

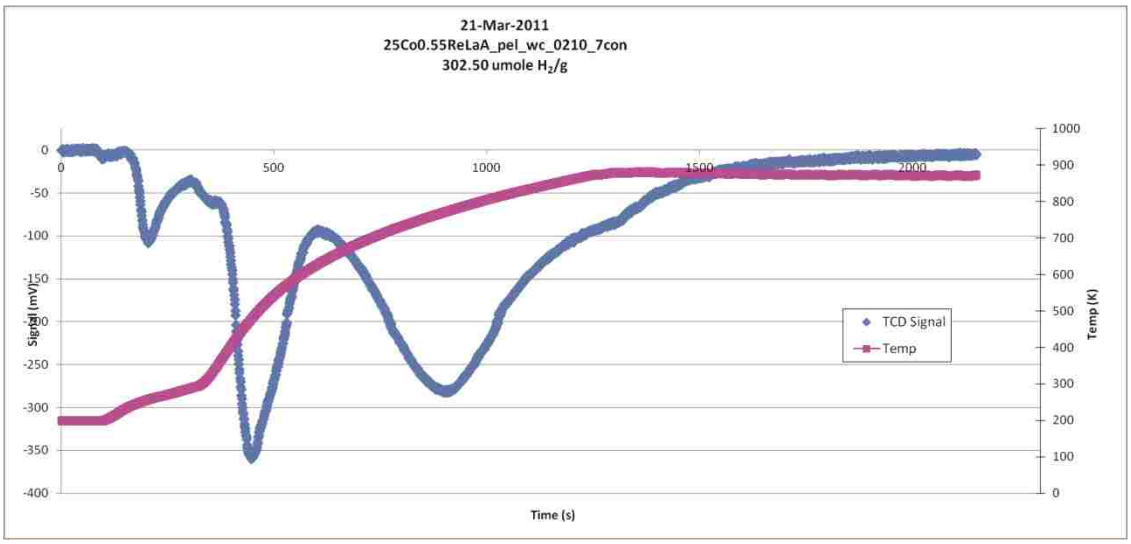

Figure 5. H_2 desorption curve for the Co/Re-seq catalyst

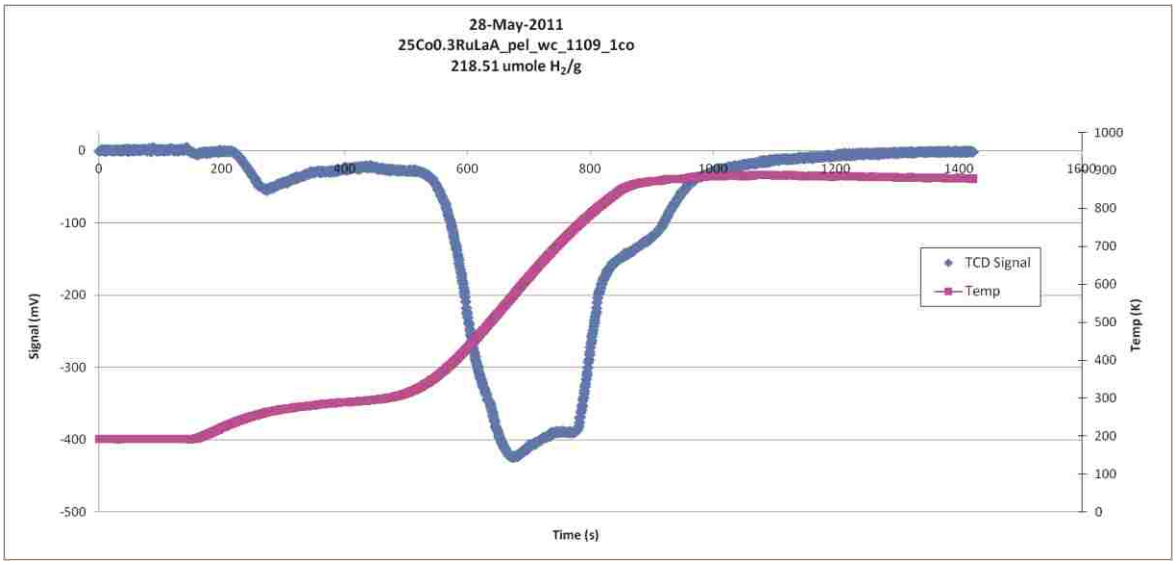

Figure 6. H_2 desorption curve for the Co/Ru-co catalyst

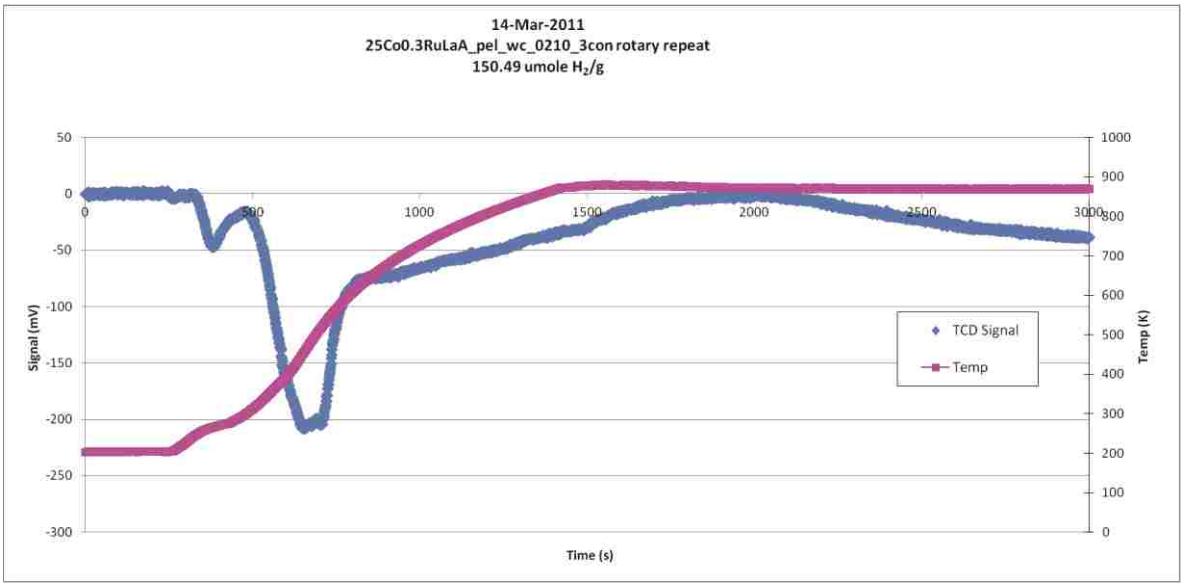

Figure 7. H_2 desorption curve for the Co/Ru-co catalyst

APPENDIX G FIXED BED

For each catalyst, the fixed bed conditions are given in rows 1-32 with the condition listed in the 1st column and the value listed in the 2nd column. In the cases where multiple runs were performed an additional (3rd) column lists in conditions for that repeat run that were different. Starting in row 33 the GC peak areas and temperatures are giving for each condition along with companioning calculated properties.

The excel versions of each of these files is included as part of the electronic Appendix (available from Dr. Hecker, hecker@byu.edu , or the BYU Chemical Engineering Department). In the folder, Fixed Bed/Catalysts Summaries where:

1.xls=Co/Ru-co
2.xls=Co/Pt-co
3.xls=Co/Ru-seq
4.xls=Co/Pt-seq
5.xls=Co only
6.xls=Co/Re-co
7.xls=Co/Re-seq

The mathematica file used for nonlinear regression fits of k for E_A.are included as part of the electronic Appendix (available from Dr. Hecker, hecker@byu.edu , or the BYU Chemical Engineering Department). In the folder, Fixed Bed/Catalysts Summaries where:

1=Co/Ru-co
2=Co/Pt-co
3=Co/Ru-seq
4=Co/Pt-seq
5=Co only
6=Co/Re-co
7=Co/Re-seq

Table 1. Fixed bed reaction conditions and raw data for the unpromoted catalyst

Weight of Catalyst (g_{cat})			0.2583	0.2530															
H_2 uptake (□mol/g_{cat})			65																
Baseline CO/Ar			6.80	6.6474803															
□			-2																
$P_{reactor}$ (psi)			313																
Density			0.697																
Fits			**Nonlinear**	**Linear**															
A			4638.20	8493.0206															
E_{App}/Rg			9359.45	9649.5															
E_{App} (kJ/mol)			**77.81**	**80.23**															
200°C, 20 atm, 50% X_{co} , 2:1 H_2:CO																			
r_{co} (mmol/g_{cat}.hr)			8.06																
TOF *10^3 (s^{-1})			-																
200°C, P_{CO} 30 psi, P_{H2} 130 psi																			
r_{co} (mmol/g_{cat}.hr)			12.00																
TOF *10^3 (s^{-1})			-																
Rxn Gases (mL/min)			61.76	60.50															
V_{H2} (mL/min) STP	0.402494		24.86	24.35															
V_{He} (mL/min) STP	0.489013		30.20	29.59															
V_{COAR} (mL/min) STP	0.108493		6.70	6.56															
V_{CO} (mL/min) STP			5.95	5.82															
V_{AR} (mL/min) STP			0.75	0.75															
Rxn Gases (mol/min)			2.76E-03	2.70E-03															
n_{H2} (mol/min) STP			1.11E-03	1.09E-03															
n_{He} (mol/min) STP			1.35E-03	1.32E-03															
n_{COAr} (mol/min) STP			2.99E-04	2.93E-04															
n_{CO} (mol/min) STP			2.65E-04	2.60E-04															
n_{Ar} (mol/min) STP			3.35E-05	3.33E-05															
Rxn Gases (mol %)			1.000																
y_{H2} (mol%)			0.402																
y_{He} (mol%)			0.489																
y_{COAr} (mol%)			0.108																
y_{CO} (mol%)			0.096																
y_{Ar} (mol%)			0.012																
H_2 area	Ar area	CO area	CH_4 area	CO_2 area	CO/Ar	Temp (°C)	Temp (K	X_{CO}	X_{H2calc}	S_{CH4}	r_{co} (mol/g_{cat}.min	r_{co} (mmol/g_{cat}.h	TOF (s^{-1})	TOF*10^3(s^{-1})	TOF (hr^{-1})	r_{CO} avg (ps	r_{H2} avg (ps	(mol/g_{cat}.min.psi^{α}	r_{calc} (mol/g_{cat}.min.$psi^{0.6}$
9788626.8	8306601	56493065			6.80	Baseline													
9612314	8363387	55632538	56333	12634	6.65	157	430	2.19%	1.23%	5.4%	2.25E-05	1.35	0.003	2.89	10.39	29.89	125.58	1.51E-06	1.65E-06
8409609	7586607	49530858	127173	14073	6.53	167	440	4.00%	2.25%	6.6%	4.11E-05	2.47	0.005	5.27	18.97	29.66	125.25	2.76E-06	2.70E-06
8387173	7741576	48875508	271235	16728	6.31	179	452	7.17%	4.04%	7.9%	7.37E-05	4.42	0.009	9.44	33.98	29.27	124.67	4.94E-06	4.75E-06
10520128	5869596	36748387	305372	15097	6.2608	183.6	456.75	5.82%	3.27%		6.10E-05	3.66	0.008	7.82	28.15	29.44	124.92	4.09E-06	5.85E-06
8127100	7824399	46578703	638399	23954	5.95	189	462	12.47%	7.02%	10.7%	1.28E-04	7.69	0.016	16.42	59.10	28.60	123.68	8.60E-06	7.43E-06
7849235	8023389	43722333	1390823	104676	5.45	201	474	19.87%	11.19%	14.6%	2.04E-04	12.26	0.026	26.17	94.20	27.64	122.26	1.37E-05	1.24E-05
10003816	6112508	33188220	1666535	39073	5.4296	204	477.15	18.32%	10.31%		1.92E-04	11.53	0.025	24.63	88.65	27.84	122.56	1.29E-05	1.40E-05

Table 2. Fixed bed reaction conditions and raw data for the Co/Pt-co catalyst

Weight of Catalyst (g_{cat})		0.25		0.2576
H_2 uptake ($\mu mol/g_{cat}$)		**297**		
Baseline CO/Ar		6.53		7.11
□		-2		
$P_{reactor}$ (psi)		313		
Density		0.697		
Fits		**Nonlinear**	**Linear**	
A		2453.00	3579.219	
E_{App}/Rg		8764.61	8944.5	
E_{App} (kJ/mol)		72.87	74.36	
200°C, 20 atm, 50% X_{co} , 2:1 H_2:CO				
r_{co} ($mmol/g_{cat}.hr$)		14.99		
TOF $*10^3$ (s^{-1})		7.01		
200°C, P_{CO} 30 psi, P_{H2} 130 psi				
r_{co} ($mmol/g_{cat}.hr$)		19.76		
TOF $*10^3$ (s^{-1})		9.23		
Rxn Gases (mL/min)		63.93	33.08	61.60
V_{H2} (mL/min) STP	0.478952	30.62	15.85	24.79
V_{He} (mL/min) STP	0.377414	24.13	12.49	30.12
V_{COAR} (mL/min) STP	0.143644	9.18	4.75	6.68
V_{CO} (mL/min) STP		8.15	4.22	5.93
V_{AR} (mL/min) STP		1.03	0.53	0.75
Rxn Gases (mol/min)		2.85E-03	1.48E-03	2.75E-03
n_{H2} (mol/min) STP		1.37E-03	7.07E-04	1.11E-03
n_{He} (mol/min) STP		1.08E-03	5.57E-04	1.34E-03
n_{COAr} (mol/min) STP		4.10E-04	2.12E-04	2.98E-04
n_{CO} (mol/min) STP		3.64E-04	1.88E-04	2.65E-04
n_{Ar} (mol/min) STP		4.59E-05	2.37E-05	3.34E-05
Rxn Gases (mol %)		1.000	1.000	1.000
y_{H2} (mol%)		0.479	0.479	0.402
y_{He} (mol%)		0.377	0.377	0.489
y_{COAr} (mol%)		0.144	0.144	0.108
y_{CO} (mol%)		0.128	0.128	0.096
y_{Ar} (mol%)		0.016	0.016	0.012

H_2 area	Ar area	CO area	CH_4 area	CO_2 area	CO/Ar	Temp (°C)	Temp (K)	X_{CO}	X_{H2calc}	S_{CH4}	r_{co} ($mol/g_{cat}.min$)	r_{co} ($mmol/g_{cat}.hr$)	TOF (s^{-1})	TOF$*10^3$(s^{-1})	TOF (hr^{-1})	P_{CO} avg (psi)	P_{H2} avg (psi)	k ($mol/g_{cat}.min.psi^{0.5}$)	k_{calc} ($mol/g_{cat}.min.psi^{0.5}$)
5566232	3396463	22168980			6.53	Baseline													
12867273	8493859	42335766	2092039	69370	4.98	200	473	23.64%	14.80%	13.49%	3.44E-04	20.64	0.01	9.64	34.69	36.18	144.71	2.17E-05	2.21E-05
8747336.67	9098775.60	48212689.00	1696225.60	39298.21	5.30	194.00	467.15	25.52%	14.36%	13.93%	2.62E-04	15.74	0.01	7.35	26.45	26.89	121.15	1.76E-05	1.74E-05
13594622	8221180	46411122	701100	49276	5.65	185	458	13.51%	8.46%	7.91%	1.97E-04	11.80	0.01	5.51	19.83	37.84	147.02	1.24E-05	1.21E-05
9183830.20	8842890.73	52462180.00	726731.06	25804.21	5.93	184.00	457.15	16.61%	9.35%	9.17%	1.71E-04	10.24	0.00	4.78	17.21	28.07	122.89	1.15E-05	1.16E-05
9359631.25	8622784.40	54497017.00	259395.99	24417.07	6.32	173.00	446.15	11.16%	6.28%	4.87%	1.15E-04	6.88	0.00	3.21	11.57	28.77	123.93	7.69E-06	7.21E-06
13729370	8055186	47373258	386827	46772	5.88	170	443	9.90%	6.20%	11.51%	7.45E-05	4.47	0.00	2.09	7.52	38.42	147.81	4.68E-06	6.31E-06
9494845.50	8533779.30	56016660.00	112220.81	21212.34	6.56	164.00	437.15	7.73%	4.35%	3.04%	7.95E-05	4.77	0.00	2.23	8.01	29.20	124.57	5.33E-06	4.81E-06

Table 3. Fixed bed reaction conditions and raw data for the Co/Pt-seq catalyst

Weight of Catalyst (g_{cat})			0.2505																
H_2 uptake ($\mu mol/g_{cat}$)			251																
Baseline CO/Ar			6.68																
□			-2																
$P_{reactor}$ (psi)			313																
Density			0.697																
Fits			**Nonlinear**	**Linear**															
A			4.12E+06	5.91E+07															
E_{App}/Rg			12616.3	13862															
E_{App} (kJ/mol)			104.89	115.25															
200°C, 20 atm, 50% X_{co} , 2:1 H_2:CO																			
r_{co} ($mmol/g_{cat}.hr$)			7.34																
TOF $*10^3$ (s^{-1})			4.06																
200°C, P_{CO} 30 psi, P_{H2} 130 psi																			
r_{co} ($mmol/g_{cat}.hr$)			9.70																
TOF $*10^3$ (s^{-1})			5.37																
Rxn Gases (mL/min)			59.90																
V_{H2} (mL/min) STP		0.4024935	24.11																
V_{He} (mL/min) STP		0.4890133	29.29																
V_{COAR} (mL/min) STP		0.1084931	6.50																
V_{CO} (mL/min) STP			5.77																
V_{AR} (mL/min) STP			0.73																
Rxn Gases (mol/min)			2.67E-03																
n_{H2} (mol/min) STP			1.08E-03																
n_{He} (mol/min) STP			1.31E-03																
n_{COAr} (mol/min) STP			2.90E-04																
n_{CO} (mol/min) STP			2.57E-04																
n_{Ar} (mol/min) STP			3.25E-05																
Rxn Gases (mol %)			1.000																
y_{H2} (mol%)			0.402																
y_{He} (mol%)			0.489																
y_{COAr} (mol%)			0.108																
y_{CO} (mol%)			0.096																
y_{Ar} (mol%)			0.012																
H_2 area	Ar area	CO area	CH_4 area	CO_2 area	CO/Ar	Temp (°C)	Temp (K)	X_{CO}	X_{H2calc}	S_{CH4}	r_{co} ($mol/g_{cat}.min$)	r_{co} ($mmol/g_{cat}.hr$)	TOF (s^{-1})	OF*10^3(s^{-1})	TOF (hr^{-1})	P_{CO} avg (psi)	P_{H2} avg (psi)	$mol/g_{cat}.min.psi^n$	k_{calc} ($mol/g_{cat}.min.psi^{0.5}$)
10928566	9477460	63318975			6.68	Baseline													
10807180	9435070	62186125	79783	19825	6.59	163	436	1.35%	0.76%	12.8%	1.39E-05	0.83	0.00	0.46	1.65	29.99	125.74	9.28E-07	1.13E-06
9654605	8639780	56356590	143563	21490	6.52	172	445	2.37%	1.33%	13.1%	2.43E-05	1.46	0.00	0.81	2.90	29.87	125.55	1.63E-06	2.02E-06
9581539	8813642	55257958	352331	23969	6.27	183	456	6.16%	3.47%	12.3%	6.33E-05	3.80	0.00	2.10	7.56	29.40	124.86	4.24E-06	4.01E-06
9334950	8906943	53163651	879698	31749	5.97	193	466	10.66%	6.00%	17.8%	1.10E-04	6.57	0.00	3.63	13.08	28.83	124.02	7.35E-06	7.25E-06
8980478	9064793	49491079	1858328	52300	5.46	203	476	18.28%	10.29%	21.9%	1.88E-04	11.27	0.01	6.23	22.44	27.85	122.57	1.26E-05	1.28E-05

Table 4. Fixed bed reaction conditions and raw data for the Co/Re-co catalyst

Weight of Catalyst (g_{cat})			**0.2576**																	
H_2 uptake ($\mu mol/g_{cat}$)			**268**																	
Baseline CO/Ar			6.76																	
□			-2																	
$P_{reactor}$ (psi)			313																	
Density			0.697																	
Fits			**Nonlinear**	**Linear**																
A			6.36E+06	1.21E+07																
E_{App}/Rg			12526.3	12825																
E_{App} (kJ/mol)			104.14	106.63																
200°C, 20 atm, 50% X_{co} , 2:1 H_2:CO																				
r_{co} ($mmol/g_{cat}.hr$)			13.70																	
TOF $*10^3$ (s^{-1})			7.09																	
200°C, P_{CO} 30 psi, P_{H2} 130 psi																				
r_{co} ($mmol/g_{cat}.hr$)			18.11																	
TOF $*10^3$ (s^{-1})			9.38																	
Rxn Gases (mL/min)			61.60																	
V_{H2} (mL/min) STP	0.402494		24.79																	
V_{He} (mL/min) STP	0.489013		30.12																	
V_{COAR} (mL/min) STP	0.108493		6.68																	
V_{CO} (mL/min) STP			5.93																	
V_{AR} (mL/min) STP			0.75																	
Rxn Gases (mol/min)			2.75E-03																	
n_{H2} (mol/min) STP			1.11E-03																	
n_{He} (mol/min) STP			1.34E-03																	
n_{COAr} (mol/min) STP			2.98E-04																	
n_{CO} (mol/min) STP			2.65E-04																	
n_{Ar} (mol/min) STP			3.34E-05																	
Rxn Gases (mol %)			1.000																	
y_{H2} (mol%)			0.402																	
y_{He} (mol%)			0.489																	
y_{COAr} (mol%)			0.108																	
y_{CO} (mol%)			0.096																	
y_{Ar} (mol%)			0.012																	
H_2 area	Ar area	CO area	CH_4 area	CO_2 area	CO/Ar	Temp (°C)	Temp (K)	X_{CO}	X_{H2calc}	S_{CH4}	**r_{co} ($mol/g_{cat}.min$)**	**r_{co} ($mmol/g_{cat}.hr$)**	**TOF (s^{-1})**	**TOF$*10^3$(s^{-1})**	**TOF (hr^{-1})**	P_{CO} avg (psi)	P_{H2} avg (psi)	**k ($mol/g_{cat}.min.psi^{0.5}$)**	**k_{calc} ($mol/g_{cat}.min.psi^{0.5}$)**	
9017758.3	7727390	52260345			6.76	Baseline														
8887048	7809771	51301118	82352	21732	6.57	162	435	2.87%	1.62%	6.0%	2.95E-05	1.77	0.00	0.92	3.30	29.80	125.46	1.98E-06	2.00E-06	
8476517	8635403	55490684	167062	27010	6.43	172	445	4.98%	2.80%	7.0%	5.12E-05	3.07	0.00	1.59	5.72	29.54	125.07	3.43E-06	3.82E-06	
8233807	8827418	53262251	540497	32231	6.03	182	455	10.78%	6.07%	10.5%	1.11E-04	6.65	0.00	3.44	12.38	28.81	124.00	7.43E-06	7.10E-06	
7791655	8962395	49523055	1296478	43493	5.53	192	465	18.30%	10.30%	14.8%	1.88E-04	11.28	0.01	5.84	21.01	27.85	122.57	1.26E-05	1.28E-05	
7265027	9229767	45388483	2713834	80419	4.92	203	476	27.29%	15.36%	20.8%	2.80E-04	16.83	0.01	8.70	31.33	26.65	120.79	1.89E-05	2.39E-05	
6403575	9683238	39090439	5665109	195446	4.04	213	486	40.31%	22.69%	29.4%	4.14E-04	24.86	0.01	12.86	46.29	24.84	118.11	2.79E-05	4.10E-05	

Table 5. Fixed bed reaction conditions and raw data for the Co/Re-seq catalyst

Weight of Catalyst (g_{cat})			**0.2505**																	
H_2 uptake ($\mu mol/g_{cat}$)			**302**																	
Baseline CO/Ar			6.71																	
□			-2																	
$P_{reactor}$ (psi)			313																	
Density			0.697																	
Fits			**Nonlinear**	**Linear**																
A			1.13E+06	3.89E+08																
E_{App}/Rg			12149.6	14896																
E_{App} (kJ/mol)			101.01	123.85																
200°C, 20 atm, 50% X_{co} , 2:1 H_2:CO																				
r_{co} ($mmol/g_{cat}.hr$)			5.38																	
TOF $*10^3$ (s^{-1})			2.47																	
200°C, P_{CO} 30 psi, P_{H2} 130 psi																				
r_{co} ($mmol/g_{cat}.hr$)			7.57																	
TOF $*10^3$ (s^{-1})			3.47																	
Rxn Gases (mL/min)			59.90																	
V_{H2} (mL/min) STP	0.4024935		24.11																	
V_{He} (mL/min) STP	0.4890133		29.29																	
V_{COAR} (mL/min) STP	0.1084931		6.50																	
V_{CO} (mL/min) STP			5.77																	
V_{AR} (mL/min) STP			0.73																	
Rxn Gases (mol/min)			2.67E-03																	
n_{H2} (mol/min) STP			1.08E-03																	
n_{He} (mol/min) STP			1.31E-03																	
n_{COAr} (mol/min) STP			2.90E-04																	
n_{CO} (mol/min) STP			2.57E-04																	
n_{Ar} (mol/min) STP			3.25E-05																	
Rxn Gases (mol %)			1.000																	
y_{H2} (mol%)			0.402																	
y_{He} (mol%)			0.489																	
y_{COAr} (mol%)			0.108																	
y_{CO} (mol%)			0.096																	
y_{Ar} (mol%)			0.012																	
H_2 area	Ar area	CO area	CH_4 area	CO_2 area	CO/Ar	Temp (°C)	Temp (K)	X_{CO}	X_{H2calc}	S_{CH4}	**r_{co} ($mol/g_{cat}.min$)**	**r_{co} ($mmol/g_{cat}.hr$)**	**TOF (s^{-1})**	**TOF$*10^3$(s^{-1})**	**TOF (hr^{-1})**	P_{CO} avg (psi)	P_{H2} avg (psi)	**k ($mol/g_{cat}.min.psi^{0.5}$)**	**k_{calc} ($mol/g_{cat}.min.psi^{0.5}$)**	
9113624.3	7887468	52949093			6.71	Baseline														
9110451	7898797	52754639	36033	19154	6.68	159	432	0.51%	0.29%	15.2%	5.24E-06	0.31	0.00	0.14	0.52	30.09	125.89	3.51E-07	6.88E-07	
8738413	8699975	57608682	81313	26810	6.62	169	442	1.36%	0.77%	12.9%	1.40E-05	0.84	0.00	0.39	1.39	29.99	125.73	9.37E-07	1.30E-06	
8668855	8742376	56859917	173505	29262	6.50	179	452	3.12%	1.75%	12.0%	3.20E-05	1.92	0.00	0.88	3.17	29.77	125.42	2.14E-06	2.39E-06	
8488754	8735208	54754263	440162	33958	6.27	189	462	6.63%	3.73%	14.3%	6.81E-05	4.09	0.00	1.87	6.75	29.34	124.77	4.56E-06	4.27E-06	
8199404	8951917	52903802	1147126	49203	5.91	200	473	11.97%	6.73%	20.7%	1.23E-04	7.38	0.00	3.39	12.19	28.66	123.77	8.25E-06	7.88E-06	
7822952	9130308	50208449	2179848	85403	5.50	209	482	18.08%	10.18%	26.0%	1.86E-04	11.15	0.01	5.12	18.42	27.87	122.61	1.25E-05	1.27E-05	

Table 6. Fixed bed reaction conditions and raw data for the Co/Ru-co catalyst

Weight of Catalyst (g_{cat})			0.2513	0.25																
H_2 uptake ($\mu mol/g_{cat}$)			**219**																	
Baseline CO/Ar			6.62	6.73																
□			-2																	
$P_{reactor}$ (psi)			313																	
Density			0.697																	
Fits			**Nonlinear**	**Linear**																
A			9.97E+04	2.00E+07																
E_{App}/Rg			10835.5	13315																
E_{App} (kJ/mol)			90.09	110.70																
200°C, 20 atm, 50% X_{co} , 2:1 H_2:CO																				
r_{co} ($mmol/g_{cat}.hr$)			7.66																	
TOF $*10^3$ (s^{-1})			4.87																	
200°C, P_{CO} 30 psi, P_{H2} 130 psi																				
r_{co} ($mmol/g_{cat}.hr$)			11.83																	
TOF $*10^3$ (s^{-1})			7.52																	
Rxn Gases (mL/min)			60.09	42.00	17.13															
V_{H2} (mL/min) STP		0.402494	24.19	20.11	8.20															
V_{He} (mL/min) STP		0.489013	29.39	15.85	6.46															
V_{COAR} (mL/min) STP		0.108493	6.52	6.03	2.46															
V_{CO} (mL/min) STP			5.79	5.36	2.18															
V_{AR} (mL/min) STP			0.73	0.68	0.28															
Rxn Gases (mol/min)			2.68E-03	1.87E-03	7.64E-04															
n_{H2} (mol/min) STP			1.08E-03	8.97E-04	3.66E-04															
n_{He} (mol/min) STP			1.31E-03	7.07E-04	2.88E-04															
n_{COAr} (mol/min) STP			2.91E-04	2.69E-04	1.10E-04															
n_{CO} (mol/min) STP			2.58E-04	2.39E-04	9.75E-05															
n_{Ar} (mol/min) STP			3.26E-05	3.01E-05	1.23E-05															
Rxn Gases (mol %)			1.000	1.000																
y_{H2} (mol%)			0.402	0.479																
y_{He} (mol%)			0.489	0.377																
y_{COAr} (mol%)			0.108	0.144																
y_{CO} (mol%)			0.096	0.128																
y_{Ar} (mol%)			0.012	0.016																
H_2 area	Ar area	CO area	CH_4 area	CO_2 area	CO/Ar	Temp (°C)	Temp (K)	X_{CO}	X_{H2calc}	S_{CH4}	**r_{co} ($mol/g_{cat}.min$)**	**r_{co} ($mmol/g_{cat}.hr$)**	**TOF (s^{-1})**	**TOF$*10^3$(s^{-1}**	**TOF (hr^{-1})**	P_{CO} avg (psi	P_{H2} avg (psi)	**ol/g_{cat}.min.p**	**r_{calc} ($mol/g_{cat}.min.psi^{0.5}$**
7899247.3	10224518	67722333			6.62	Baseline														
1882119	1752991	11791590	0	0	7	Baseline														
7296550	5935229	37191359	164824	43022	6	170	443	6.84%	3.81%	13.70%	2.65E-05	1.59	0.00	1.01	3.64	38.89	148.93	1.66E-06	2.40E-06
7356658	6014857	37377208	241085	43655	6	185	458	7.62%	3.81%	7.34%	7.24E-05	4.35	0.00	2.76	9.94	38.77	149.23	4.53E-06	5.34E-06
7361786.5	10697614	64185054	566929	60878	6.00	187	460	9.41%	5.24%	12.93%	9.68E-05	5.81	0.00	3.69	13.27	28.99	124.30	6.49E-06	5.92E-06
7180411.3	10857616	62912771	882297.8667	70688.46	5.79	193	466	12.52%	6.26%	15.13%	1.29E-04	7.72	0.00	4.90	17.65	28.59	124.28	8.60E-06	8.01E-06
7653776	10572552	58005778	1450023	77445	5.49	198	471	17.17%	8.58%	18.14%	1.76E-04	10.59	0.01	6.72	24.21	27.99	123.62	1.18E-05	1.03E-05
6752387	11145969	50928638	50928639	77446	4.57	199	472	31.01%	15.50%	352.62%	3.19E-04	19.13	0.01	12.15	43.73	26.14	121.60	2.13E-05	1.08E-05
7104556	6171433	34895893	872753	63577	6	200	473	15.94%	8.86%	12.71%	1.52E-04	9.10	0.01	5.78	20.80	37.45	147.57	9.49E-06	1.13E-05

Table 7. Fixed bed reaction conditions and raw data for the Co/Ru-seq catalyst

Weight of Catalyst (g_{cat})			0.2511																		
H_2 uptake ($\mu mol/g_{cat}$)			**150**																		
Baseline CO/Ar			6.21																		
			-2																		
$P_{reactor}$ (psi)			313																		
Density			0.697																		
Fits			**Nonlinear**	**Linear**																	
A			2.83E+07	2.79E+07																	
E_{App}/Rg			13572	13565																	
E_{App} (kJ/mol)			112.84	112.78																	
200°C, 20 atm, 50% X_{co} , 2:1 H_2:CO																					
r_{co} ($mmol/g_{cat}.hr$)			6.68																		
TOF $*10^3$ (s^{-1})			6.19																		
200°C, P_{CO} 30 psi, P_{H2} 130 psi																					
r_{co} ($mmol/g_{cat}.hr$)			8.83																		
TOF $*10^3$ (s^{-1})			8.17																		
Rxn Gases (mL/min)			60.04																		
V_{H2} (mL/min) STP		0.40249355	24.17																		
V_{He} (mL/min) STP		0.48901333	29.36																		
V_{COAR} (mL/min) STP		0.10849312	6.51																		
V_{CO} (mL/min) STP			5.78																		
V_{AR} (mL/min) STP			0.73																		
Rxn Gases (mol/min)			2.68E-03																		
n_{H2} (mol/min) STP			1.08E-03																		
n_{He} (mol/min) STP			1.31E-03																		
n_{COAr} (mol/min) STP			2.91E-04																		
n_{CO} (mol/min) STP			2.58E-04																		
n_{Ar} (mol/min) STP			3.26E-05																		
Rxn Gases (mol %)			1.000																		
y_{H2} (mol%)			0.402																		
y_{He} (mol%)			0.489																		
y_{COAr} (mol%)			0.108																		
y_{CO} (mol%)			0.096																		
y_{Ar} (mol%)			0.012																		
H_2 area	Ar area	CO area	CH_4 area	CO_2 area	CO/Ar	Temp (°C)	Temp (K)	X_{CO}	X_{H2calc}	S_{CH4}	**r_{co} ($mol/g_{cat}.min$)**	**r_{co} ($mmol/g_{cat}.hr$)**	**TOF (s^{-1})**	**TOF$*10^3$(s^{-1})**	**TOF (hr^{-1})**	P_{CO} avg (psi)	P_{H2} avg (psi)	**k ($mol/g_{cat}.min.psi^{0.5}$)**	**k_{calc} ($mol/g_{cat}.min.psi^{0.5}$)**		
15409924	7194640	44663063.6			6.21	Baseline															
15294336	7302501	41563640	629388	50654	5.69	191	464	8.31%	4.68%	16.3%	8.55E-05	5.13	0.00	4.74	17.08	29.13	124.46	5.73E-06	5.67E-06		
15336550	7436027	41153505	1101339	68933	5.53	196	469	10.85%	6.11%	21.8%	1.12E-04	6.69	0.01	6.19	22.28	28.81	123.98	7.48E-06	7.59E-06		
14859977	7523540	37258167	2290733	74399	4.95	206	479	20.23%	11.38%	24.3%	2.08E-04	12.47	0.01	11.54	41.54	27.59	122.19	1.40E-05	1.39E-05		
14080557	7936380	28964913	6124802	119733	3.65	221	494	41.21%	23.19%	31.9%	4.24E-04	25.41	0.02	23.51	84.64	24.71	117.92	2.85E-05	3.30E-05		